Complexes of ditopic and tritopic 4'-substituted- 2,2':6',2''-terpyridine ligands

Inauguraldissertation

zur

Erlangung der Würde eines Doktors der Philosophie

vorgelegt der

Philosophisch-Naturwissenschaftlichen Fakultät

der Universität Basel

von

Paulina Chwalisz

aus Brzeg Dolny, Polen

Basel, 2010

creative commons

Namensnennung-Keine kommerzielle Nutzung-Keine Bearbeitung 2.5 Schweiz

Sie dürfen:

das Werk vervielfältigen, verbreiten und öffentlich zugänglich machen

Zu den folgenden Bedingungen:

Namensnennung. Sie müssen den Namen des Autors/Rechteinhabers in der von ihm festgelegten Weise nennen (wodurch aber nicht der Eindruck entstehen darf, Sie oder die Nutzung des Werkes durch Sie würden entlohnt).

Keine kommerzielle Nutzung. Dieses Werk darf nicht für kommerzielle Zwecke verwendet werden.

Keine Bearbeitung. Dieses Werk darf nicht bearbeitet oder in anderer Weise verändert werden.

- Im Falle einer Verbreitung müssen Sie anderen die Lizenzbedingungen, unter welche dieses Werk fällt, mitteilen. Am Einfachsten ist es, einen Link auf diese Seite einzubinden.

- Jede der vorgenannten Bedingungen kann aufgehoben werden, sofern Sie die Einwilligung des Rechteinhabers dazu erhalten.

- Diese Lizenz lässt die Urheberpersönlichkeitsrechte unberührt.

Quelle: http://creativecommons.org/licenses/by-nc-nd/2.5/ch/   Datum: 3.4.2009

Genehmigt von der Philosophisch-Naturwissenschaftlichen Fakultät
auf Antrag von

Prof. Dr. Edwin Constable
Prof. Dr. Thorfinnur Gunnlaugsson

Basel, den 21.09.2010

Prof. Dr. Martin Spiess

Dekan

2

"As our circle of knowledge expands,
so does the circumference of darkness surrounding it."

A. Einstein

Acknowledgements

Contents

Abstract

Chapter 1 gives a brief introduction to supramolecular chemistry, metallosupramolecular chemistry and 2,2':6',2''-terpyridine-based ligands and their complexes.

Chapter 2 discusses the synthesis and characterization of new ditopic ligands **L1**-**L4** and **L6**-**L7.** These ligands are based on a benzene unit connected to two 4'-substituted-2,2':6',2''-terpyridine moieties through polyethyleneoxy spacers. The variability of this group of compounds was achieved by using different length ethyleneoxy chains and changing the substitution position on the benzene unit. The ligands were also preliminary studied for interactions with Group 1 metals.

Chapter 3 describes the synthesis and characterization of heteroleptic dinuclear ruthenium(II) complexes formed with ligands **L1**-**L2**, **L4** and **L6**-**L7**.

Chapter 4 describes the synthesis and characterization of a homoleptic mononuclear zinc(II) complex with a ditopic 4'-substituted- 2,2':6',2''-terpyridine ligand **L4**.

Chapter 5 discusses the synthesis and characterization of ligand **L5** which contain three 2,2':6',2''-terpyridine metal-binding domains as well as the synthesis and characterization of a heteroleptic trinuclear ruthenium(II) complex of this ligand. Three 2,2':6',2''-terpyridine domains on the ligand **L5** are linked at their 4'-positions to a benzene unit through diethylene glycol spacers.

Chapter 6 describes the synthesis and characterization of homoleptic mononuclear europium(III) and terbium(III) complexes of tritopic 4'-substituted- 2,2':6',2''-terpyridine ligand **L5**.

Abbreviations

Cl-tpy	4'-chloro-2,2':6',2"-terpyridine
COSY	correlated spectroscopy
CV	cyclic voltammetry
bpy	2,2'-bipyridine
br	broad
d	doublet
δ	chemical shift
DCM	dichloromethane
DEPT	distortionless enhancement by polarisation transfer
DMF	N,N'-dimethylformamide
DMSO	dimethylsulfoxide
ε	molar extinction coefficient
ESI	electrospray ionisation
EtOH	ethanol
Fc	ferrocene
Fc^{+}	ferrocenium
HMBC	heteronuclear multiple bond correlation
HMQC	heteronuclear multiple quantum correlation
HPLC	high performance liquid chromatography
Hz	hertz, s^{-1}
IR	infrared spectroscopy
IUPAC	International Union of Pure and Applied Chemistry
J	coupling constant
λ	wavelength
LC	ligand centred
m	multiplet or medium (IR)
M	molarity
M	parent ion mass
MALDI	matrix assisted laser desorption ionisation

MC	metal centred
MLCT	metal to ligand charge transfer
m.p.	melting point
MS	mass spectrometry
m/z	mass to charge ratio
ν	frequency (cm^{-1} or Hz)
NMR	nuclear magnetic resonance spectroscopy
NOESY	nuclear overhauser effect spectroscopy
ppm	parts per million
RT	room temperature
REOSY	Rotating frame nuclear Overhauser effect spectroscopy
s	singlet or strong (IR)
t	triplet
td	triplet of doublets
τ	lifetime of emission
TOF	time of flight
tpy	2,2':6',2"-terpyridine
UV-Vis	ultra-violet visible spectroscopy
w	weak (IR)

General experimental

Microwave reactor

Microwave reactions were carried out in a Biotage Initiator 8 reactor with sealed tubes allowing pressures of up to 20 bars.

NMR spectroscopy

NMR spectra were recorded on Bruker AM250 (250 MHz), Bruker AVANCE 300 (300 MHz), Bruker DPX400 (400 MHz) and Bruker DRX500 (500 MHz). For full assignments COSY, DEPT, HMBC, HMQC and NOESY experiments were recorded on the Bruker DRX500. ^{1}H and ^{13}C spectra were recorded at 25 °C and chemical shifts are relative to residual solvent peaks (^{1}H: CDCl$_3$ 7.24 ppm, acetonitrile-*d$_3$* 1.94 ppm; ^{13}C: CDCl$_3$ 77.00 ppm, acetonitrile-*d$_3$* 1.39 ppm).

Mass spectrometry

Electrospray ionisation (ESI) mass spectra were measured using Finnigan MAT LCQ or Bruker esquire 3000^{plus} instruments. MALDI-TOF mass spectra were recorded with a PerSeptive Biosystems Voyager mass spectrometer, using a supporting matrix (sinapinic acid or α-cyano-4-hydroxycinnamic acid).

Infrared spectroscopy

IR spectra were recorded on a Shimadzu FTIR-8400S spectrophotometer with neat samples using a golden gate attachment.

Melting points

Melting points were determined on a Stuart Scientific melting point apparatus SMP3.

UV-Vis spectroscopy

UV-visible absorption spectra were measured in 1-cm quartz cuvettes on a Varian Cary 50 spectrophotometer. Baseline correction was applied for all spectra.

Emission spectroscopy

Emission (Fluorescence, phosphorescence and excitation) spectra were recorded on a Varian Cary Eclipse Fluorimeter. Quartz cells with a 1 cm path length from Hellma were used for these measurements. The temperature was kept constant throughout the measurements by using a thermostated unit block

Microanalysis

The microanalyses were performed with a Leco CHN-900 microanalyser by W. Kirsch.

Electrochemistry

Electrochemical measurements were done on an Eco Chemie Autolab PGSTAT 20 using a glassy carbon working electrode, a platinum mesh for the counter electrode, and a silver wire as the reference electrode. The redox potentials ($E_{1/2}^{ox}$, $E_{1/2}^{red}$ [V]) were determined by cyclic voltammetry (CV) and by square wave and differential pulse voltammetry. The compounds were dissolved and measured in dry and degassed acetonitrile in the presence of 0.1 M [n-Bu$_4$N][PF$_6$] unless otherwise stated. The scanning rate for the CV was 100 mV·s^{-1} in all cases and ferrocene (Fc) was added as an internal standard at the end of every experiment.

CHAPTER 1

Introduction

In this chapter, a brief introduction to this thesis is presented. The three most important subjects are described below: supramolecular chemistry, metallosupramolecular chemistry and 2,2':6',2''-terpyridine-based molecules in supramolecular chemistry.

1.1 Supramolecular chemistry

Stoddart has defined chemistry as follows:[1]

Chemistry can be likened to "language". The atoms are the "letters". The molecules are the "words". Assemblies of molecules make up the "sentences". The sets of assembled molecules or supermolecules are the "paragraphs". The ways in which the molecular assemblies and supramolecular arrays contain and express information are the "chapters". The manner in which this information is conveyed at both a molecular level is the "book". Ultimately, chemistry has to tell a "story".

Chemists are writing their own "stories". They know how to produce the "words". They are still learning how to write the "sentences". The "grammar" they use has been dictated by the nature of the noncovalent bond.

Supramolecular chemistry was defined by Jean-Marie Lehn as "chemistry beyond the molecule, bearing on the organized entities of higher complexity that result from the association of two or more chemical species".[2-4]

Supramolecular chemistry is an interdisciplinary field of science which covers the chemical, physical, and biological features of chemical species. In contrast to molecular chemistry which is based on the covalent bond, supramolecular chemistry is the chemistry of molecular assemblies and of the intermolecular (noncovalent) bond. All

weak intermolecular interactions can be used in supramolecular chemistry: electrostatic interactions, hydrogen bonds, van der Waals forces, π-π stacking, charge transfer interactions and hydrophobic interactions.[5]

There are two probable mechanisms which work together and lead to supramolecules: molecular recognition and self-assembly. Molecular recognition is a process involving both binding and selection of substrate by a given receptor molecule.[6] Self-assembly is a spontaneous assembly of molecules into structured, stable, non-covalently joined aggregates.[3]

One of the most known examples of a supramolecule comes from nature and is deoxyribonucleic acid (DNA). The double helix form of DNA is based on hydrogen bonds between complementary bases in two oligonucleotides. The structure of DNA became an inspiration for some chemists to synthesize similar systems. Lehn and his group have reported bpy-based double helices held by three copper(I) metal ions (**Figure 1.1**).[7,8]
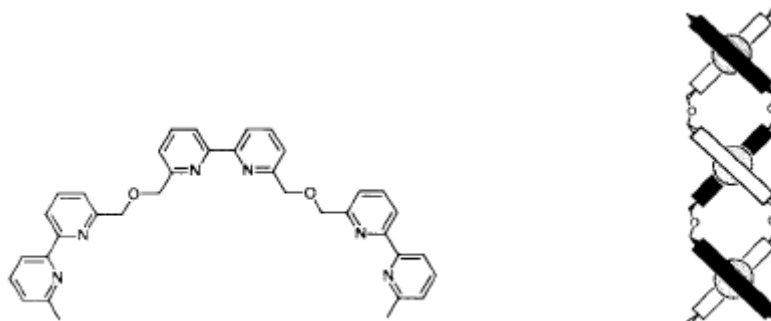
Figure 1.1. Self assembly interactions between three copper(I) ions and two tris(2,2'-bipirydyne) ligands.[7,8]

Jean-Marie Lehn found his interest in the supramolecular chemistry field more than 20 years before he published copper(I) double helices.[7,8] Everything started in the 1960's with cryptands[3,4] and Pedersen joined him with his studies of crown ethers.[9] Since then supramolecular chemistry became one of the biggest and fastest developing field of studies.

16

1.2 Metallosupramolecular chemistry

Introducing metals into supramolecular chemistry appeared to be one of the best ideas. Metallosupramolecules are based on strong metal-ligand bonds, ~ 200 kJ/mol. The ligands can be described as the building blocks, which form larger structures and the metal ions are like molecular "glue", which hold these structures together. The number and orientation of the coordination sites of ligand and coordination number and geometry of metal ion allows very often to design a large number of various highly directional and geometrically well-defined species.

One of the most simple examples of metallosupramolecules are 2-dimensional molecular squares. The geometry of these systems is well defined by platinum(II) or palladium(II) ions acting as 90 degree corners. Fujita, Yazaki, and Ogura have reported self-assembling molecular squares based on metal coordination chemistry. When $[M(en)(NO_3)_2]$ (M = Pt, Pd) is treated with bipyridine, a cyclic tetrameric macrocycle - a molecular square - is formed as the thermodynamically preferred product (**Figure 1.2**).[10,11]
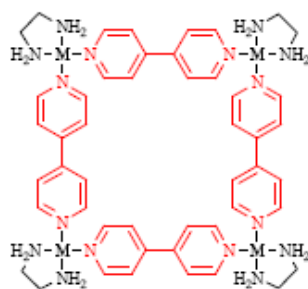
M = Pt(II) or Pd(II)

Figure 1.2. Tetrameric bipyridine macrocycles.[10,11]

Hupp and co-workers have prepared a number of molecular squares which have been used as catalysts.[12] **Figure 1.3** shows a structure in which manganese(II) porphyrin is encapsulated in a square built from four zinc(II) porphyrins and four rhenium complexes. It has been suggested that this could act as an artificial enzyme.
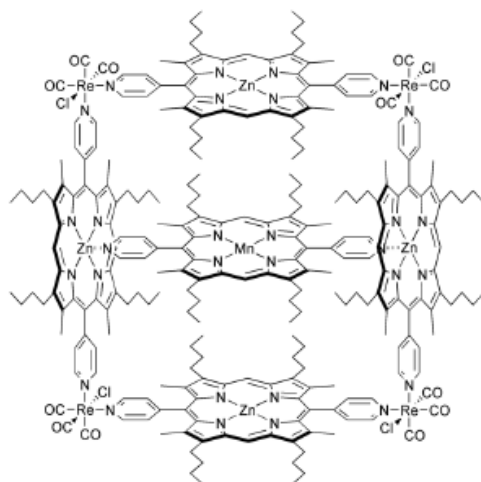
Figure 1.3. A molecular square with an encapsulated Mn(II) porphyrin, prepared by Hupp.[12]

The supramolecular structures containing copper ions and bidentate or tridentate ligands are very good examples to demonstrate how important the metal ion geometry is and the number of the coordination sites of ligand. The Cu(I) ion has a d^{10} electron configuration and it prefers a coordination number of 4 and a tetrahedral geometry[13] whereas the Cu(II) ion has a d^9 electron configuration and prefers to be octahedral or 5-coordinate.[14] There are a lot of examples of the use of preferences of metal ions to direct the assembly of multi-component structures.

a   b
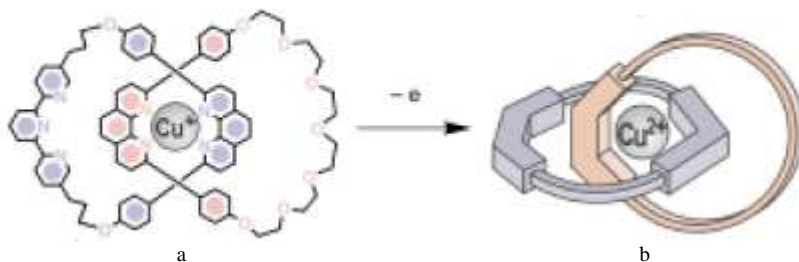
Figure 1.4. 4-Coordinated copper(I) (a) and 5-coordinated copper(II) (b).[14]

Rotaxanes are a class of molecules in which a dumbbell shaped component is encircled by a macrocycle; the two components are linked mechanically rather than by a covalent bond. A generally accepted method for the synthesis of rotaxanes is threading.[15] The

complex formed between these two species can then be modified with blocking groups to produce the [2]rotaxane.[15]

Sauvage has reported a rotaxane in which the thread contains two different ligand domains: 1,10-phenanthroline and 2,2':6',2"-terpyridine, whereas the ring is built out of a bidentate 1,10-phenathroline unit.[16,17] The system can be switched from a four-coordinate Cu(I) to a five-coordinate Cu(II) and back, by oxidizing and reducing the metal (**Figure 1.5**).[18]
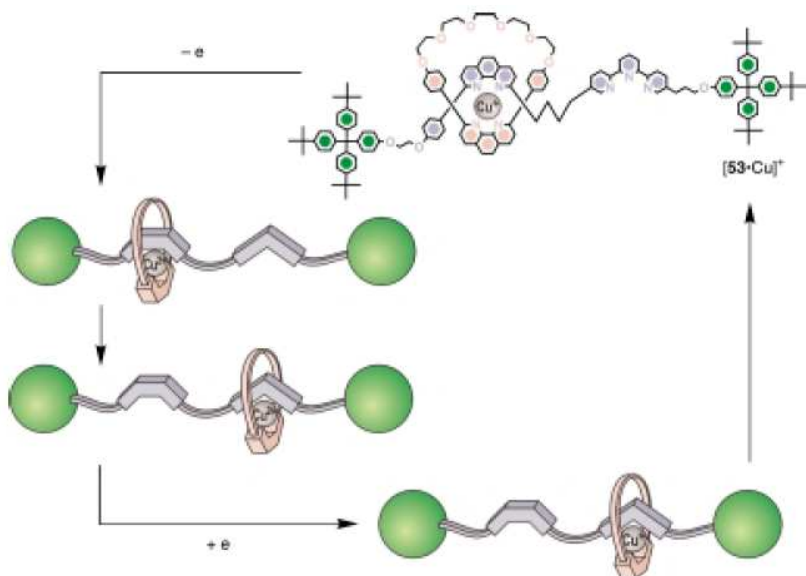
Figure 1.5. The molecular motion of the rotaxane driven by reduction and oxidation.[18]
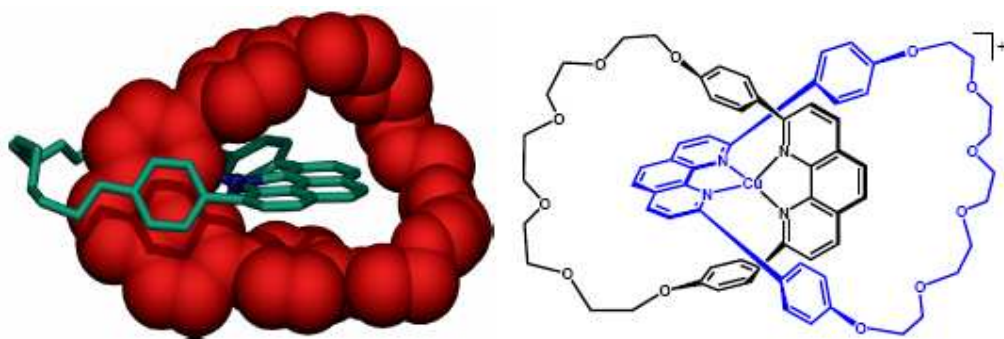
Figure 1.6. The first X-ray crystal structure of a catenate, prepared by Sauvage *et al.*[25]

The efficient synthesis of interlocked or catenated molecules[19-24] requires that one ring be threaded by the precursor of the second ring, and that this assembly be held together as the second ring is formed, simply: one macrocycle must act as a template for the formation of the second macrocycle. One of the very first Cu(I) based catenates was prepared in the Sauvage group.[25] The X-ray structure has confirmed the structure of the product (**Figure 1.6**).

The Sauvage group has also shown that catenates could be extended to multinuclear systems substituted with multiple bridged porphyrin groups (**Figure 1.7**).[26]
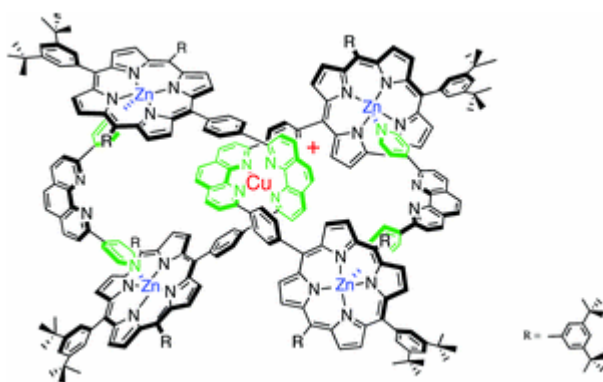
Figure 1.7. An example of catenate containing porphyrin groups.[26]

From the above examples, we understand how important it is to design ligands with the correct number and orientation of the coordination sites as well as a choice of metal ions with the correct coordination number and geometry. **Figure 1.8** shows that smaller molecules can be used as tools, to template the formation of larger systems. Sanders and co-workers have investigated the flexible bisporphyrin receptors.[27,28] In a directed self-assembly process, novel porphyrin-containing macrocycles could be obtained. Although the macrocyclic porphyrin trimer (**Figure 1.8**) can be synthesized by untemplated oxidative coupling of the diacetylenic porphyrin monomer (**Figure 1.8**), the yield is relatively low (47%). If the monomer (**Figure 1.8**) is oxidatively coupled in the presence of s-2,4,6-tri-4-pyridyltriazine, the amount of cyclic trimer formed is dramatically enhanced. The s-2,4,6-tri-4-pyridyltriazine acts as a "negative template": it promotes trimer formation passively by inhibiting dimer formation actively.[29,30]

20
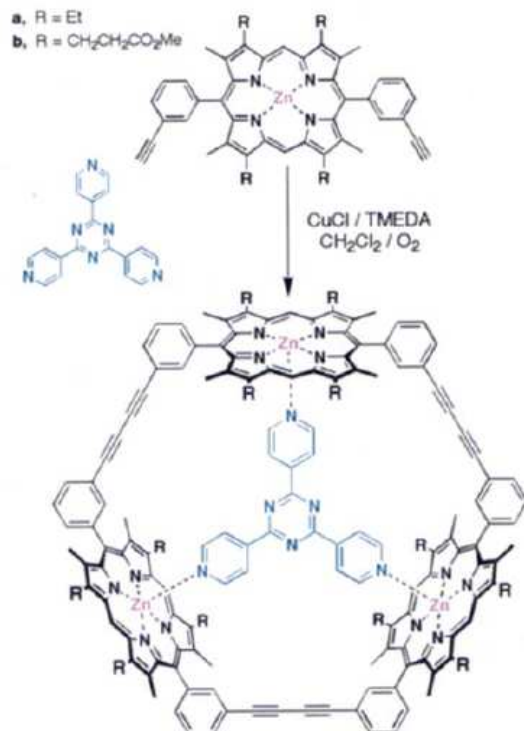
Figure 1.8. Trimeric macrocyclic porphyrin array prepared by Sanders *et al*.[29,30]

Many metal complexes contain more than one metal centre. Some of these dinuclear or multinuclear complexes exhibit electron transfer and energy transfer properties.

Anderson has studied the porphyrin-based macrocycles and that led him to present successful syntheses of electron transporting molecular wires (**Figure 1.9**).[31,32] He also reported new π-conjugated porphyrin nanorings[33] (**Figure 1.10**), which could be obtained by bending and connecting these molecular wires.
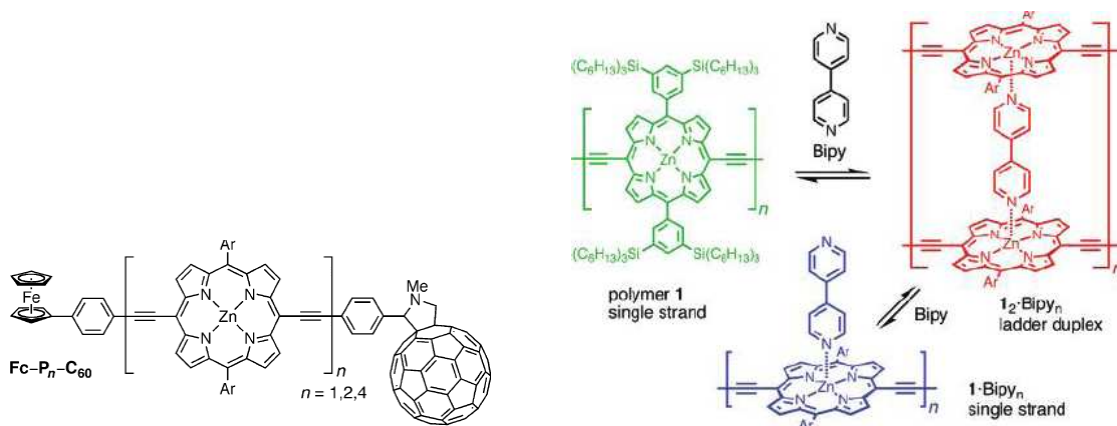
Figure 1.9. Electron transporting molecular wires.[31,32]
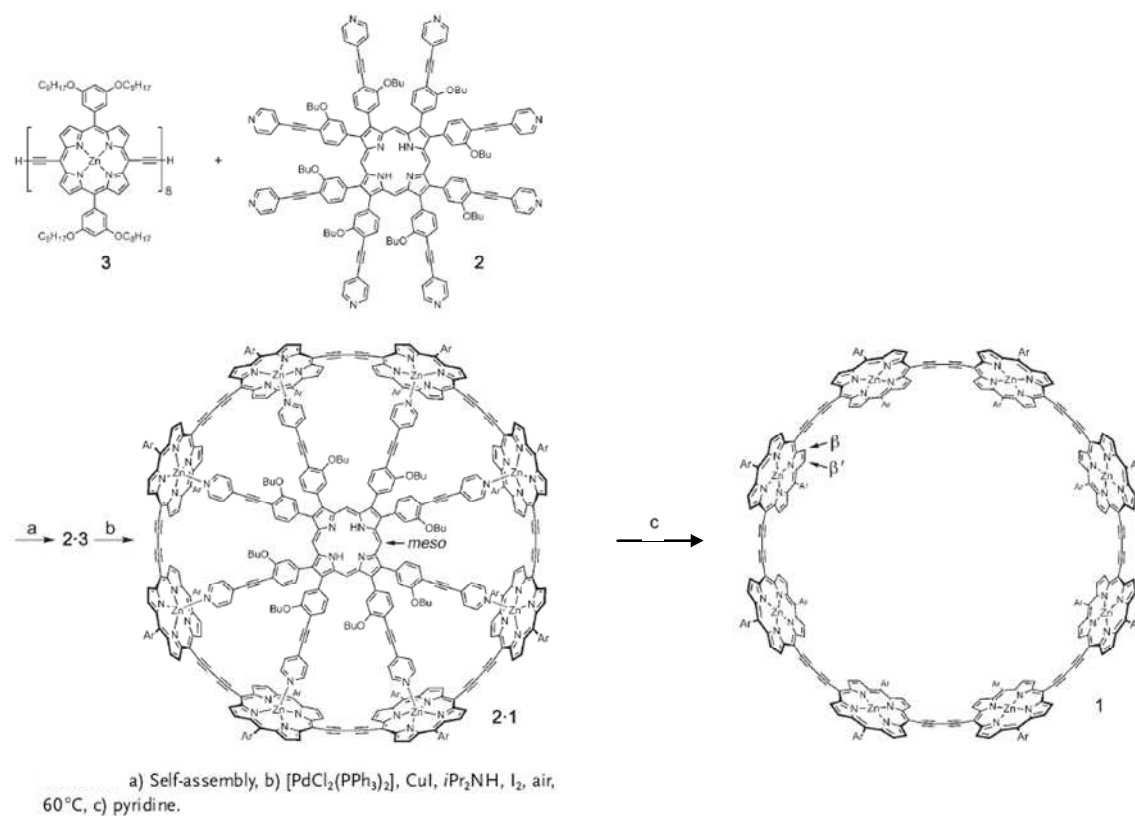
Figure 1.10. Template-directed synthesis of a π-conjugated porphyrin nanoring.[33]

Lehn and co-workers have explored the use of metal coordination for the construction of molecular racks, ladders, and grids (**Figure 1.11**).[34-38] After mixing the ligand presented in **Figure 11** with 1.5 eq. of $AgSO_3CF_3$, a three-by-three molecular grid self-assembles spontaneously from nine Ag(I) ions and six ligands (**Figure 1.11**).
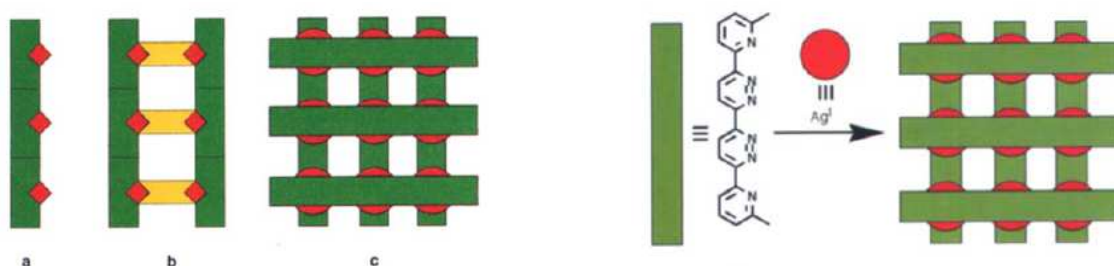
Figure 1.11. Rack (a), ladder (b), and grid structures (c) and self-assembled molecular grid with Ag(I) ions prepared by Lehn.[34-38]

1.3   2,2':6',2''-Terpyridine in Supramolecular chemistry

2,2':6',2''-Terpyridine (tpy) and its derivatives are some of the most popular chelating ligands in supramolecular chemistry. This ligand forms very stable octahedral complexes with a large variety of metal ions.[39,40] In contrast to the bidentate analogue 2,2'-bipyridine (bpy), $\{M(tpy)_2\}^{n+}$ complexes are achiral (provided that only non-substituted or symmetrically substituted tpy ligands are used). The $\{M(bpy)_3\}^{n+}$ complexes exist in two enantiomeric forms: Λ and Δ.
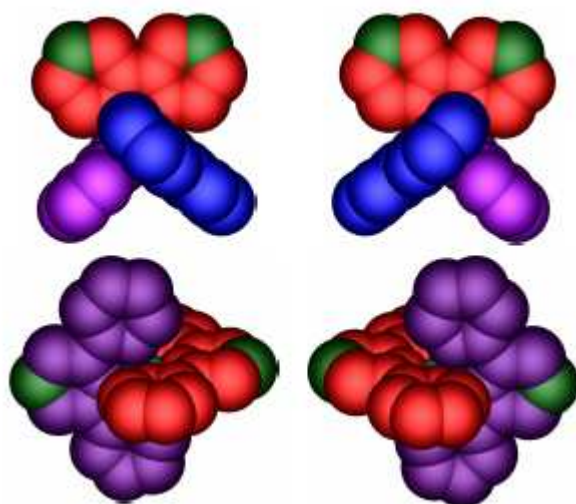
Figure 1.12. The Λ and Δ enantiomers of $\{M(bpy)_3\}^{n+}$ (top) and an achiral $\{M(tpy)_2\}^{n+}$ with symmetrical ligands (bottom).

Tpy can be functionalized at several different positions, such as the 4' position of the central ring and the 6 and 6'' positions of the terminal pyridine rings, but the most known and studied are the 4'-substituted tpy derivatives.

Constable and Housecroft have reported many different 2,2':6',2''-terpyridine ligands substituted with functional groups in 4'-position. Azacrown[41,42] (**Figure 1.13**) and fullerene[43,44] (**Figure 1.14**) functionalized ligands have been synthesized, as well as their metal complexes. These have been studied further of or their electronic and luminescent properties.
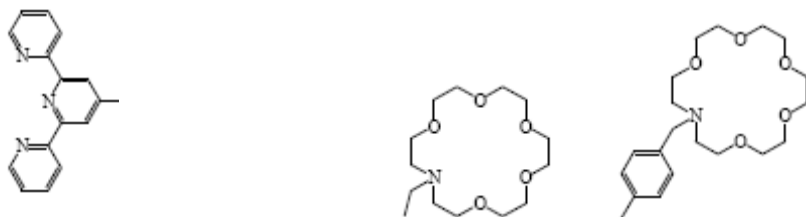
Figure 1.13. Azacrown functionalized tpy ligands.[41,42]

n=0,1
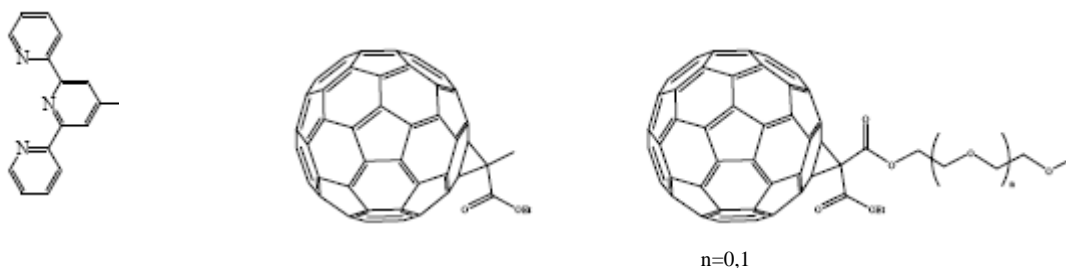
Figure 1.14. Fullerene functionalized tpy ligands.[43,44]

A cyclopentadiene functionalized tpy was used to synthesize the corresponding ferrocene tpy ligand[45] (**Figure 1.15 a**). The 4'-cyclodextrin functionalized[46-48] (**Figure 1.15 b**) and anthryl substituted[49] (**Figure 1.15 c**) tpy ligands have been also synthesized. Their ruthenium and osmium complexes have been studied.

a   b   c
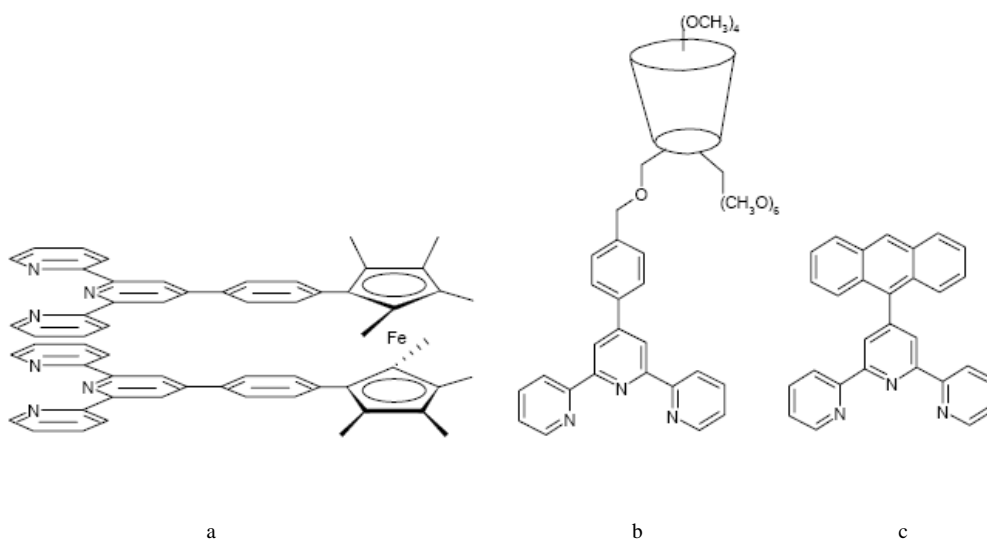
Figure 1.15. Ferrocene (a), cyclodextrin (b) and anthryl (c) substituted tpy.[45-49]

24

Other functional groups have also been used in the syntheses of the 4'-substituted tpy ligands: 2,2'-bipyridine[50], diphenylphosphine[51,52], porphyrins[53-56], thienyl groups[57,58], sugars[59] and much more.

2- and 3-furyl and thiophene have been used to synthesize 4'-substituted tpy ligands and then have been studied for their potential application in anticancer therapy (**Figure 1.16**).[60,61]
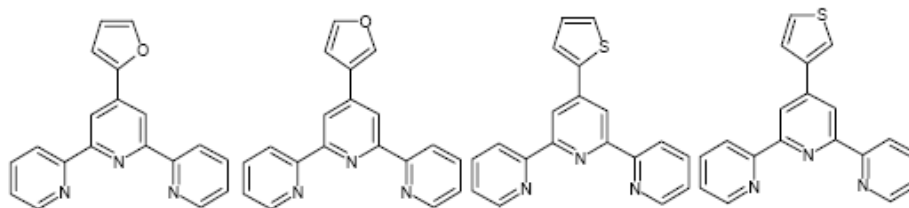
Figure 1.16. Furyl and thiophene substituted tpy ligands.[60,61]

The other well-studied substitution position is the 6-position of the terminal pyridine ring. A series of 6-substituted tpy ligands has been synthesized[62-64]: 6-bromo tpy (**Figure 1.17 a**), chiral 6-bornyloxy tpy ligands (**Figure 1.17 b-e**) and quaterpyridine ligand (**Figure 1.17 f**), synthesized in coupling reaction[65]. A chiral cobalt(II) complex of 6-bromo tpy (**Figure 1.17 a**) has been well studied in Constable group.[66] In contrast to cobalt(II) complexes of 4'-substituted tpy, [Co(II)(6-bromo tpy)$_2$] complex is a high spin system.
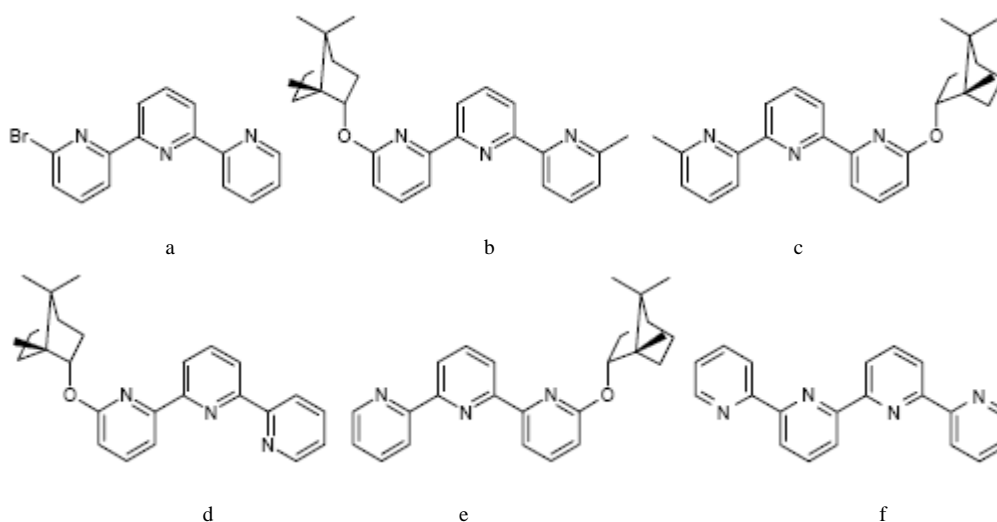
Figure 1.17. 6-Bromo tpy (a), chiral 6-bornyloxy tpy ligands (b-e) and quaterpyridine ligand (f).[62-66]

More than one 2,2':6',2"-terpyridine domain can be used to synthesize different groups of ligands. There is great interest in studying ligands containing two or more tpy units, these are called "bridged" ligands. A variety of ligands with two 2,2':6',2"-terpyridine groups linked with different spacers have been reported. An introduction of the spacer into a molecule allows one to control the supramolecular structure, distances and angles, and/or to control transfer of electrons or energy through the bonds. Depending on the type of the spacer, either rod-like[67-78] or macrocyclic[79-82] complexes are preferred.
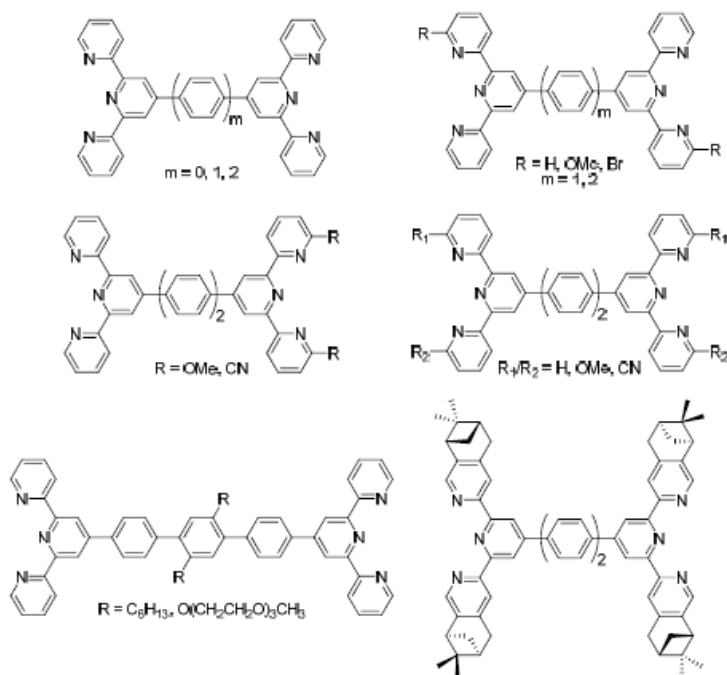
Figure 1.18. Ditopic bis(2,2':6',2"-terpyridine) ligands with rigid phenylene-based spacers.[67-78]
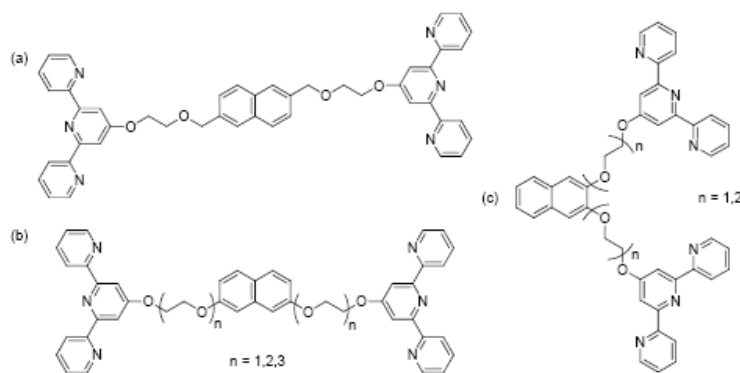
Figure 1.19. Ditopic bis(2,2':6',2"-terpyridine) ligands with naphthalene spacers.[79-82]

26

Figure 1.20 shows bridged ligands containing three (a), four (b) and six tpy (c) domains. These kind of ligands have been used as the core for the synthesis of metallostars[83,84] and metallodendrimers.[85]

a   b   c
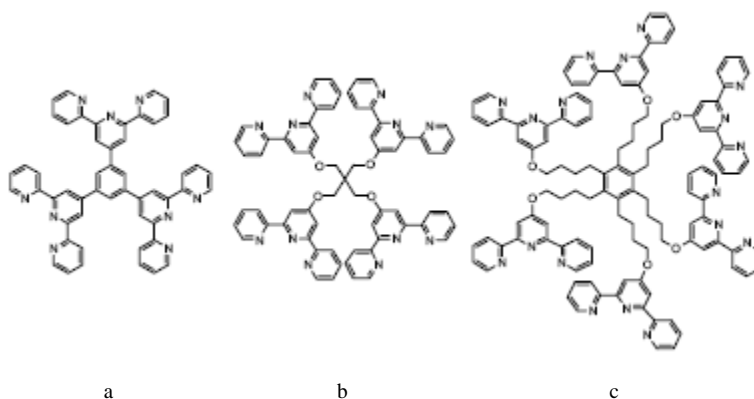
Figure 1.20. Tpy based ligands with three, four and six tpy domains.[83-85]

The triruthenium complex (**Figure 1.21**) has been reacted with hexakis(bromomethyl)benzene to give the desired octadecanuclear complex (**Figure 1.21**). The center of the complex is built from six tpy domains – dendrimeric core, and therefore is a very similar to that presented on **Figure 1.20 c**.[86]
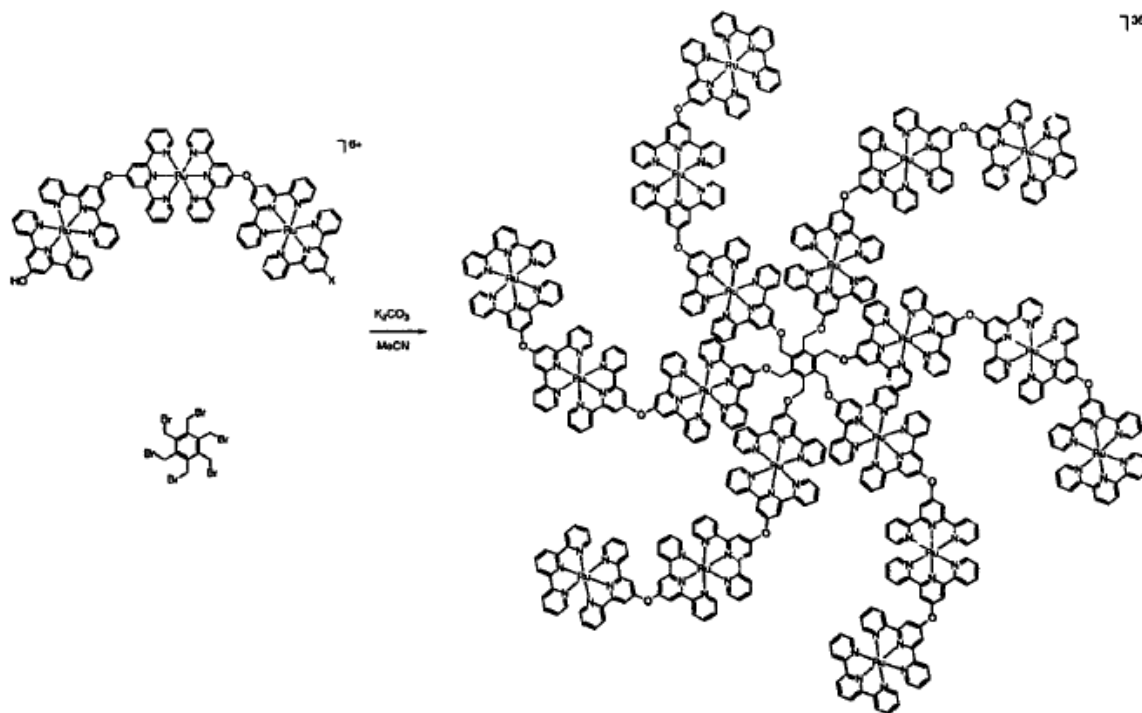
Figure 1.21. Reaction scheme for the synthesis of the octadecaruthenium complex.[86]

A first generation tetranuclear complex has been synthesized by reacting together pentaerythritol functionalised with 2,2′:6′,2″-terpyridine and ruthenium(III) complex. For a second generation dendrimer, the tetranuclear metal species has been coupled with a [Ru(tpy)(Cl-tpy)]$^{2+}$ complex (**Figure 1.22**).[85]
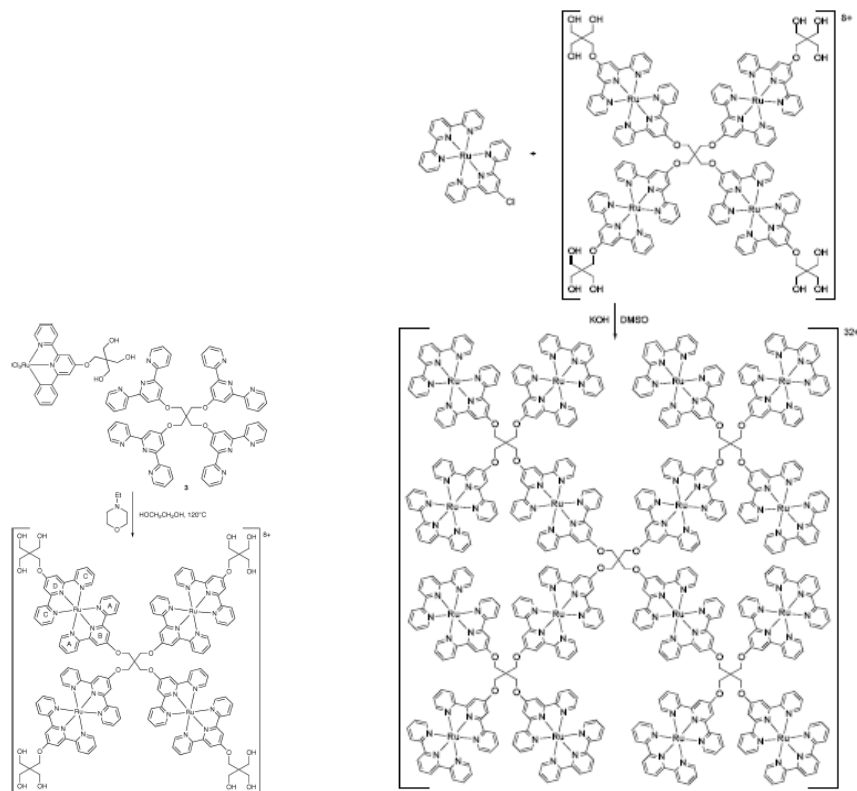
Figure 1.22. Reaction scheme for the synthesis of metallodendrimers.[85]

Metallodendrimers and metallostars pictured in **Figure 1.21** and **1.22** are examples of typical examples of the use of tpy-based ligands, as the building blocks for larger systems, namely – metal complexes. Due to the photophysical properties (they absorb a significant portion of the visible spectrum, have relatively long-lived excited states (>1 μs) and exhibit good photochemical stability),[87] ruthenium(II) tpy complexes have been the focus of big research interest. From all of the enormous possible applications only two of the most spectacular are mentioned here: light-powered molecular machines[88,89] and dye sensitized solar cells (Grätzel cells).[90-95]

As already mentioned, ligands with two or more 2,2':6',2"-terpyridine units, depending on the type of the spacer used, allows one to obtain basically two types of different complexes, either rod-like[67-78] (or sometimes linear polymeric) or macrocyclic.[79-82] Some examples of the linear multinuclear complexes are shown on **Figure 1.23**. Metallomacrocyclic iron(II) complexes shown in **Figure 1.24** are the thermodynamic products although the initial kinetic products are oligomeric.
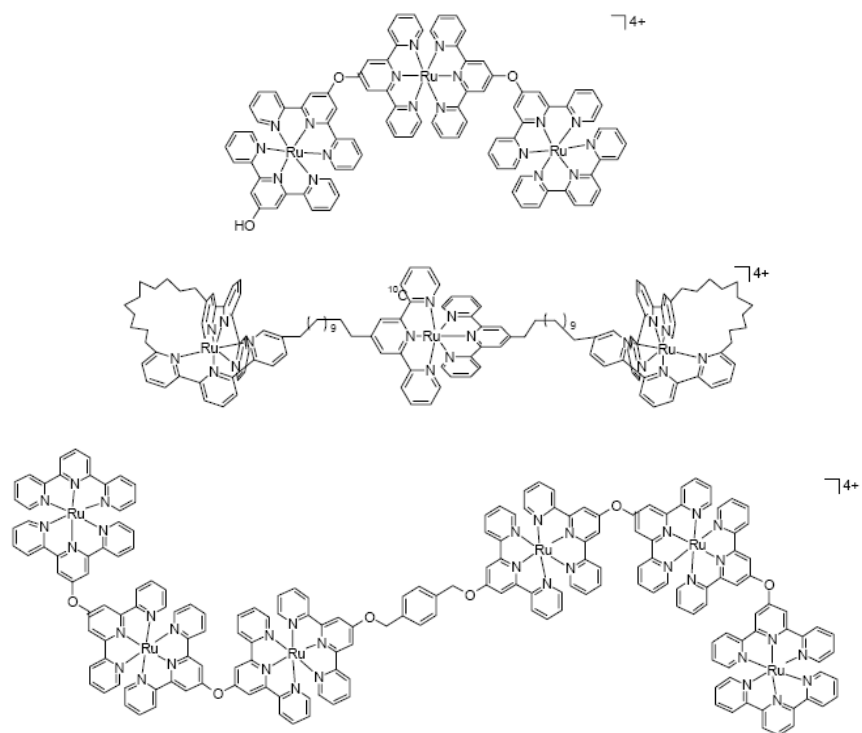
Figure 1.23. Linear multinuclear complexes.[67-78]
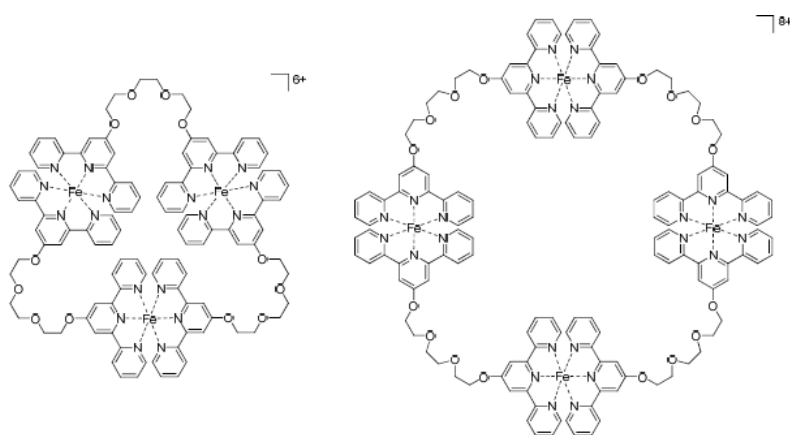
Figure 1.24. Macrocyclic multinuclear iron(II) complexes.[79-82]

1.4 Aims of this thesis

The aim of this thesis is to synthesize and characterize a series of ligands containing two or three 2,2':6',2''-terpyridine domains, linked by flexible oligo(ethylene glycol) chains separated additionally with a phenyl spacer. These ditopic 2,2':6',2''-terpyridine – based ligands (L1 – L4, L6 - L7) are the building blocks for heteroleptic dinuclear ruthenium(II) as well as homoleptic mononuclear zinc(II) complexes.

The tritopic 2,2':6',2''-terpyridine ligand (L5) is also a template for binding ruthenium(II) into trinuclear complex but due to its flexibility and higher number of coordination sites (9), this particular ligand can be used for binding europium(III) and terbium(III).

All of these complexes, containing a number of metal centers can be further investigated for the applications in the energy transfer processes between metal centers.

CHAPTER 2

Synthesis of ditopic 4'-substituted- 2,2':6',2''-tpy ligands and preliminary study of interactions with Group 1 metals

2.1 Introduction

2,2':6',2''-Terpyridine contains three pyridine rings connected through the α carbon atoms with respect to the nitrogen atoms. There are two major methodologies for the synthesis of the 2,2':6',2''-terpyridine ligand and its derivatives: ring assembly (**Scheme 2.1**) and cross-coupling procedures (**Scheme 2.2**).[96] In the first method an intermediate diketone undergoes a ring closing reaction in the last step in the presence of ammonium acetate and ethanol.
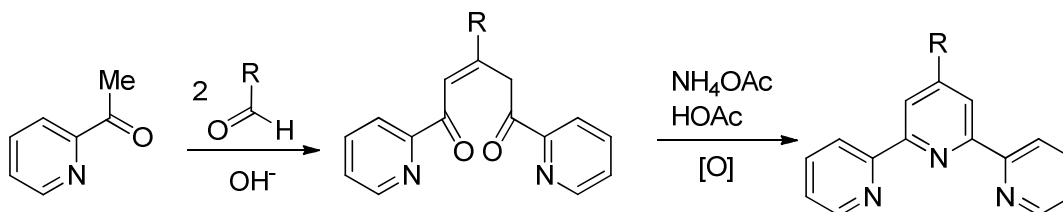
Scheme 2.1. The ring-coupling procedure for the synthesis of tpy.
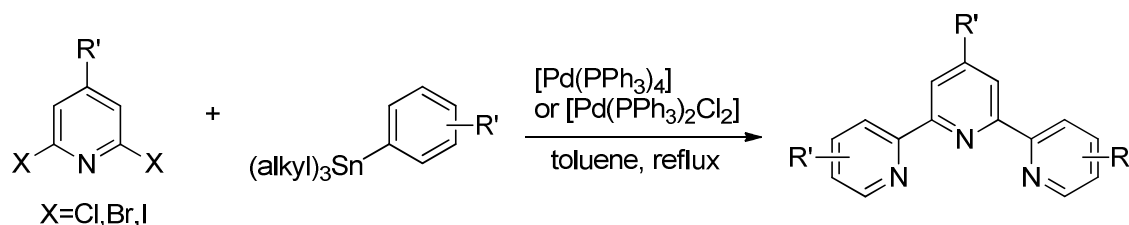
Scheme 2.2. The cross-coupling procedure for the synthesis of tpy, R – alkyl or aryl.

The coupling reaction can also be used to prepare "back-to-back" ditopic terpyridine ligands,[97-100] some examples are shown in **Scheme 2.3**. A range of 2,5-diethynyl-3,4-dibutylthiophene-bridged "back-to-back" terpyridine ligands have been prepared by the Ziessel group.[101]
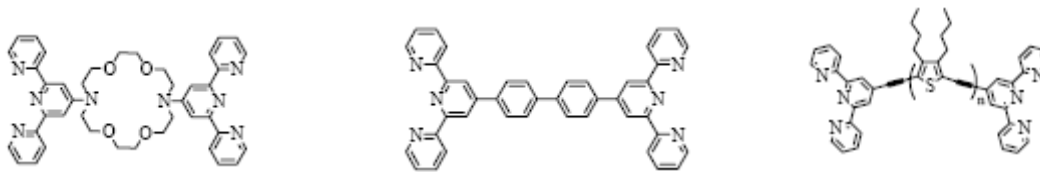
Scheme 2.3. "Back-to-back" ditopic tpy ligands.[97-101]

In this chapter the syntheses of several new ditopic ligands (**L1-L4**, **L6-L7**) based on a benzene unit connected to two 4'-substituted-2,2':6',2"-terpyridine moieties through polyethyleneoxy spacers are discussed. The variability of this group of compounds was achieved by using different length ethyleneoxy chains and changing the substitution position on the benzene unit (**Scheme 2.4**).

L1 n = 1
L2 n = 5
L3 n = 2

L4

L6

L7
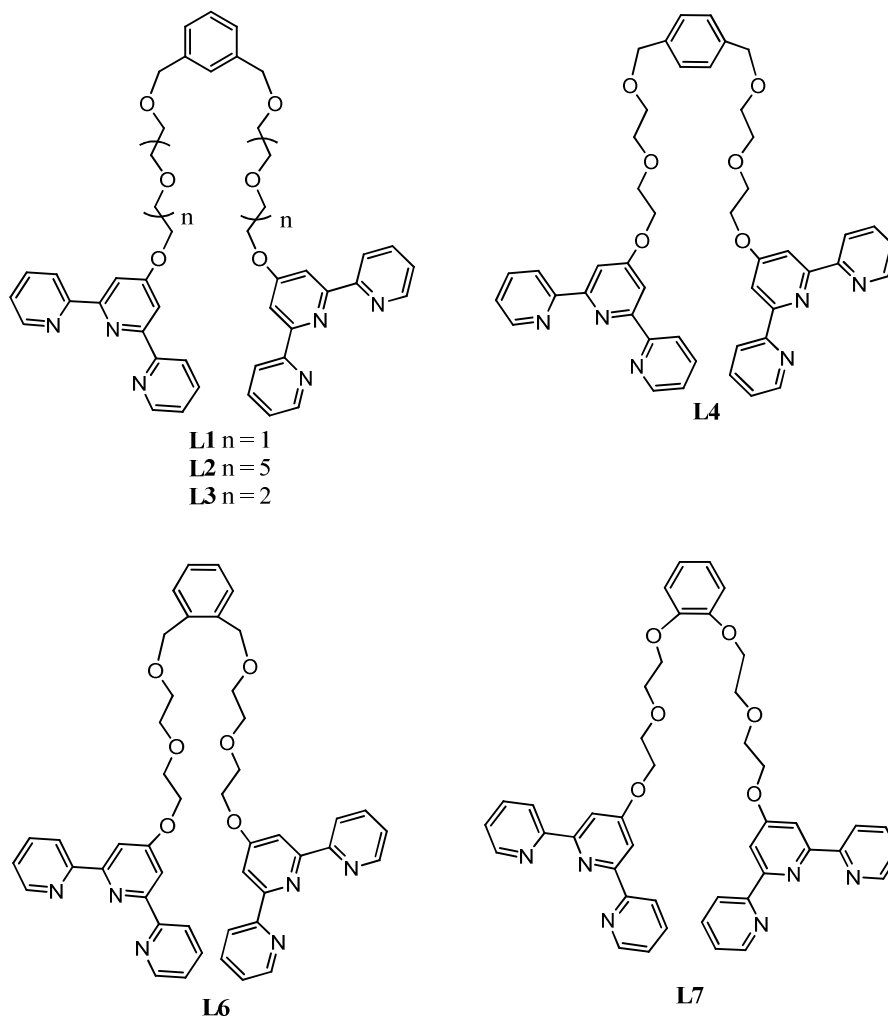
Scheme 2.4. Ditopic ligands **L1-L4**, **L6-L7.**

2.2 Synthesis

All of the ligands were prepared in two steps by nucleophilic substitution reactions. For ligands **L1-L4** and **L6**, firstly the appropriate benzene functionalized with two ethylene glycol chains was obtained (**L1a-L4a, L6a**) by nucleophilic substitution of the dibromobenzene derivative (**Schemes 2.6, 2.8, 2.10**). In the second step a nucleophile was generated by deprotonation of the terminal hydroxyl groups, this was then reacted further with Cl-tpy (**Schemes 2.7, 2.8, 2.11**). **L7** was synthesized by two nucleophilic substitution reactions. In both steps deprotonated hydroxyl groups were reacted with electrophilic halogenated reagents.

4'- Chloro-2,2':6',2"-terpyridine (Cl-tpy) was prepared as previously reported in the literature[102] (**Scheme 2.5**).
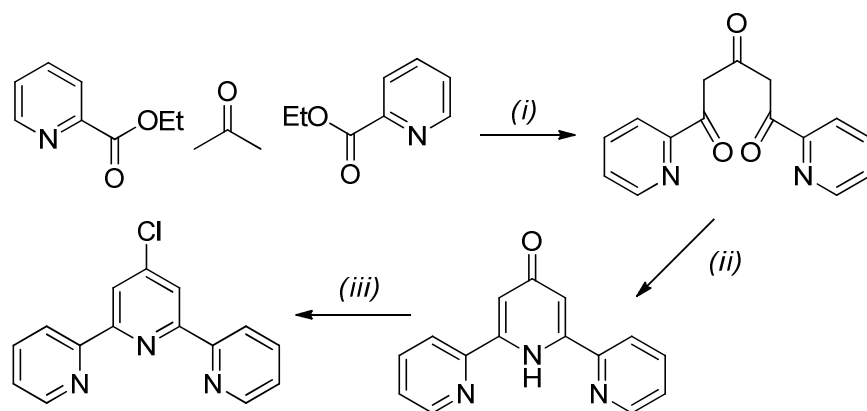
Scheme 2.5. Synthesis of Cl-tpy[102] : *(i)* NaH, MeOCH$_2$CH$_2$OMe; *(ii)* [NH$_4$][O$_2$CMe], EtOH; *(iii)* PCl$_5$, POCl$_3$.

The syntheses of the ditopic 4'-substituted-2,2':6',2"-terpyridine based ligands (**L1-L4, L6-L7**) are described below. The syntheses of three intermediate products: 2,2'-(((((1,3-phenylenebis(methylene))bis(oxy))bis(ethane-2,1-diyl))bis(oxy))diethanol (**L1a**), 1,1'-(1,3-phenylene)bis(2,5,8,11,14,17-hexaoxanonadecan-19-ol) (**L2a**) and 2,2'-((((((1,3-phenylenebis(methylene))bis(oxy))bis(ethane-2,1-diyl))bis(oxy))bis(ethane-2,1-diyl))bis(oxy))diethanol (**L3a**) are shown in **Scheme 2.6**.
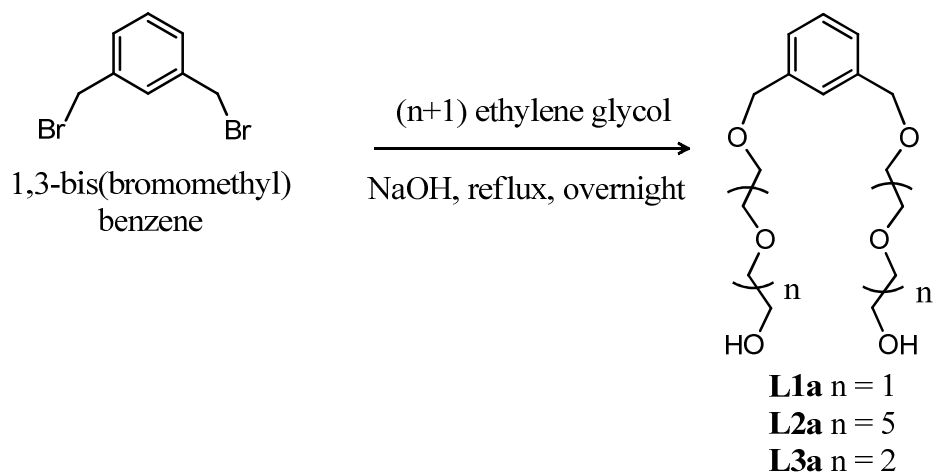
Scheme 2.6. Syntheses of **L1a-L3a**.

L1a-L3a were prepared from 1,3-bis(bromomethyl)benzene, which was heated under reflux in the appropriate (n+1)ethylene glycol with sodium hydroxide overnight.

In the next step, after deprotonation of two terminal hydroxyl groups with KOH in hot DMSO, intermediate product (**L1a/L2a/L3a**) was reacted further with Cl-tpy. After three days the desired products were obtained in 55-70% yield after work up.
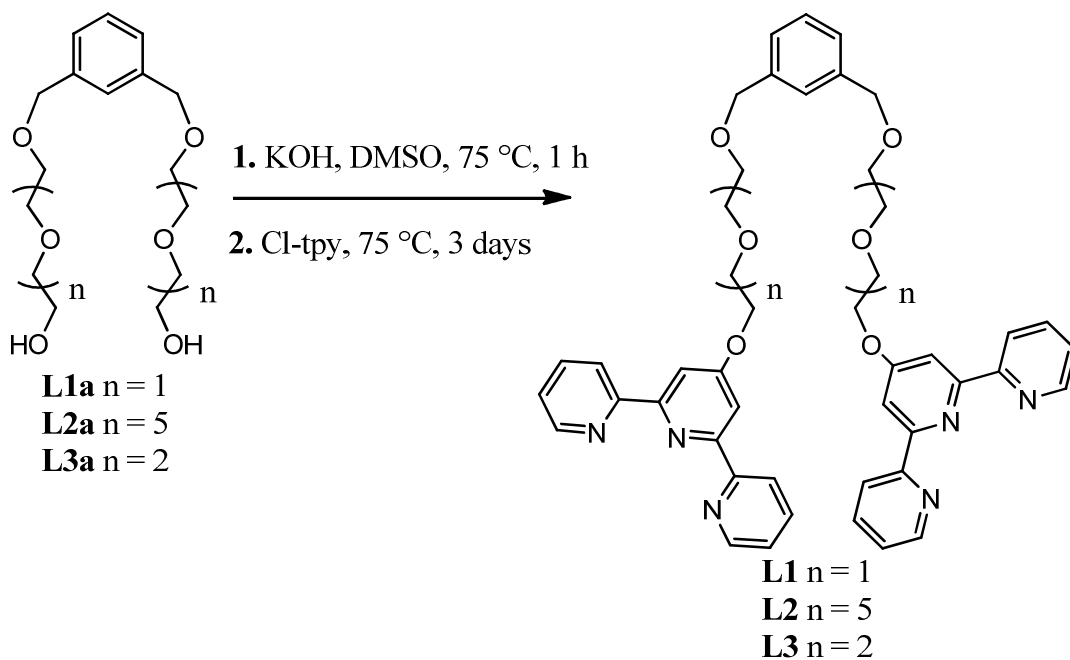
Scheme 2.7. Syntheses of **L1-L3**.
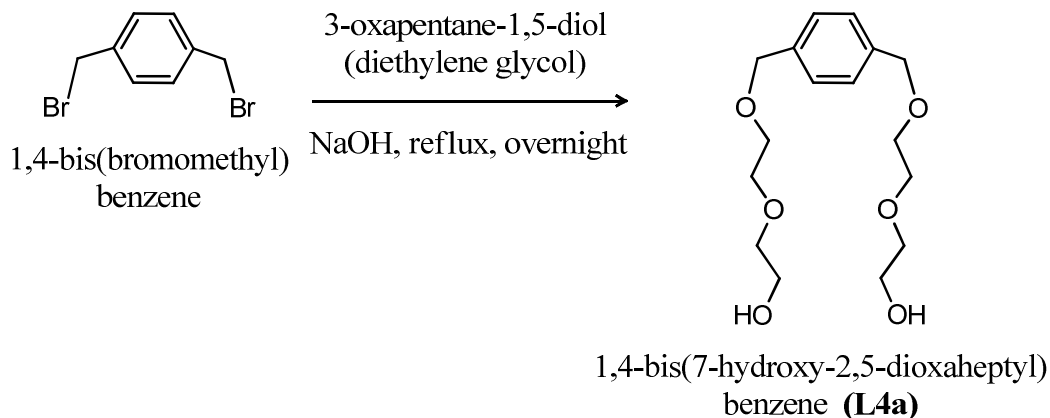
Scheme 2.8. Synthesis of **L4a**.

L4a was prepared from 1,4-bis(bromomethyl)benzene, under reflux, overnight. The hydroxyl groups of 2,2'-oxydiethanol (diethylene glycol) were deprotonated with sodium hydroxide. Diethylene glycol was playing in this reaction a double role: as a reagent and as the solvent (**Scheme 2.8**). **L4a** was then reacted as described above for **L1a-L3a** (**Scheme 2.9**), yielding 68% of a yellow powder after work up. Other tpy containing products were not isolated.
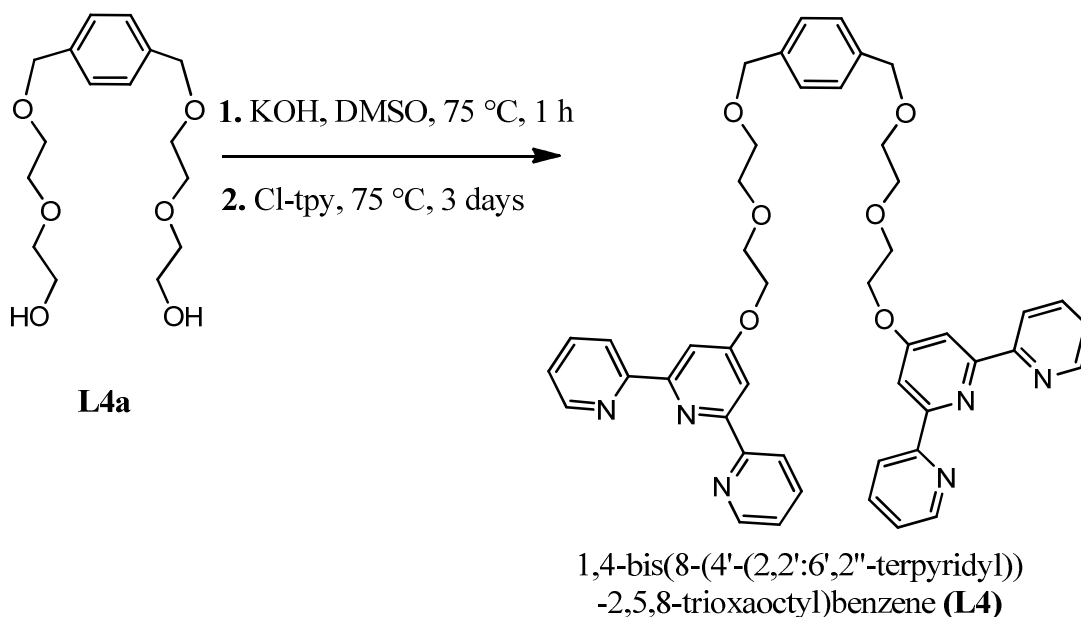
Scheme 2.9. Synthesis of **L4**.
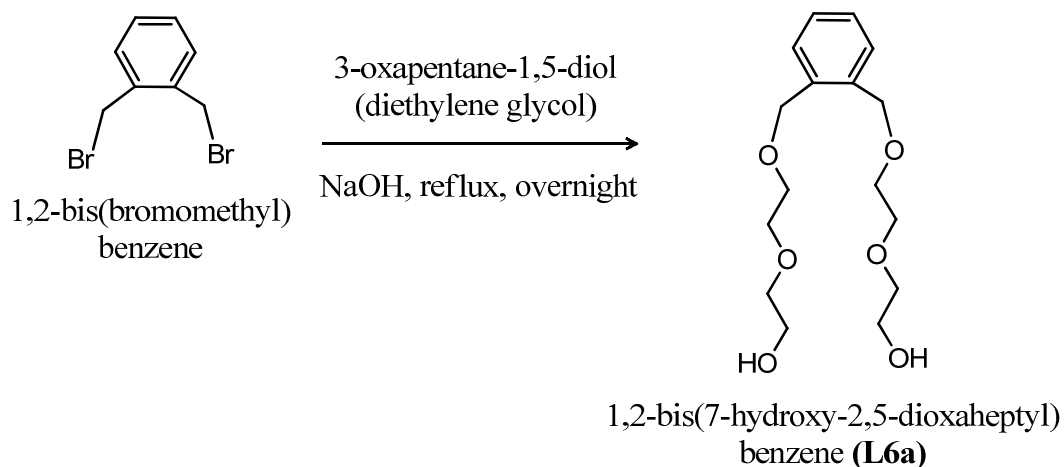
Scheme 2.10. Synthesis of **L6a**.

In the synthesis of **L6a**, 1,2-bis(bromomethyl)benzene (*o*-xylylene dibromide) was mixed with deprotonated diethylene glycol overnight (**Scheme 2.10**). The intermediate was then reacted with Cl-tpy, followed by purification by column chromatography on alumina with CHCl$_3$ resulting in 65% of **L6**, as a yellow oil (**Scheme 2.11**).
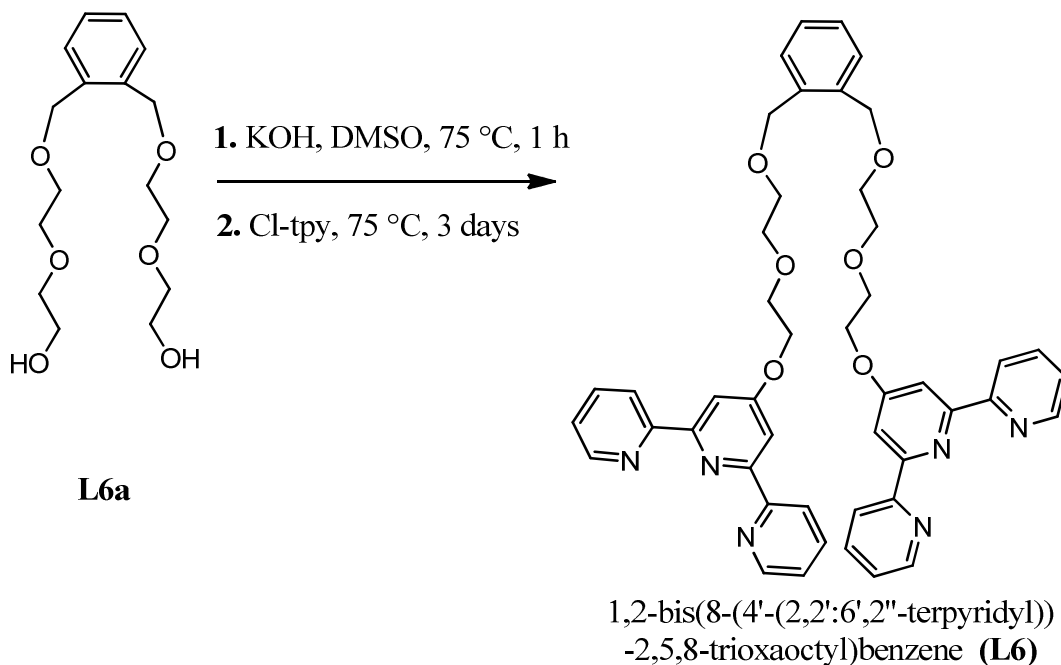
Scheme 2.11. Synthesis of **L6**.
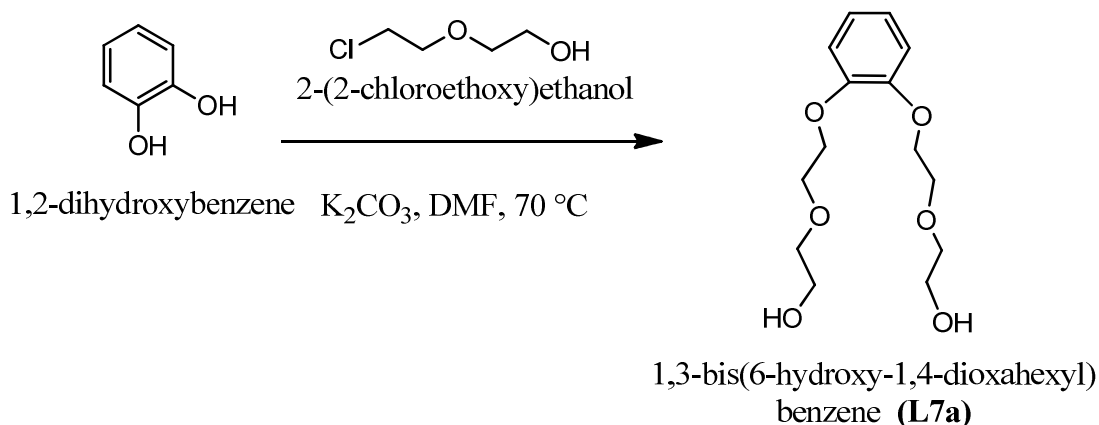
Scheme 2.12. Synthesis of **L7a**.

The synthesis of **L7a** required a different strategy than preparations of the previous intermediate products, **L1a-L4a** and **L6a**. Both of the hydroxyl groups of the 1,2-dihydroxybenzene were deprotonated with potassium carbonate and 2-(2-chloroethoxy)ethanol was added to the reaction mixture (**Scheme 2.12**). **L7a** was reacted further as described previously with Cl-tpy in DMSO. After column chromatography (Al$_2$O$_3$, CHCl$_3$), **L7** in 63% yield was obtained as a yellow powder. Other tpy containing products were not isolated.
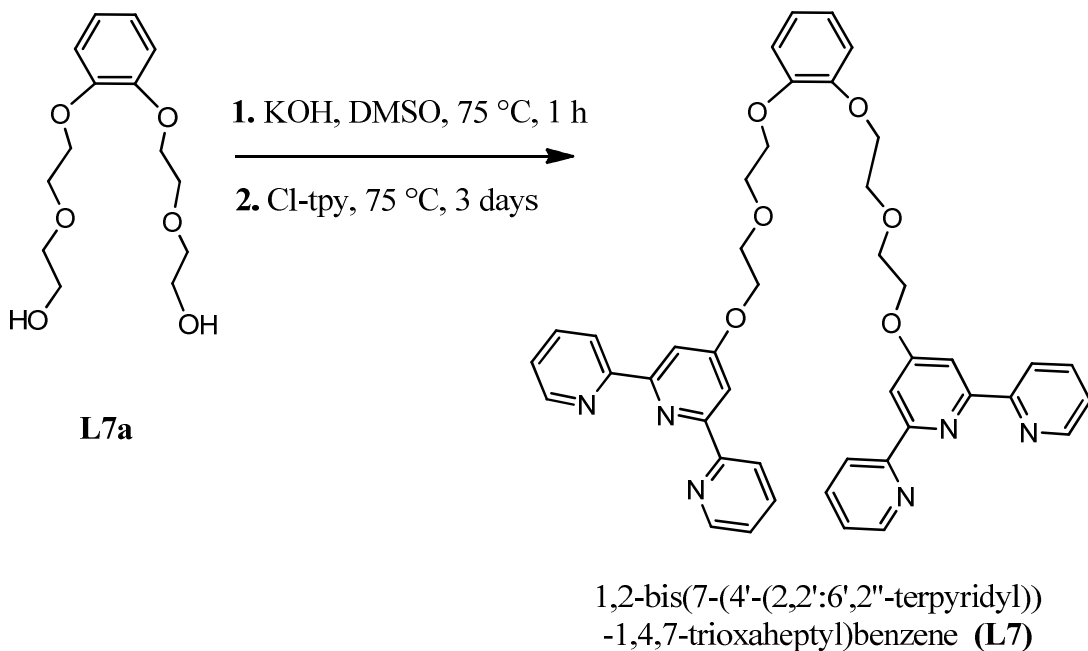
Scheme 2.13. Synthesis of **L7**.

2.3 ^{1}H NMR spectroscopy

All of the intermediate products **L1a-L4a, L6a-L7a** (**Scheme 2.14**) and the ligands **L1-L4, L6-L7** (**Scheme 2.15**) were characterized by ^{1}H NMR spectroscopy in CDCl$_3$. The ^{1}H NMR spectra of intermediates **L1a-L4a, L6a-L7a** compare well with those of similar crown ether systems[8-10] and they are almost identical with each other (**Table 2.1**).
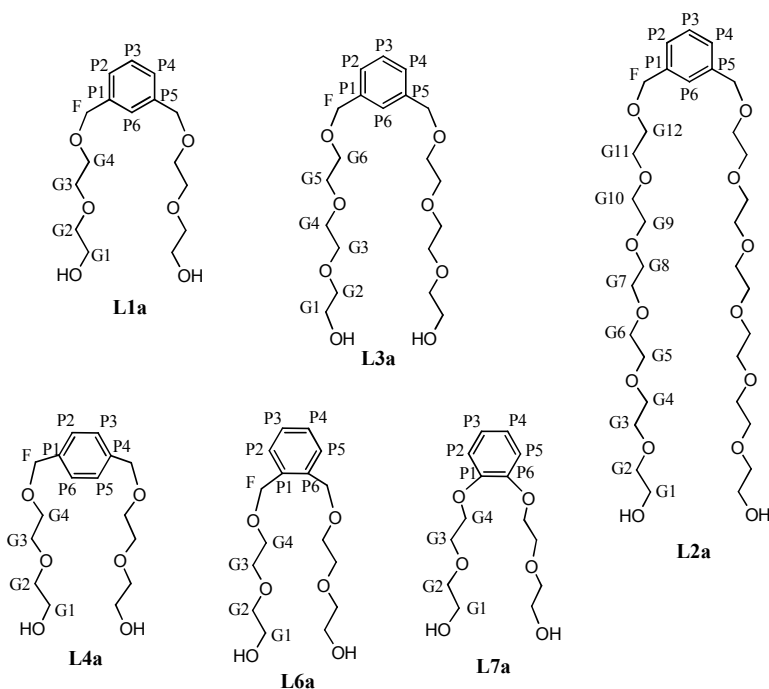
Scheme 2.14. Labeling for **L1a-L4a, L6a-L7a** intermediates.

The **H^P** protons from compound **L1a-L3a** and **L7a** appear in the ^{1}H NMR spectrum as a multiplet. Only the **H^P** proton from **L6a** shows a different multiplicity (singlet), due to the higher symmetry of the compound. All of the signals corresponding to the ethylene glycol chain **H$^{G1-G4/G6/G12}$** can be found, as expected in the aliphatic region 3.55-3.80 ppm. The signal around 4.55 ppm is assigned to **H^F** from the -CH$_2$- bridge connecting the benzene ring to the ethylene glycol chain.

L	$H^{G2-G4/G6/G12}$	H^{G1}	H^F	H^{OH}	H^P
L1a	3.59–3.76 (m)	3.57 (m)	4.56 (s)	3.34 (br)	7.18-7.39 (m)
L2a	3.60–3.77 (m)	3.55 (m)	4.55 (s)	3.32 (br)	7.18-7.40 (m)
L3a	3.55–3.75 (m)	3.59 (m)	4.57 (s)	3.36 (br)	7.20-7.40 (m)
L4a	3.59–3.77 (m)	3.57 (m)	4.57 (s)	3.36 (br)	7.32 (s)
L6a	3.59–3.76 (m)	3.55 (m)	4.58 (s)	3.35 (br)	7.18-7.39 (m)
L7a	3.60–3.80 (m)	3.58 (m)		3.34 (br)	7.18-7.39 (m)

Table 2.1. ^{1}H NMR spectroscopic data, δ_H [ppm], (400 MHz, 295 K, CDCl$_3$) for **L1a-L4a**, **L6a-L7a** (see page 38 for scheme of labeling).

Ditopic intermediates **L1a-L4a, L6a-L7a** were considered as closely related to crown ethers (especially benzo-crown ethers); for this reason all of the spectroscopic data were compared with the literature and gave very good agreement with these.[103-105] **L1a** intermediate has been already discibed in literature[103] and its ^{1}H NMR spectrum matched that reported.

Upon substitution of the free hydroxyl groups on the ethylene glycol chain with chloro-tpy a lot of changes in chemical shifts can be observed. **Table 2.2** shows chemical shifts for the protons on ethylene glycol chains $\mathbf{H}^{\mathbf{G1\text{-}G4/G6/G12}}$ and the -CH$_2$-bridge $\mathbf{H}^{\mathbf{F}}$. The aromatic protons from tpy and the phenyl spacer are shown in **Table 2.3**.
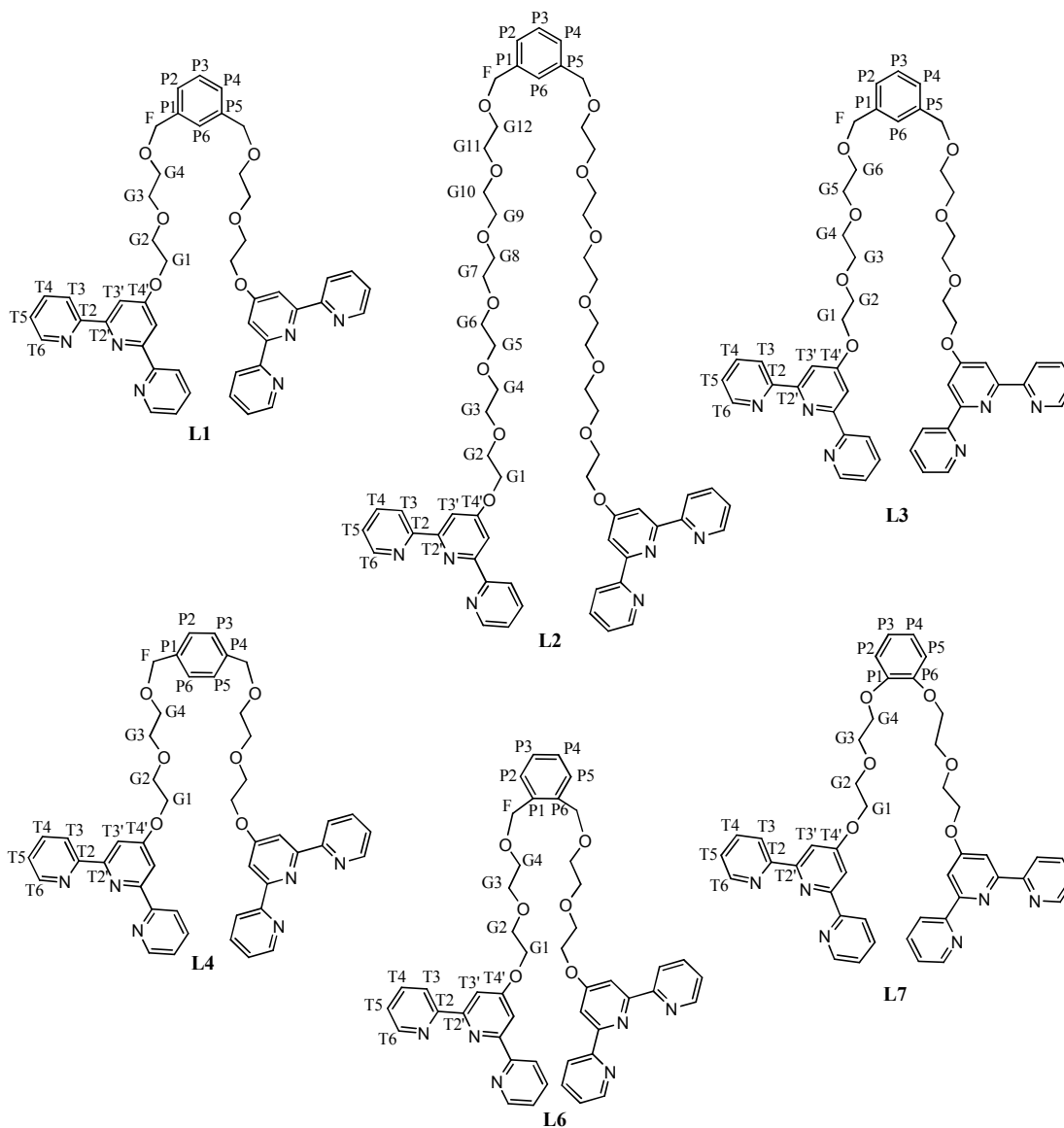
Scheme 2.15. Labeling for **L1-L4, L6-L7** ligands.

40

L	$H^{G4/-G6/-G12}$	H^{G3}	H^{G2}	H^{G1}	H^F
L1	3.63 (m)	3.75 (m)	3.91 (m)	4.37 (m)	4.54 (s)
L2	3.50-3.65 (m)	3.69 (m)	3.86 (m)	4.32 (m)	4.47 (s)
L3	3.45-3.75 (m)	3.45-3.75 (m)	3.87 (m)	4.34 (m)	4.49 (s)
L4	3.62 (t) J 5.0 Hz	3.73 (t) J 5.0 Hz	3.91 (t) J 5.0 Hz	4.38 (t) J 5.0 Hz	4.53 (s)
L6	3.27 (m)	3.34 (m)	3.48 (m)	3.94 (m)	4.26 (s)
L7	4.17 (m)	3.92 (m)	3.96 (m)	4.34 (m)	—

Table 2.2. ^{1}H NMR spectroscopic shift data, δ_H [ppm], (500 MHz, 295 K, CDCl$_3$) for **L1-L2, L4, L6-L7**. As an exception **L3** was measured at 400 MHz, 295 K, CDCl$_3$.

L	H^{T5}/H^P	H^{T4}	$H^{T3'}$	H^{T3}	H^{T6}
L1	7.27-7.31 (m)/ 7.21-7.27(m), 7.27-7.31 (m)	7.81 (td) J 1.5, 7.8 Hz	8.02 (s)	8.58 (d) J 8.0 Hz	8.65 (d) J 4.1 Hz
L2	7.15-7.30 (m)/ 7.15-7.30 (m)	7.76 (t) J 7.7 Hz	7.98 (s)	8.54 (d) J 8.0 Hz	8.61 (d) J 4.2 Hz
L3	7.15-7.30 (m)/ 7.15-7.30 (m)	7.79 (td) J 1.7, 7.8 Hz	7.99 (s)	8.55 (d) J 8.0 Hz	8.62 (d) J 3.9 Hz
L4	7.30 (m)/ 7.29 (s)	7.81 (td) J 1.8, 7.7 Hz	8.02 (s)	8.58 (d) J 8.0 Hz	8.66 (d) J 4.7 Hz
L6	6.92 (m)/ 6.88 (m), 7.01 (m)	7.44 (t) J 7.6 Hz	7.65 (s)	8.20 (d) J 8.0 Hz	8.28 (d) J 3.9 Hz
L7	7.25 (m)/ 6.84-6.88 (m), 6.88-6.92 (m)	7.77 (td) J 1.6, 7.8 Hz	7.99 (s)	8.54 (d) J 7.9 Hz	8.62 (d) J 4.7 Hz

Table 2.3. ^{1}H NMR spectroscopic shift data, δ_H [ppm], (500 MHz, 295 K, CDCl$_3$) for **L1-L2, L4, L6-L7**. As an exception **L3** was measured at 400 MHz, 295 K, CDCl$_3$.
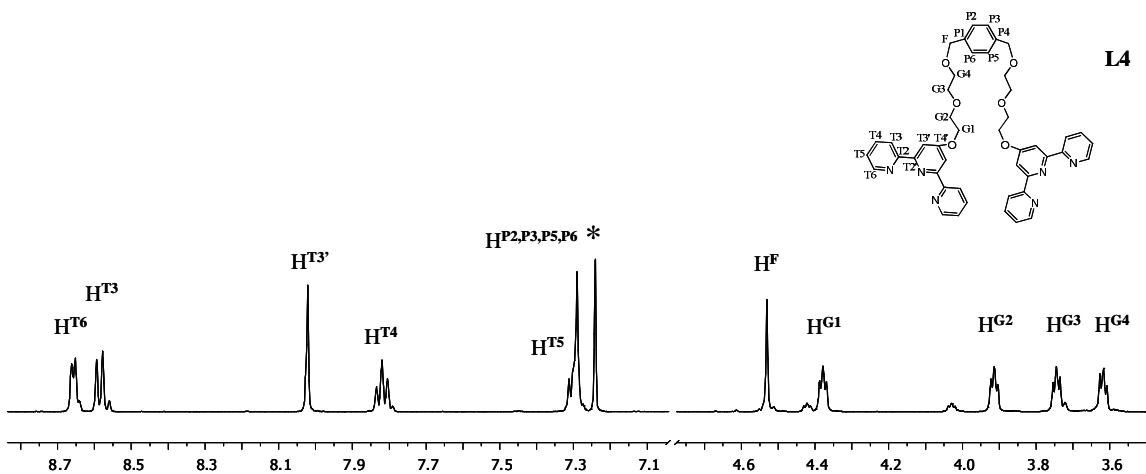
Figure 2.1. ^{1}H NMR spectrum (500 MHz, 295 K) of **L4** in CDCl$_3$. The signal marked with * is the signal for CHCl$_3$.

The ^{1}H NMR spectrum of ligand **L4** shows six signals in the aromatic region: five signals for the protons on tpy: **H^{T5}, H^{T3}, H$^{T3'}$, H^{T4}, H^{T5}** and the sixth signal comes from the protons on the phenyl spacer. Due to the symmetrical substitution on the benzene ring all of the phenyl protons are equivalent and give rise to a singlet (**Figure 2.1**).
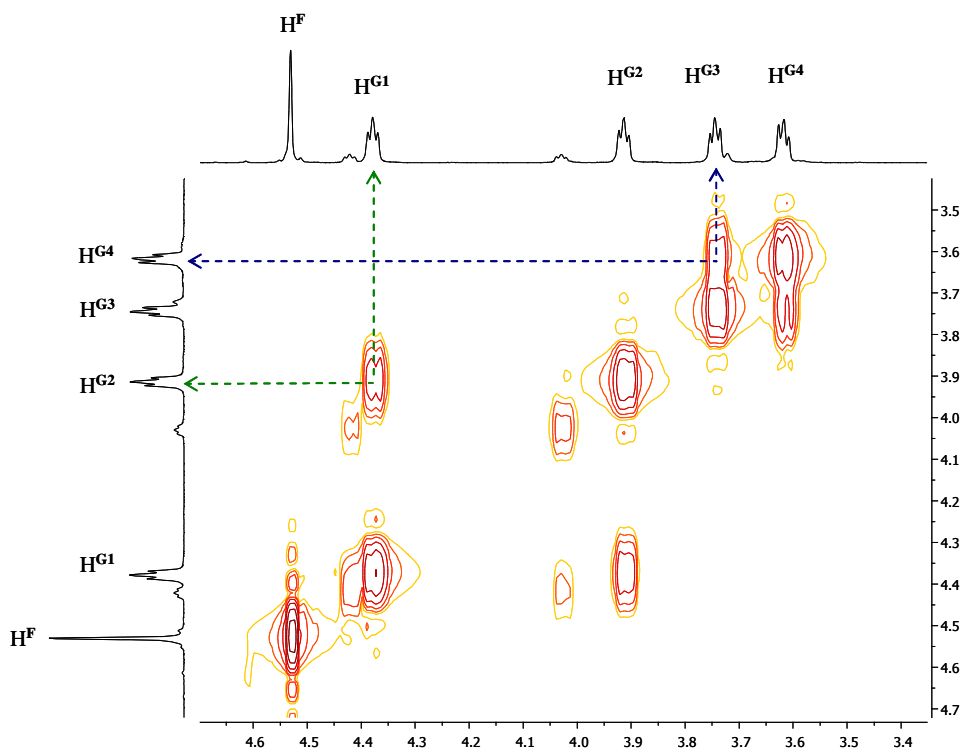
Figure 2.2. Aliphatic region of the ^{1}H-^{1}H COSY spectrum (500 MHz, 295 K) of **L4** in CDCl$_3$.

42

In the aliphatic region, in the NMR spectrum of ligand **L4,** there is one singlet for the H^F proton and four well separated triplets from the H^G protons on the diethylene glycol chains. The signal for H^{G1} is the strongest shifted downfield due to its close proximity to the tpy unit. The assignment of the H^{G1}, H^{G2}, H^{G3} and H^{G4} protons of the **L4** ligand was made using the COSY technique (**Figure 2.2**). The signal for H^{G1} gives a COSY cross peak to the signal H^{G2} at δ 3.91 ppm (**Figure 2.2**). The signal for H^{G3} gives a COSY cross peak to the signal at δ 3.62 ppm, and this signal is assigned to H^{G4} (**Figure 2.2**).
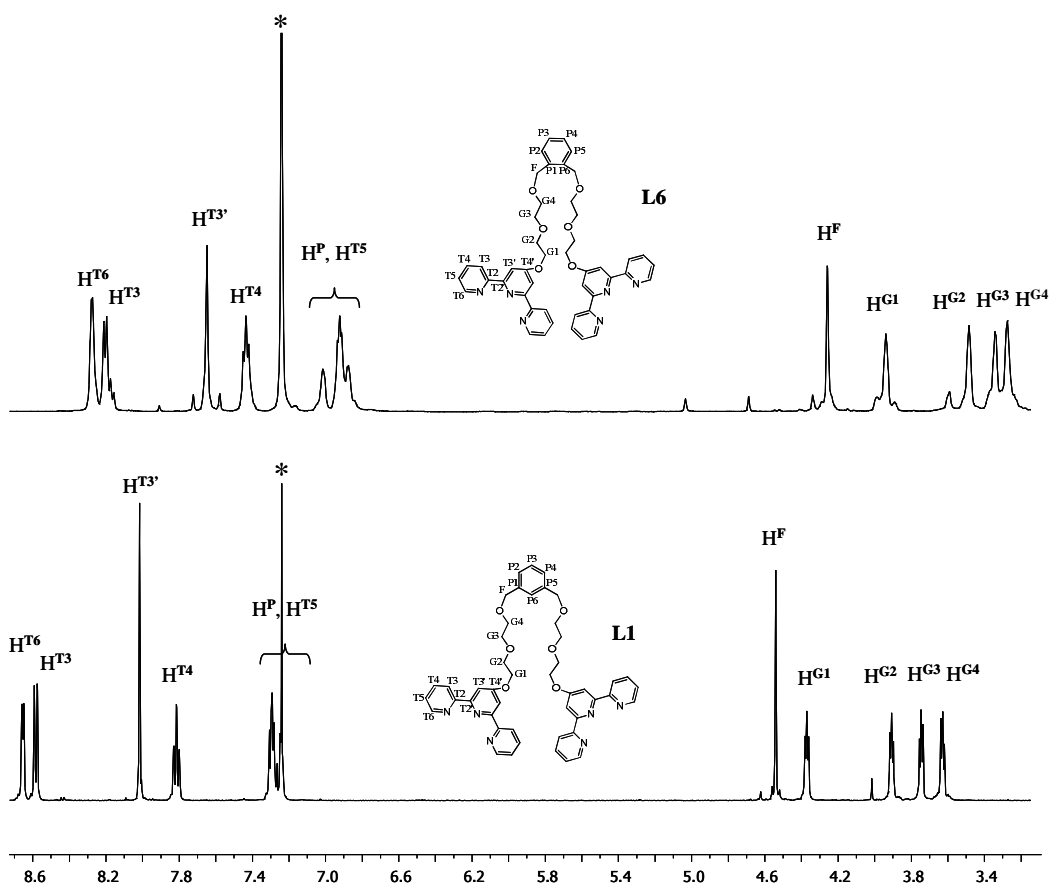
Figure 2.3. ^{1}H NMR spectra (500 MHz, 295 K) of **L6** (above) and **L1** (below) in CDCl$_3$. The signal marked with * is the signal for CHCl$_3$. Spectrum exhibits some residues of the starting material, which could not be removed by column chromatography or other purification methods.

In **Figure 2.3** the ^{1}H NMR spectra of ligands **L6** and **L1** are compared. Both spectra have the usual features of this group of terpyridine ligands and are almost identical to each

other, but the signals for protons of **L6** are all shifted upfield. The reason for these changes in the NMR spectrum is most probably the *ortho-* substitution on the benzene ring in ligand **L6**.
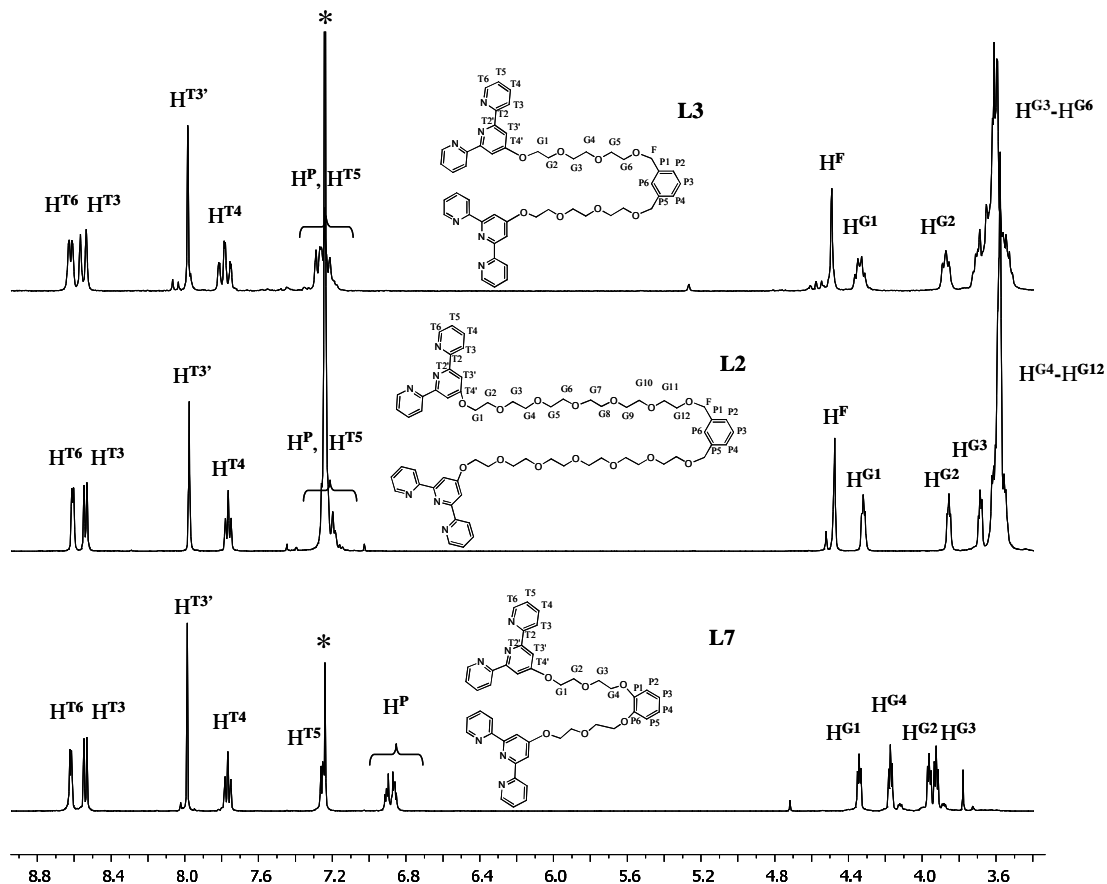
Figure 2.4. ^{1}H NMR spectra (500 MHz, 295 K, for **L3** 400 MHz, 295 K) of **L3** (above), **L2** (middle) and **L7** (below) in CDCl$_3$. The signal marked with * is the signal for CHCl$_3$.

The ligands **L2** and **L3** have the longest glycol spacers with six and three -CH$_2$-CH$_2$- groups respectively. Most of the protons **H^G** from the ethylene glycol chains of ligand **L2** and ligand **L3** overlap on the ^{1}H NMR spectrum and can be found together as one multiplet between δ 3.40-3.80 ppm. The signal at δ 4.47 ppm, for ligand **L2** and at δ 4.49 ppm, for ligand **L3** is assigned to proton **H^F.** There are six signals excluding the signal for CHCl$_3$, in the aromatic region for both ligands **L2** and **L3**: **H^{T6}**, **H^{T3}**, **H$^{T3'}$**, **H^{T4}**, **H^P** and **H^{T5}** are overlapping.

The ^{1}H NMR spectrum of ligand **L7** looks very different from those discussed above (**Figure 2.4**). Ligand **L7** has two flexible glycol chains directly attached to the benzene ring through the oxygen, unlike ligands **L1-L4**, **L6**, in which the glycols are attached through a -CH$_2$- bridge. This does not affect any of the protons on the terpyridine: H^{T6}, H^{T3}, $H^{T3'}$, H^{T4}, H^{T5} of ligand **L7**, but has a strong influence on the H^P protons on the phenyl ring. From the NOESY spectrum (**Figure 2.5**), the two multiplets at δ 6.84-6.88 and 6.88-6.92 ppm can be assigned to $H^{P3/P4}$ and $H^{P2/P5}$. Both signals, from protons $H^{P3/P4}$ and $H^{P2/P5}$, give cross peaks to the signal for H^{G4} at δ 4.17 ppm, which is the closest glycol proton to the benzene ring. Due to the *ortho-* substitution on the benzene ring proton H^{P3} is equivalent to proton H^{P4}, and proton H^{P2} to H^{P5}.
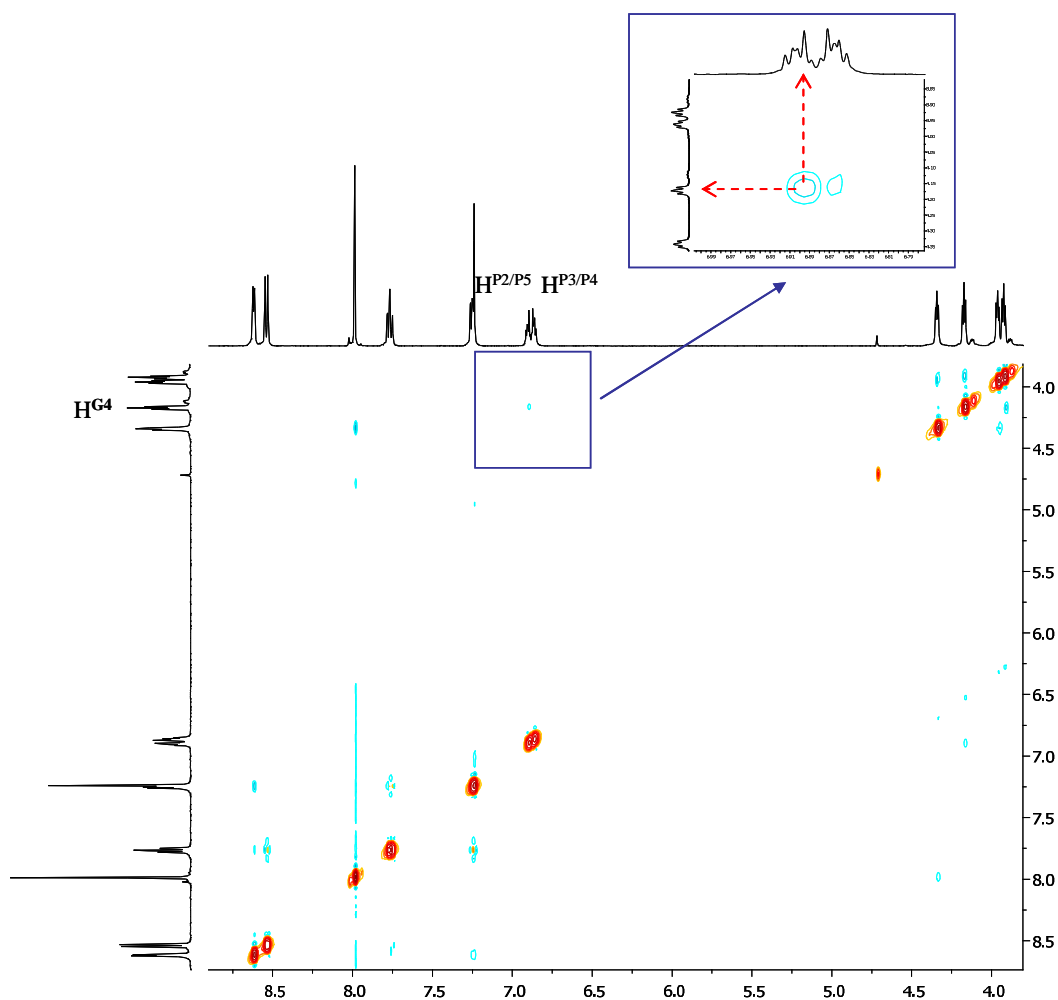
Figure 2.5. NOESY spectrum (500 MHz, 295 K) of **L7** in CDCl$_3$.

From the ^{1}H-^{1}H COSY spectrum, all of the protons in the aliphatic region can be assigned. As in the other ligands **L1-L4** and **L6**, proton **H^{G1}** of the glycol chains of ligand **L7** is most shifted downfield, influenced by the tpy substituent. Proton **H^{G1}** gives a COSY cross peak to the signal for **H^{G2}** at δ 3.96 ppm. The signals for **H^{G3}** and **H^{G4}** couple with each other giving a cross peak in the COSY spectrum. In comparison with the ligands **L1-L4** and **L6**, the signals for both **H^{G3}** and **H^{G4}** are downfield shifted, which is an effect of the phenyl ring and the lack of the -CH$_2$- bridge.
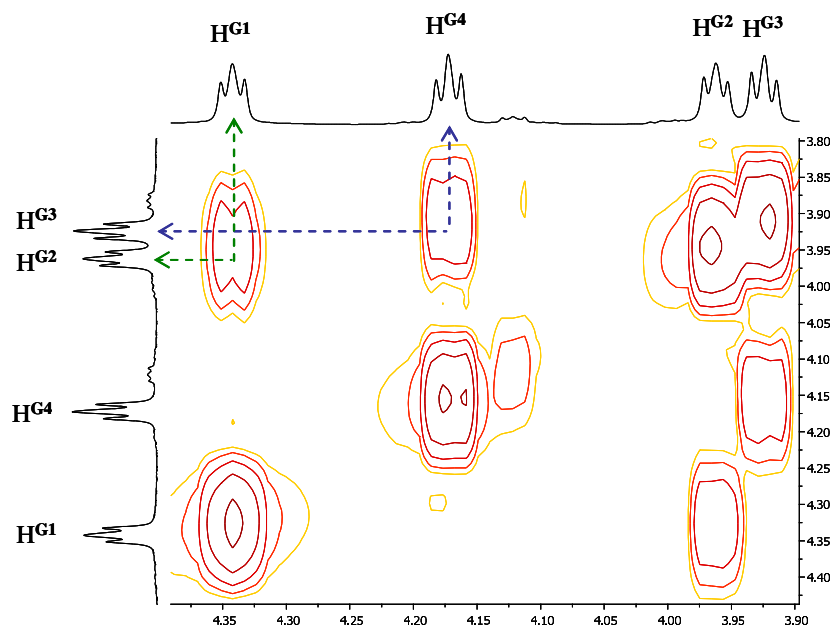
Figure 2.6. Part of the COSY spectrum (500 MHz, 295 K) of **L7** in CDCl$_3$ showing the aliphatic region. Spectrum exhibits some residues of the starting material, which could not be removed by column chromatography or other purification methods.

2.4 ^{13}C NMR spectroscopy

Table 2.4 shows the ethylene glycol **C^G**, **C^F** and phenyl **C^P** carbon signals for **L1-L4** and **L6-L7** in CDCl$_3$ solution. All of the terpyridine carbon signals are shown in the **Table 2.5**. The assignments were made using HMQC and HMBC techniques.

46

L	C^{G1}	C^{G2}	C^{G3}	$C^{G4}/$ C^{G5-G12}	C^F	$C^P/$ $^{(\#)}C^P$ (quaternary)
L1	68.0	69.8	71.2	69.7	73.4	127.2 127.3 128.7 $^{(\#)}$138.6
L2	67.8	69.5	71.0	69.4/ 70.6 70.6 70.7	73.2	127.0 127.1 $^{(\#)}$138.4
L4	67.7	69.7	71.2	68.0	73.3	128.0 $^{(\#)}$137.7
L6	67. 0	68.5	70.1	68.9	70.0	126.9 127.9 $^{(\#)}$135.7
L7	68.0	69.8	70.3	69.2	—	115.2 121.9 $^{(\#)}$149.2

Table 2.4. ^{13}C NMR spectroscopic shift data, δ_C [ppm], (125 MHz, 295 K, CDCl$_3$) for **L1-L2, L4, L6-L7** (see page 40 for scheme of labeling).

L	$C^{T3'}$	C^{T3}	C^{T5}	C^{T4}	C^{T6}	C^{T2}	$C^{T2'}$	$C^{T4'}$
L1	107.7	121.5	124.0	136.9	149.2	156.3	157.3	167.2
L2	107.5	121.3	123.9	136.8	149.1	156.0	157.1	167.0
L4	107.6	121.5	124.0	137.00	149.2	156.3	157.3	167.1
L6	106.5	120.5	123.3	136.1	148.3	155.0	156.2	166.1
L7	107.6	121.4	123.9	136.8	149.2	156.1	157.2	167.1

Table 2.5. ^{13}C NMR spectroscopic shift data, δ_C [ppm], (125 MHz, 295 K, CDCl$_3$) for **L1-L2, L4, L6-L7** (see page 40 for scheme of labeling).
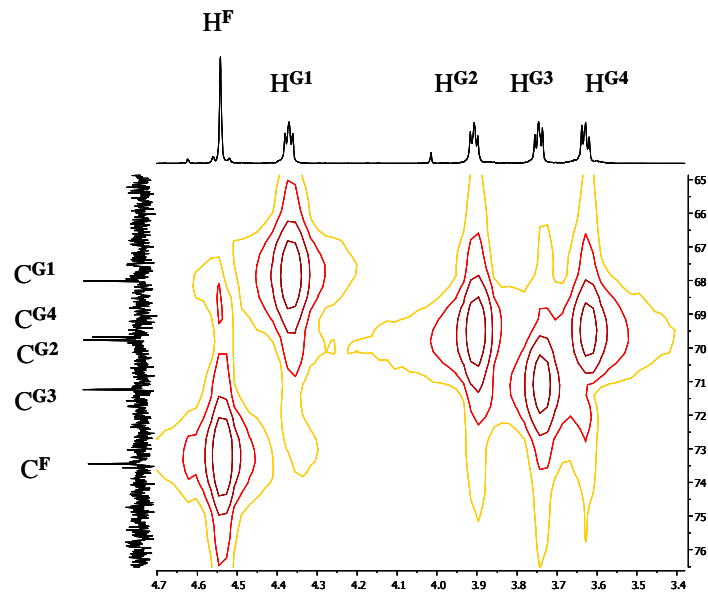
Figure. 2.7. Part of the HMQC spectrum (500 MHz, 295 K) of **L1** in CDCl$_3$.

In the **Figure 2.7** the cross peaks of the aliphatic protons of the ligand **L1** : **H**$^{\text{G1-4}}$ and **H**$^{\text{F}}$ to the direct carbons signal are shown. The signals could be easily assigned using the HMQC spectrum. The HMBC spectrum (**Figure 2.8**) exhibits the expected cross-peaks consistent with the proposed molecular structure. The signal for **H**$^{\text{G3}}$ is coupling with the signals for carbon **C**$^{\text{G2}}$ and **C**$^{\text{G4}}$ and the for **H**$^{\text{G4}}$ is coupling with the signals for carbon **C**$^{\text{G3}}$ and **C**$^{\text{F}}$.
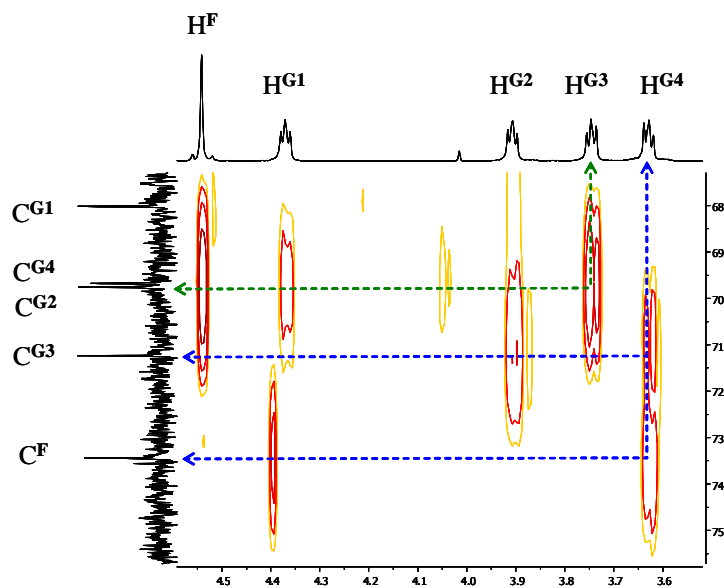
Figure. 2.8. Part of the HMBC spectrum (500 MHz, 295 K) of **L1** in CDCl$_3$.
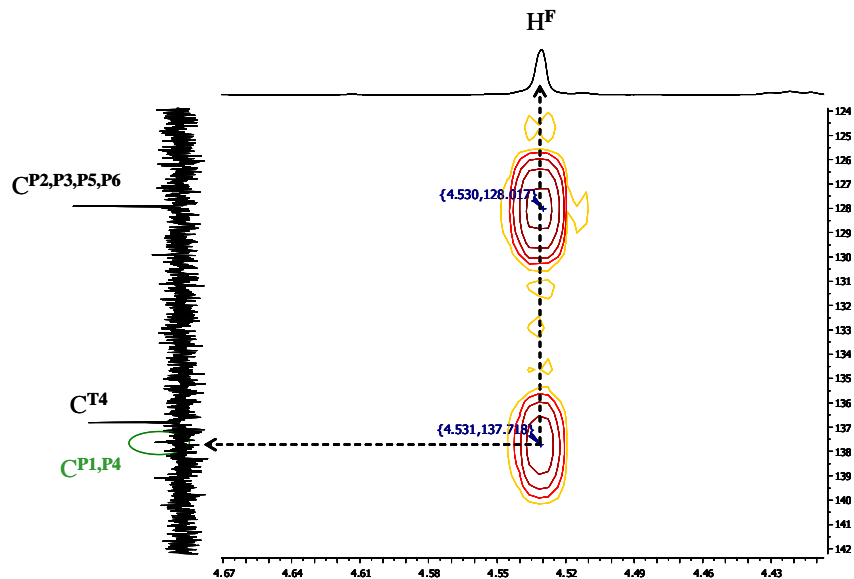
Figure 2.9. Part of the HMBC spectrum (500 MHz, 295 K) of **L4** in CDCl$_3$.

In the HMBC spectrum, the signal for the quaternary carbons $\mathbf{C^{P1,P4}}$ of ligand **L4** couples over two bonds to the $\mathbf{H^F}$ proton. Using this method, this small peak could be assigned (**Figure 2.9**). In **Figure 2.10** two carbon-proton cross peaks for $\mathbf{H^{P2,P3,P5,P6}}$ to $\mathbf{C^{P2,P3,P5,P6}}$ and $\mathbf{H^{T5}}$ to $\mathbf{C^{T5}}$ are shown.
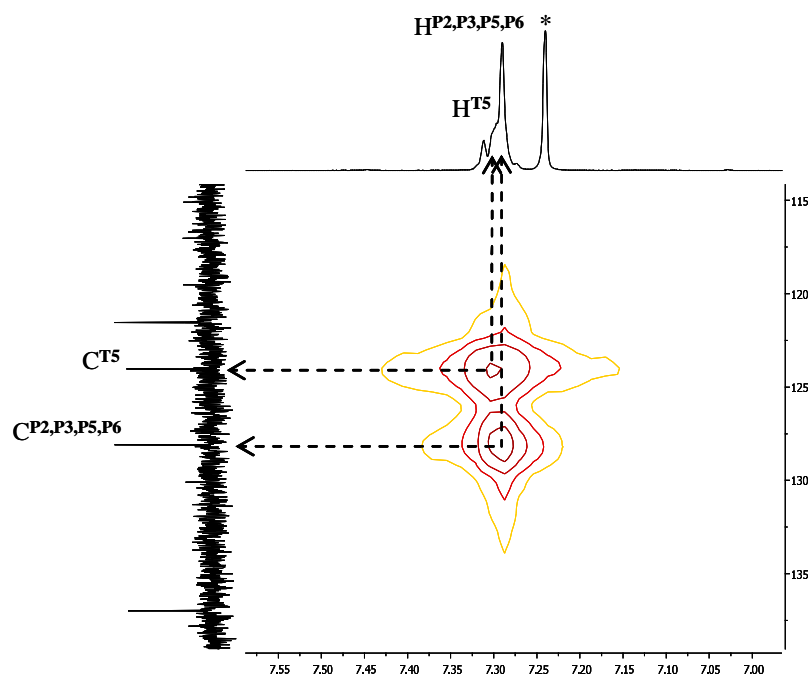
Figure 2.10. Part of the HMQC spectrum (500 MHz, 295 K) of **L4** in CDCl$_3$.
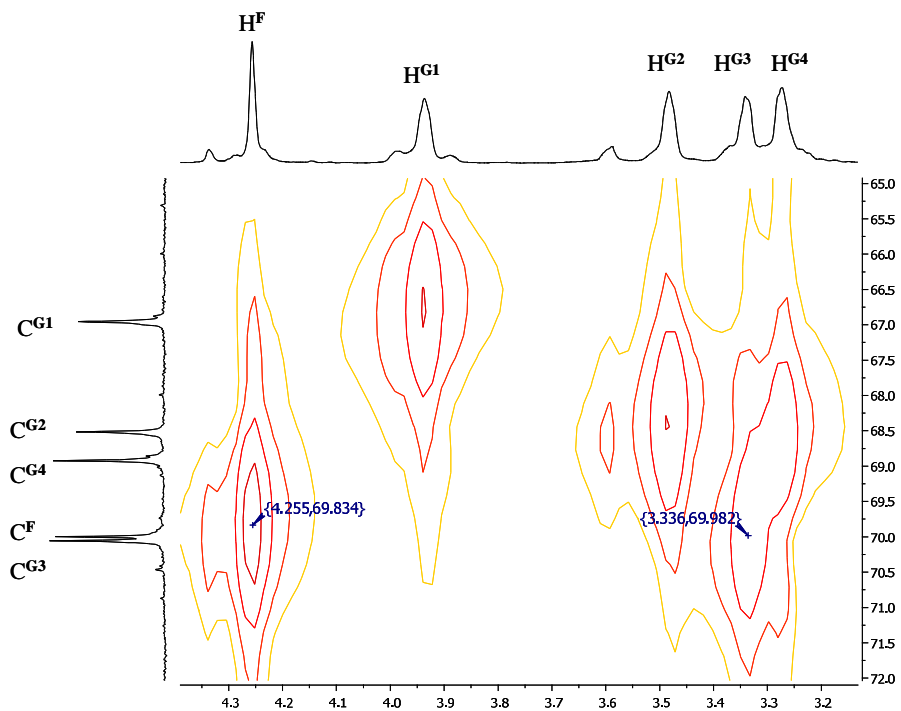
Figure 2.11. Part of the HMQC spectrum (500 MHz, 295 K) of **L6** in CDCl$_3$.
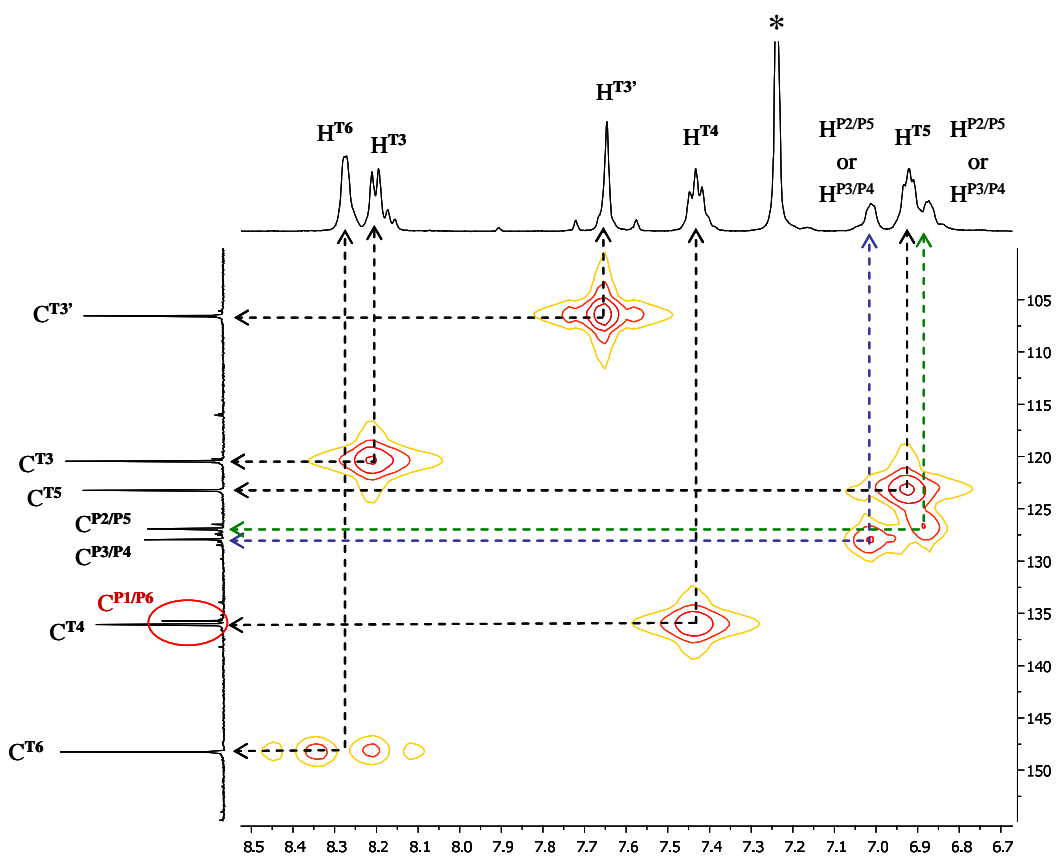
Figure 2.12. Part of the HMQC spectrum (500 MHz, 295 K) of **L6** in CDCl$_3$.

As already observed for the proton signals of ligand **L6** the carbon signals are also shifted upfield (**Table 2.4** and **2.5**). In the aliphatic region there are some additional changes in comparison to the other ligands. The carbon $\mathbf{C^F}$ is influenced very strongly and shifted upfield, to the frequency even lower than carbon $\mathbf{C^{G3}}$. The signal for $\mathbf{C^{G2}}$ carbon is shifted upfield more than one ppm and in contrast to the other ligands it is shifted to the lower energy than carbon $\mathbf{C^{G4}}$ (**Figure 2.11**). In **Figure 2.12** the assignments for the carbon signals for tpy and phenyl are shown. The missing signal for quaternary carbons $\mathbf{C^{P1,P6}}$ were observed next to the carbon $\mathbf{C^{T4}}$.

For the ligand **L7** only carbon signals for $\mathbf{C^{G3}}$ and $\mathbf{C^{G4}}$ protons are upfield shifted (**Table 2.4**). These are the carbons the closest to the phenyl ring and this is most probably an effect of the lack of the -CH$_2$- bridge. In the HMBC spectrum there is the cross peak for the proton $\mathbf{H^{G4}}$ to the carbon $\mathbf{C^{T5}}$, which suggests that signal for quaternary carbons $\mathbf{C^{P1,P6}}$ must be overlapping with signal for carbon $\mathbf{C^{T5}}$ (**Figure 2.13**). In the same figure one can observe that the proton $\mathbf{H^{G1}}$ couples over three bonds to carbon $\mathbf{C^{T4'}}$. Both carbon signals for phenyl protons $\mathbf{C^{P2/P5}}$ and $\mathbf{C^{P3/P4}}$ could be assigned using the HMQC technique (**Figure 2.14**).
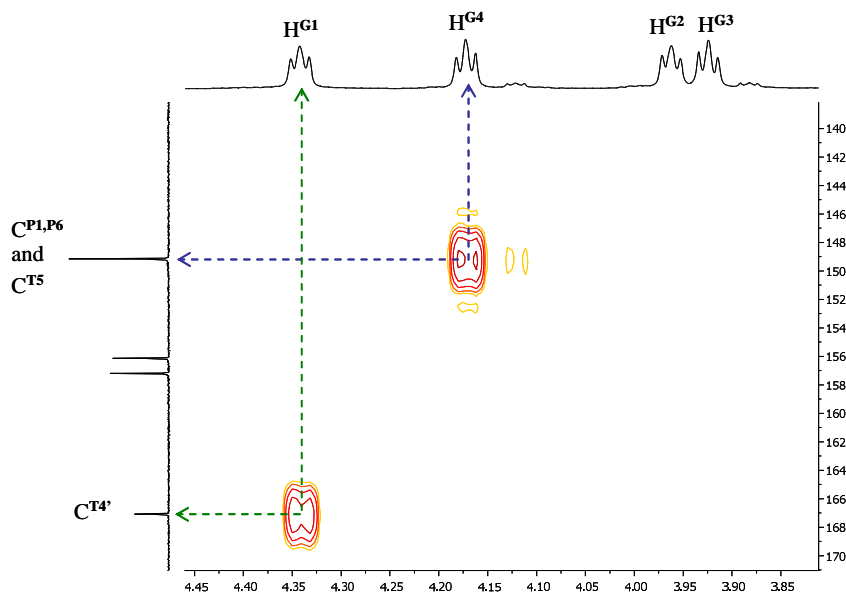
Figure 2.13. Part of the HMBC spectrum (500 MHz, 295 K) of **L7** in CDCl$_3$. Spectrum exhibits some residues of the starting material, which could not be removed by column chromatography or other purification methods.
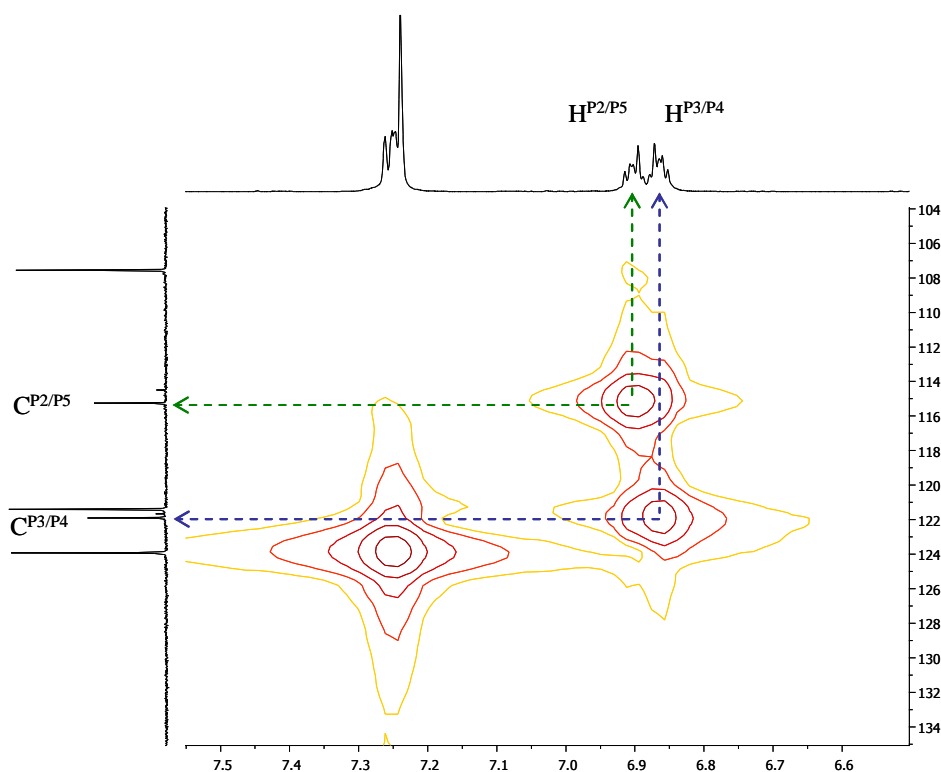
Figure 2.14. Part of the HMQC spectrum (500 MHz, 295 K) of **L7** in CDCl$_3$.

2.5 Mass spectrometric characterization

Electrospray ionization (ESI) and MALDI-TOF mass spectrometry, both in positive mode, were used to characterize intermediates **L1a-L4a** and **L6a-L7a** and ligands **L1-L4** and **L6-L7**. Normally, the [**L**+H]$^+$ peak was found as the major peak. In some measurements [**L**+Na]$^+$ could also be observed. Scanning with a laser in the MALDI-TOF method is a harder method and can cause fragmentation of some compounds (for example fragmentation on one or both of the glycol chains).

2.6 NMR titrations of ligand L1 with alkali metal ions: Na$^+$ and Li$^+$

Despite the important role of alkali metal ions in biological and material sciences,[107,108] their coordination chemistry, especially with classical ligands, has received little attention, in comparison with transition metal ions.[109] Although the discovery of crown ethers[110] and cryptands[111] opened a new era in coordination chemistry of the alkali metal ions, their complexes with more conventional ligands have remained much less investigated. Pedersen reported in 1967, thirty-three cyclic polyethers, derived from aromatic vicinal diols and containing from 9 to 60 atoms including 3 to 20 oxygen atoms in the ring. Many of those containing five to ten oxygen atoms form stable complexes with some or all of the cations of: Li, Na, NH$_4$, RNH$_3$, K, Rb, Cs, Ag(I), Au(I), Ca, Sr, Ba, Cd, Hg(I), Hg(II), La(III), Tl(I), Ce(III) and Pb(II).[110] Most of the attempts to study these alkali metals complexes were focused on the isolation of the solid adducts of the alkali metal salts with a variety of chelating and non-chelating ligands.[109] Morita and co-workers have prepared a number of complexes with dicyano-monoalkyl-tetraaza macrocycles with lithium salts and the properties of resulting macrocycle complexes were examined in detail by means of ^{1}H NMR spectroscopy.[112] An unsymmetrical macrocycle has exhibited intriguing features, such as high selectivity for binding to the Li$^+$ ion. The unusual Li$^+$ complexation reactions have their origin in the unique properties of the metal free macrocycle, due to the fact that macrocycle has a strong intramolecular hydrogen bond in the macrocyclic ring and the highly strained macrocyclic ring by unsymmetrical structure consisting of nonplanar and planar moieties.[112] Recently Baulin and Kurochkina have reported the sodium, calcium and potassium complexes of benzo-15-crown-5-substituted terpyridines.[113] In the Ishimori group, highly effective and selective synergistic extraction of Li$^+$ has been found using 2-naphthoyltrifluoroacetone (Hnta) as an acidic chelating agent and 2,9-dimethyl-1,10-phenanthroline (dmp) or 2,9-dimethyl-4,7-diphenyl-1,10-phenanthroline (dmdpp) as a neutral coligands.[114] The electronic and steric effects of the methyl groups at 2,9-positions of phen on the thermodynamic functions of adduct formation as well as the high lithium selectivity were quantitatively elucidated.[114] Starova and Denisova have been investigating the solid

phase formed in acetone at a 1,10-phenanthroline (phen):LiClO$_4$ concentration ratio close to 2: 1. According to X-ray diffraction data, the molecular structure of bis(1,10-phenanthroline)lithium perchlorate consists of a flattered tetrahedron Li(phen)$_2{}^+$ cation. The IR spectral data show that the complex dissociates in acetone to a 1:1 complex and a phen molecule.[115] The role of nitrogen in the charge transfer and storage capacity of lithium-intercalated heterocyclic oligophenylenes was investigated using photoelectron spectroscopy by Doherty and Friedlein. The development of new occupied states at low binding energies in the valence band region, as well as core level chemical shifts at both carbon and nitrogen sites, demonstrates partial charge transfer from lithium atoms to the organic component during formation of the intercalated compound. In small compounds, i.e., biphenyl and bipyridine derivatives, the position of the nitrogen heteroatom significantly affects the spacing between gap states in the Li-intercalated film; yet it has minimal effects on the charge storage capacity. In larger, branched systems, the presence of nitrogen in the aromatic system significantly enhances the charge storage capacity while the Li-N bond strength at high intercalation levels is significantly weakened relative to the nitrogen-free derivative. These observations have important implications for improved deintercalation processes in organic electrodes in lithium-ion batteries.[116] A new sodium tetrafluoroborate bridged neutral helical coordination polymer, formulated as [Na(1,10-phenanthroline)BF$_4$]$_{(n)}$, has been synthesized and characterized by Huang, W. and H. F. Qian. X-ray single crystal determination reveals that the Na center has hexa-coordinate distorted octahedron coordination geometry and the BF$_4{}^-$ anion serves as a multidentate bridging ligand coordinated to three adjacent sodium cations forming an infinite one-dimensional single-strand helix. Mostly likely this complex is an unprecedented type of helical structure in which only coordinated alkali metal sodium and bridging tetrafluoroborate are present.[117] Sauvage has reported a compound in which Li$^+$ is used as an assembling centre to generate a double-stranded helical complex from two linear coordinating fragments, each containing three 1,10-phenanthroline units and bearing terminal olefins at their ends; ruthenium-catalyzed ring-closing metathesis on the helical precursor leads to a 4-crossing [2]-catenane in 30% yield, making the procedure reasonably preparative (**Figure 2.15**).[118]
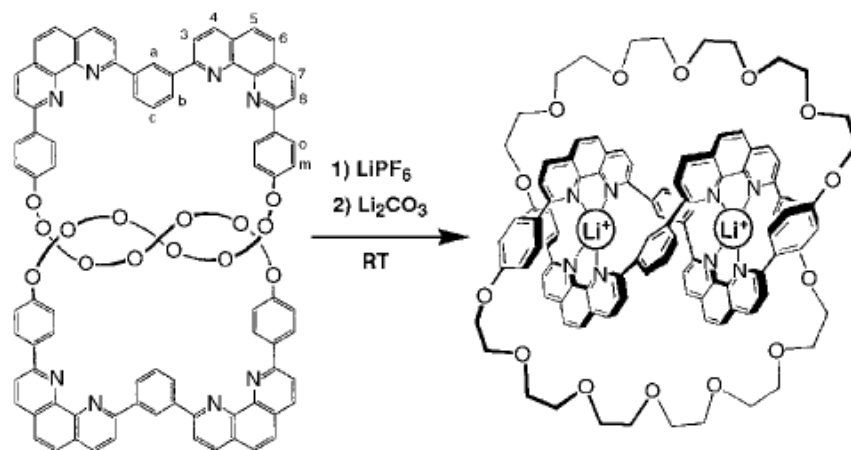
Figure 2.15. Synthesis of a dilithium catenate.[118]

A few attempts have been made to study such alkali complexes in solutions, and particularly in nonaqueous solutions.[119,120] The reason for such a low interest in the solution studies is the fact that the interactions of conventional ligands with alkali metal ions are relatively weak and most of the physicochemical techniques are not sensitive enough.

In this section we report an NMR study of the complexation of Na$^+$ and Li$^+$ ions with the new ditopic 4'-substituted- 2,2':6',2''-terpyridine ligand **L1** in acetonitrile.

To determine conditional stability constants, NMR titrations of ligand **L1** with NaClO$_4$ and LiClO$_4$ solutions were performed. A 1.3×10^{-2} M solution of ligand **L1** was titrated with 1 M NaClO$_4$ and ^{1}H NMR spectra were recorded after each addition of Na$^+$ starting from 0.8 eq up to a total concentration ratio $R = $ Na$^+$/**L1** = 12. For titration with LiClO$_4$, to 1.3×10^{-2} M ligand **L1** solution 0.5 M Li$^+$ was added and ^{1}H NMR spectra were recorded after each addition of metal solution starting from 0.2 eq up to a total concentration ratio $R = $ Li$^+$/**L1** = 4.6. All of the titrations were conducted in CD$_3$CN solution (**Figures 2.16, 2.17. 2.18 and 2.19**).
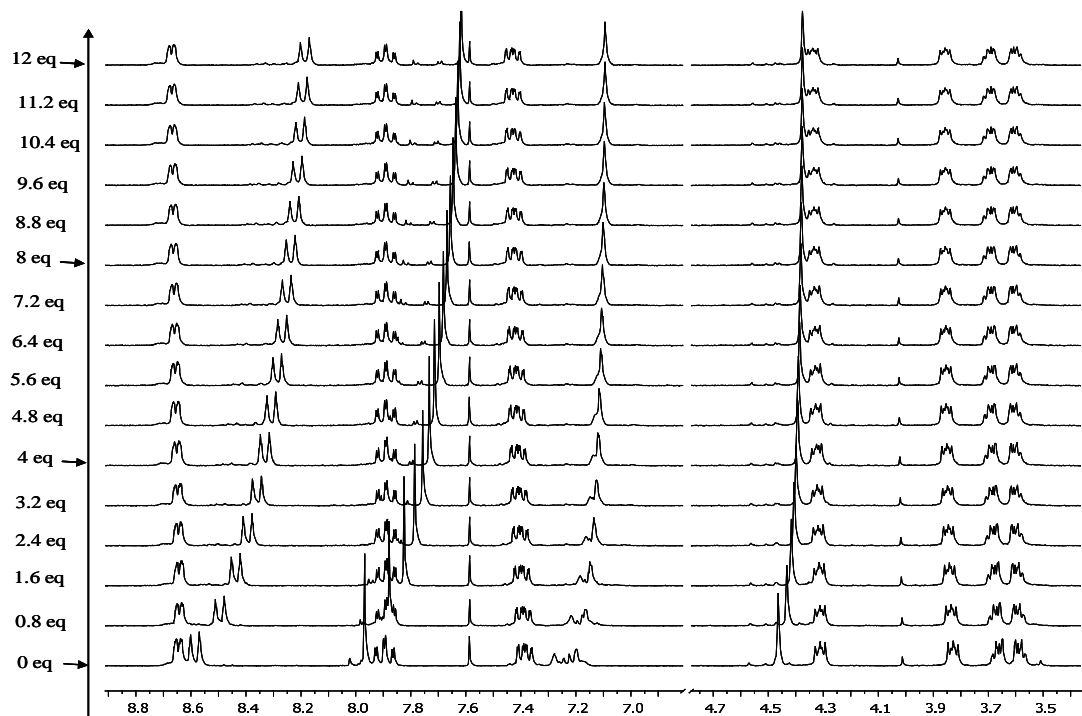
Figure 2.16. Part of the ^{1}H NMR spectra (500 MHz, 295 K) of **L1** (bottom spectrum) with increasing amount of NaClO$_4$ (from bottom up) in CD$_3$CN.
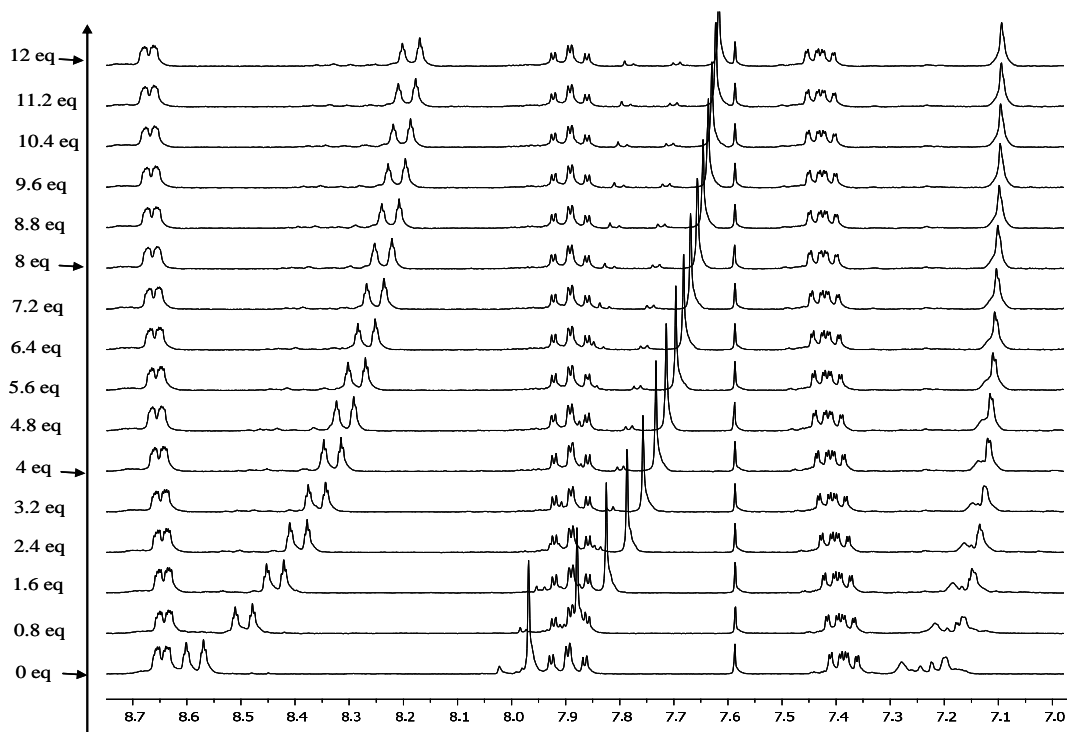
Figure 2.17. Aromatic region of the ^{1}H NMR spectra (500 MHz, 295 K) of **L1** (bottom spectrum) with increasing amount of NaClO$_4$ (from bottom up) in CD$_3$CN.

56

Addition of the $NaClO_4$ solution results in a few significant changes in the ^{1}H NMR spectrum of ligand **L1** (**Figures 2.16** and **2.17**). In the aromatic region, signals assigned to the protons $\mathbf{H^{T6}}$ and $\mathbf{H^{T3'}}$ of ligand **L1** are both strongly shifted upfield. Also the multiplet for protons $\mathbf{H^P}$ is shifted upfield and additionally is changing its multiplicity to a singlet. This suggests that upon addition of $NaClO_4$, the geometry of the created species changes in such a way that all of the protons on the benzene ring are equivalent. In the aliphatic region of the ^{1}H NMR spectrum of ligand **L1,** after addition of the $NaClO_4$, only small changes are observed. The signal at δ 4.54 ppm which is assigned to $\mathbf{H^F}$ from the -CH_2- bridge connecting the benzene ring to the ethylene glycol chain is slightly shifted upfield. After addition of the 8 equivalents of $NaClO_4$, further addition resulted in no more significant changes in the ^{1}H NMR spectrum being observed.

The addition of the $LiClO_4$ results in more marked changes in the ^{1}H NMR spectrum of ligand **L1** (**Figures 2.18** and **2.19)**. In the aromatic region, the signal assigned to proton $\mathbf{H^{T3}}$ is slightly shifted downfield. Proton $\mathbf{H^{T6}}$ is shifted strongly upfield and after the addition of 1.5 equivalents of $LiClO_4$, overlaps with a triplet from proton $\mathbf{H^{T4}}$. The most affected by the addition of $LiClO_4$ is the signal for proton $\mathbf{H^{T3'}}$, this signal is shifted upfield from δ 8.02 ppm to δ 7.17 ppm, at the end of the titration. Also the signal for protons $\mathbf{H^P}$ is shifted upfield and this multiplet separates to two signals. In the aliphatic region of the ^{1}H NMR spectrum of ligand **L1** after addition of $LiClO_4$, similar changes to the titration with $NaClO_4$ can be observed, namely the signal at δ 4.54 ppm from proton $\mathbf{H^F}$ is slightly shifted upfield. After the addition of 1.5 equivalents of $LiClO_4$ salt, no more significant changes in the ^{1}H NMR spectrum are observed.

The signal at δ 7.58 ppm is the signal for chloroform. A small amount of this solvent was used to dissolve ligand.
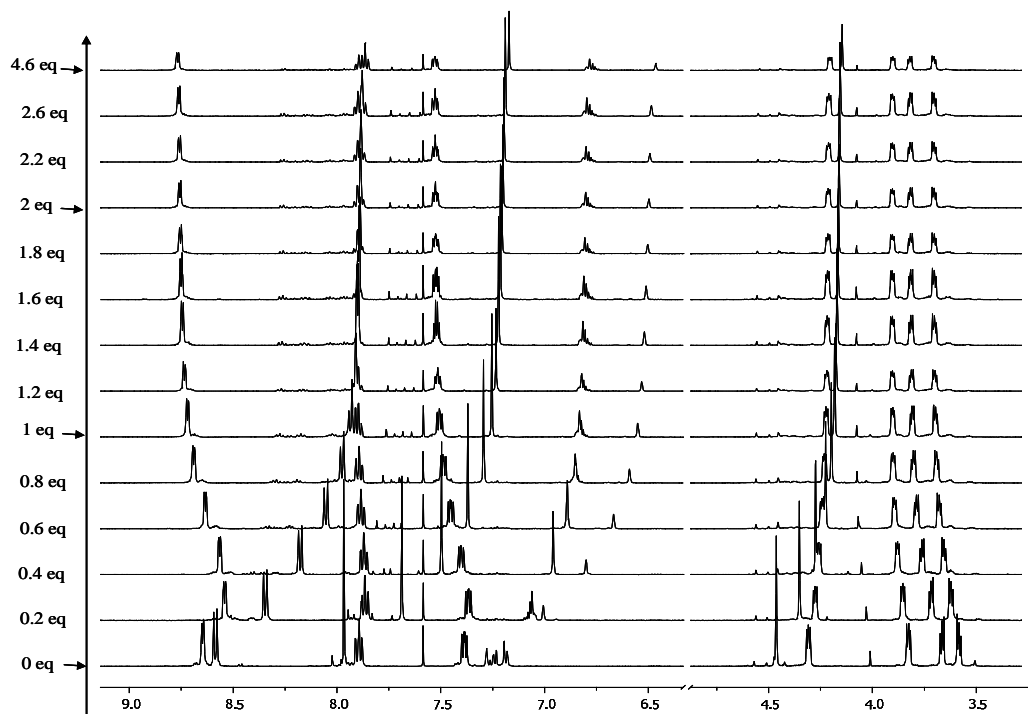
Figure 2.18. Part of the ^{1}H NMR spectra (500 MHz, 295 K) of **L1** (bottom spectrum) with increasing amount of LiClO$_4$ (from bottom up) in CD$_3$CN.
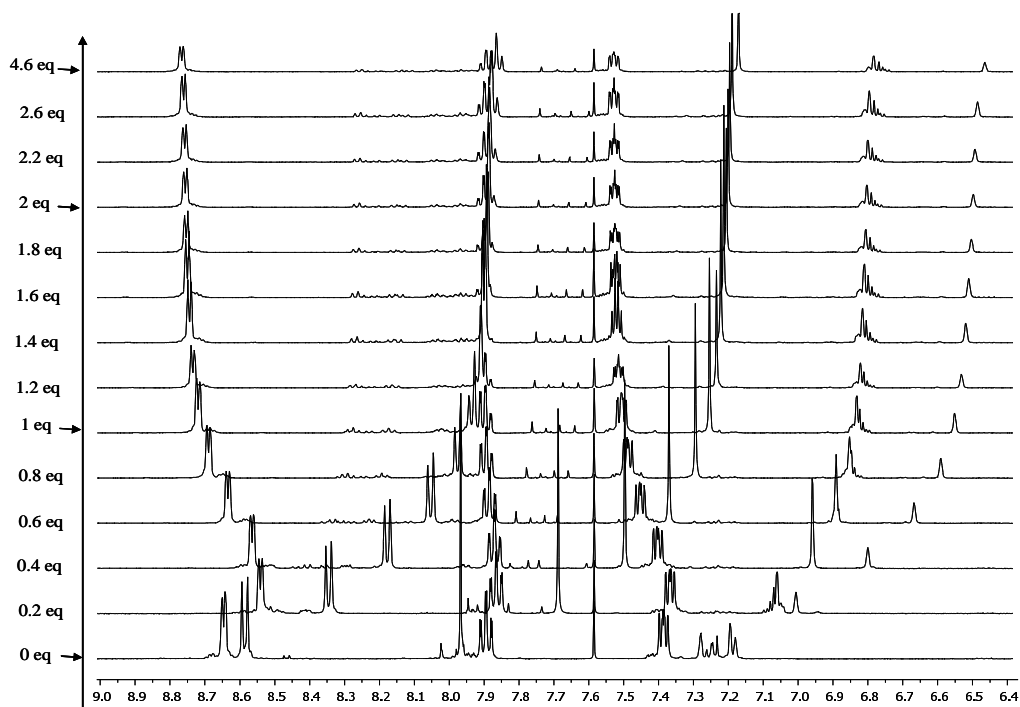
Figure 2.19. Aromatic region of the ^{1}H NMR spectra (500 MHz, 295 K) of **L1** (bottom spectrum) with increasing amount of LiClO$_4$ (from bottom up) in CD$_3$CN.

58

All of the changes in chemical shifts in ^{1}H NMR spectra after addition of NaClO$_4$ (**Tabele 2.6**) or LiClO$_4$ (**Tabele 2.7**) are shown below. As one can notice from tables, the less affected by metal addition proton signals are $\mathbf{H^G}$, $\mathbf{H^{T4}}$ and $\mathbf{H^{T6}}$. In contrast, the most sensitive to increasing amounts of sodium or lithium perchlorate is proton $\mathbf{H^{T3'}}$.

The changes in chemical shifts of $\mathbf{H^{T3'}}$ ($\Delta\delta\,\mathbf{H^{T3'}}$ [ppm]) as a function of added NaClO$_4$ or LiClO$_4$ are shown in **Figures 2.20** and **2.21**.

^{1}H	Before addition [ppm]	After addition [ppm]	$\Delta\delta$
H^{G4}	3.63	3.60	-0.03
H^{G3}	3.75	3.69	-0.06
H^{G2}	3.91	3.86	-0.05
H^{G1}	4.37	4.32	-0.05
H^{F}	4.54	4.38	-0.19
H^{P}	7.24	7.09	-0.15
H^{T5}	7.29	7.42	0.13
H^{T4}	7.81	7.89	0.07
$H^{T3'}$	8.02	7.62	-0.40
H^{T3}	8.58	8.18	-0.40
H^{T6}	8.65	8.67	0.02

Table 2.6. Changes in chemical shifts of ^{1}H ($\Delta\delta$ H) after addition of NaClO$_4$ (12 eq).

^1H	Before addition [ppm]	After addition [ppm]	$\Delta\delta$
H^{G4}	3.63	3.70	0.07
H^{G3}	3.75	3.82	0.07
H^{G2}	3.91	3.90	-0.01
H^{G1}	4.37	4.20	-0.17
H^{F}	4.54	4.15	-0.39
H^{P}	7.24	6.46 6.77	-0.78 -0.47
H^{T5}	7.29	7.56	0.27
H^{T4}	7.81	7.89	0.08
$H^{T3'}$	8.02	7.17	-0.85
H^{T3}	8.58	7.89	-0.69
H^{T6}	8.65	8.77	0.12

Table 2.7. Changes in chemical shifts of ^1H ($\Delta\delta$ H) after addition of $LiClO_4$ (4.6 eq).
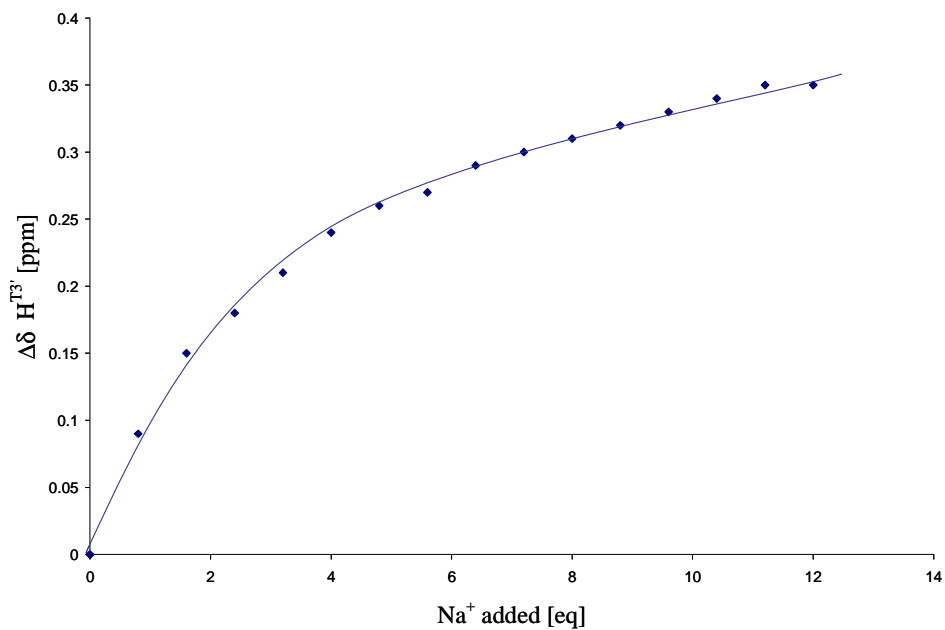
Figure 2.20. Changes in chemical shifts of $H^{T3'}$ ($\Delta\delta\ H^{T3'}$ [ppm]) as a function of added NaClO$_4$ [eq] together with best fit curve.
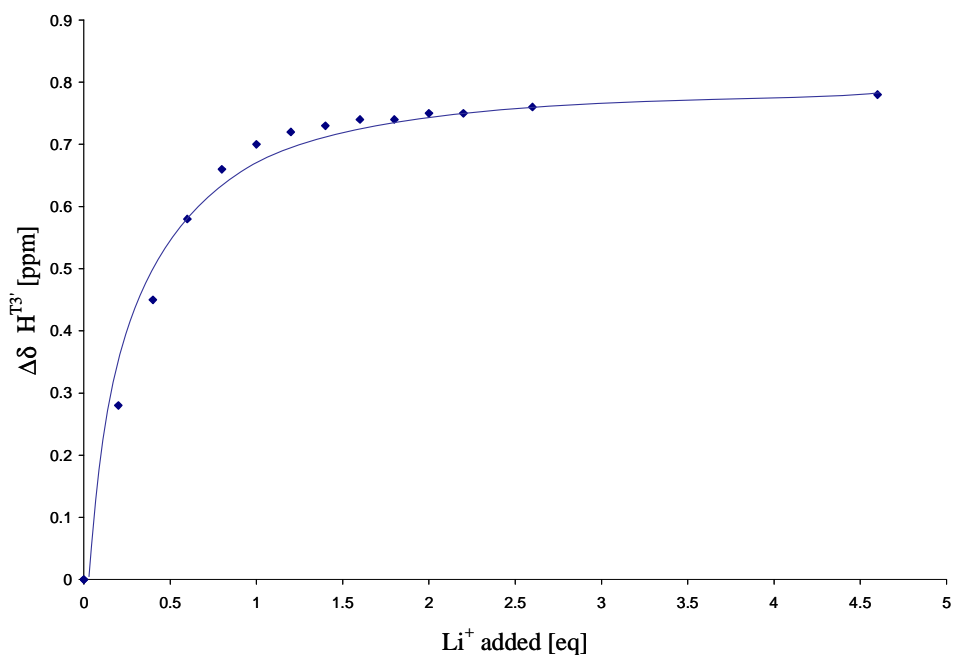
Figure 2.21. Changes in chemical shifts of $H^{T3'}$ ($\Delta\delta\ H^{T3'}$ [ppm]) as a function of added LiClO$_4$ [eq] together with best fit curve.

The stability of the resulting complexes were evaluated from non-linear least-squares fitting of the chemical shift-mole ratio data of the 3' proton to appropriate equations by using WinEQNMR2 (Version 2.00 by Michael J. Hynes, National University of Ireland, Galway).

$$Na^+ \; + \; \mathbf{L1} \leftrightarrow [Na\mathbf{L1}]^+ \qquad \log K$$

$$Li^+ \; + \; \mathbf{L1} \leftrightarrow [Li\mathbf{L1}]^+ \qquad \log K$$
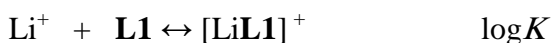
	$\mathrm{Log}K^{a}$
Na^+	1.03
Li^+	2.69

Table 2.8. Conditional stability constants for $[Na\mathbf{L1}]^+$ and $[Li\mathbf{L1}]^+$ in CD_3CN. [a] esd values on calculated K values were 15 (Li) and 0.6 (Na).

The overall stability of the resulting Li^+ complex with the ditopic 4'-substituted-2,2':6',2''-terpyridine ligand $\mathbf{L1}$ is higher than that of the corresponding Na^+ complex (**Table 2.6**). The lithium ion, with a higher charge density and harder character, is expected to form more stable complex with tpy ligands.

It seems reasonable to assume that the nitrogen atoms of tpy substituent act as more effective donating groups than the oxygen atoms of the glycol chains for Li^+ and Na^+ ions.

For comparison conditional stability constant values of sodium and lithium complexes with bpy and phen in acetonitrile and with tpy and bpy in nitromethane are shown in **Table 2.9**. The orders of magnitude of logK values are comparable to the conditional

62

stability constants found for $[NaL1]^+$ and $[LiL1]^+$ in CD_3CN. It is imported to notice that conditional stability constant of tpy complex with lithium in nitromethane is higher than this of $[LiL1]^+$ in acetonitrile by almost one order of the magnitude and conditional stability constant of tpy complex with sodium in nitromethane is slightly smaller than this of $[NaL1]^+$ in acetonitrile.

	$\mathrm{Log}K_1$
bpy + Na^+ (in acetonitrile)	$1.31(7)$[121]
bpy + Li^+ (in acetonitrile)	$2.11(7)$[121]
phen+ Na^+ (in acetonitrile)	$1.55(7)$[121]
phen + Li^+ (in acetonitrile)	$2.28(7)$[121]
bpy + Na^+ (in nitromethane)	$2.39(7)$[121]
bpy + Li^+ (in nitromethane)	$2.44(7)$[121]
tpy + Na^+ (in nitromethane)	$1.67(7)$[121]
tpy + Li^+ (in nitromethane)	$3.24(6)$[121]

Table 2.9. Conditional stability constants for some 1:1 Na^+ and Li^+ complexes.[121]

In **Table 2.10** conditional stability constant of transition metals tpy complexes are shown. All of the presented in table transition metals are binding tpy ligands much stronger, from two to six times, than the alkali metal ions: Li^+ and Na^+.

	Log$K$1	Log$K$2
tpy + Fe^{2+}	7.1(4)[122]	12.9(5)[122]
tpy + Co^{2+}	8.4(4)[122]	9.9(3)[122]
tpy + Mn^{2+}	4.4(5)[122]	-
tpy + Cd^{2+}	5.1(2)[122]	-
tpy + Ni^{2+}	10.7(5)[122]	11.1(2)[122]
tpy + Zn^{2+}	6.0(1)[122]	-

Table 2.10. Conditional stability constants for transition metal tpy complexes.[122]

2.7 Conclusion

In this chapter, several new ditopic intermediates **L1a-L4a, L6a-L7a** and ligands **L1-L4, L6-L7**, which are based on a benzene unit connected to two 4'-substituted- 2,2':6',2''-terpyridine moieties through different polyethyleneoxy spacers were synthesized and characterized by ^{1}H and ^{13}C NMR spectroscopy, mass spectrometry (ESI-MS and MALDI-TOF), IR spectroscopy, UV-Vis spectroscopy and elemental analysis. The ligands were also preliminary studied for interactions with Group 1 metals.

2.8   Experimental

❖ 1,3-Bis(7-hydroxy-2,5-dioxaheptyl)benzene (**L1a**)

❖ 1,3-Bis(19-hydroxy-2,5,8,11,14,17-hexaoctanonadecyl)benzene (**L2a**)

❖ 1,3-Bis(10-hydroxy-2,5,8-trioxadecyl)benzene (**L3a**)

❖ 1,4-Bis(7-hydroxy-2,5-dioxaheptyl)benzene (**L4a**)

❖ 1,2-Bis(7-hydroxy-2,5-dioxaheptyl)benzene (**L6a**)

❖ 1,3-Bis(6-hydroxy-1,4-dioxahexyl)benzene (**L7a**)

4'- Chloro-2,2':6',2''-terpyridine was prepared as previously reported in the literature.[102]

❖ 1,3-Bis(7-hydroxy-2,5-dioxaheptyl)benzene (**L1a**)
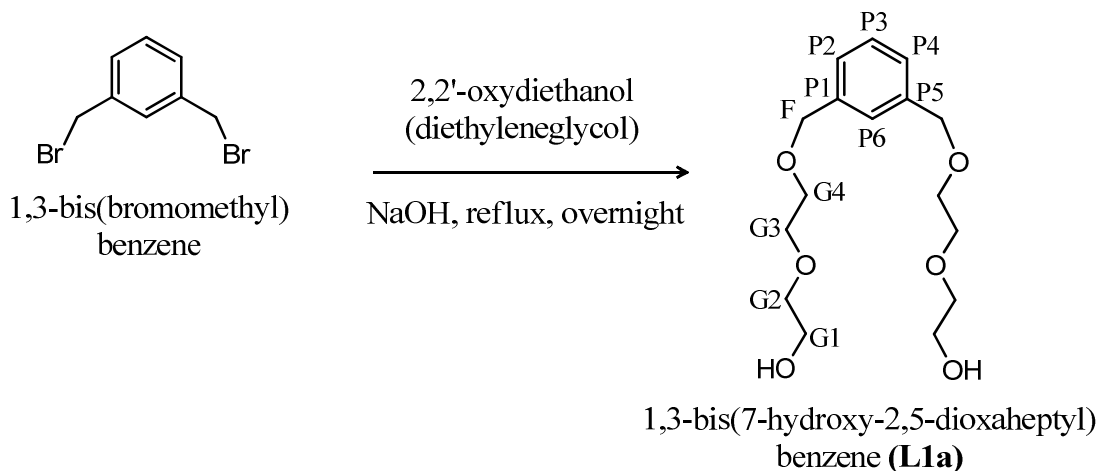
Molecular formula: $C_{16}H_{26}O_6$
Molecular weight: 314.37

General procedure for ditopic intermediates L1a-L4a, L6a-L7a

The intermediates were only characterized in a crude form by ^{1}H NMR spectroscopy and MALDI MS.

1,3-Bis(bromomethyl)benzene (97%, Alfa Aesar) (1.0 g, 3.8 mmol) was added to a hot suspension of NaOH (0.35 g, 8.8 mmol) in 50 mL diethylene glycol. The reaction mixture was stirred overnight at 125 °C under nitrogen. After 10 h the reaction mixture was cooled to room temperature and quenched with 100 mL water, then extracted with CHCl$_3$ (4x100 mL). The organic layer was dried (MgSO$_4$) filtered and the solvent was removed *in vacuo*. The product **L1a** was collected as a yellow oil (0.95 g, 3.0 mmol, 80%) after column chromatography (Al$_2$O$_3$, CHCl$_3$).

The reaction could be also performed in a microwave reactor at 125 °C for 15 minutes but on a much smaller scale. 1,3-Bis(bromomethyl)benzene (97%, Alfa Aesar) was reacted with NaOH (0.040 g, 0.88 mmol) in 10 mL diethylene glycol. After work up, the product **L1a** was obtained in 50% yield (0.063 g, 0.19 mmol). Other tpy containing products were not isolated. Despite the lower yield, this method allowed the reaction time to be shortened from 10 hours to 15 minutes.

^{1}H NMR (400 MHz, CDCl$_3$) δ_H 3.34 (br, 2H, H^{OH}), 3.57 (m, 4H, H^{G1}), 3.59–3.76 (m, 12H, H^{G2-G4}), 4.56 (s, 4H, H^F), 7.18-7.39 (m, 4H, H$^{P2, P3, P4, P6}$).

MS (MALDI-TOF, sinapinic acid): m/z = 337.5 [**L1a**+Na]$^+$ (calc. 337.5), 315.5 [**L1a**+H]$^+$ (calc. 315.5).

❖ 1,3-Bis(19-hydroxy-2,5,8,11,14,17-hexaoctanonadecyl)benzene (**L2a**)

3,6,9,12,15-pentaoxa
heptadecane-1,17-diol
(haxaethylene glycol)

NaOH, reflux, overnight

1,3-bis(bromomethyl)
benzene

1,3-bis(19-hydroxy-2,5,8,11,14,17-
hexaoctanonadecyl)benzene **(L2a)**

Molecular formula: $C_{32}H_{58}O_{14}$
Molecular weight: 666.79

Compound **L2a** was synthesized according to general procedure for ditopic intermediates with 1,3-bis(bromomethyl)benzene (97%, Alfa Aesar) (1.0 g, 3.8 mmol), NaOH (0.35 g, 8.8 mmol) and hexaethylene glycol (2.2 g, 7.6 mmol) in 50 mL DMSO. The product **L2a** was collected as a yellow oil (2.1 g, 3.1 mmol, 82%) after column chromatography (Al_2O_3, $CHCl_3$).

^{1}H NMR (400 MHz, CDCl$_3$) δ_H 3.32 (br, 2H, H^{OH}), 3.55 (m, 4H, H^{G1}), 3.60–3.77 (m, 44H, H$^{G2\text{-}G12}$), 4.55 (s, 4H, H^F), 7.18-7.40 (m, 4H, H$^{P2,\ P3,\ P4,\ P6}$).

MS (MALDI-TOF, sinapinic acid): m/z = 667.8 [**L2a**+H]$^+$ (calc. 667.5).

❖ 1,3-Bis(10-hydroxy-2,5,8-trioxadecyl)benzene (**L3a**)
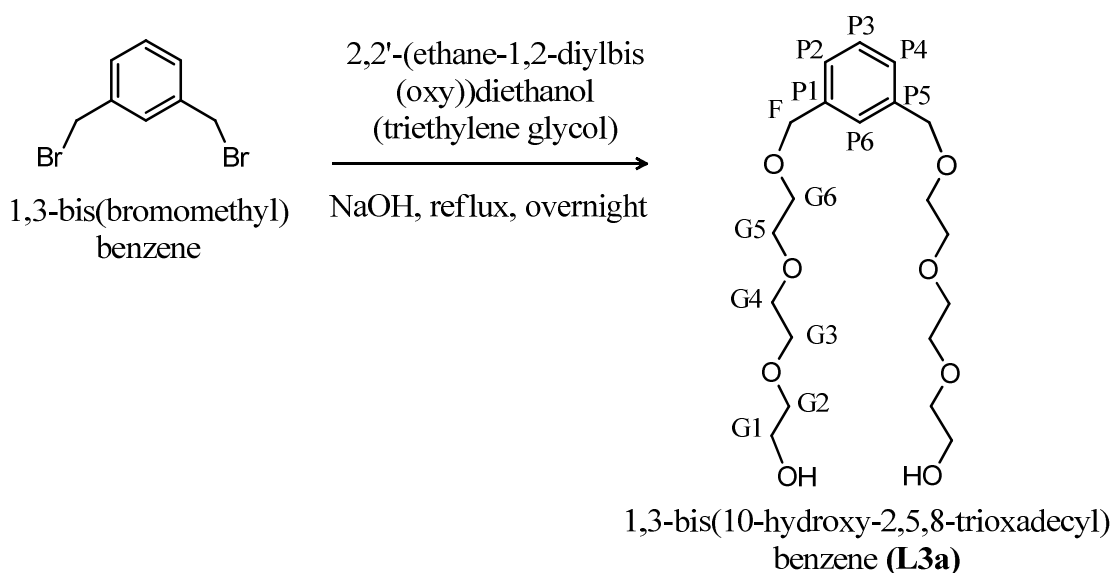
Molecular formula:C$_{20}$H$_{34}$O$_8$
Molecular weight: 402.48

Compound **L3a** was synthesized according to general procedure for ditopic intermediates with 1,3-bis(bromomethyl)benzene (97%, Alfa Aesar) (1.0 g, 3.8 mmol) and NaOH (0.35 g, 8.8 mmol) in 50 mL triethylene glycol. The product **L3a** was collected as a yellow oil (1.2 g, 3.0 mmol, 80%) after column chromatography (Al$_2$O$_3$, CHCl$_3$).

The reaction could be also performed in a microwave reactor at 125 °C for 15 minutes but on a much smaller scale. 1,3-Bis(bromomethyl)benzene (97%, Alfa Aesar) was reacted with NaOH (0.040 g, 0.88 mmol) in 10 mL diethylene glycol. After work up, the product **L3a** was obtained in 50% yield (0.076 g, 0.19 mmol). Despite the lower yield, this method allowed the reaction time to be shortened from 10 hours to 15 minutes.

^{1}H NMR (400 MHz, CDCl$_3$) δ_H 3.36 (br, 2H, H^{OH}), 3.59 (m, 4H, H^{G1}), 3.55–3.75 (m, 20H, H$^{G2\text{-}G6}$), 4.57 (s, 4H, H^F), 7.20-7.40 (m, 4H, H$^{P2,\,P3,\,P4,\,P6}$).

MS (MALDI-TOF, sinapinic acid): *m/z* = 425.5 [**L3a**+Na]$^+$ (calc. 425.5), 403.5 [**L3a**+H]$^+$ (calc. 403.5).

❖ 1,4-Bis(7-hydroxy-2,5-dioxaheptyl)benzene (**L4a**)

1,4-bis(7-hydroxy-2,5-dioxaheptyl) benzene **(L4a)**
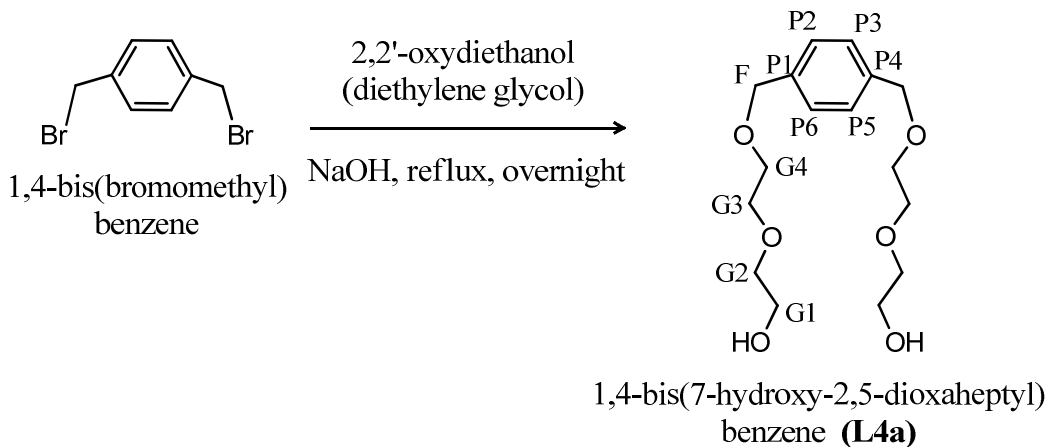
Molecular formula:C$_{16}$H$_{26}$O$_6$
Molecular weight: 314.37

Compound **L4a** was synthesized according to general procedure for ditopic intermediates with 1,4-bis(bromomethyl)benzene (97%, Alfa Aesar) (1.0 g, 3.8 mmol) and NaOH (0.35 g, 8.8 mmol) in 50 mL diethylene glycol. The product **L4a** was collected as a yellow oil (1.1 g, 3.4 mmol, 90%) after column chromatography (Al_2O_3, $CHCl_3$).

The reaction could be also performed in a microwave reactor at 125 °C for 15 minutes but on a much smaller scale. 1,4-Bis(bromomethyl)benzene (97%, Alfa Aesar) was reacted with NaOH (0.040 g, 0.88 mmol) in 10 mL diethylene glycol. After work up, the product **L4a** was obtained in 60% yield (0.072 g, 0.23 mmol). Despite the lower yield, this method allowed the reaction time to be shortened from 10 hours to 15 minutes.

^{1}H NMR (400 MHz, $CDCl_3$) δ_H 3.36 (br, 2H, H^{OH}), 3.57 (m, 4H, H^{G1}), 3.59–3.77 (m, 12H, $H^{G2\text{-}G4}$), 4.57 (s, 4H, H^F), 7.32 (s, 4H, $H^{P2, P3, P5, P6}$).

MS (MALDI-TOF, sinapinic acid): *m/z* = 315.4 [**L4a**+H]$^+$ (calc. 315.5).

❖ 1,2-Bis(7-hydroxy-2,5-dioxaheptyl)benzene (**L6a**)

1,2-bis(7-hydroxy-2,5-dioxaheptyl)
benzene **(L6a)**

Molecular formula:$C_{16}H_{26}O_6$
Molecular weight: 314.37

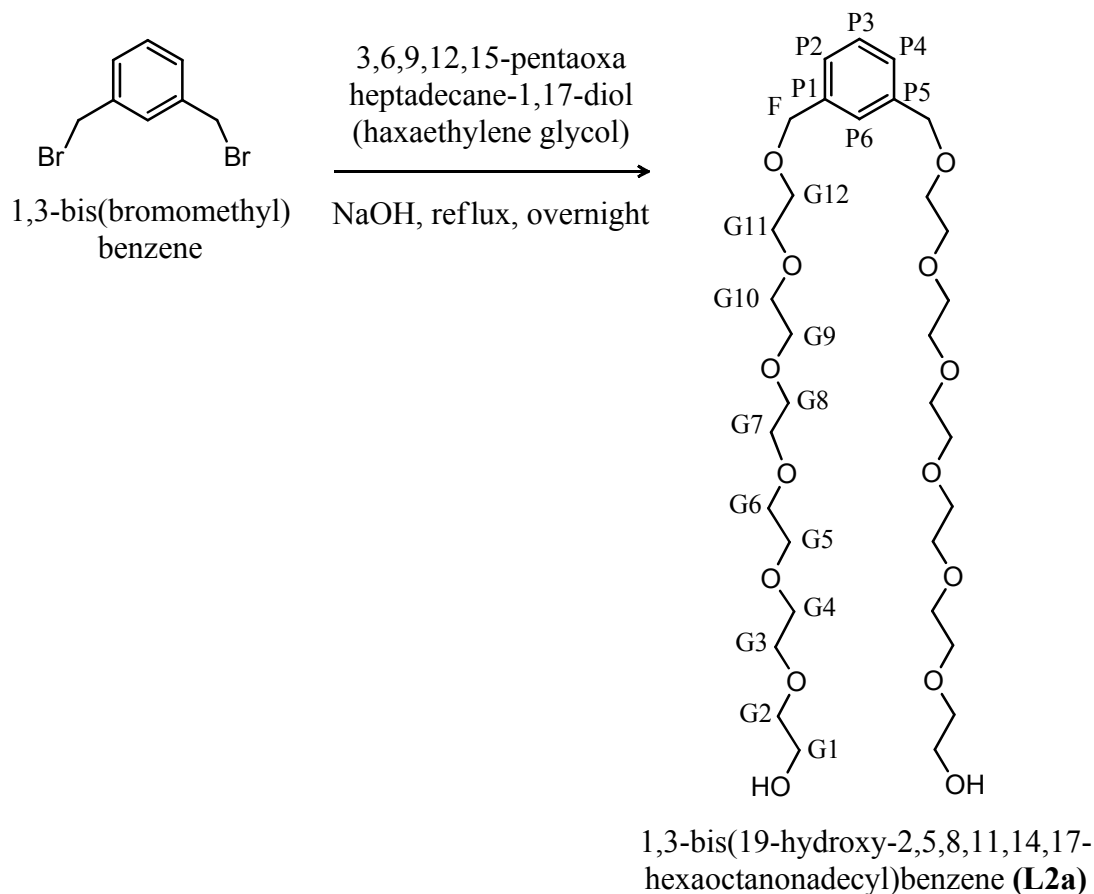Compound **L6a** was synthesized according to general procedure for ditopic intermediates with 1,2-bis(bromomethyl)benzene (97%, Alfa Aesar) (1.0 g, 3.8 mmol) and NaOH (0.35 g, 8.8 mmol) in 50 mL diethylene glycol. The product **L6a** was collected as a yellow oil (1.0 g, 3.2 mmol, 85%) after column chromatography (Al_2O_3, $CHCl_3$).

The reaction could be also performed in a microwave reactor at 125 °C for 15 minutes but on a much smaller scale. 1,2-Bis(bromomethyl)benzene (97%, Alfa Aesar) was reacted with NaOH (0.040 g, 0.88 mmol) in 10 mL diethylene glycol. After work up, the product **L6a** was obtained in 50% yield (0.063 g, 0.19 mmol).

^{1}H NMR (400 MHz, $CDCl_3$) δ_H 3.35 (br, 2H, H^{OH}), 3.55 (m, 4H, H^{G1}), 3.59–3.76 (m, 12H, H^{G2-G4}), 4.58 (s, 4H, H^F), 7.18-7.39 (m, 4H, $H^{P2,\ P3,\ P4,\ P5}$).

MS (MALDI-TOF, sinapinic acid): m/z = 327.5 [**L6a**+Na]$^+$ (calc. 327.5), 315.5 [**L6a**+H]$^+$ (calc. 315.5).

❖ 1,3-Bis(6-hydroxy-1,4-dioxahexyl)benzene (**L7a**)

1,2-dihydroxybenzene   K$_2$CO$_3$, DMF, 70 °C

1,3-bis(6-hydroxy-1,4-dioxahexyl)
benzene **(L7a)**

Molecular formula: C$_{14}$H$_{22}$O$_6$
Molecular weight: 286.32
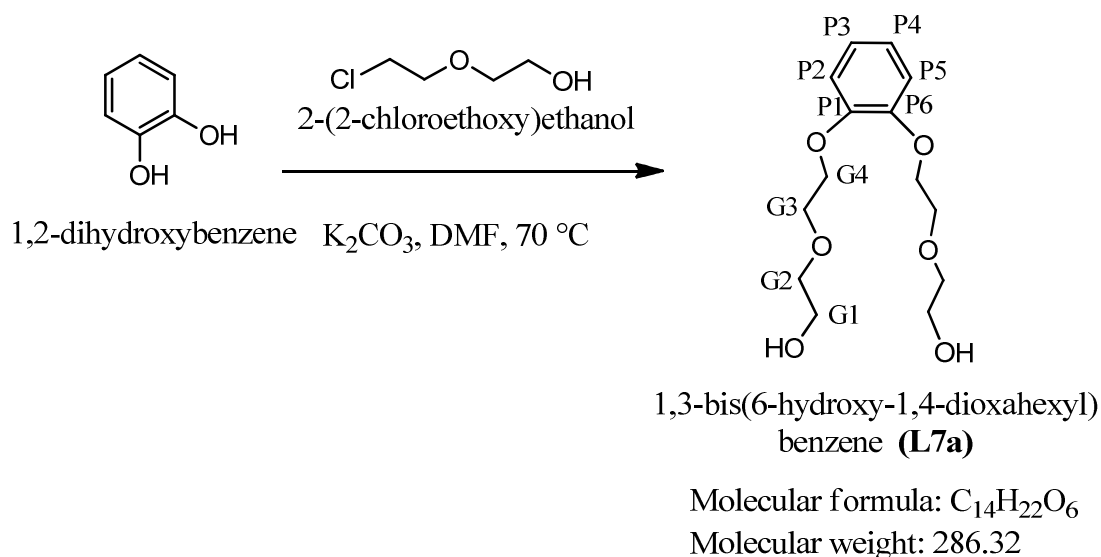
1,2-Dihydroxybenzene (>98%, Fluka) (1.0 g, 9.1 mmol) was added to a hot mixture of K$_2$CO$_3$ (3.5 g, 25 mmol) and 2-(2-chloroethoxy)ethanol (2.5 g, 20 mmol) in 50 mL DMF. The reaction mixture was stirred overnight at 70 °C under nitrogen. After 10 h the reaction mixture was cooled to room temperature and quenched with 100 mL water, then extracted with CHCl$_3$ (4x100 mL). The organic layer was dried (MgSO$_4$) filtered and the solvent was removed *in vacuo*. The product **L7a** was collected as a yellow oil (2.1 g, 7.3 mmol, 80%) after column chromatography (Al$_2$O$_3$, CHCl$_3$).

^{1}H NMR (400 MHz, CDCl$_3$) δ_H 3.34 (br, 2H, H^{OH}), 3.58 (m, 4H, H^{G1}), 3.60–3.80 (m, 12H, H^{G2-G4}), 7.18-7.39 (m, 4H, H$^{P2, P3, P4, P5}$).

MS (MALDI-TOF, sinapinic acid): *m/z* = 289.3 [**L7a**+H]$^+$ (calc. 289.5).

72

- 1,3-Bis(8-(4'-(2,2':6',2''-terpyridyl))-2,5,8-trioxaoctyl)benzene (**L1**)

- 1,3-Bis(20-(4'-(2,2':6',2''-terpyridyl))-2,5,8,11,14,17,20-heptaoxaeikosyl)benzene (**L2**)

- 1,3-Bis(11-(4'-(2,2':6',2''-terpyridyl))-2,5,8,11-tetraoxaundecyl)benzene (**L3**)

- 1,4-Bis(8-(4'-(2,2':6',2''-terpyridyl))-2,5,8-trioxaoctyl)benzene (**L4**)

- 1,2-Bis(8-(4'-(2,2':6',2''-terpyridyl))-2,5,8-trioxaoctyl)benzene (**L6**)

- 1,2-Bis(7-(4'-(2,2':6',2''-terpyridyl))-1,4,7-trioxaheptyl)benzene (**L7**)

- 1,3-Bis(8-(4'-(2,2':6',2''-terpyridyl))-2,5,8-trioxaoctyl)benzene (**L1**)
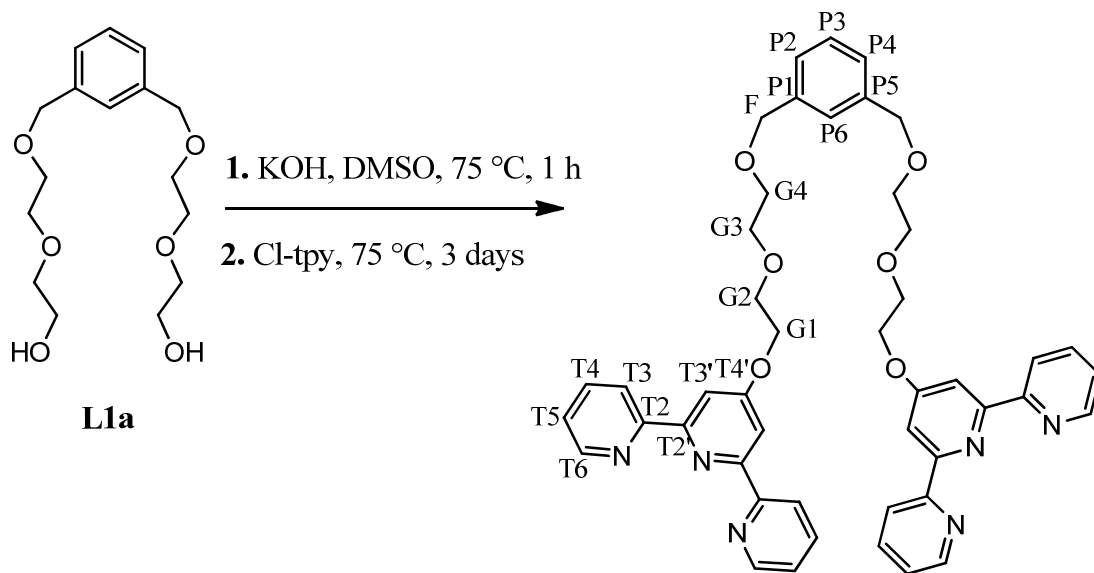
1,3-bis(8-(4'-(2,2':6',2''-terpyridyl))
-2,5,8-trioxaoctyl)benzene **(L1)**

Molecular formula: $C_{46}H_{44}N_6O_6$
Molecular weight: 776.81

General procedure for ditopic ligands L1-L4 and L6-L7

Compound **L1a** (0.50 g, 1.6 mmol) and finely powdered potassium hydroxide (0.31 g, 5.0 mmol) were stirred in 20 mL DMSO at 75 °C under nitrogen for 1 hour. Cl-tpy (1.4 g, 5.0 mmol) was added to the suspension and the mixture was stirred for 3 days at 75 °C. The reaction mixture was cooled to room temperature and quenched with 200 mL water, then extracted with $CHCl_3$ (3x200 mL). The organic layer was dried ($MgSO_4$), filtered and the solvent was removed. After column chromatography (Al_2O_3, $CHCl_3$), **L1** (0.85 g, 1.1 mmol, 68%) was obtained as a yellow oil. Other tpy containing products were not isolated.

^{1}H NMR (500 MHz, $CDCl_3$) δ_H 3.63 (m, 4H, H^{G4}), 3.75 (m, 4H, H^{G3}), 3.91 (m, 4H, H^{G2}), 4.37 (m, 4H, H^{G1}), 4.54 (s, 4H, H^F), 7.21-7.27 (m, 2H, $H^{P2/P4}$ or H^{P3} and H^{P6}), 7.27-7.31 (m, 6H, H^{T5} and $H^{P2/P4}$ or H^{P3} and H^{P6}), 7.81 (td, J 1.5, 7.8 Hz, 4H, H^{T4}), 8.02 (s, 4H, $H^{T3'}$), 8.58 (d, J 8.0 Hz, 4H, H^{T3}), 8.65 (d, J 4.1 Hz, 4H, H^{T6}).

^{13}C NMR (125 MHz, $CDCl_3$) δ_C 68.0 (C^{G1}), 69.7 (C^{G4}), 69.8 (C^{G2}), 71.2 (C^{G3}), 73.4 (C^F), 107.7 ($C^{T3'}$), 121.5 (C^{T3}), 124.0 (C^{T5}), 127.3 ($C^{P2/P4}$ or C^{P3} or C^{P6}), 127.3 ($C^{P2/P4}$ or C^{P3} or C^{P6}), 128.7 ($C^{P2/P4}$ or C^{P3} or C^{P6}), 136.9 (C^{T4}), 138.6 ($C^{P1,P5}$), 149.2 (C^{T6}), 156.3 (C^{T2}), 157.3 ($C^{T2'}$), 167.2 ($C^{T4'}$).

MS (ESI) m/z = 777.8 [**L1**+H]$^+$ (calc. 777.5).

IR (oil, $\tilde{v}$/cm^{-1}): 2864w, 1599m, 1582s, 1562s, 1556s, 1504m, 1468m, 1441s, 1406s, 1367m, 1348m, 1323m, 1292w, 1252w, 1203m, 1123s, 1091s, 1058s, 1038s, 991s, 971m, 963m, 941m, 929s, 903m, 845m, 791s, 743s, 733s, 697s, 656s, 646m, 621m.

UV/VIS (CH_2Cl_2):λ_{max}/ nm (ε_{max}, M^{-1} cm^{-1}) 241 (56.7 x 10^3), 279 (55.4 x 10^3).

Elemental Analysis : Found: C, 64.21; H, 5.83; N, 9.45. Calc. for $C_{46}H_{44}N_6O_6 \cdot 2H_2O \cdot 0.5CHCl_3$: C, 64.00; H, 5.60; N, 9.63%.

❖ 1,3-Bis(20-(4'-(2,2':6',2''-terpyridyl))-2,5,8,11,14,17,20-heptaoxaeikosyl)benzene (**L2**)

1. KOH, DMSO, 75 °C, 1 h

2. Cl-tpy, 75 °C, 3 days

L2a

1,3-bis(20-(4'-(2,2':6',2''-terpyridyl))
-2,5,8,11,14,17,20-heptaoxaeikosyl)benzene **(L2)**
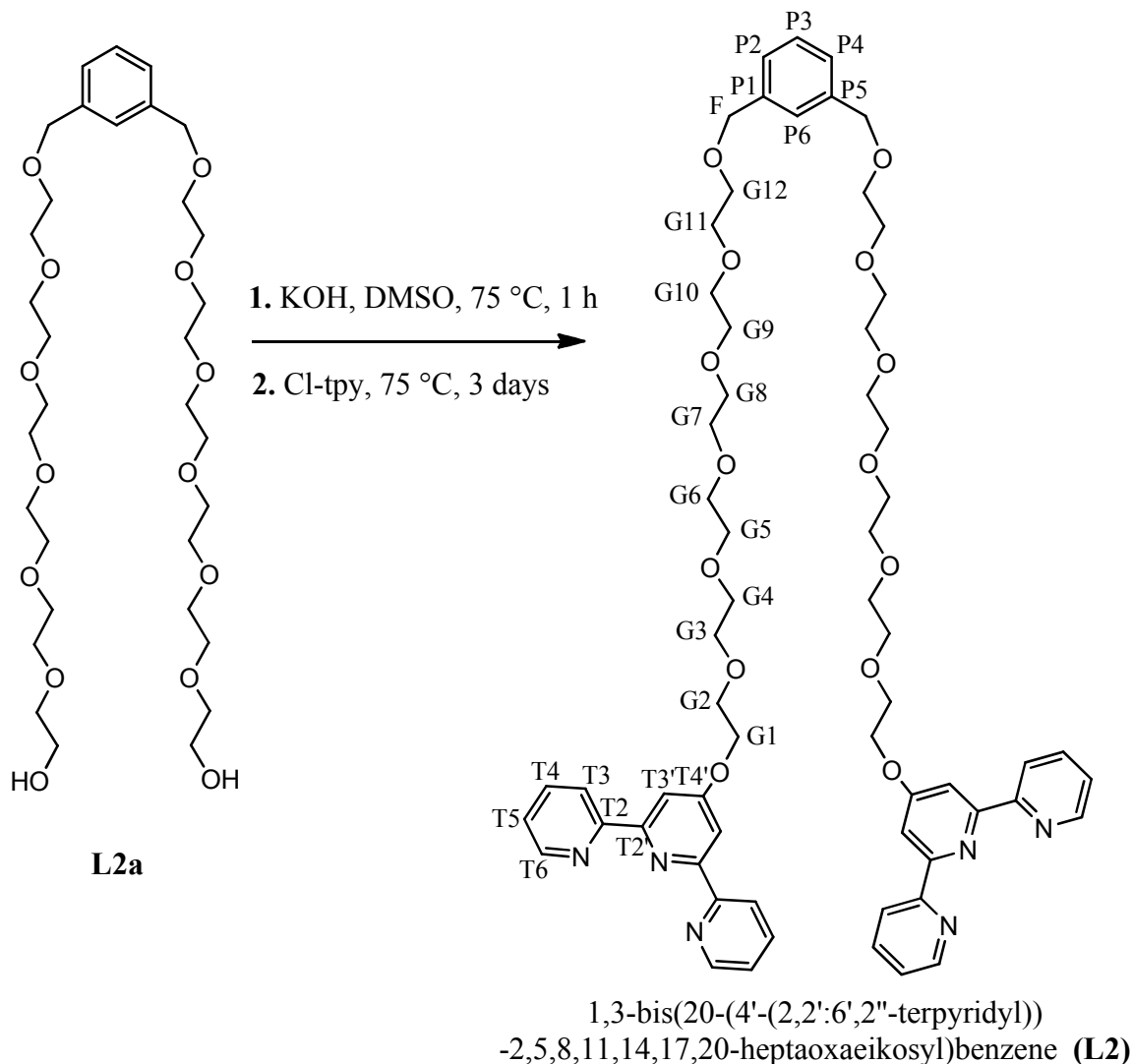
Molecular formula: $C_{62}H_{76}N_6O_{14}$
Molecular weight:1129.31

Compound **L2** was synthesized according to general procedure for ditopic ligands with intermediate **L2a** (0.50 g, 0.75 mmol), finely powdered potassium hydroxide (0.31 g, 5.0 mmol) and Cl-tpy (1.4 g, 5.0 mmol). After column chromatography (Al_2O_3, $CHCl_3$), **L2** (0.55 g, 0.49 mmol, 65%) was obtained as a yellow oil. Other tpy containing products were not isolated.

^{1}H NMR (500 MHz, CDCl$_3$) δ_H 3.50-3.65 (m, 36H, H^{G4-G12}), 3.69 (m, 4H, H^{G3}), 3.86 (m, 4H, H^{G2}), 4.32 (m, 4H, H^{G1}), 4.47 (s, 4H, H^F), 7.15-7.30 (m, 8H, H^{T5}, H$^{P2/P4}$ and H$^{P3/P6}$), 7.76 (t, J 7.7 Hz, 4H, H^{T4}), 7.98 (s, 4H, H$^{T3'}$), 8.54 (d, J 8.0 Hz, 4H, H^{T3}), 8.61 (d, J 4.2 Hz, 4H, H^{T6}).

^{13}C NMR (125 MHz, CDCl$_3$) δ_C 67.8 (C^{G1}), 69.4 (C^{G4}), 69.5 (C^{G2}), 70.6 (C^{G5-G12}), 70.6 (C^{G5-G12}), 70.7 (C^{G5-G12}), 71.0 (C^{G3}), 73.2 (C^F), 107.5 (C$^{T3'}$), 121.3 (C^{T3}), 123.9 (C^{T5}), 127.0 (C$^{P2/P4}$ or C^{P3} or C^{P6}), 127.1 (C$^{P2/P4}$ or C^{P3} or C^{P6}), 136.8 (C^{T4}), 138.4 (C^{P1,P5}), 149.1 (C^{T6}), 156.0 (C^{T2}), 157.1 (C$^{T2'}$), 167.0 (C$^{T4'}$).

MS (ESI) m/z = 1130.3 [**L2**+H]$^+$ (calc. 1130.5).

IR (oil, $\widetilde{\nu}$/cm^{-1}): 1598m, 1581s, 1563s, 1501m, 1467m, 1441m, 1404s, 1368s, 1348m, 1323s, 1291w, 1254w, 1205m, 1124s, 1091s, 1059m, 1038s, 991s, 971m, 963m, 943s, 931s, 905m, 844m, 789m, 744s, 735m, 697s, 656s, 645m, 621m.

UV/VIS (CH$_2$Cl$_2$):λ_{max}/ nm (ε_{max}, M^{-1} cm^{-1}) 241 (56.5 x 10^3), 279 (55.5 x 10^3).

Elemental Analysis : Found: C, 63.27; H, 6.38; N, 7.15. Calc. for C$_{62}$H$_{76}$N$_6$O$_{14}$·0.5CHCl$_3$: C, 63.14 H, 6.49; N, 7.07%.

❖ 1,3-Bis(11-(4'-(2,2':6',2"-terpyridyl))-2,5,8,11-tetraoxaundecyl)benzene (**L3**)

1,3-bis(11-(4'-(2,2':6',2"-terpyridyl))-2,5,8,11-
tetraoxaundecyl)benzene **(L3)**
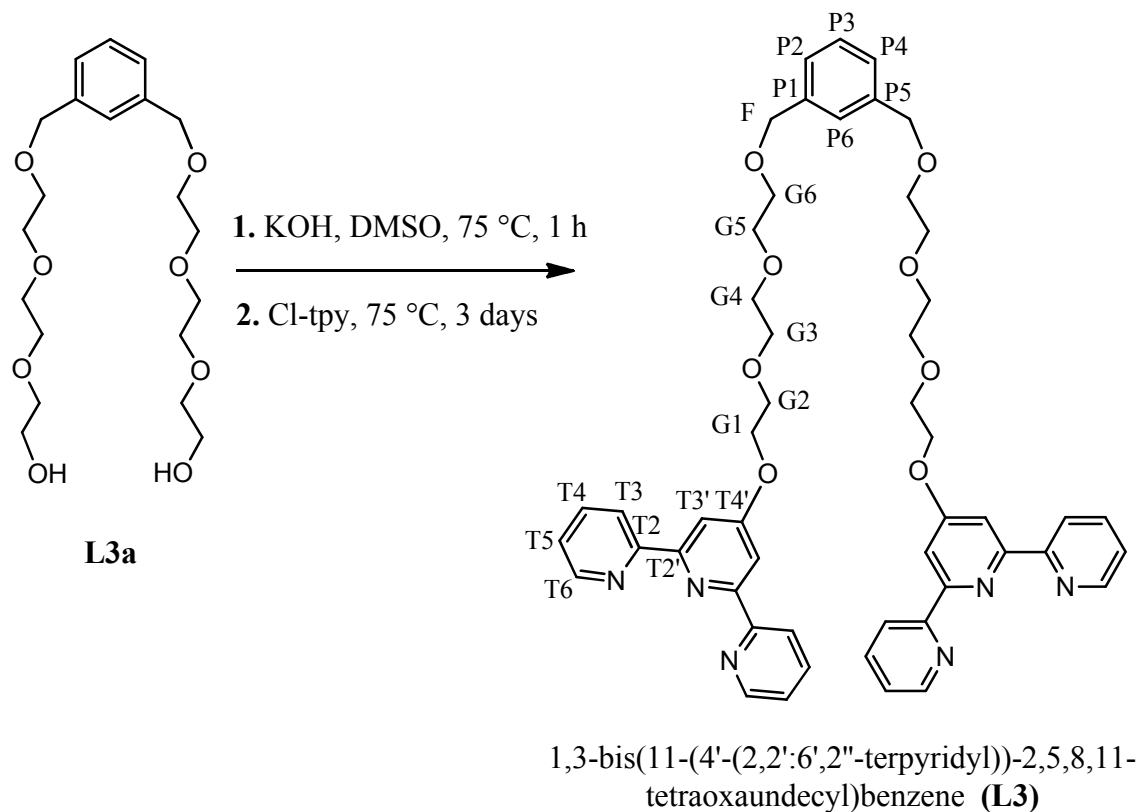
Molecular formula: $C_{50}H_{52}N_6O_8$
Molecular weight: 864.98

Compound **L3** was synthesized according to general procedure for ditopic ligands with intermediate **L3a** (0.50 g, 1.2 mmol), finely powdered potassium hydroxide (0.31 g, 5.0 mmol) and Cl-tpy (1.4 g, 5.0 mmol). After column chromatography (Al₂O₃, CHCl₃), **L3** (0.58 g, 0.67 mmol, 56%) was obtained as a yellow oil. Other tpy containing products were not isolated.

^{1}H NMR (400 MHz, CDCl₃) δ_H 3.45-3.75 (m, 16H, H^{G3-G6}), 3.87 (m, 4H, H^{G2}), 4.34 (m, 4H, H^{G1}), 4.49 (s, 4H, H^F), 7.15-7.30 (m, 8H, H^{T5}, H$^{P2/P4}$ and H$^{P3/P6}$), 7.79 (td, *J* 1.7, 7.8 Hz, 4H, H^{T4}), 7.99 (s, 4H, H$^{T3'}$), 8.55 (d, *J* 8.0 Hz, 4H, H^{T3}), 8.62 (d, *J* 3.9 Hz, 4H, H^{T6}).

MS (MALDI-TOF, sinapinic acid): m/z = 866.0 [**L3**+H]$^+$ (calc. 866.0).

UV/VIS (CH$_2$Cl$_2$):λ_{max}/ nm (ε_{max}, M^{-1} cm^{-1}) 241 (54.5 x 10^3), 279 (55.5 x 10^3).

❖ 1,4-Bis(8-(4'-(2,2':6',2''-terpyridyl))-2,5,8-trioxaoctyl)benzene (**L4**)

1,4-bis(8-(4'-(2,2':6',2''-terpyridyl))
-2,5,8-trioxaoctyl)benzene **(L4)**

Molecular formula: C$_{46}$H$_{44}$N$_6$O$_6$
Molecular weight: 776.88

Compound **L4** was synthesized according to general procedure for ditopic ligands with intermediate **L4a** (0.50 g, 1.6 mmol), finely powdered potassium hydroxide (0.31 g, 5.0 mmol) and Cl-tpy (1.4 g, 5.0 mmol). After column chromatography (Al$_2$O$_3$, CHCl$_3$), **L4** (0.85 g, 1.1 mmol, 68%) was obtained as a yellow oil. Other tpy containing products were not isolated.

^{1}H NMR (500 MHz, CDCl$_3$) δ_H 3.62 (t, J 5.0 Hz, 4H, H^{G4}), 3.73 (t, J 5.0 Hz, 4H, H^{G3}), 3.91 (t, J 5.0 Hz, 4H, H^{G2}), 4.38 (t, J 5.0 Hz, 4H, H^{G1}), 4.53 (s, 4H, H^F), 7.29 (s, 4H, H^{P2,} $^{P3, P5, P6}$), 7.30 (m, 4H, H^{T5}), 7.81 (td, J 1.8, 7.7 Hz, 4H, H^{T4}), 8.02 (s, 4H, H$^{T3'}$), 8.58 (d, J 8.0 Hz, 4H, H^{T3}), 8.66 (d, J 4.7 Hz, 4H, H^{T6}).

^{13}C NMR (125 MHz, CDCl$_3$) δ_C 67.7 (C^{G1}), 68.0 (C^{G4}), 69.7 (C^{G2}), 71.2 (C^{G3}), 73.3 (C^F), 107.6 (C$^{T3'}$), 121.5 (C^{T3}), 124.0 (C^{T5}), 128.0 (C^{P2,P3,P5,P6}), 137.0 (C^{T4}), 137.7 (C^{P1,P4}), 149.2 (C^{T6}), 156.3 (C^{T2}), 157.3 (C$^{T2'}$), 167.1 (C$^{T4'}$).

MS (ESI) m/z = 777.9 [**L4**+H]$^+$ (calc. 778.0).

m.p.: 97-100 °C

IR (oil, $\tilde{v}$/cm^{-1}): 1599m, 1582m, 1555m, 1466w, 1441w, 1406m, 1348w, 1325m, 1294w, 1277w, 1252w, 1236w, 1202m, 1124m, 1086m, 1049m, 1038m, 1022m, 989m, 968m, 930m, 868m, 847m, 835m, 814m, 791m, 771m, 733m, 700m, 660w, 621w.

UV/VIS (CH$_2$Cl$_2$):λ_{max}/ nm (ε_{max}, M^{-1} cm^{-1}) 241 (56.8 x 10^3), 279 (55.3 x 10^3).

Elemental Analysis . Found: C, 66.57; H, 5.48; N, 10.35. Calc for C$_{46}$H$_{44}$N$_6$O$_6$·0.5CHCl$_3$: C, 66.76; H, 5.36; N, 10.05%.

❖ 1,2-Bis(8-(4'-(2,2':6',2''-terpyridyl))-2,5,8-trioxaoctyl)benzene (**L6**)

L6a
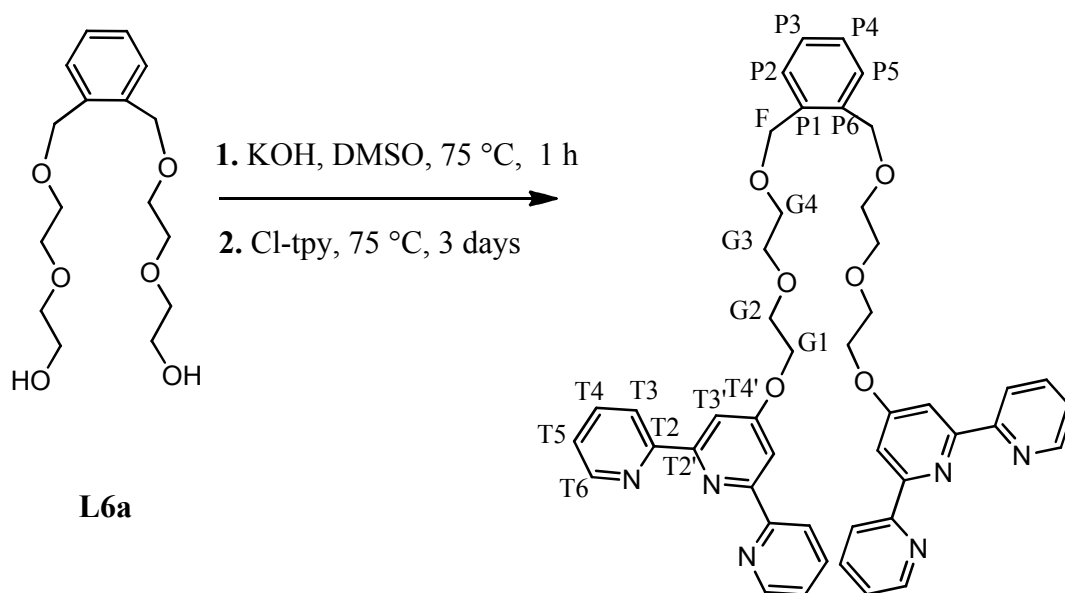
1,2-bis(8-(4'-(2,2':6',2''-terpyridyl))
-2,5,8-trioxaoctyl)benzene **(L6)**

Molecular formula: $C_{46}H_{44}N_6O_6$
Molecular weight: 776.88

Compound **L6** was synthesized according to general procedure for ditopic ligands with intermediate **L6a** (0.50 g, 1.6 mmol), finely powdered potassium hydroxide (0.31 g, 5.0 mmol) and Cl-tpy (1.4 g, 5.0 mmol). After column chromatography (Al$_2$O$_3$, CHCl$_3$), **L6** (0.78 g, 1.0 mmol, 65%) was obtained as a yellow oil. Other tpy containing products were not isolated.

^{1}H NMR (500 MHz, CDCl$_3$) δ$_H$ 3.27 (m, 4H, H^{G4}), 3.34 (m, 4H, H^{G3}), 3.48 (m, 4H, H^{G2}), 3.94 (m, 4H, H^{G1}), 4.26 (s, 4H, H^F), 6.88 (m, 2H, H$^{P2/P5}$ or H$^{P3/P4}$), 6.92 (m, 4H, H^{T5}), 7.01 (m, 2H, H$^{P2/P5}$ or H$^{P3/P4}$), 7.44 (t, *J* 7.6 Hz, 4H, H^{T4}), 7.65 (s, 4H, H$^{T3'}$), 8.20 (d, *J* 8.0 Hz, 4H, H^{T3}), 8.28 (d, *J* 3.9 Hz, 4H, H^{T6}).

^{13}C NMR (125 MHz, CDCl$_3$) δ_C 67. 0 (C^{G1}), 68.5 (C^{G2}), 68.9 (C^{G4}), 70.0 (C^{F}), 70.0 (C^{G3}), 106.5 (C$^{T3'}$), 120.5 (C^{T3}), 123.3 (C^{T5}), 126.9 (C$^{P2/P5}$ or C$^{P3/P4}$), 127.9 (C$^{P2/P5}$ or C$^{P3/P4}$), 135.7 (C^{P1,P6}), 136.1 (C^{T4}), 148.3 (C^{T6}), 155.0 (C^{T2}), 156.2 (C$^{T2'}$), 166.1 (C$^{T4'}$).

MS (ESI) m/z = 777.9 [**L6**+H]$^+$ (calc. 778.0).

IR (oil, $\widetilde{\nu}$/cm^{-1}): 1598m, 1583s, 1563s, 1556s, 1503s, 1468m, 1443s, 1404s, 1368m, 1348m, 1323m, 1291m, 1252w, 1205m, 1123s, 1091s, 1059s, 1037s, 991s, 973s, 967m, 941m, 929s, 904m, 847s, 791s, 743m, 733s, 697m, 655s, 644m, 621m.

UV/VIS (CH$_2$Cl$_2$):λ_{max}/ nm (ε_{max}, M^{-1} cm^{-1}) 241 (56.5 x 10^3), 279 (55.6 x 10^3).

Elemental Analysis . Found: C, 65.60; H, 5.80; N, 9.55. Calc. for C$_{46}$H$_{44}$N$_6$O$_6$·H$_2$O·0.5CHCl$_3$: C, 65.35; H, 5.48; N, 9.83%.

❖ 1,2-Bis(7-(4'-(2,2':6',2"-terpyridyl))-1,4,7-trioxaheptyl)benzene (**L7**)
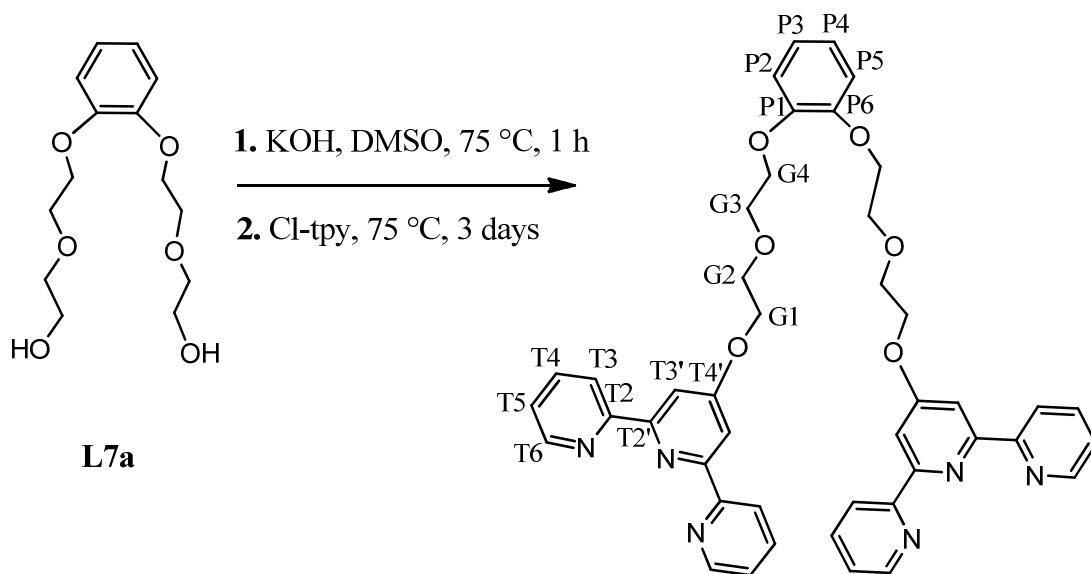
1,2-bis(7-(4'-(2,2':6',2"-terpyridyl))
-1,4,7-trioxaheptyl)benzene **(L7)**

Molecular formula: $C_{44}H_{40}N_6O_6$
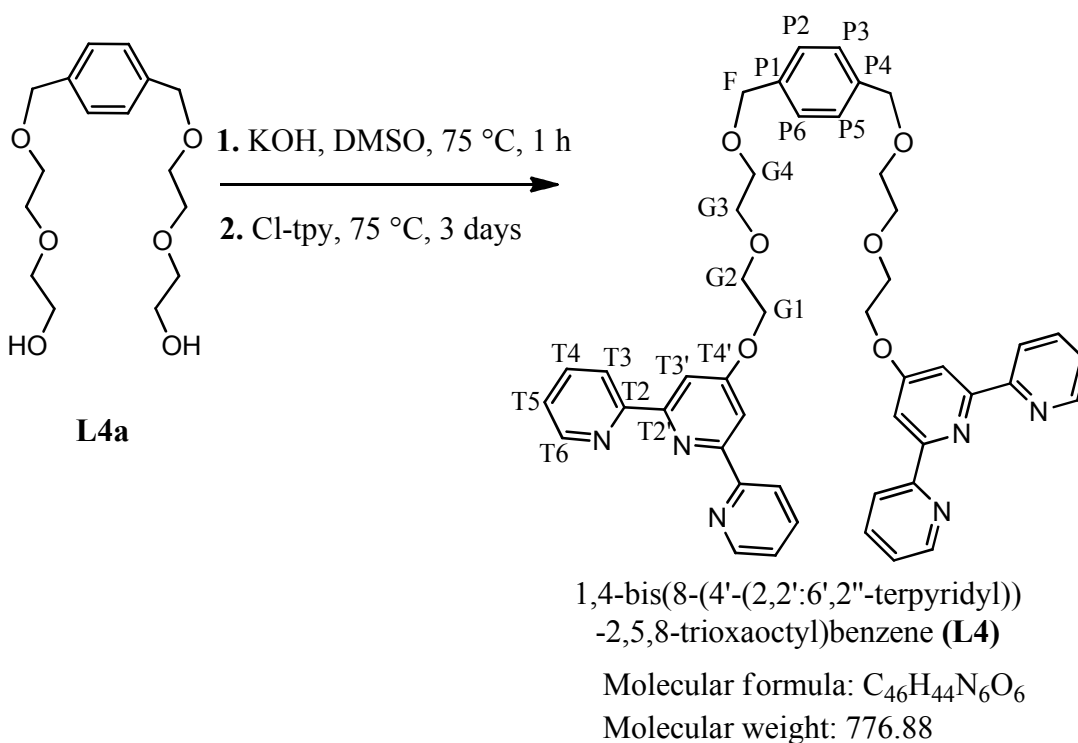Molecular weight: 748.83

Compound **L7** was synthesized according to general procedure for ditopic ligands with intermediate **L7a** (0.50 g, 1.8 mmol), finely powdered potassium hydroxide (0.31 g, 5.0 mmol) and Cl-tpy (1.4 g, 5.0 mmol). After column chromatography (Al_2O_3, $CHCl_3$), **L7** (0.82 g, 1.1 mmol, 63%) was obtained as a yellow oil. Other tpy containing products were not isolated.

^{1}H NMR (500 MHz, $CDCl_3$) δ_H 3.92 (m, 4H, H^{G3}), 3.96 (m, 4H, H^{G2}), 4.17 (m, 4H, H^{G4}), 4.34 (m, 4H, H^{G1}), 6.84-6.88 (m, 2H, $H^{P3/P4}$), 6.88-6.92 (m, 2H, $H^{P2/P5}$), 7.25 (m, 4H, H^{T5}), 7.77 (td, J 1.6, 7.8 Hz, 4H, H^{T4}), 7.99 (s, 4H, $H^{T3'}$), 8.54 (d, J 7.9 Hz, 4H, H^{T3}), 8.62 (d, J 4.7 Hz, 4H, H^{T6}).

^{13}C NMR (125 MHz, CDCl$_3$) δ_C 68.0 (C^{G1}), 69.2 (C^{G4}), 69.8 (C^{G2}), 70.3 (C^{G3}), 107.6 (C$^{T3'}$), 115.3 (C$^{P2/P5}$), 121.4 (C^{T3}), 121.9 (C$^{P3/P4}$), 123.9 (C^{T5}), 136.8 (C^{T4}), 149.2 (C^{T6} and C$^{P1/P6}$), 156.1 (C^{T2}), 157.2 (C$^{T2'}$), 167.1 (C$^{T4'}$).

MS (ESI) m/z = 749.9 [**L7**+H]$^+$ (calc. 750.0).

m.p.: 99-102 °C

IR (oil, $\widetilde{\nu}$/cm^{-1}): 1599m, 1582s, 1556s, 1504m, 1468m, 1441s, 1404s, 1369m, 1350s, 1323m, 1300w, 1292w, 1254s, 1234m, 1202s, 1124s, 1097s, 1090s, 1053s, 1039s, 991s, 972m, 962m, 941m, 928s, 905m, 866s, 845m, 823m, 790s, 741s, 730s, 698s, 657s, 646m, 621m.

UV/VIS (CH$_2$Cl$_2$):λ_{max}/ nm (ε_{max}, M^{-1} cm^{-1}) 241 (57.5 x 10^3), 279 (55.6 x 10^3).

Elemental Analysis : Found: C, 61.67; H, 5.47; N, 9.75. Calc. for C$_{44}$H$_{40}$N$_6$O$_6$·2H$_2$O·0.75CHCl$_3$: C, 61.47; H, 5.16; N, 9.61%.

CHAPTER 3

Synthesis of heteroleptic dinuclear ruthenium(II) complexes of ditopic 4'-substituted- 2,2':6',2''-terpyridine ligands

3.1   Introduction

The photochemical and photophysical properties of ruthenium(II) complexes of 2,2'-bipyridine (bpy) and its derivatives have been widely studied over the past 30 years.[123-138] Most widely investigated are their redox properties, luminescence intensities and excited state lifetimes.[123,124,139] Despite the fact that ruthenium(II) complexes of 2,2':6',2''-terpyridine derivatives show lower luminescence intensities and shorter excited state lifetimes at room temperature than those of 2,2'-bipyridine and its derivatives, they are still of great interest, due to their synthetic and structural advantages (see Section 1.3).[124,139,140] Their potential applications as energy- and electron- transmitters has been explored in details.[141-159]

2,2':6',2''-Terpyridine derivatives can form metal complexes with a variety of transition metal ions. When tridentate tpy-based ligands react with ruthenium(II) ions, achiral octahedral complexes are usually formed (**Scheme 3.1**).[160] Ruthenium(II) is a d^6 ion, in the low-spin state. Its complexes are kinetically inert and relatively stable.
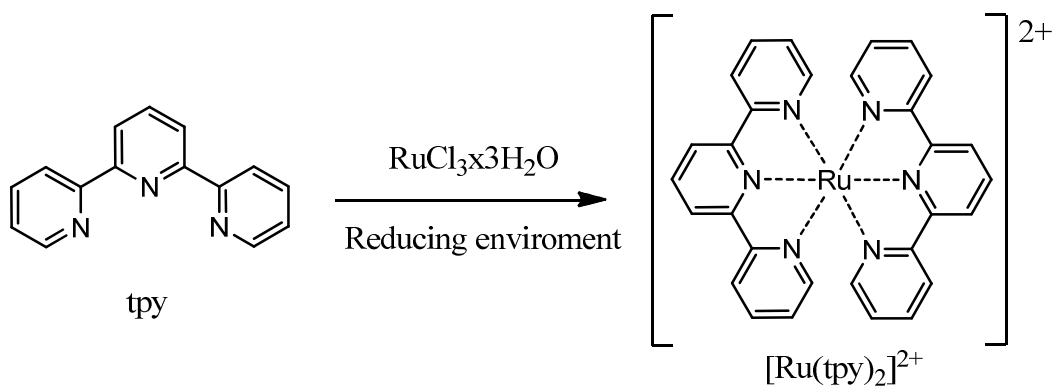
Scheme 3.1. Reaction of 2,2':6',2''-terpyridine with $RuCl_3x3H_2O$ in reducing enviroment.

In this chapter, heteroleptic dinuclear ruthenium(II) complexes of ditopic 4'-substituted-2,2':6',2"-terpyridine ligands are discussed (**Scheme 3.2**).

[(*p*-ttpy)Ru(**L1**)(Ru)(*p*-ttpy)][PF$_6$]$_4$

[(tpy)Ru(**L2**)(Ru)(tpy)][PF$_6$]$_4$

[(tpy)Ru(**L4**)(Ru)(tpy)][PF$_6$]$_4$

[(tpy)Ru(**L7**)(Ru)(tpy)][PF$_6$]$_4$

[(tpy)Ru(**L6**)(Ru)(tpy)][PF$_6$]$_4$
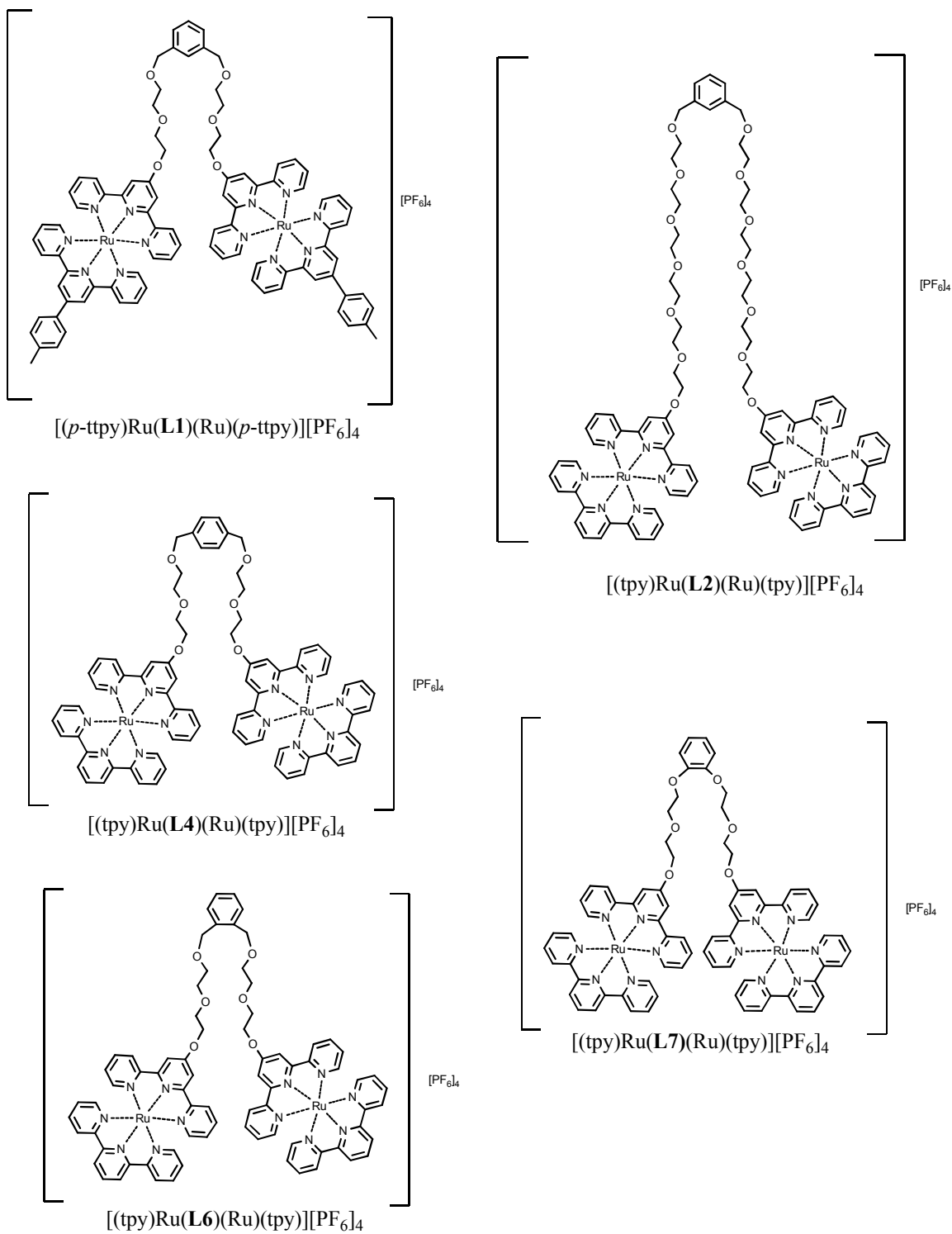
Scheme 3.2. Ruthenium(II) complexes of ditopic 4'-substituted- 2,2':6',2"-terpyridine ligands studied in this chapter.

3.2 Synthesis

Heteroleptic dinuclear ruthenium(II) complexes of ligands **L1**, **L2**, **L4**, **L6** and **L7** were prepared stepwise in a Biotage microwave reactor. First one equivalent of $RuCl_3 \cdot 3H_2O$ and one equivalent of *p*-ttpy (for complex with ligand **L1**) (**Scheme 3.3**) or tpy (for complexes with ligands **L2**, **L4**, **L6** and **L7**) (**Scheme 3.4**) were heated under microwave conditions in ethanol at 135 °C for 15 minutes. Then 0.5 equivalent of ditopic ligand (**L^b**) and the reducing agent *N*-ethylmorpholine (NEM) were added and the mixture was again treated as described above. Red ruthenium(II) complexes were precipitated from solution with excess aqueous NH_4PF_6 and then filtered and collected. The yield of [(X-tpy)Ru(**L^b**)(Ru)(X-tpy)][PF_6]$_4$ complexes ranged from 89-93%.

1. $RuCl_3 \cdot 3H_2O$, EtOH, 135 °C, 15 min, microwave reactor

2. L1, EtOH, NEM, 135 °C, 30 min, microwave reactor

3. NH_4PF_6

[(*p*-ttpy)Ru(**L1**)(Ru)(*p*-ttpy)][PF_6]$_4$

p-ttpy = 4'-(*p*-tolyl)-2,2':6',2''-terpyridine
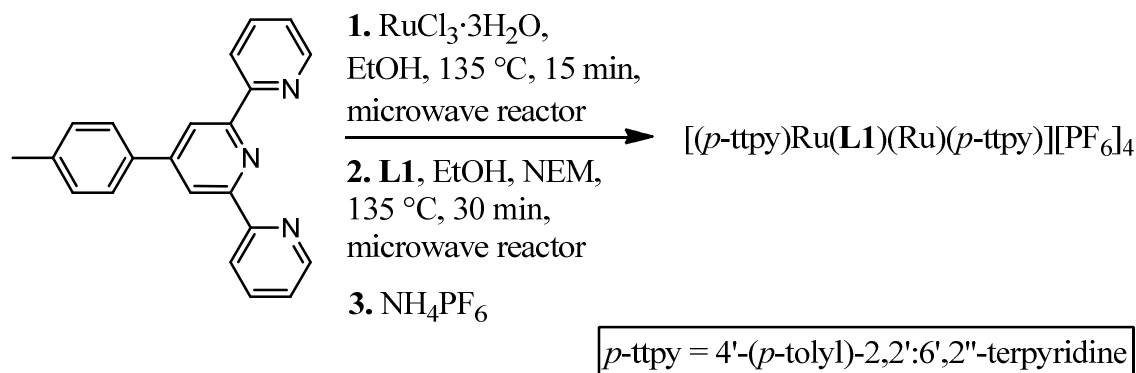
Scheme 3.3. Synthesis of [(*p*-ttpy)Ru(**L1**)(Ru)(*p*-ttpy)][PF_6]$_4$.

1. $RuCl_3 \cdot 3H_2O$, EtOH, 135 °C, 15 min, microwave reactor

2. L^b, EtOH, NEM, 135 °C, 30 min, microwave reactor

3. NH_4PF_6

[(tpy)Ru(**L^b**)(Ru)(tpy)][PF_6]$_4$
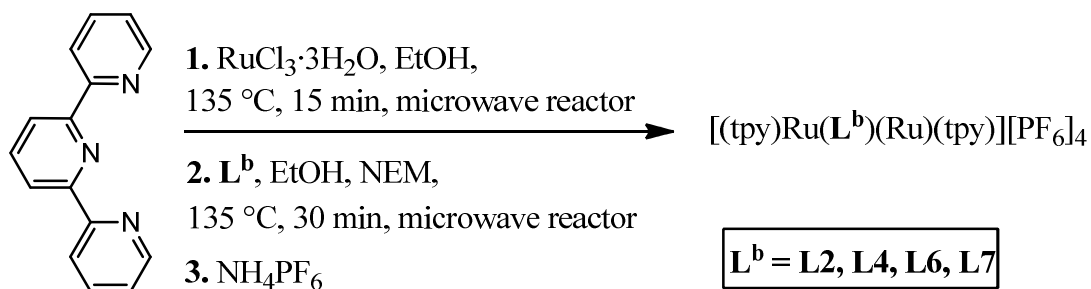
L^b = L2, L4, L6, L7

Scheme 3.4. The general synthesis of [(tpy)Ru(**L^b**)(Ru)(tpy)][PF_6]$_4$, where **L^b = L2**, **L4**, **L6**, **L7**.

3.3 ^{1}H NMR spectroscopy

All of the complexes were characterized by ^{1}H NMR spectroscopy in CD$_3$CN solution. The ^{1}H NMR spectra of the complexes were similar to those of other related bis(terpyridine) systems. The terpyridine proton signals, from both types of tpy units – from ditopic ligand **L** and the monotopic tpy ligand - are very similar or almost identical in all complexes (**Tables 3.1** and **3.2**).

The aromatic part of the ^{1}H NMR spectrum of [(tpy)Ru(**L4**)(Ru)(tpy)][PF$_6$]$_4$ in CD$_3$CN is shown in **Figure 3.1**. The proton signals from rings A and B of the unsubstituted tpy are highlighted in green, the proton signals from ligand **L4** in red.
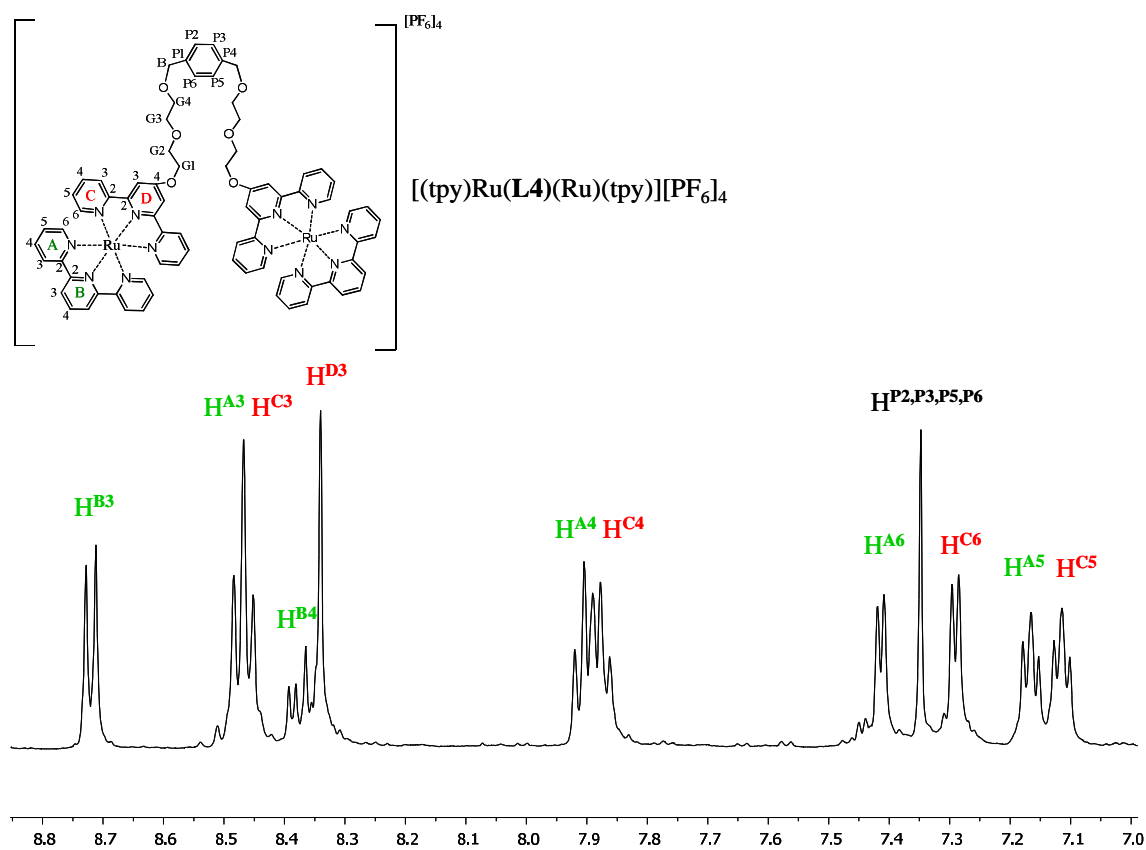
Figure 3.1. Aromatic region of the ^{1}H NMR spectrum (500 MHz, 295 K) of [(tpy)Ru(**L4**)(Ru)(tpy)][PF$_6$]$_4$ in CD$_3$CN. Signals for **H^{A3}** and **H^{C3}** overlap to give in experiment triplet (see experimental for integrations).
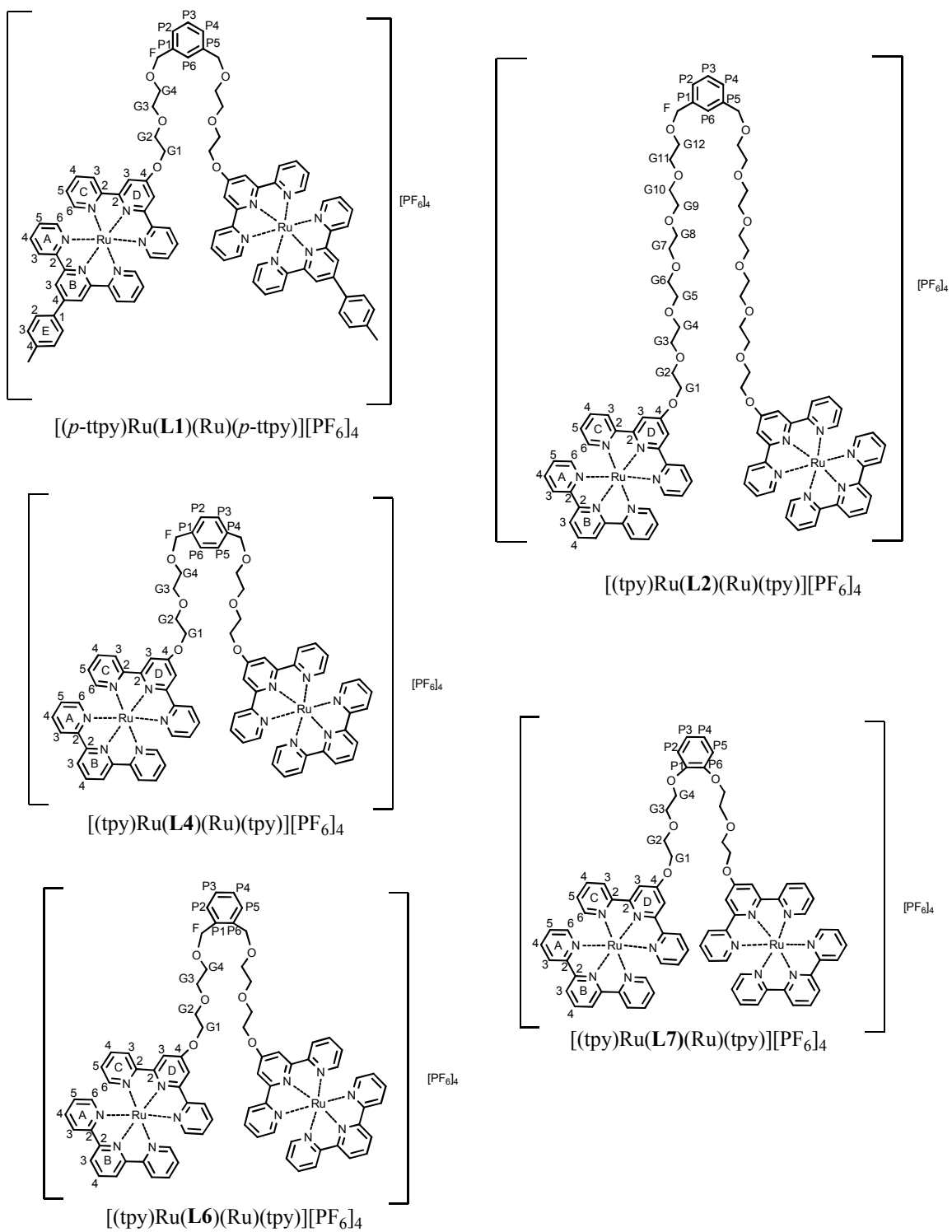
Scheme 3.5. Labeling for ruthenium(II) complexes of ditopic 4'-substituted- 2,2':6',2"-terpyridine ligands studied in this chapter.

	$H^{G4/-G12}$	H^{G3}	H^{G2}	H^{G1}	H^{F}	H^{B3}	H^{D3}	H^{B4} or $H^{E3,E3}$
[(p-ttpy)Ru(**L1**)(Ru)(p-ttpy)][PF$_6$]$_4$	3.72 (m)	3.79 (m)	4.02 (m)	4.66 (m)	4.63 (s)	8.72 (d) J 8.2 Hz	8.33 (s)	8.34-8.40 (m)
[(tpy)Ru(**L2**)(Ru)(tpy)][PF$_6$]$_4$	3.65-3.75 (m)	3.80 (m)	4.06 (m)	4.67 (m)	4.56 (s)	8.72 (d) J 8.1 Hz	8.30-8.45 (m)	8.30-8.45 (m)
[(tpy)Ru(**L4**)(Ru)(tpy)][PF$_6$]$_4$	3.69 (m)	3.80 (m)	4.06 (m)	4.67 (m)	4.54 (s)	8.72 (d) J 8.1 Hz	8.34 (s)	8.33-8.45 (m)
[(tpy)Ru(**L6**)(Ru)(tpy)][PF$_6$]$_4$	3.75 (m)	3.83 (m)	4.06 (m)	4.67 (m)	4.70 (s)	8.73 (d) J 8.2 Hz	8.34 (s)	8.35-8.45 (m)
[(tpy)Ru(**L7**)(Ru)(tpy)][PF$_6$]$_4$	4.26 (m)	4.03 (m)	4.15 (m)	4.72 (m)	—	8.72 (d) J 8.2 Hz	8.34 (s)	8.35-8.43 (m)

Table 3.1. ^{1}H NMR spectroscopic data, δ_H [ppm], (500 MHz, 295 K, CD$_3$CN) for ruthenium(II) complexes of ligands **L1**, **L2**, **L4**, **L6** and **L7** (see page 89 for scheme of labeling).

	H^{C3}	H^{C4}	H^{C5}	H^{C6}	H^{A3}	H^{A4}	H^{A5}	H^{A6}
[(p-ttpy)Ru(**L1**)(Ru)(p-ttpy)][PF$_6$]$_4$	8.45 (d) J 9.0 Hz	7.75- 7.95 (m)	7.11 (m)	7.25- 7.45 (m)	8.46 (d) J 9.0 Hz	7.75- 7.95 (m)	7.16 (m)	7.25- 7.45 (m)
[(tpy)Ru(**L2**)(Ru)(tpy)][PF$_6$]$_4$	8.45- 8.50 (m)	7.82- 7.94 (m)	7.11 (m)	7.29 (d) J 5.3 Hz	8.45- 8.50 (m)	7.82- 7.94 (m)	7.17 (m)	7.41 (d) J 4.9 Hz
[(tpy)Ru(**L4**)(Ru)(tpy)][PF$_6$]$_4$	8.46 (d) J 8.0 Hz	7.82- 7.94 (m)	7.11 (m)	7.29 (d) J 5.5 Hz	8.47 (d) J 8.0 Hz	7.82- 7.94 (m)	7.17 (m)	7.41 (d) J 5.4 Hz
[(tpy)Ru(**L6**)(Ru)(tpy)][PF$_6$]$_4$	8.46 (d) J 9.2 Hz	7.85- 7.95 (m)	7.11 (m)	7.30 (d) J 5.3 Hz	8.47 (d) J 9.2 Hz	7.85- 7.95 (m)	7.15 (m)	7.43 (d) J 5.6 Hz
[(tpy)Ru(**L7**)(Ru)(tpy)][PF$_6$]$_4$	8.43- 8.51 (m)	7.85- 7.95 (m)	7.10 (m)	7.29 (d) J 5.3 Hz	8.43- 8.51 (m)	7.85- 7.95 (m)	7.16 (m)	7.42 (d) J 5.3 Hz

Table 3.2. ^{1}H NMR spectroscopic data, δ_H [ppm], (500 MHz, 295 K, CD$_3$CN) for ruthenium(II) complexes of ligands **L1**, **L2**, **L4**, **L6** and **L7** (see page 89 for scheme of labeling).
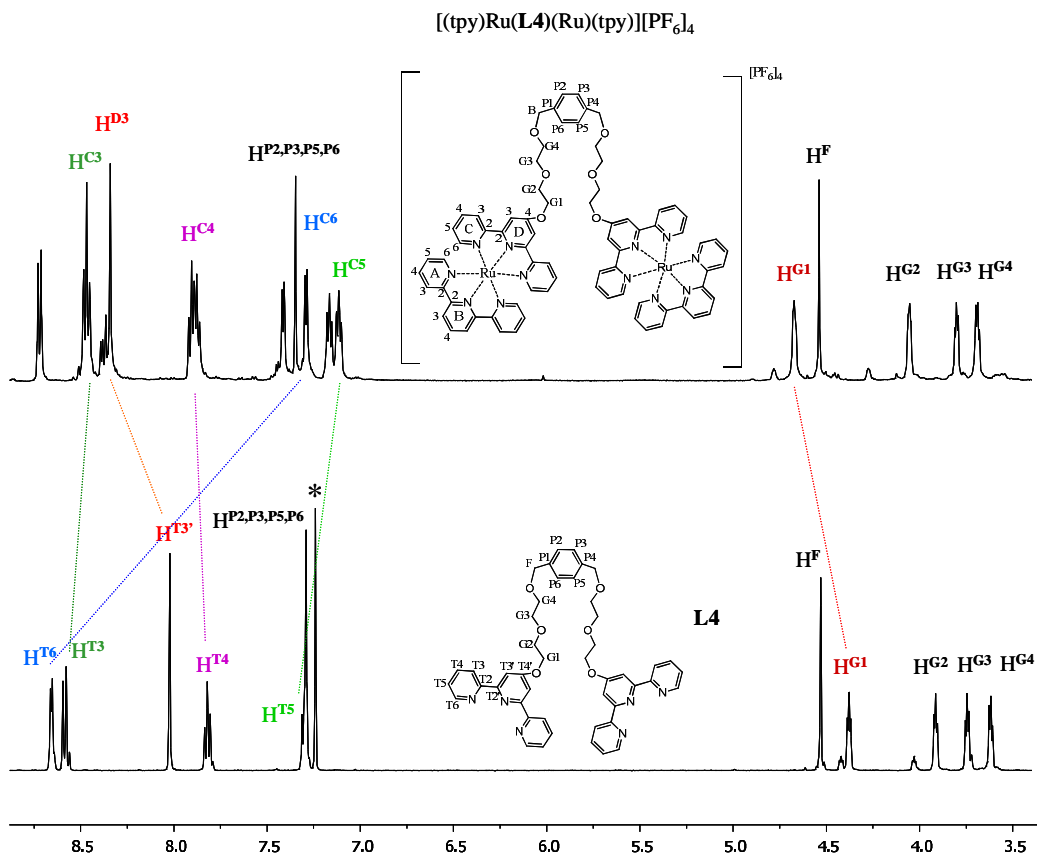
Figure 3.2. ^{1}H NMR spectra (500 MHz, 295 K) of **L4** in CDCl$_3$ (below) and [(tpy)Ru(**L4**)(Ru)(tpy)][PF$_6$]$_4$ in CD$_3$CN (above). Spectra exhibit some residues of the starting material, which could not be removed by purify.

Figure 3.2 shows how the ^{1}H NMR spectrum of ligand **L4** changes, after complexation with ruthenium(II). All of the signals are influenced by addition of the ruthenium(II) to the system but most changed is the proton signal **H^{T6}** of ligand **L4**, which is shifted 1.37 ppm upfield (**H^{C6}**). The proton signals for **H$^{T3'}$** and **H^{G1}** of ligand **L4** are both shifted around 0.3 ppm downfield in the ^{1}H NMR spectrum of [(tpy)Ru(**L4**)(Ru)(tpy)][PF$_6$]$_4$.

The proton signals in the aliphatic region for heteroleptic ruthenium(II) complexes of ligands **L1** and **L2** exhibit the same behavior as ligand **L4**. However, the signal assigned to the **H^F** proton of the complex with ligand **L7** is shifted much further downfield than the signal from the **H^F** proton of any other complex. Also the **H^G** proton signals of ligand **L7** are all shifted downfield in comparison to other complexes (**Table 3.1**).

3.4 ^{13}C NMR spectroscopy

Table 3.3 shows the ethylene glycol $\mathbf{C^G}$, $\mathbf{C^F}$ and phenyl $\mathbf{C^P}$ carbon signals for heteroleptic dinuclear ruthenium(II) complexes of ligands **L1-L2, L4** and **L6-L7** in CD$_3$CN solution. All of the terpyridine carbon signals, from both types of tpy units – from ditopic ligand **L** and the monotopic tpy ligand - are shown in **Tables 3.4** and **3.5**. The assignments were made using HMQC and HMBC techniques. The terpyridine carbon signals are similar in all of the complexes and comparable to other related bis(terpyridine) systems[79-82].

	$C^{G4/-G12}$	C^{G3}	C^{G2}	C^{G1}	C^F	C^P	C^P quatern.	C^E
[(p-ttpy)Ru(**L1**)(Ru)(p-ttpy)][PF$_6$]$_4$	70.3	71.9	69. 8	70.7	68.6	128.5	138.9	128.5, 138.9
[(tpy)Ru(**L2**)(Ru)(tpy)][PF$_6$]$_4$	70.5, 70.6, 70.6, 70. 7	71.69	70.0	70.9	73.5	128.5	139.0	—
[(tpy)Ru(**L4**)(Ru)(tpy)][PF$_6$]$_4$	70.6	71.69	70.0	70.9	73.5	128.8	139.0	—
[(tpy)Ru(**L6**)(Ru)(tpy)][PF$_6$]$_4$	70.7	71.3	70.0	70.9	71.6	128.7, 129.6	139.0	—
[(tpy)Ru(**L7**)(Ru)(tpy)][PF$_6$]$_4$	69.7	70.9	70.2	70.8	—	115.7, 124.8	149.9	—

Table 3.3. ^{13}C NMR spectroscopic data, δ_H [ppm], (125 MHz, 295 K, CD$_3$CN) for ruthenium(II) complexes of ligands **L1**, **L2**, **L4**, **L6** and **L7** (see page 89 for scheme of labeling).

	C^{C2}	C^{C3}	C^{C4}	C^{C5}	C^{C6}	C^{D2}	C^{D3}	C^{D4}
[(p-ttpy)Ru(**L1**)(Ru)(p-ttpy)][PF$_6$]$_4$	157.0	125.5	138.9	128.5	153.8	159.0	112.1	167.2
[(tpy)Ru(**L2**)(Ru)(tpy)][PF$_6$]$_4$	157.0	125.5	138.9	128.5	153.8	159.1	112.0	167.3
[(tpy)Ru(**L4**)(Ru)(tpy)][PF$_6$]$_4$	157.0	125.5	138.9	128.5	153.8	159.1	112.2	167.3
[(tpy)Ru(**L6**)(Ru)(tpy)][PF$_6$]$_4$	157.0	125.5	138.9	128.5	153.7	159.1	112.2	167.3
[(tpy)Ru(**L7**)(Ru)(tpy)][PF$_6$]$_4$	157.0	125.4	138.9/ 139.0	128.5	153.8	159.1	112.2	167.3

Table 3.4. ^{13}C NMR spectroscopic data, δ_H [ppm], (125 MHz, 295 K, CD$_3$CN) for ruthenium(II) complexes of ligands **L1**, **L2**, **L4**, **L6** and **L7** (see page 89 for scheme of labeling).

	C^{A2}	C^{A3}	C^{A4}	C^{A5}	C^{A6}	C^{B2}	C^{B3}	C^{B4}
[(p-ttpy)Ru(**L1**)(Ru)(p-ttpy)][PF$_6$]$_4$	156.9	125.3	138.9	128.5	153.3	159.3	124.7	136.3
[(tpy)Ru(**L2**)(Ru)(tpy)][PF$_6$]$_4$	156.9	125.3	138.9	128.5	153.3	159.3	124.6	136.3
[(tpy)Ru(**L4**)(Ru)(tpy)][PF$_6$]$_4$	156.9	125.3	138.9	128.5	153.3	159.3	124.7	136.3
[(tpy)Ru(**L6**)(Ru)(tpy)][PF$_6$]$_4$	156.9	125.3	138.9	128.5	153.3	159.3	124.7	136.3
[(tpy)Ru(**L7**)(Ru)(tpy)][PF$_6$]$_4$	156.9	125.3	138.9/ 139.0	128.5	153.3	159.2	124.7	136.3

Table 3.5. ^{13}C NMR spectroscopic data, δ_H [ppm], (125 MHz, 295 K, CD$_3$CN) for ruthenium(II) complexes of ligands **L1**, **L2**, **L4**, **L6** and **L7** (see page 89 for scheme of labeling).

3.5 Mass spectroscopic characterization

Electrospray ionization mass spectroscopy (ESI) was used to characterize the new heteroleptic dinuclear ruthenium(II) complexes. The peaks are observed as the ratio of mass to the charge of the species (m/z). All of the peaks show the typical isotope distribution of two ruthenium atoms. Normally, the $[\mathbf{M}\text{-}2PF_6]^{2+}$ peak was found as the major peak for these dinuclear ruthenium(II) complexes but $[\mathbf{M}\text{-}3PF_6]^{3+}$ and $[\mathbf{M}\text{-}4PF_6]^{4+}$ can be also observed. Charge on the ion was confirmed by the peak separations in each peak-envelope, as shown in **Figure 3.3** for a 2+ ion.

	$[\mathbf{M}\text{-}2PF_6]^{2+}$	$[\mathbf{M}\text{-}3PF_6]^{3+}$	$[\mathbf{M}\text{-}4PF_6]^{4+}$
[(*p*-ttpy)Ru(**L1**)(Ru)(*p*-ttpy)][PF$_6$]$_4$	958.2	590.5	—
[(tpy)Ru(**L2**)(Ru)(tpy)][PF$_6$]$_4$	1044.2	—	449.6
[(tpy)Ru(**L4**)(Ru)(tpy)][PF$_6$]$_4$	868.3	530.5	361.7
[(tpy)Ru(**L6**)(Ru)(tpy)][PF$_6$]$_4$	868.1	530.4	—
[(tpy)Ru(**L7**)(Ru)(tpy)][PF$_6$]$_4$	854.1	521.1	354.6

Table 3.6. The ESI-MS data for ruthenium(II) complexes with **L1, L2, L4, L6** and **L7**

In **Figure 3.3** the ESI-MS spectrum of [(tpy)Ru(**L4**)(Ru)(tpy)][PF$_6$]$_4$ is shown. The major signal is a peak at m/z 530.5 and was assigned to $[\mathbf{M}\text{-}3PF_6]^{3+}$. The other two signals at m/z 868.3 and 361.7 correspond to $[\mathbf{M}\text{-}2PF_6]^{2+}$ and $[\mathbf{M}\text{-}4PF_6]^{4+}$, respectively. The inset shows an expansion of the peak at m/z 868.3 ($[\mathbf{M}\text{-}2PF_6]^{2+}$). The observed isotope pattern matches that of the simulated spectrum.
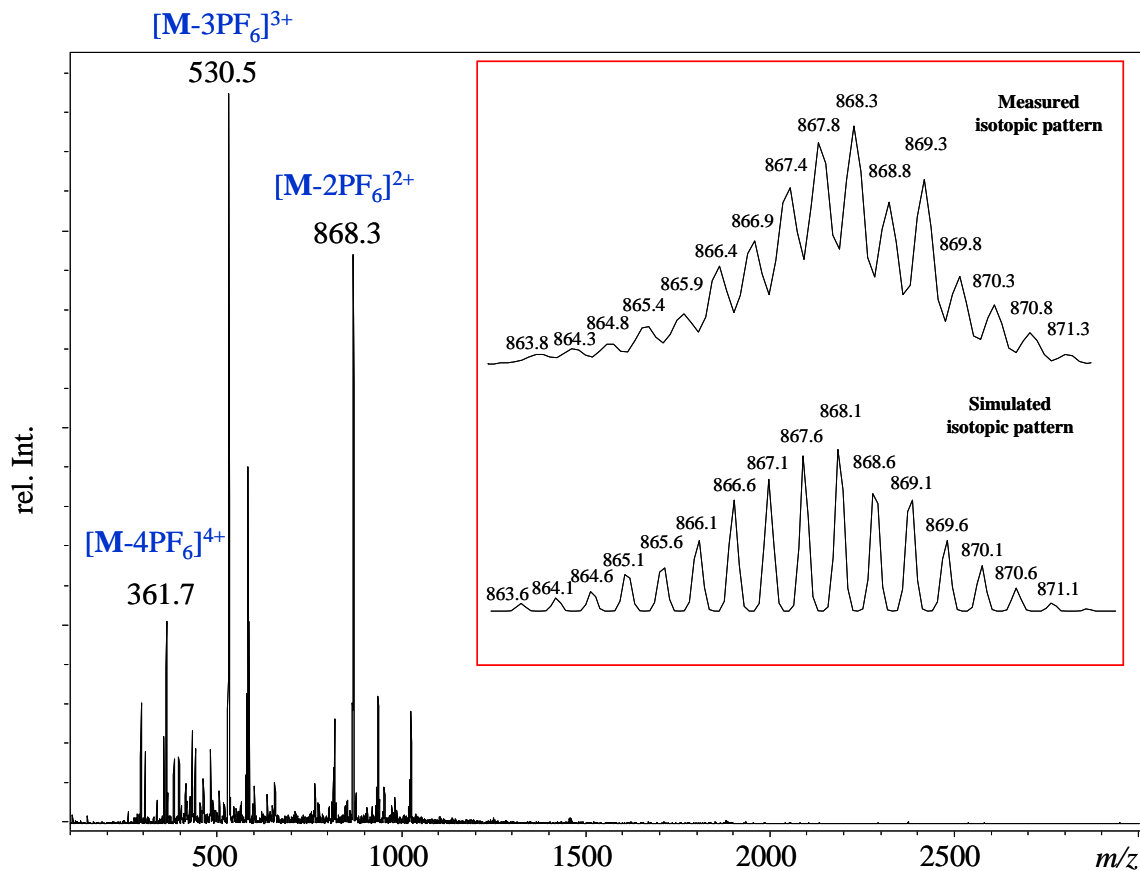
Figure 3.3. ESI-MS spectrum of [(tpy)Ru(**L4**)(Ru)(tpy)][PF$_6$]$_4$.

3.6 Electrochemical studies

The redox properties of the ruthenium(II) complexes have been investigated using the cyclic voltammetry method (CV). One typical example is shown in **Figure 3.4** for the cyclic voltammogram of [(tpy)Ru(**L4**)(Ru)(tpy)][PF$_6$]$_4$ in degassed acetonitrile solution. The oxidation of ruthenium(II) in the complexes introduced in this chapter typically occurs around 830 mV (**Table 3.7**). There are three reduction processes, two of them are reversible, around -1.69 and -1.92 V, one is irreversible, at -2.44 V (**Table 3.7**). The potentials were measured versus Ferrocene^0/Ferrocenium$^+$ (Fc/Fc$^+$).
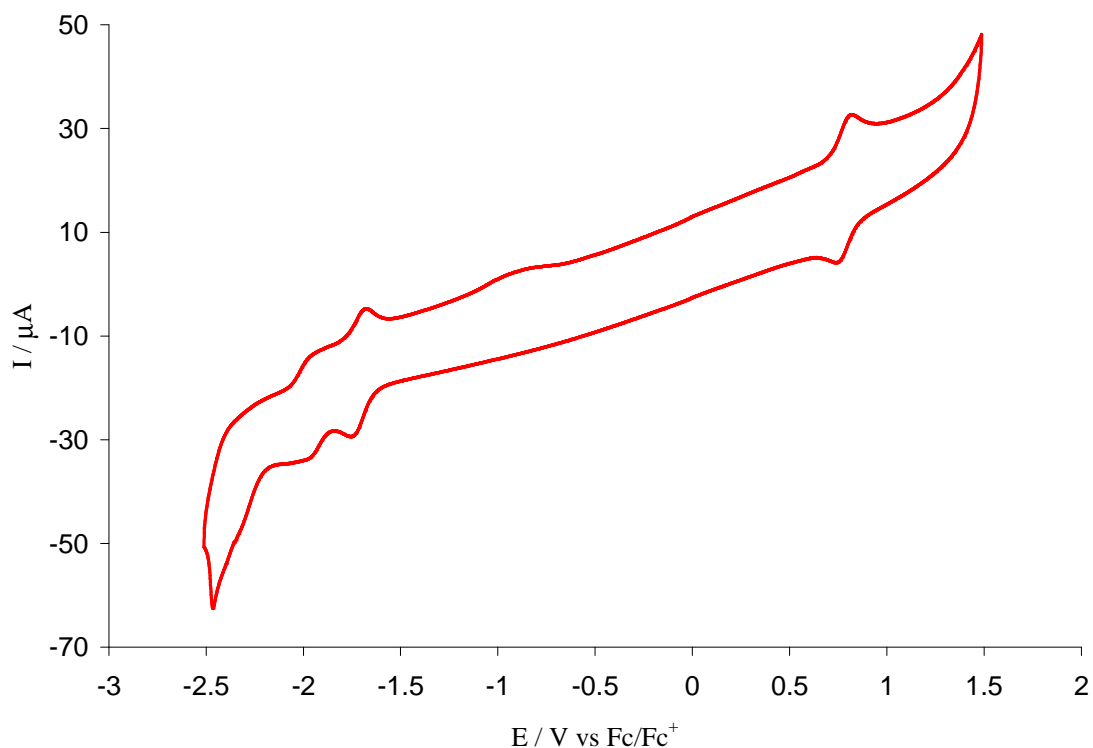
Figure 3.4. Cyclic voltammogram of [(tpy)Ru(**L4**)(Ru)(tpy)][PF$_6$]$_4$ (1 mM) in degassed acetonitrile containing 0.1 M [^{n}Bu$_4$N][PF$_6$], scan rate = 100 mVs^{-1}.

	Potential [V] vs Fc/Fc$^+$	
	oxidation	reduction
[(Ru)(tpy)$_2$][PF$_6$]$_2$	0.92[a]	-1.67[a], -1.92[a]
[(p-ttpy)Ru(**L1**)(Ru)(p-ttpy)][PF$_6$]$_4$	0.83[a]	-1.69[a], -1.92[a], -2.44[b]
[(tpy)Ru(**L2**)(Ru)(tpy)][PF$_6$]$_4$	0.83[a]	-1.69[a], -1.92[a], -2.44[b]
[(tpy)Ru(**L4**)(Ru)(tpy)][PF$_6$]$_4$	0.83[a]	-1.69[a], -1.92[a], -2.44[b]
[(tpy)Ru(**L6**)(Ru)(tpy)][PF$_6$]$_4$	0.83[a]	-1.69[a], -1.92[a], -2.44[b]
[(tpy)Ru(**L7**)(Ru)(tpy)][PF$_6$]$_4$	0.83[a]	-1.69[a], -1.92[a], -2.44[b]

Table 3.7. Redox potentials measured for ruthenium(II) complexes in argon-purged solutions of acetonitrile. E$_{1/2}$ values are given for reversible processes ([a]) from the cyclic voltammetry and for irreversible processes ([b]) from square wave.

For comparison, in **Table 3.7** oxidation and reduction potentials for the homoleptic ruthenium(II) complex $[(Ru)(tpy)_2][PF_6]_2$ are also shown This homoleptic complex shows the Ru(II)/Ru(III) process at higher reduction/oxidation potential than the ruthenium(II) complexes introduced in this chapter. This indicates that these substituents in the 4'-position of the terpyridine ligands (**L1-L2**, **L4** and **L6-L7**) have higher electron donating properties than a hydrogen atom in the 4'-position of 2,2':6',2"-terpyridine.[160]

3.7 Absorption spectroscopic characterization

The electronic spectra of the heteroleptic dinuclear ruthenium(II) complexes were recorded in HPLC grade acetonitrile solution. The very intense bands in the UV region are assigned to the ligand-centered (LC) $\pi^* \leftarrow \pi$ transitions (**Table 3.8**). The ruthenium(II) complexes exhibit a low energy metal-to-ligand charge transfer (MLCT) transition with λ_{max} at 480 nm (**Table 3.8**). The MLCT transitions occur when an electron is transferred from the metal-centered d orbital to an unfilled ligand-centered π^* orbital.

For comparison, in **Table 3.8** electronic spectroscopic data for the homoleptic ruthenium(II) complex $[(Ru)(tpy)_2][PF_6]_2$ are also shown The MLCT bands of heteroleptic ruthenium(II) complexes are red shifted in comparison to the homoleptic $[(Ru)(tpy)_2][PF_6]_2$ complex. Balzani and Constable *et al.*[161] have reported that there is a red shift of the MLCT band of ruthenium(II) complexes irrespective of whether the substituent at the 4'-position of the terpyridine ligand is electron-donating or electron-accepting.

It seems that there is no influence on the absorption data when the length of the linkage is changed, nor when the substitution position on the benzyl ring is altered.

	λ_{max}/nm ($\varepsilon_{max}/10^3$ M^{-1} cm^{-1})	
	LC	MLCT
[(Ru)(tpy)$_2$][PF$_6$]$_2$	268 (67), 305 (111)	473 (25)
[(*p*-ttpy)Ru(**L1**)(Ru)(*p*-ttpy)][PF$_6$]$_4$	241 (110), 269 (115), 305 (140)	480 (40)
[(tpy)Ru(**L2**)(Ru)(tpy)][PF$_6$]$_4$	241 (107), 269 (116), 305 (141)	480 (41)
[(tpy)Ru(**L4**)(Ru)(tpy)][PF$_6$]$_4$	241 (108), 269 (116), 305 (140)	480 (40)
[(tpy)Ru(**L6**)(Ru)(tpy)][PF$_6$]$_4$	241 (108), 269 (115), 305 (139)	480 (39)
[(tpy)Ru(**L7**)(Ru)(tpy)][PF$_6$]$_4$	241 (105), 269 (113), 305 (139)	480 (38)

Table 3.8. Electronic spectroscopic data for the ruthenium(II) complexes in acetonitrile solution.
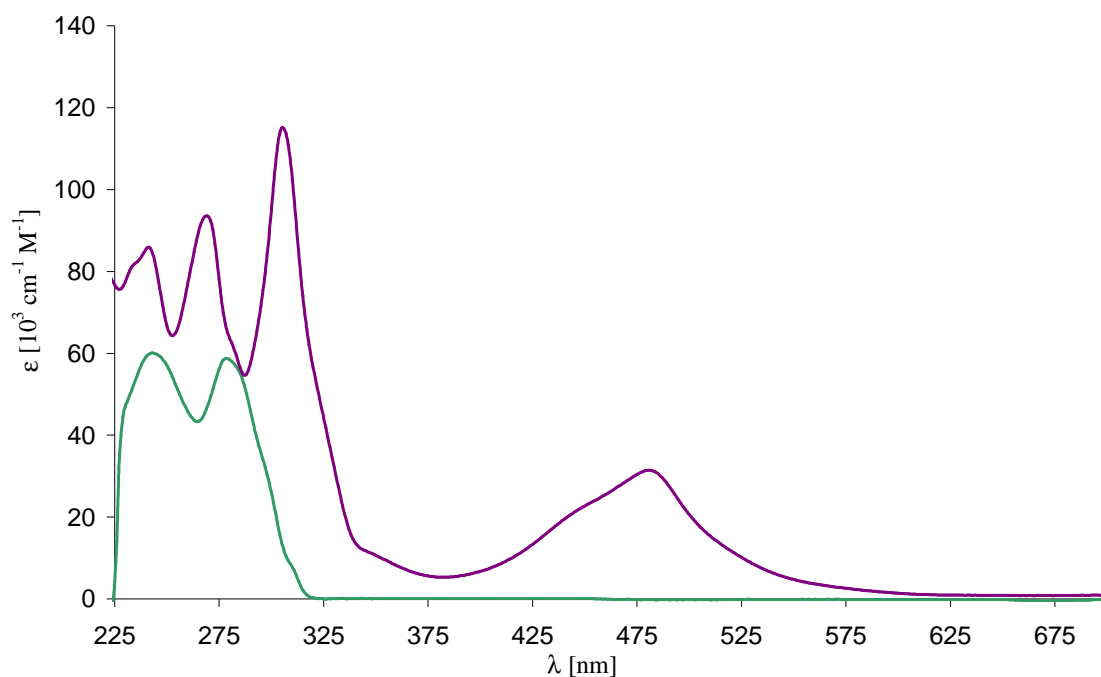
Figure 3.3. Absorption spectra of ligand **L4** in CH$_2$Cl$_2$ (in green) and [(tpy)Ru(**L4**)(Ru)(tpy)][PF$_6$]$_4$ in CH$_3$CN (in violet).

In **Figure 3.3** absorption spectra of ligand **L4** (in green) and [(tpy)Ru(**L4**)(Ru)(tpy)][PF$_6$]$_4$ (in violet) are shown for comparison. In contrast to the absorption spectrum of [(tpy)Ru(**L4**)(Ru)(tpy)][PF$_6$]$_4$, for uncomplexed ligand **L4** there are only two bands in the high energy UV region, assigned to ligand-centered (LC) $\pi^* \leftarrow \pi$ and/or $\pi^* \leftarrow$ n transitions with λ_{max} at 241 and 279 nm. Both bands are only half as intense as the LC bands for [(tpy)Ru(**L4**)(Ru)(tpy)][PF$_6$]$_4$, ($\varepsilon_{max}/10^3$ M^{-1} cm^{-1} : 56.8 and 55.3).

3.8 Conclusion

The heteroleptic dinuclear ruthenium(II) complexes of the ditopic 4'-substituted-2,2':6',2''-terpyridine ligands **L1-L2**, **L4** and **L6-L7,** which are based on a benzene unit connected to two 4'-substituted-2,2':6',2''-terpyridine moieties through different polyethyleneoxy spacers, have been synthesized. The complexes were characterized by ^{1}H and ^{13}C NMR spectroscopy, mass spectrometry (ESI-MS), IR spectroscopy, UV-Vis spectroscopy, cyclic voltammetry and elemental analysis.

The microanalitical data for many of these compounds required the inclusion of NaPF$_6$ in the material. This is not unexpected in view of the affinity of Group 1 metal ions for poly(oxethylene) chains and we have recently reported a crystallographically characterized example of a compound capturing serendipitous sodium ions.[154]

3.9 Experimental

❖ [(*p*-ttpy)Ru(**L1**)(Ru)(*p*-ttpy)][PF$_6$]$_4$

❖ [(tpy)Ru(**L2**)(Ru)(tpy)][PF$_6$]$_4$

❖ [(tpy)Ru(**L4**)(Ru)(tpy)][PF$_6$]$_4$

❖ [(tpy)Ru(**L6**)(Ru)(tpy)][PF$_6$]$_4$

❖ [(tpy)Ru(**L7**)(Ru)(tpy)][PF$_6$]$_4$

L1, **L2**, **L4**, **L6** and **L7** were prepared as described in Chapter 2. RuCl$_3$·3H$_2$O and NH$_4$PF$_6$ are commercially available compounds and were used as received.

❖ [(*p*-ttpy)Ru(**L1**)(Ru)(*p*-ttpy)][PF$_6$]$_4$

General procedure for [Ru(*p*-ttpy)Cl$_3$] and [Ru(tpy)Cl$_3$] complexes

RuCl$_3$·3H$_2$O (0.011 g, 0.043 mmol, 1.0 eq) and *p*-ttpy (for complex with ligand **L1,** 0.014 g, 0.043 mmol, 1.0 eq) or tpy (for complexes with ligands **L2, L4**, **L6** and **L7,** 0.010 g, 0.043 mmol, 1.0 eq) were heated under microwave conditions in 15 mL ethanol at 135 °C for 15 minutes. The crude product was used for the next step reactions.

General procedure for ruthenium(II) complexes

Compound **L1** (0.015 g, 0.019 mmol, 1.0 eq) and [Ru(*p*-ttpy)Cl$_3$] (0.021 g, 0.038 mmol, 2.0 eq) with a few drops of *N*-ethylmorpholine (NEM) were heated at 135 °C in 15 mL ethanol in a microwave reactor for 30 minutes. Excess of solid ammonium hexafluorophosphate was added to give a red precipitate. This was collected by filtration through celite, washed with water and diethyl ether, then redissolved in acetonitrile. The solvent was removed *in vacuo* to give a red solid (0.038 g, 0.017 mmol, 90%).

1. RuCl$_3$·3H$_2$O, EtOH, 135 °C, 15 min, microwave reactor

2. L1, EtOH, NEM, 135 °C, 30 min, microwave reactor

3. NH$_4$PF$_6$

[(*p*-ttpy)Ru(**L1**)(Ru)(*p*-ttpy)][PF$_6$]$_4$

p-ttpy = 4'-(*p*-tolyl)-2,2':6',2''-terpyridine

$[(p\text{-ttpy})\text{Ru}(\textbf{L1})(\text{Ru})(p\text{-ttpy})][\text{PF}_6]_4$
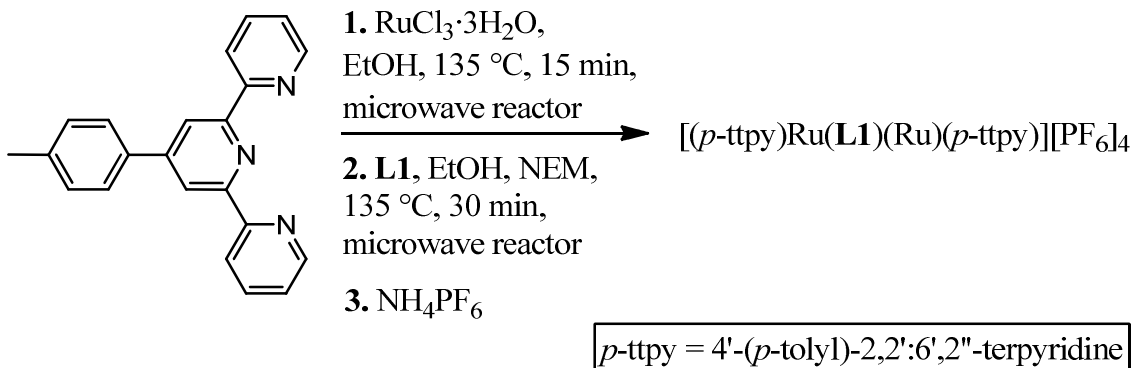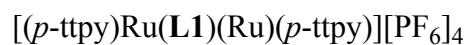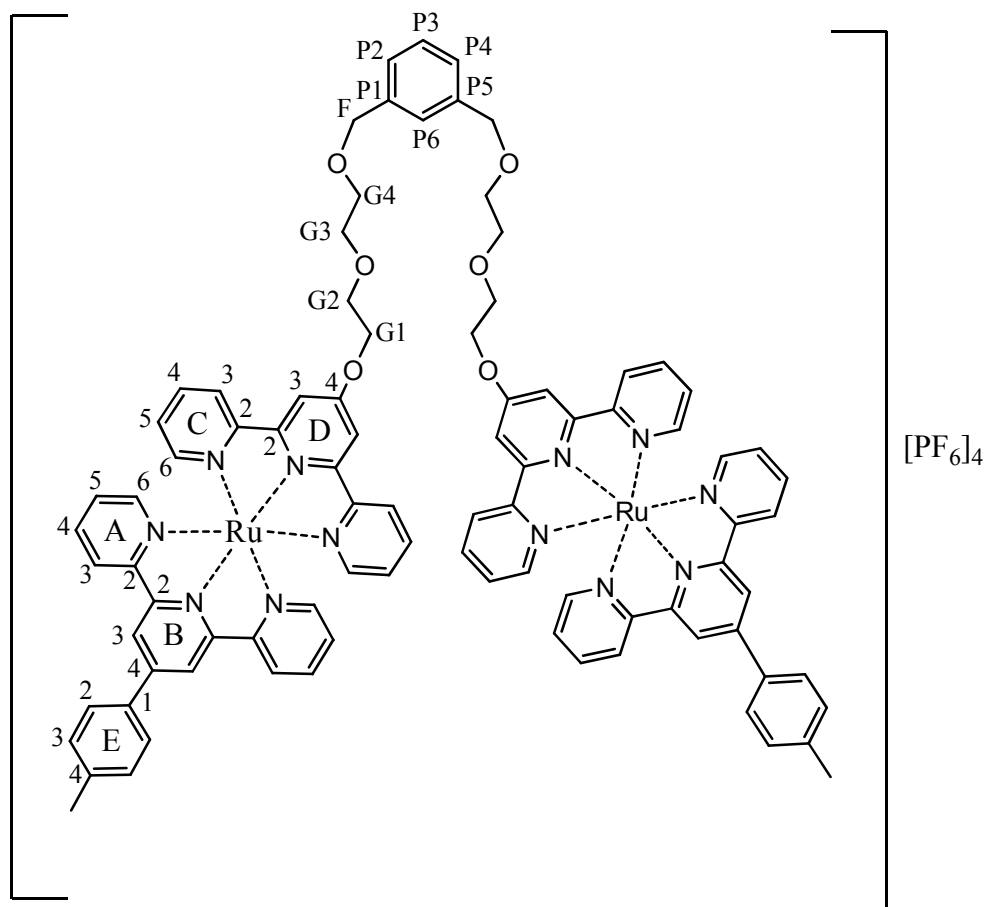
Molecular formula: $C_{90}H_{78}F_{24}N_{12}O_6P_4Ru_2$

Molecular weight: 2206.28

^{1}H NMR (500 MHz, CD$_3$CN) δ_H 2.46 (s, 6H, H^{Mes}), 3.72 (m, 4H, H^{G4}), 3.79 (m, 4H, H^{G3}), 4.02 (m, 4H, H^{G2}), 4.63 (s, 4H, H^F), 4.66 (m, 4H, H^{G1}), 7.11 (m, 4H, H^{C5}), 7.16 (m, 4H, H^{A5}), 7.25-7.45 (m, 12H, H^{C6}, H$^{P2/P4}$, H^{P3}, H^{P6}, H^{A6}), 7.75-7.95 (m, 8H, H^{C4} and H^{A4}), 8.33 (s, 4H, H^{D3}), 8.34-8.40 (m, 8H, H^{E2} and H^{E3}), 8.45 (d, J 9.0 Hz, 4H, H^{C3}), 8.46 (d, J 9.0 Hz, 4H, H^{A3}), 8.72 (d, J 8.2 Hz, 4H, H^{B3}).

^{13}C NMR (125 MHz, CD$_3$CN) δ_C 16.0 (C^{Mes}), 68.6 (C^F), 69.8 (C^{G2}), 70.3 (C^{G4}), 70.7 (C^{G1}), 71.9 (C^{G3}), 112.1 (C^{D3}), 124.7 (C^{B3}), 125.3 (C^{A3}), 125.5 (C^{C3}), 128.5 (C^{A5}, C^{C5}, C$^{P2/P4}$, C^{P3}, C^{P6} and C^{E2}, C^{E3}), 136.3 (C^{B4}), 138.9 (C^{A4}, C^{C4}, C^{E1}, C^{E4} and C$^{P1/P5}$), 153.3 (C^{A6}), 153.8 (C^{C6}), 156.9 (C^{A2}), 157.0 (C^{C2}), 159.0 (C^{D2}), 159.3 (C^{B2}), 167.2 (C^{D4}).

MS (ESI) m/z = 958.2 [**M**-2PF$_6$]$^{2+}$ (calc. 958.0), 590.5 [**M**-3PF$_6$]$^{3+}$ (calc. 590.5).

IR (solid, $\tilde{\nu}$/cm^{-1}): 3661w, 2923w, 2867w, 2833w, 1956w, 1700w, 1669w, 1613m, 1605m, 1560w, 1490w, 1467m, 1448m, 1420m, 1388m, 1350w, 1285w, 1209m, 1162w, 1130w, 1116w, 1090m, 1065m, 1045m, 1029m, 1019w, 987w, 964w, 926w, 877w, 824s, 820s, 786s, 765s, 750s, 735s, 725s, 696s, 673m, 665m, 645m, 638m, 617w.

Cyclic voltammetry data (CH$_3$CN, 0.1 M [^{n}Bu$_4$N][PF$_6$], Fc/Fc$^+$): +0.83 V, - 1.69 V, -1.92 V, -2.44 V.

UV/VIS (CH$_3$CN):λ_{max}/ nm (ε_{max}, M^{-1} cm^{-1}) 241 (110 x 10^3), 269 (115 x 10^3), 305 (140 x 10^3), 480 (40 x 10^3).

Elemental Analysis . Found: C, 47.76; H, 3.61; N, 7.62. Calc. for C$_{90}$H$_{78}$F$_{24}$N$_{12}$O$_6$P$_4$Ru$_2$· 1/3NaPF$_6$: C, 47.80; H, 3.48; N, 7.43%.

❖ [(tpy)Ru(**L2**)(Ru)(tpy)][PF$_6$]$_4$
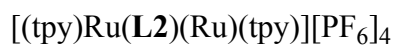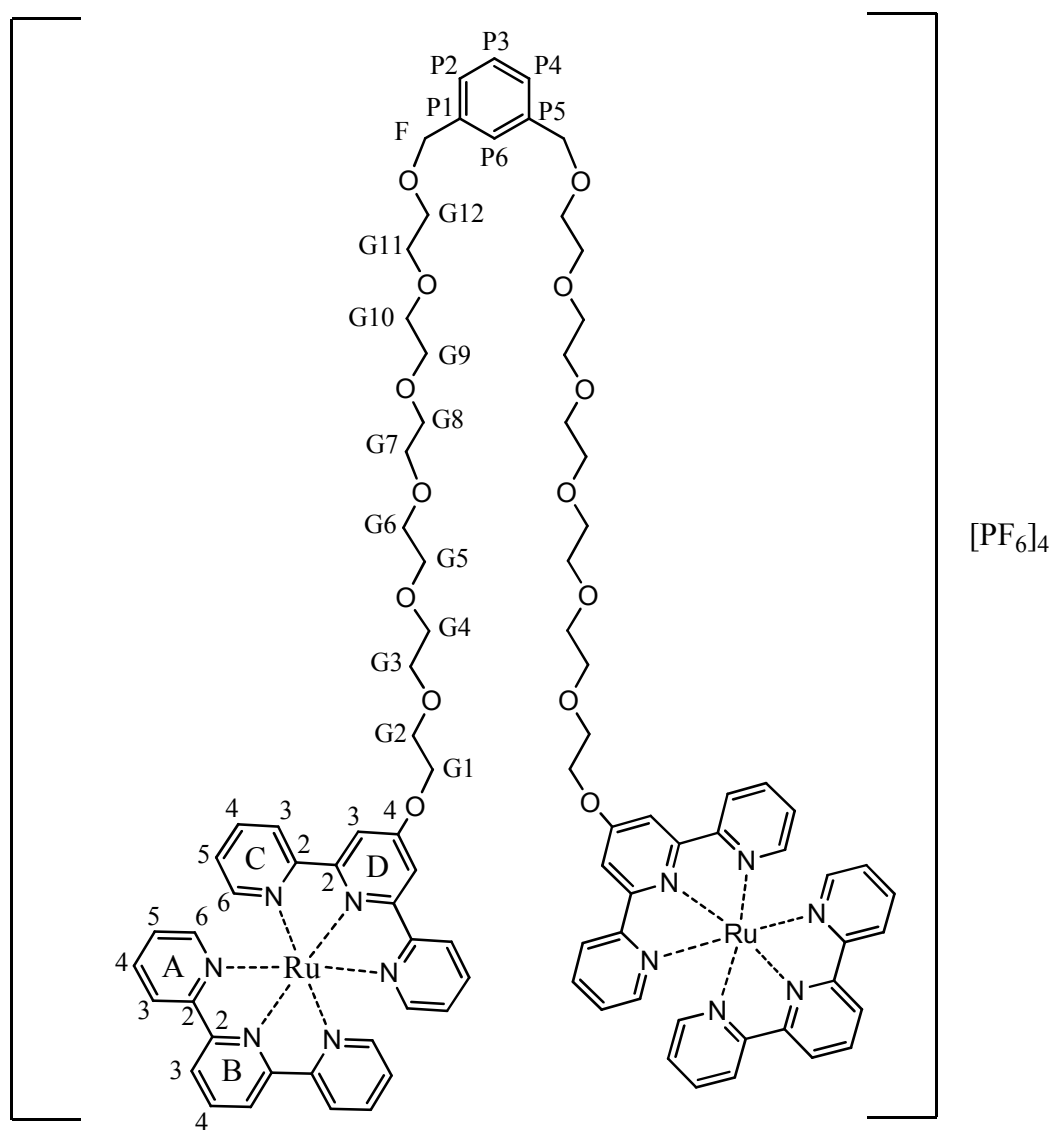
[(tpy)Ru(**L2**)(Ru)(tpy)][PF$_6$]$_4$

Molecular formula: $C_{92}H_{98}F_{24}N_{12}O_{14}P_4Ru_2$
Molecular weight: 2378.40

Complex [(tpy)Ru(**L2**)(Ru)(tpy)][PF$_6$]$_4$ was synthesized according to general procedure for ruthenium(II) complexes with **L2** (0.015 g, 0.013 mmol, 1.0 eq) and [Ru(tpy)Cl$_3$] (0.012 g, 0.027 mmol, 2.0 eq). The product was collected by filtration through celite, as a red solid (0.029 g, 0.012 mmol, 93%).

1. $RuCl_3 \cdot 3H_2O$, EtOH, 135 °C, 15 min, microwave reactor

2. $\mathbf{L^b}$, EtOH, NEM, 135 °C, 30 min, microwave reactor

3. NH_4PF_6

$[(tpy)Ru(\mathbf{L^b})(Ru)(tpy)][PF_6]_4$

$\boxed{\mathbf{L^b = L2, L4, L6, L7}}$
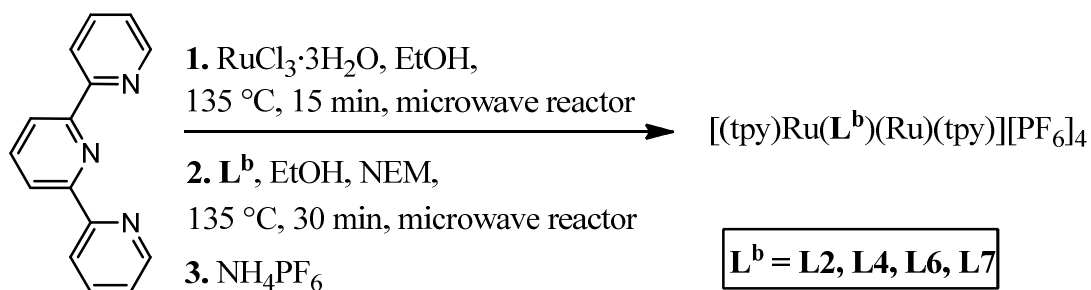
^{1}H NMR (500 MHz, CD$_3$CN) δ_H 3.65-3.75 (m, 36H, H^{G4-G12}), 3.80 (m, 4H, H^{G3}), 4.06 (m, 4H, H^{G2}), 4.56 (s, 4H, H^F), 4.67 (m, 4H, H^{G1}), 7.11 (m, 4H, H^{C5}), 7.17 (m, 4H, H^{A5}), 7.29 (d, J 5.3 Hz, 4H, H^{C6}), 7.30-7.40 (m, 4H, H$^{P2,\ P3,\ P4,\ P6}$), 7.41 (d, J 4.9 Hz, 4H, H^{A6}), 7.82-7.94 (m, 8H, H^{C4} and H^{A4}), 8.30-8.45 (m, 6H, H^{B4} and H^{D3}), 8.45-8.50 (m, 8H, H^{C3} and H^{A3}), 8.72 (d, J 8.1 Hz, 4H, H^{B3}).

^{13}C NMR (125 MHz, CD$_3$CN) δ_C 70.0 (C^{G2}), 70.5 (C^{G4}), 70.6 (C^{G5-G12}), 70.6 (C^{G5-G12}), 70.7 (C^{G5-G12}), 70.9 (C^{G1}), 71.6 (C^{G3}), 73.5 (C^F), 112.0 (C^{D3}), 124.6 (C^{B3}), 125.3 (C^{A3}), 125.5 (C^{C3}), 128.5 (C^{A5}, C^{C5} and C^{P2,P3,P4,P6}), 136.3 (C^{B4}), 138.9 (C^{A4} and C^{C4}), 139.0 (C$^{P1/P5}$), 153.3 (C^{A6}), 153.8 (C^{C6}), 156.9 (C^{A2}), 157.0 (C^{C2}), 159.1 (C^{D2}), 159.3 (C^{B2}), 167.3 (C^{D4}).

MS (ESI) m/z = 1044.2 [$\mathbf{M}$-2PF$_6$]$^{2+}$ (calc. 1044.0), 449.6 [$\mathbf{M}$-4PF$_6$]$^{4+}$ (calc. 450.0).

IR (solid, $\tilde{\nu}$/cm^{-1}): 3662w, 3086w, 2925w, 2868w, 2853w, 2833w, 1956w, 1700w, 1668w, 1613m, 1603m, 1560w, 1547w, 1488w, 1467m, 1448m, 1439m, 1421m, 1388m, 1347w, 1287w, 1245w, 1207m, 1162w, 1130w, 1115w, 1091m, 1061m, 1045m, 1027m, 1017w, 985w, 964w, 923w, 877w, 824s, 764s, 750s, 741s, 735s, 725s, 698s, 673m, 663m, 638m, 614w.

Cyclic voltammetry data (CH$_3$CN, 0.1 M [^{n}Bu$_4$N][PF$_6$], Fc/Fc$^+$): +0.83 V, - 1.69 V, -1.92 V, -2.44V.

UV/VIS (CH$_3$CN):λ_{max}/ nm (ε_{max}, M^{-1} cm^{-1}) 241 (107 x 10^3), 269 (116 x 10^3), 305 (141 x 10^3), 480 (41 x 10^3).

Elemental Analysis . Found: C, 44.34; H, 4.30; N, 6.92. Calc. for C$_{92}$H$_{98}$F$_{24}$N$_{12}$O$_{14}$P$_4$Ru$_2$·NaPF$_6$: C, 44.89; H, 4.01; N, 6.83%.

❖ [(tpy)Ru(**L4**)(Ru)(tpy)][PF$_6$]$_4$
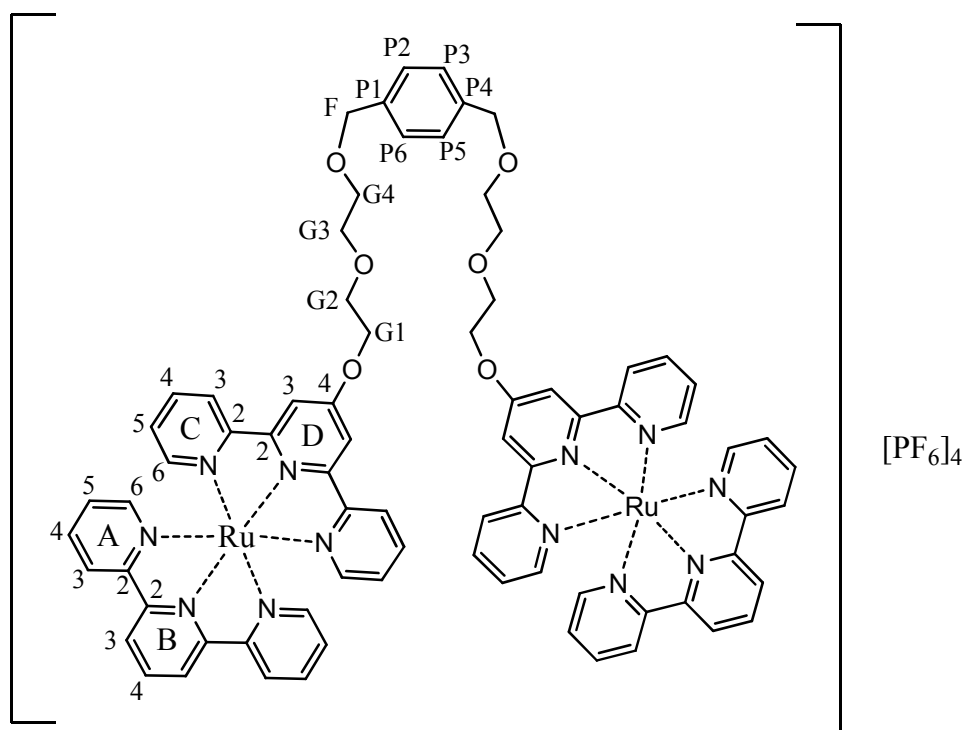
[(tpy)Ru(**L4**)(Ru)(tpy)][PF$_6$]$_4$

Molecular formula: C$_{76}$H$_{66}$F$_{24}$N$_{12}$O$_6$P$_4$Ru$_2$
Molecular weight: 2026.19

Complex [(tpy)Ru(**L4**)(Ru)(tpy)][PF$_6$]$_4$ was synthesized according to general procedure for ruthenium(II) complexes with **L4** (0.015 g, 0.019 mmol, 1.0 eq) and [Ru(tpy)Cl$_3$]

(0.017 g, 0.038 mmol, 2.0 eq). The product was collected as a red solid (0.035 g, 0.017 mmol, 92%).

^{1}H NMR (500 MHz, CD$_3$CN) δ_H 3.69 (m, 4H, H^{G4}), 3.80 (m, 4H, H^{G3}), 4.06 (m, 4H, H^{G2}), 4.54 (s, 4H, H^F), 4.67 (m, 4H, H^{G1}), 7.11 (m, 4H, H^{C5}), 7.17 (m, 4H, H^{A5}), 7.29 (d, J 5.5 Hz, 4H, H^{C6}), 7.35 (s, 4H, H$^{P2, P3, P5, P6}$), 7.41 (d, J 5.4 Hz, 4H, H^{A6}), 7.82-7.94 (m, 8H, H^{C4} and H^{A4}), 8.34 (s, 4H, H^{D3}), 8.33-8.45 (m, 2H, H^{B4}), 8.46 (d, J 8.0 Hz, 4H, H^{C3}), 8.47 (d, J 8.0 Hz, 4H, H^{A3}), 8.72 (d, J 8.1 Hz, 4H, H^{B3}).

^{13}C NMR (125 MHz, CD$_3$CN) δ_C 70.0 (C^{G2}), 70.6 (C^{G4}), 70.9 (C^{G1}), 71.6 (C^{G3}), 73.5 (C^F), 112.2 (C^{D3}), 124.7 (C^{B3}), 125.3 (C^{A3}), 125.5 (C^{C3}), 128.5 (C^{A5} and C^{C5}), 128.8 (C^{P2,P3,P5,P6}), 136.3 (C^{B4}), 138.9 (C^{A4} and C^{C4}), 139.0 (C$^{P1/P4}$), 153.3 (C^{A6}), 153.8 (C^{C6}), 156.9 (C^{A2}), 157.0 (C^{C2}), 159.1 (C^{D2}), 159.3 (C^{B2}), 167.3 (C^{D4}).

MS (ESI) m/z = 868.3 [**M**-2PF$_6$]$^{2+}$ (calc. 868.5), 530.5 [**M**-3PF$_6$]$^{3+}$ (calc. 530.5), 361.7 [**M**-4PF$_6$]$^{4+}$ (calc. 362.0).

IR (solid, $\tilde{\nu}$/cm^{-1}): 3662w, 3086w, 2922w, 2868w, 2851w, 2833w, 1956w, 1700w, 1668w, 1613m, 1603m, 1560w, 1546w, 1488w, 1467m, 1448m, 1437m, 1420m, 1388m, 1349w, 1285w, 1245w, 1207m, 1162w, 1130w, 1115w, 1090m, 1061m, 1045m, 1027m, 1017w, 987w, 964w, 925w, 877w, 824s, 820s, 786s, 764s, 750s, 741s, 735s, 725s, 696s, 673m, 663m, 645m, 638m, 614w.

Cyclic voltammetry data (CH$_3$CN, 0.1 M [^{n}Bu$_4$N][PF$_6$], Fc/Fc$^+$): +0.83 V, - 1.69 V, -1.92 V, -2.44 V.

UV/VIS (CH$_3$CN):λ_{max}/ nm (ε_{max}, M^{-1} cm^{-1}) 241 (108 x 10^3), 269 (116 x 10^3), 305 (140 x 10^3), 480 (40 x 10^3).

Elemental Analysis . Found: C, 42.34; H, 3.50; N, 7.92. Calc. for C$_{76}$H$_{66}$F$_{24}$N$_{12}$O$_6$P$_4$Ru$_2$ ·2/3NaPF$_6$: C, 42.71; H, 3.11; N, 7.86%.

❖ [(tpy)Ru(**L6**)(Ru)(tpy)][PF$_6$]$_4$
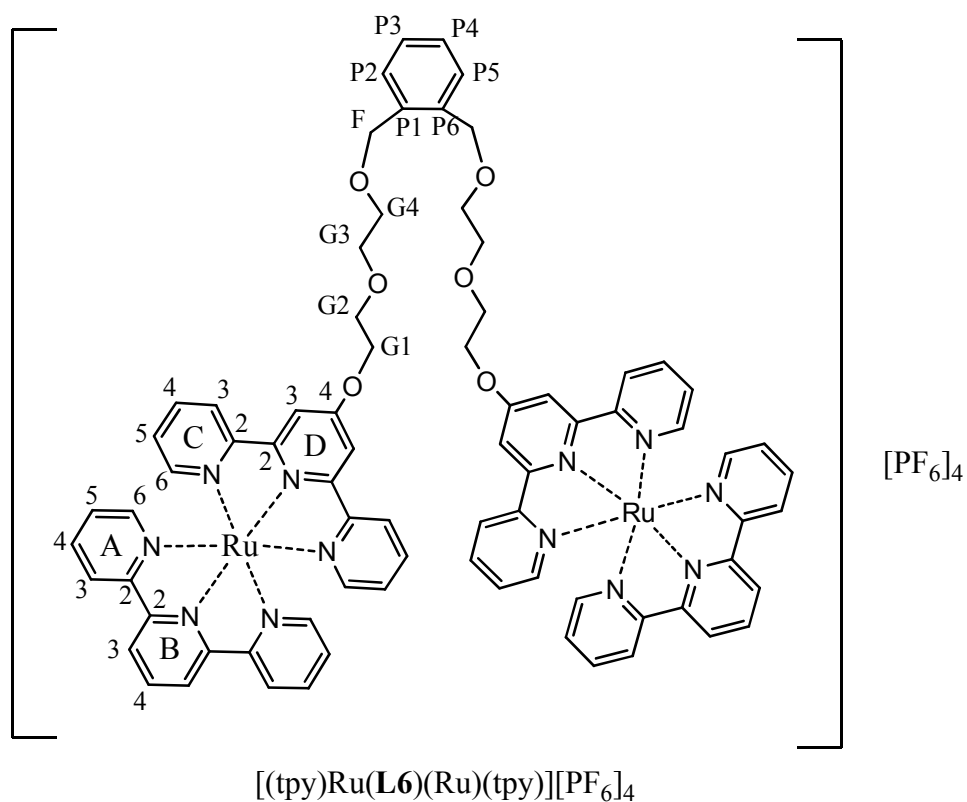
[(tpy)Ru(**L6**)(Ru)(tpy)][PF$_6$]$_4$

Molecular formula: C$_{76}$H$_{66}$F$_{24}$N$_{12}$O$_6$P$_4$Ru$_2$
Molecular weight: 2026.19

Complex [(tpy)Ru(**L6**)(Ru)(tpy)][PF$_6$]$_4$ was synthesized according to general procedure for ruthenium(II) complexes with **L6** (0.015 g, 0.019 mmol, 1.0 eq) and [Ru(tpy)Cl$_3$] (0.017 g, 0.038 mmol, 2.0 eq). The product was collected as a red solid (0.035 g, 0.017 mmol, 90%).

^{1}H NMR (500 MHz, CD$_3$CN) δ$_H$ 3.75 (m, 4H, H^{G4}), 3.83 (m, 4H, H^{G3}), 4.06 (m, 4H, H^{G2}), 4.67 (m, 4H, H^{G1}), 4.70 (s, 4H, H^F), 7.11 (m, 4H, H^{C5}), 7.15 (m, 4H, H^{A5}), 7.27 (m, 2H, H$^{P2/P5}$ or H$^{P3/P4}$), 7.30 (d, *J* 5.3 Hz, 4H, H^{C6}), 7.34 (m, 2H, H$^{P2/P5}$ or H$^{P3/P4}$), 7.43 (d, *J* 5.6 Hz, 4H, H^{A6}), 7.85-7.95 (m, 8H, H^{C4} and H^{A4}), 8.34 (s, 4H, H^{D3}), 8.35-8.45 (m, 2H, H^{B4}), 8.46 (d, *J* 9.2 Hz, 4H, H^{C3}), 8.47 (d, *J* 9.2 Hz, 4H, H^{A3}), 8.73 (d, *J* 8.2 Hz, 4H, H^{B3}).

^{13}C NMR (125 MHz, CD$_3$CN) δ_C 70.0 (C^{G2}), 70.7 (C^{G4}), 70.9 (C^{G1}), 71.3 (C^{G3}), 71.6 (C^F), 112.2 (C^{D3}), 124.7 (C^{B3}), 125.3 (C^{A3}), 125.5 (C^{C3}), 128.5 (C^{A5} and C^{C5}), 128.7 (C$^{P2/P5}$ or C$^{P3/P4}$), 129.6 (C$^{P2/P5}$ or C$^{P3/P4}$), 136.3 (C^{B4}), 138.9 (C^{A4} and C^{C4}), 139.0 (C$^{P1/P6}$), 153.3 (C^{A6}), 153.7 (C^{C6}), 156.9 (C^{A2}), 157.0 (C^{C2}), 159.1 (C^{D2}), 159.3 (C^{B2}), 167.3 (C^{D4}).

MS (ESI) m/z = 868.1 [**M**-2PF$_6$]$^{2+}$ (calc. 861.5), 530.4 [**M**-3PF$_6$]$^{3+}$ (calc.530.5).

IR (solid, $\tilde{\nu}$/cm^{-1}): 3662w, 3086w, 2851w, 2833w, 1956w, 1705w, 1665w, 1613m, 1603m, 1561w, 1545w, 1488w, 1467m, 1448m, 1437m, 1420m, 1385m, 1349w, 1285w, 1246w, 1205m, 1162w, 1130w, 1065m, 1045m, 1027m, 1017w, 987w, 965w, 925w, 877w, 824s, 825s, 786s, 764s, 750s, 741s, 735s, 725s, 696s, 673m, 663m, 645m, 635m, 615w.

Cyclic voltammetry data (CH$_3$CN, 0.1 M [^{n}Bu$_4$N][PF$_6$], Fc/Fc$^+$): +0.83 V, - 1.69 V, -1.92 V, -2.44 V.

UV/VIS (CH$_3$CN):λ_{max}/ nm (ε_{max}, M^{-1} cm^{-1}) 241 (108 x 10^3), 269 (115 x 10^3), 305 (139 x 10^3), 480 (39 x 10^3).

Elemental Analysis . Found: C, 44.34; H, 3.75; N, 8.72. Calc. for C$_{76}$H$_{66}$F$_{24}$N$_{12}$O$_6$P$_4$Ru$_2$ ·0.1NaPF$_6$: C, 44.70; H, 3.26; N, 8.23%.

❖ [(tpy)Ru(**L7**)(Ru)(tpy)][PF$_6$]$_4$
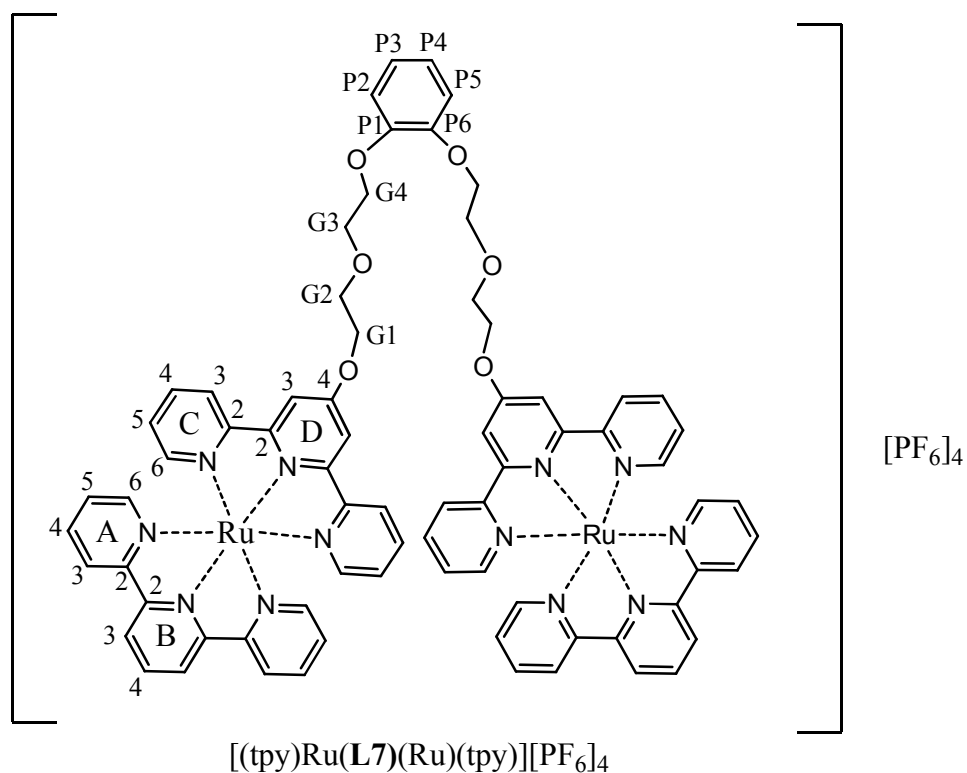
[(tpy)Ru(**L7**)(Ru)(tpy)][PF$_6$]$_4$

Molecular formula: C$_{74}$H$_{62}$F$_{24}$N$_{12}$O$_6$P$_4$Ru$_2$
Molecular weight: 1998.16

Complex [(tpy)Ru(**L7**)(Ru)(tpy)][PF$_6$]$_4$ was synthesized according to general procedure for ruthenium(II) complexes with **L7** (0.015 g, 0.020 mmol, 1.0 eq) and [Ru(tpy)Cl$_3$] (0.018 g, 0.040 mmol, 2.0 eq). The product was collected as a red solid (0.036 g, 0.018 mmol, 89%).

^{1}H NMR (500 MHz, CD$_3$CN) δ_H 4.03 (m, 4H, H^{G3}), 4.15 (m, 4H, H^{G2}), 4.26 (m, 4H, H^{G4}), 4.72 (m, 4H, H^{G1}), 6.88-6.92 (m, 2H, H$^{P3/P4}$), 7.00-7.06 (m, 2H, H$^{P2/P5}$), 7.10 (m, 4H, H^{C5}), 7.16 (m, 4H, H^{A5}), 7.29 (d, *J* 5.3 Hz, 4H, H^{C6}), 7.42 (d, *J* 5.3 Hz, 4H, H^{A6}), 7.85-7.95 (m, 8H, H^{C4} and H^{A4}), 8.34 (s, 4H, H^{D3}), 8.35-8.43 (m, 2H, H^{B4}), 8.43-8.51 (m, 8H, H^{C3} and H^{A3}), 8.72 (d, *J* 8.2 Hz, 4H, H^{B3}).

^{13}C NMR (125 MHz, CD$_3$CN) δ_C 69.7 (C^{G4}), 70.2 (C^{G2}), 70.8 (C^{G1}), 70.9 (C^{G3}), 112.2 (C^{D3}), 115.7 (C$^{P2/P5}$), 124.7 (C^{B3}), 124.8 (C$^{P3/P4}$), 125.3 (C^{A3}), 125.4 (C^{C3}), 128.5 (C^{A5} and C^{C5}), 136.3 (C^{B4}), 138.9 (C^{A4} or C^{C4}), 139.0 (C^{A4} or C^{C4}), 149.9 (C$^{P1/P6}$), 153.3 (C^{A6}), 153.8 (C^{C6}), 156.9 (C^{A2}), 157.0 (C^{C2}), 159.1 (C^{D2}), 159.2 (C^{B2}), 167.3 (C^{D4}).

MS (ESI) m/z = 854.1 [**M**-2PF$_6$]$^{2+}$ (calc. 854.2), 521.1 [**M**-3PF$_6$]$^{3+}$ (calc. 521.0), 354.6 [**M**-4PF$_6$]$^{4+}$ (calc. 355.0).

IR (solid, , $\tilde{\nu}$/cm^{-1}): 3662w, 3086w, 2923w, 2868w, 2853w, 2833w, 1956w, 1700w, 1668w, 1613m, 1603m, 1560w, 1546w, 1448m, 1437m, 1423m, 1388m, 1349w, 1283w, 1243w, 1162w, 1130w, 1115w, 1090m, 1061m, 1043m, 1027m, 1017w, 983w, 964w, 925w, 877w, 824s, 820s, 786s, 764s, 750s, 741s, 733s, 725s, 696s, 673m, 663m, 645m, 638m, 613w.

Cyclic voltammetry data (CH$_3$CN, 0.1 M [^{n}Bu$_4$N][PF$_6$], Fc/Fc$^+$): +0.83 V, - 1.69 V, -1.92 V, -2.44 V.

UV/VIS (CH$_3$CN):λ_{max}/ nm (ε_{max}, M^{-1} cm^{-1}) 241 (105 x 10^3), 269 (113 x 10^3), 305 (139 x 10^3), 480 (38 x 10^3).

Elemental Analysis . Found: C, 44.64; H, 3.50; N, 8.92. Calc. for C$_{74}$H$_{62}$F$_{24}$N$_{12}$O$_6$P$_4$Ru$_2$·H$_2$O·0.5CH$_3$CN: C, 44.25; H, 3.24; N, 8.60%.

CHAPTER 4

Synthesis of a homoleptic mononuclear zinc(II) complex of a ditopic 4'-substituted- 2,2':6',2''-terpyridine ligand

4.1 Introduction

In contrast to typical octahedral ruthenium(II) complexes, zinc(II) can adopt different geometries in its complexes, depending on the type of coordinated ligand. Nevertheless, when tridentate tpy-based ligands react with zinc(II) ions octahedral complexes are usually formed (see Scheme 3.1). The zinc(II) ion with its d^{10} configuration has a filled electron shell and is a labile metal centre.
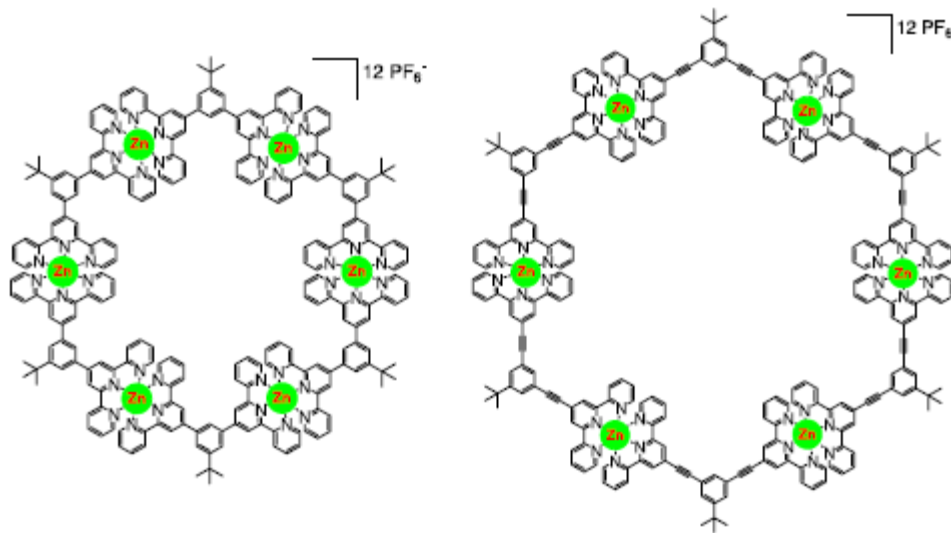
Figure 4.1. Zinc(II)-hexagonal metallomacrocycles.[155]

Zinc(II) has gained much interest as a template for the construction of photoluminescent PL) or electroluminescent (EL) metallopolymers with well-defined structures[162-169] as

well as discrete molecular architectures such as hexagonal metallomacrocycles (**Figure 4.1**).[170-171] Depending on the nature of the π-conjugated system between the terpyridine units, the emission properties can be tuned, and materials with high PL quantum yields and EL performance are accessible.

Studies of the homoleptic mononuclear Zn(II) complex of ditopic 4'-substituted-2,2':6',2"-terpyridine ligand **L4** described in Chapter 2 will be fully presented in this chapter (**Scheme 4.1**).

$$[Zn(\mathbf{L4})][BF_4]_2$$
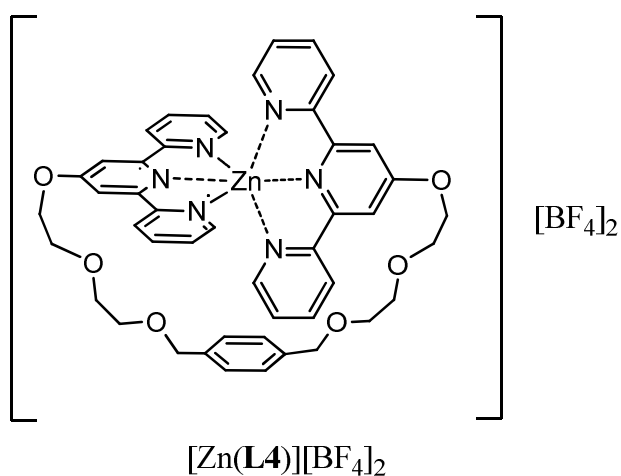
Scheme 4.1. Zn(II) complex of the ditopic 4'-substituted- 2,2':6',2"-terpyridine ligand **L4** studied in this chapter.

4.2 Synthesis

The homoleptic mononuclear Zn(II) complex of ligand **L4** was easily prepared by reacting one equivalent of ligand **L4** in CHCl$_3$ with one equivalent of Zn(BF$_4$)$_2$·6H$_2$O in acetonitrile at room temperature overnight. The solvent was removed *in vacuo* and the

desired product was obtained in 89% yield (**Scheme 4.2**). No polymeric products were observed.
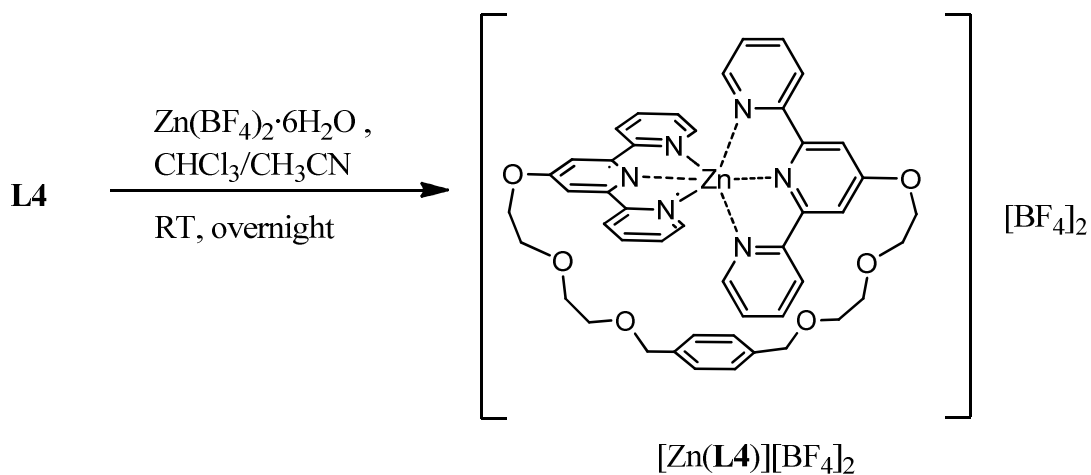
Scheme 4.2. Synthesis of [Zn(**L4**)][BF$_4$]$_2$.

4.3 Mass spectroscopic characterization

Electrospray ionization mass spectroscopy (ESI-MS) was used to characterize the new homoleptic mononuclear zinc(II) complex of ligand **L4** - [Zn(**L4**)][BF$_4$]$_2$. The peaks are observed as the ratio of mass to the charge of the species (*m/z*).

In **Figure 4.2** the ESI-MS spectrum of [Zn(**L4**)][BF$_4$]$_2$ is shown. The major peak envelope is a peak at *m/z* 420.3 and was assigned to [**M**-2BF$_4$]$^{2+}$. The other set of peaks at *m/z* 927.5 corresponds [**M**-BF$_4$]$^+$. Also shown are expansions of both peaks at *m/z* 420.3 and 927.5. The peaks show the typical isotope distribution pattern of zinc(II), a separations of peaks in a given envelope confirm the charge on the ion.
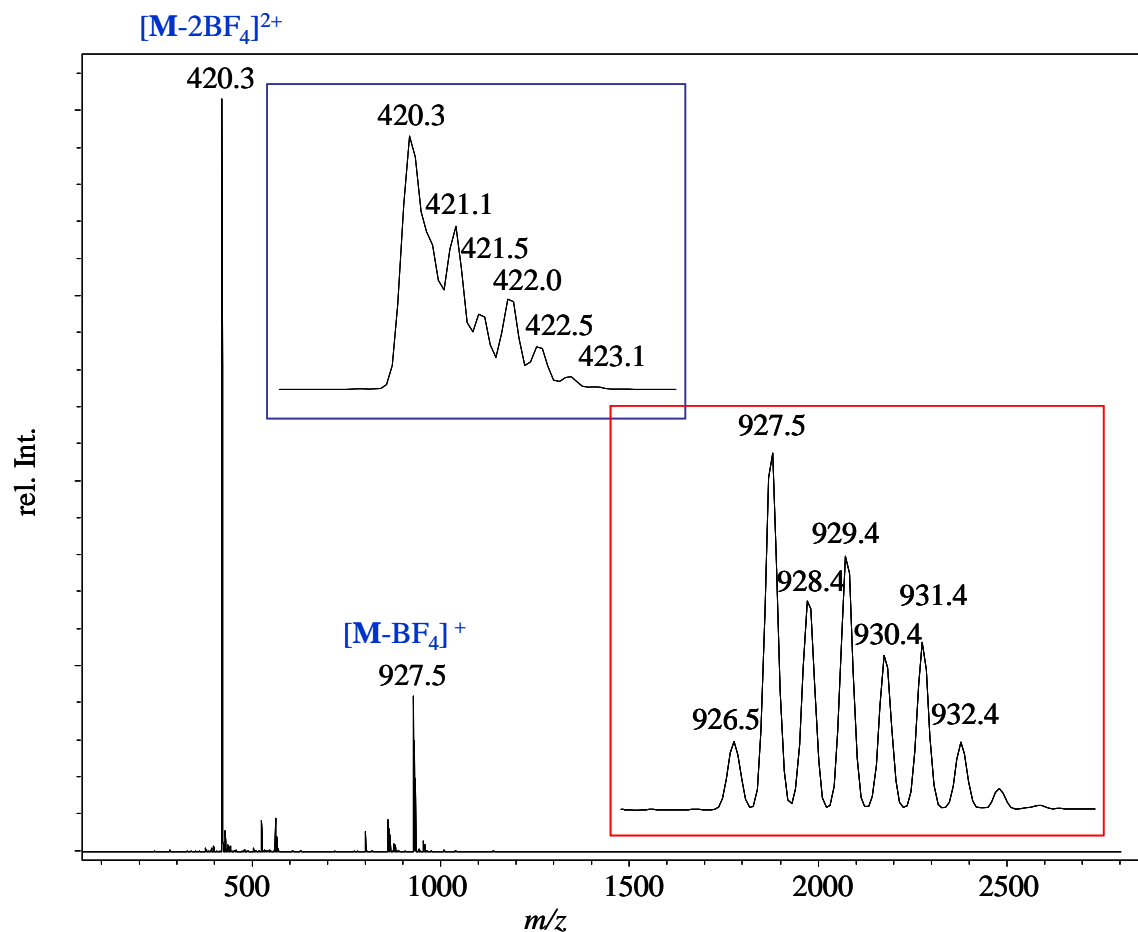
Figure 4.2. ESI-MS spectrum of $[Zn(L4)][BF_4]_2$.

4.4 ^{1}H NMR spectroscopy

The Zn(II) complex of ligand **L4** - $[Zn(L4)][BF_4]_2$, was characterized by ^{1}H NMR spectroscopy in CH_3CN solution.

A comparison between the ^{1}H NMR spectra obtained for the free ligand **L4** in $CHCl_3$ (not soluble in acetonitrile) and the zinc(II) complex $[Zn(L4)][BF_4]_2$ in acetonitrile is shown in **Figure 4.3** as well as in **Tables 4.1** and **4.2**.
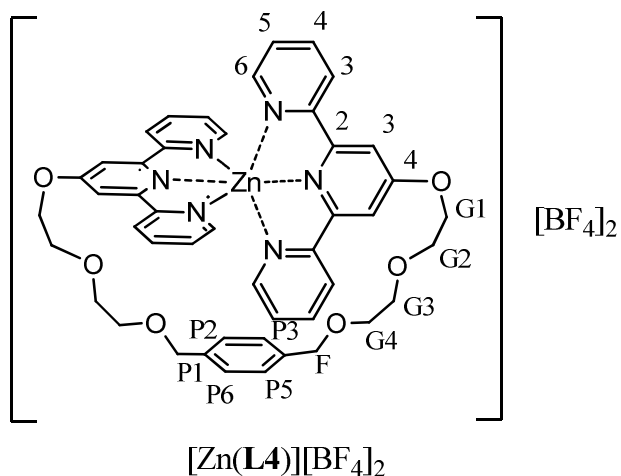
Scheme 4.3. Labeling for [Zn(**L4**)][BF$_4$]$_2$.

	H^{G4}	**H^{G3}**	**H^{G2}**	**H^{G1}**	**H^{F}**
L4	3.62 (t) J 5.0 Hz	3.73 (t) J 5.0 Hz	3.91 (t) J 5.0 Hz	4.38 (t) J 5.0 Hz	4.53 (s)
[Zn(**L4**)][BF$_4$]$_2$	3.63 (m)	3.75 (m)	3.99 (m)	4.65 (m)	4.48 (s)

Table 4.1. ^{1}H NMR spectroscopic data, δ_H [ppm] for **L4** (500 MHz, 295 K, CDCl$_3$) and [Zn(**L4**)][BF$_4$]$_2$ (500 MHz, 295 K, CD$_3$CN)**.**

In the aliphatic region of the ^{1}H NMR spectra of ligand **L4** and complex [Zn(**L4**)][BF$_4$]$_2$ there are few significant differences. After complexation the **H^{G1}** and **H^{G2}** protons are both shifted downfield by 0.27 ppm for proton **H^{G1}** and 0.08 ppm for proton **H^{G2}**, the signal assigned to proton **H^{F}** is slightly shifted upfield (**Table 4.1**).

	H^{C5}/H^{T5} /H^P	H^{C4}/H^{T4}	$H^{D3}/H^{T3'}$	H^{C3}/H^{T3}	H^{C6}/H^{T6}
L4	7.30 (m)/ 7.29 (s)	7.81 (td) J 1.8, 7.7 Hz	8.02 (s)	8.58 (d) J 8.0 Hz	8.66 (d) J 4.7 Hz
[Zn(**L4**)][BF$_4$]$_2$	7.33 (m)/ 7.30 (s)	8.08 (t) J 7.5 Hz	8.21 (s)	8.52 (d) J 8.0 Hz	7.73 (d) J 4.5 Hz

Table 4.2. ^{1}H NMR spectroscopic data, δ_H [ppm] for **L4** (500 MHz, 295 K, CDCl$_3$) and [Zn(**L4**)][BF$_4$]$_2$ (500 MHz, 295 K, CD$_3$CN).
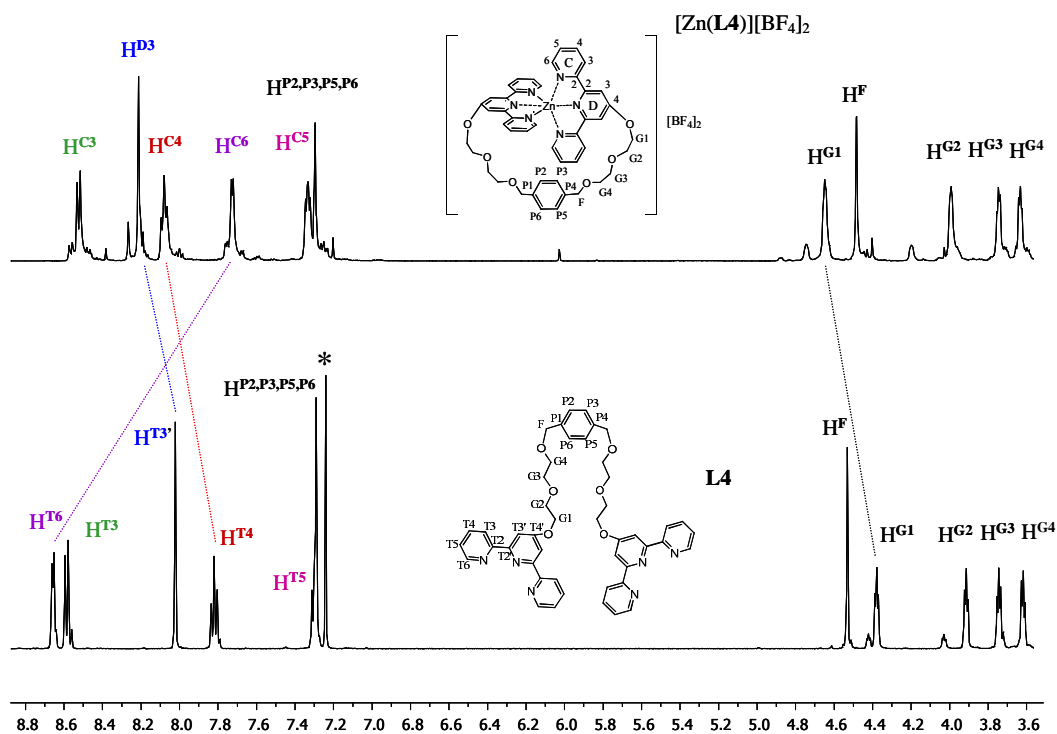
Figure 4.3. ^{1}H NMR spectrum (500 MHz, 295 K) of **L4** (below) in CDCl$_3$ and [Zn(**L4**)][BF$_4$]$_2$ (above) in CD$_3$CN. The signal marked with * is the signal for CHCl$_3$. Spectra exhibit some residues of the starting material, which could not be removed by column chromatography or other purification methods.

120

All of the terpyridine proton signals are influenced by the complexation of ligand **L4** with zinc(II), but the signal for the $\mathbf{H^{C6}}$/$\mathbf{H^{T6}}$ proton of ligand is mostly affected and is shifted 0.93 ppm upfield. It is important to notice that the signal for the $\mathbf{H^{C6}}$ proton of [(tpy)Ru(**L4**)(Ru)(tpy)][PF$_6$]$_4$ is shifted 1.37 ppm upfield. The signals for protons $\mathbf{H^{C4}}$ and $\mathbf{H^{D3}}$ of complex [Zn(**L4**)][BF$_4$]$_2$ are shifted downfield, respectively 0.27 and 0.19 ppm, in comparison to ligand **L4**.
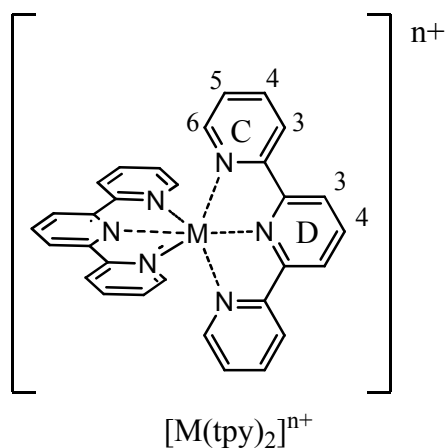
Scheme 4.4. Mononuclear metal complex of 2,2':6',2"-terpyridine [M(tpy)$_2$]$^{n+}$.

It is generally observed in [M(bpy)$_3$]$^{n+}$, [M(tpy)$_2$]$^{n+}$ and [M(phen)$_3$]$^{n+}$ complexes that the protons adjacent to the nitrogen are significantly deshielded when compared to the free ligand. The degree of upfield shifting depends on both the metal ion and the precise ligand being studied.[172-174] A number of factors contribute to the upfield shifting in these complexes, firstly, these protons are the ones closest to the metal centre and are likely to experience shielding from the t$_{2g}$ electron pair and, secondly, in the complexes (**Scheme 4.4**) the protons lie above the aromatic plane of one of the other ligands present. The pyridine ring has a magnetic anisotropy and the precise position of the proton with respect to the ring will effect where exactly it lies with respect to the shielding or deshielding effects of the paired electrons in the π^* levels. naturally, the exact spatial relationship depends on the M-N bond lengths and the precise geometry of the complex and so a metal-dependent variation is expected. A possible third influence is a

temperature independent paramagnetism in the d^6 complexes if there are suitable low lying states of T symmetry.

All of the changes in the ^{1}H NMR spectra of ligand **L4** and complex $[Zn(\textbf{L4})][BF_4]_2$ are also pictured in **Figure 4.3**.

The assignment of the $\textbf{H}^{\textbf{G1}}$, $\textbf{H}^{\textbf{G2}}$, $\textbf{H}^{\textbf{G3}}$ and $\textbf{H}^{\textbf{G4}}$ protons of the complex $[Zn(\textbf{L4})][BF_4]_2$ was made using the ^{1}H-^{1}H COSY and NOESY techniques (**Figures 4.4 and 4.5**). The signal for $\textbf{H}^{\textbf{G1}}$ gives a COSY cross peak to the signal $\textbf{H}^{\textbf{G2}}$ at δ 3.99 ppm (**Figure 4.4**). The signal for $\textbf{H}^{\textbf{G3}}$ gives a COSY cross peak to the signal at δ 3.63 ppm, and this signal is assigned to $\textbf{H}^{\textbf{G4}}$ (**Figure 4.4**).
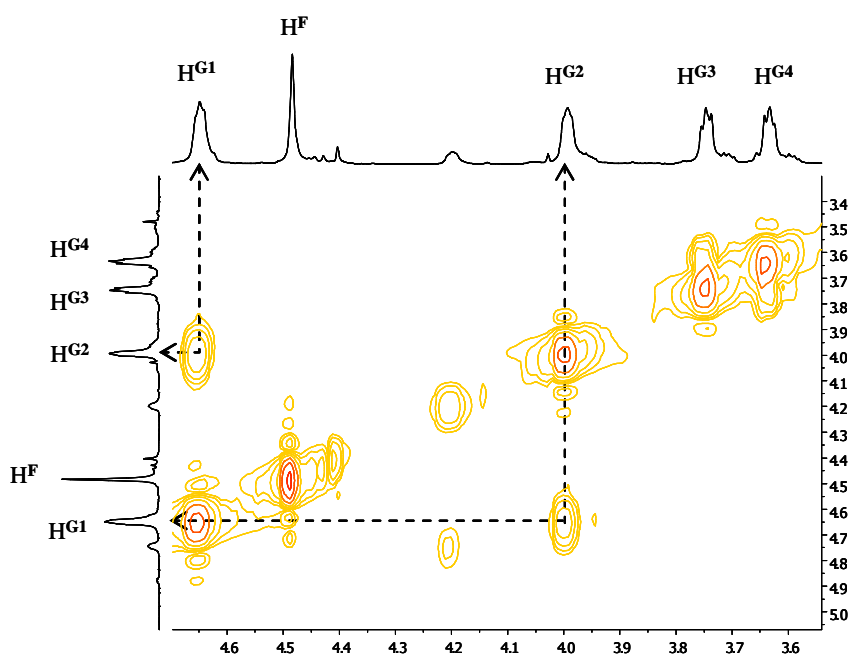
Figure 4.4. Part of the ^{1}H-^{1}H COSY spectrum (500 MHz, 295K) of $[Zn(\textbf{L4})][BF_4]_2$ in CD_3CN showing the aliphatic region. Spectrum exhibits some residues of the starting material, which could not be removed by column chromatography or other purification methods.
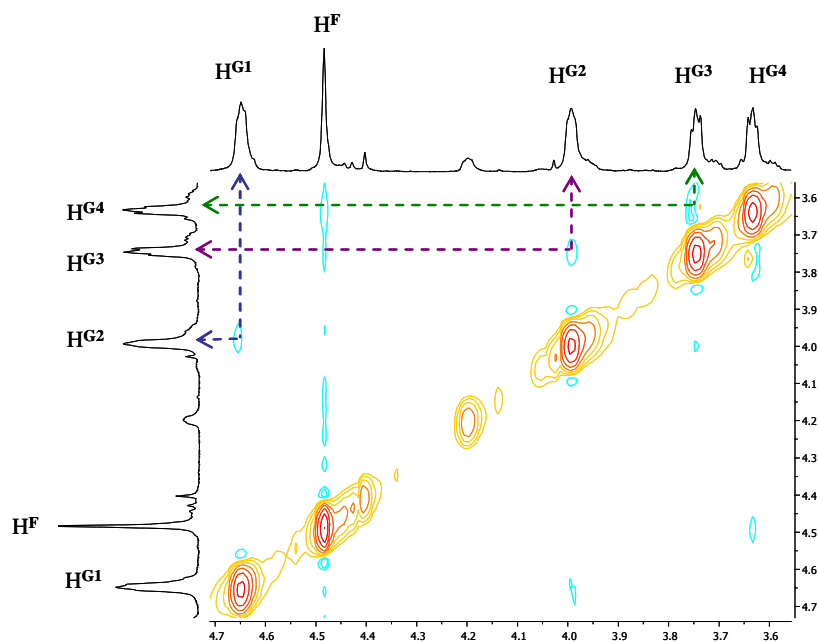
Figure 4.5. Part of the NOESY spectrum (500 MHz, 295K) of [Zn(**L4**)][BF$_4$]$_2$ in CD$_3$CN showing the aliphatic region.

4.5 ^{13}C NMR spectroscopy

For comparison, the diethylene glycol $\mathbf{C^G}$, $\mathbf{C^F}$ and phenyl $\mathbf{C^P}$ carbon signals of zinc(II) complex [Zn(**L4**)][BF$_4$]$_2$ as well as the terpyridine carbon signals of this complex were put together with carbon signals of ligand **L4** in **Tables 4.3** and **4.4**. The assignments were made using HMQC and HMBC techniques.

Table 4.3 shows how the $\mathbf{C^G}$, $\mathbf{C^F}$ and $\mathbf{C^P}$ carbon signals of ligand **L4** changes, after complexation with zinc(II). All of the signals are shifted downfield after complexation with zinc(II) but most changed are the carbon signals $\mathbf{C^{G1}}$ and $\mathbf{C^{G4}}$ of ligand **L4**, which are shifted by 3.3 and 2.4 ppm, respectively.

123

	C^{G1}	C^{G2}	C^{G3}	C^{G4}	C^F	C^P/ [#]C^P (quaternary)
L4	67.7	69.7	71.2	68.0	73.3	128.0/ [#]137.7
[Zn(**L4**)][BF$_4$]$_2$	71.0	69.8	71.5	70.5	73.4	128.8/ [#]139.0

Table 4.3. ^{13}C NMR spectroscopic data, δ_C [ppm], (125 MHz, 295 K) for **L4** in CDCl$_3$ and [Zn(**L4**)][BF$_4$]$_2$ in CD$_3$CN (see page 78 and 119 for scheme of labeling).

In **Figure 4.6** the cross peaks of the aliphatic protons $\mathbf{H^G}$ and $\mathbf{H^F}$ of the complex [Zn(**L4**)][BF$_4$]$_2$ to the signals for directly attached carbons are shown. All of the C-H signals could be easily assigned using the HMQC spectrum.

Figure 4.6. Part of the HMQC spectrum (500 MHz, 295 K) of [Zn(**L4**)][BF$_4$]$_2$ in CD$_3$CN showing the aliphatic region. Spectrum exhibits some residues of the starting material, which could not be removed by column chromatography or other purification methods.

	C^{T2} /C^{C2}	C^{T3} /C^{C3}	C^{T4} /C^{C4}	C^{T5} /C^{C5}	C^{T6} /C^{C6}	$C^{T2'}$ /C^{D2}	$C^{T3'}$ /C^{D3}	$C^{T4'}$ /C^{D4}
L4	156.3	121.5	137.0	124.0	149.2	157.3	107.6	167.1
[Zn(**L4**)] [BF$_4$]$_2$	148.8	123.9	142.2	128.4	148.8	152.0	111.1	172.4

Table 4.4. ^{13}C NMR spectroscopic data, δ_C [ppm], (125 MHz, 295 K) for **L4** in CDCl$_3$ and [Zn(**L4**)][BF$_4$]$_2$ in CD$_3$CN (see page 78 and 119 for scheme of labeling).

Table 4.4 shows in comparison the terpyridine carbon signals of ligand **L4** and zinc(II) complex [Zn(**L4**)][BF$_4$]$_2$. After complexation with zinc(II) almost all of the carbon signals are shifted downfield, accept carbons **C^{C6}**, **C^{C2}** and **C^{D2}** which are shifted upfield.

In the **Figure 4.7** the cross peaks of the terpyridine protons **H^{C3}**, **H^{D3}**, **H^{C4}**, **H^{C6}**, **H^{C5}** and **H^P** of the complex [Zn(**L4**)][BF$_4$]$_2$ to the direct carbons signal are shown. All of the signals were assigned using the HMQC spectrum.
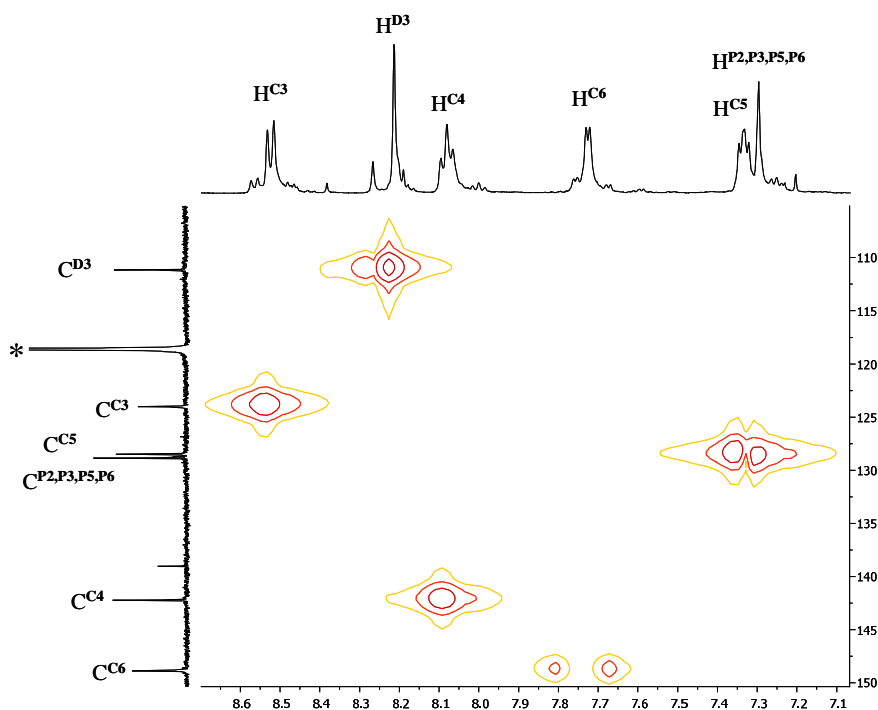
Figure 4.7. Part of the HMQC spectrum (500 MHz, 295 K) of [Zn(**L4**)][BF$_4$]$_2$ in CD$_3$CN.

The three quaternary carbons $C^{P1/P4}$, C^{C2} and C^{D2} could be only assigned using the HMBC technique, as they do not have any protons directly attached. In **Figure 4.8**, the cross peak of the benzene protons $H^{P2,P3,P5,P6}$ of the complex [Zn(**L4**)][BF$_4$]$_2$ to the indirect carbon signal $C^{P1/P4}$ is shown. The signal for proton H^{C3} couples with the signal for carbon C^{D2} and the signal for carbon C^{C2} couples with the signals for protons H^{C3}, H^{D3}, H^{C4}, H^{C6} and H^{C5}, giving the cross peaks.
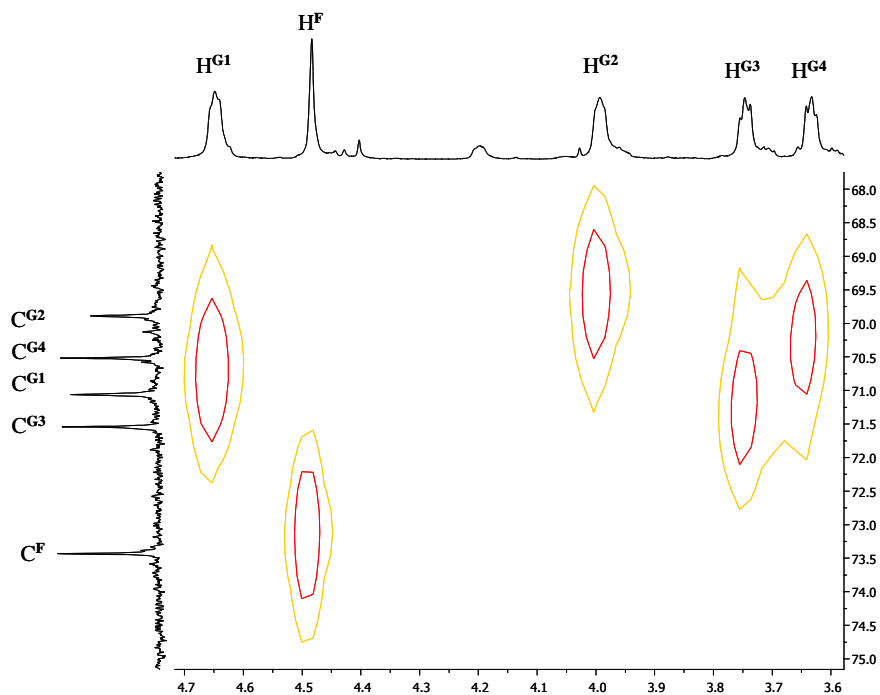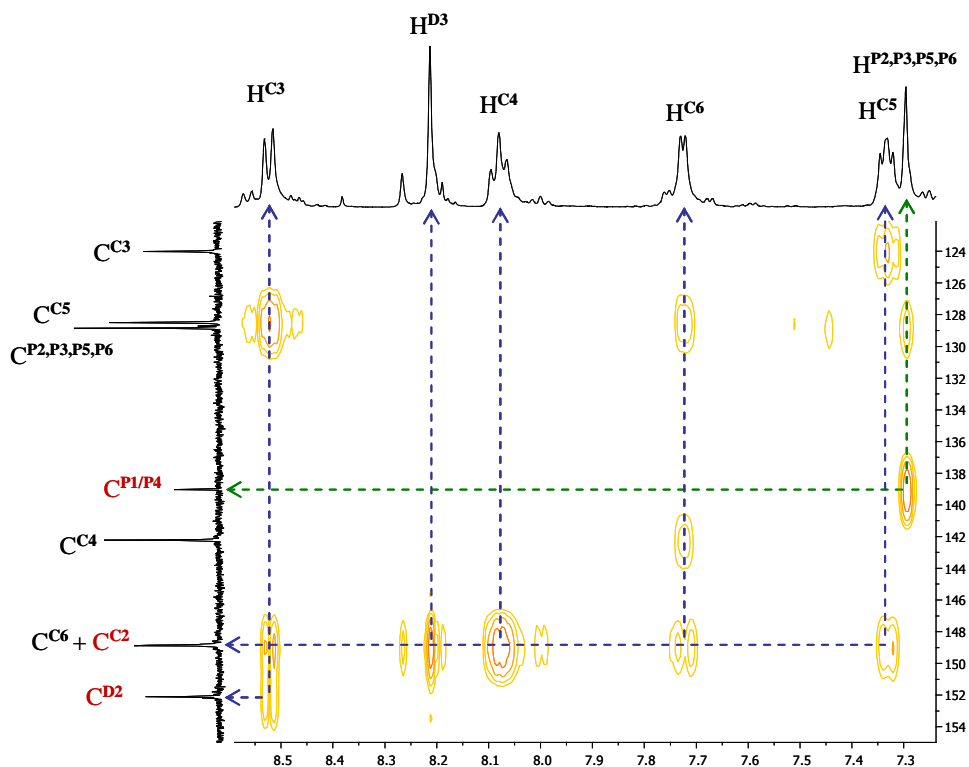

Figure 4.8. Part of the HMBC spectrum (500 MHz, 295 K) of [Zn(**L4**)][BF$_4$]$_2$ in CD$_3$CN showing the aromatic region. Spectrum exhibits some residues of the starting material, which could not be removed by column chromatography or other purification methods.

4.6 Absorption spectroscopic characterization

The electronic spectra of the homoleptic mononuclear zinc(II) complex [Zn(**L4**)][BF$_4$]$_2$ was recorded in HPLC grade acetonitrile solution. Although the ^{1}H MR spectra show the presence of small amounts of other tpy containing species, it is assumed that the observed absorption spectra represent the major component.

It is well-known from the literature that metal-to-ligand charge transfer (MLCT) processes do not occur for metal ions with filled electron shells, such as Zn(II) with its d^{10} configuration.[175] Hence, only the ligand-centered (LC) $\pi^* \leftarrow \pi$ charge transitions are observed.
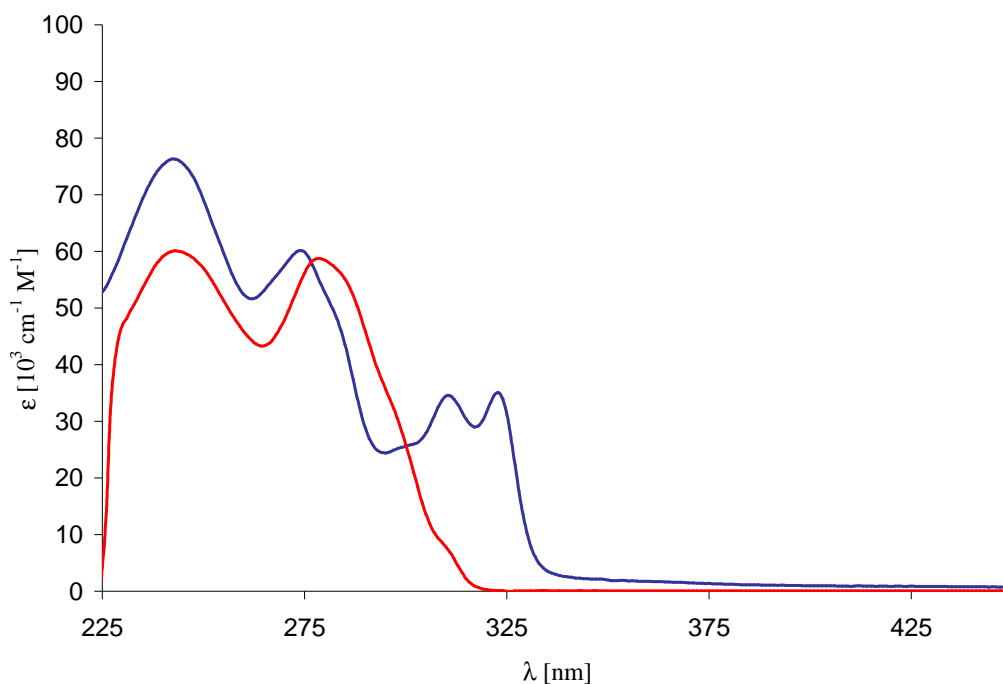
Figure 4.9. Absorption spectra of ligand **L4** in CH$_2$Cl$_2$ (in red) and [Zn(**L4**)][BF$_4$]$_2$ in CH$_3$CN (in blue).

A comparison between the UV-vis spectra obtained for free ligand **L4** (in red) and zinc(II) complex [Zn(**L4**)][BF$_4$]$_2$ (in blue) is shown in **Figure 4.9**. While the absorption spectrum of uncomplexed ligand **L4** has only two bands in the high energy UV region, assigned to the ligand-centered (LC) $\pi^* \leftarrow \pi$ transitions with λ_{max} at 241 and 279 nm

($\varepsilon_{max}/10^3$, M^{-1} cm^{-1} : 56.8 and 55.3, respectively), the electronic spectrum of zinc(II) complex [Zn(**L4**)][BF$_4$]$_2$ shows four bands: the most intense band with λ_{max} at 243 nm ($\varepsilon_{max}/10^3$, M^{-1} cm^{-1} : 76.0) and three others - λ_{max} at 274, 310 and 323 nm ($\varepsilon_{max}/10^3$, M^{-1} cm^{-1} : 60.0, 34.0 and 35.0 respectively).

4.7 DFT molecular modeling
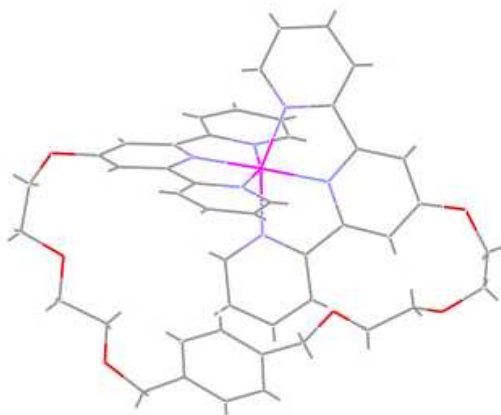
Figure 4.10. Calculated structure of [Zn(**L4**)]$^{2+}$.

The Zn(II) complex of the ditopic 4'-substituted- 2,2':6',2''-terpyridine ligand **L4** [Zn(**L4**)]$^{2+}$ was also investigated by means of SCF performed with the PM3 method. The optimized bond distances of the metal coordination environment are given in **Table 4.5**, while the optimized geometry of [Zn(**L4**)]$^{2+}$ is shown in **Figure 4.10**. The SCF calculations provide a minimum energy conformation in which the Zn(II) ion is six-coordinate, directly bound to the six available donor atoms (nitrogen on tpy) of the ligand. All of the data were compared with another [Zn(4'-X-tpy)$_2$]$^{2+}$ system with 4'-(4'''-benzo-15-crown-5)-methyloxy-2,2':6',2''-terpyridine ligand (4'-X-tpy) (**Figure 4.11**).[176] Molecular modeling shows that formation of a [1+1] metallomacrocyclic species is

possible with ligand **L4**. Both tpy moieties are almost flat, each is lying in one plane and they are coordinated to the zinc center in the characteristic perpendicular geometry, which means the planes on which tpy units are lying make a 90° angle.
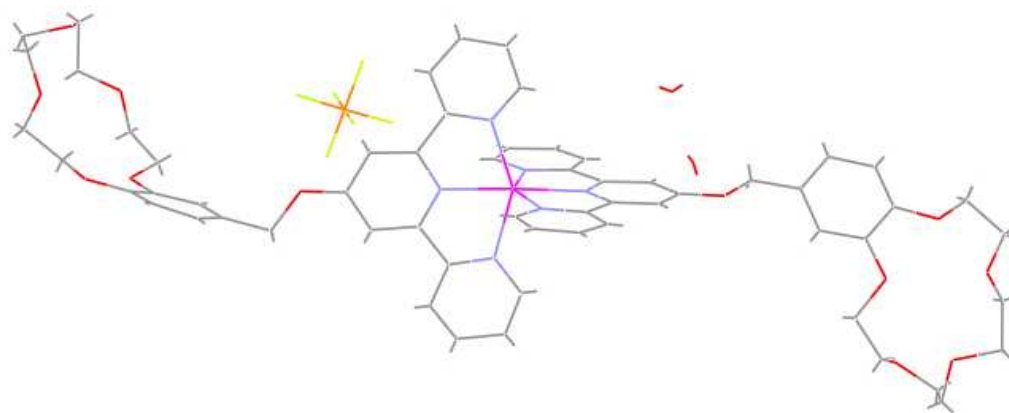
Figure 4.11. X-ray structure of $[Zn(4'-X-tpy)_2]^{2+}$, 4'-X-tpy = 4'-(4'''-benzo-15-crown-5)-methyloxy-2,2':6',2''-terpyridine

	$[Zn(\mathbf{L4})]^{2+}$	$[Zn(4'-X-tpy)_2]$
Zn-N$_{term}$	2.027	2.262(4)
Zn-N$_{cent}$	1.994	2.145(7)
Zn-N$_{term}$	2.023	2.246(3)

Table 4.5. Values of the mean distances (Å) of calculated (for $[Zn(\mathbf{L4})][BF_4]_2$) and experimental (X-ray) structures (for $[Zn(4'-X-tpy)_2]^{2+}$).

A comparison of the calculated bond distances of $[Zn(\mathbf{L4})]^{2+}$ and experimental bond distances of $[Zn(X-tpy)_2]$ shows that coordination environment in these complexes affects

the bond length, namely the Zn-N bonds in the $[Zn(\mathbf{L4})]^{2+}$ complex are shortened by 0.150-0.235 Å.

An analysis of bond length data for the IS independent $[Zn(4'-X-tpy)_2]$) structures including tpy or 4'-X-tpy ligands in the CSD using VISTA gave average $Zn-N_{term}$ 2.185 Å and $Zn-N_{cent}$ 2.081 Å.

4.8   Conclusion

The homoleptic mononuclear zinc(II) complex of the ditopic 4'-substituted-2,2':6',2"-terpyridine ligand **L4,** which is based on a benzene unit connected to two 4'-substituted-2,2':6',2"-terpyridine moieties through diethyleneoxy spacers, has been synthesized. The complex was characterized by ^{1}H and ^{13}C NMR spectroscopy, mass spectrometry (ESI-MS), IR spectroscopy, UV-Vis spectroscopy and elemental analysis. Molecular modeling of $[Zn(\mathbf{L4})]^{2+}$ using the SCF method showed that formation of a [1+1] metallomacrocyclic species is possible with this ligand.

4.9 Experimental

Ligand **L4** was prepared as described in Chapter 2. $Zn(BF_4)_2 \cdot 6H_2O$ is a commercially available compound.

❖ [Zn(**L4**)][BF$_4$]$_2$

[Zn(**L4**)][BF$_4$]$_2$
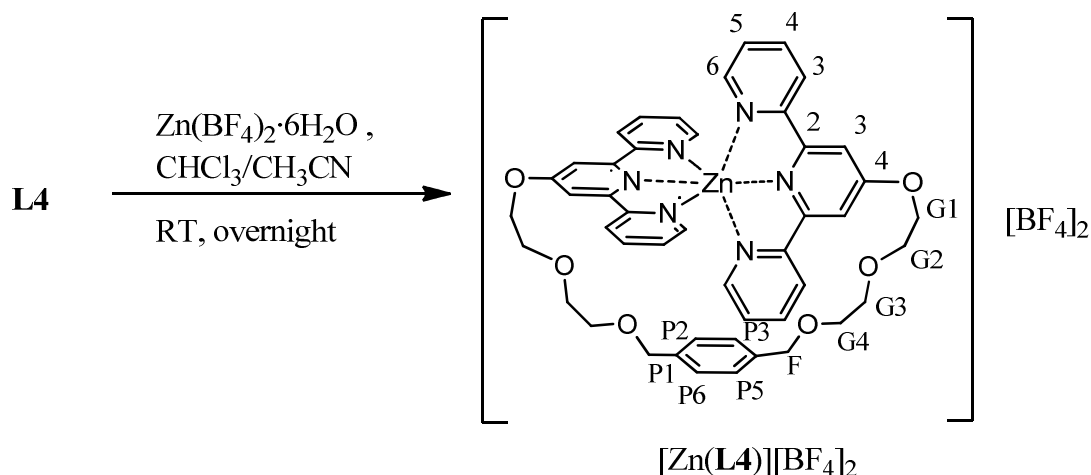
Compound **L4** (0.10 g, 0.13 mmol) dissolved in 10 mL $CHCl_3$ was added to a solution of $Zn(BF_4)_2 \cdot 6H_2O$ (0.033 g, 0.13 mmol) in 30 mL CH_3CN. The mixture was stirred overnight at room temperature. The solvent was removed *in vacuo* to give a white oil (0.12 g, 0.12 mmol, 89%).

^{1}H NMR (500 MHz, CD$_3$CN) δ_H 3.63 (m, 4H, H^{G4}), 3.75 (m, 4H, H^{G3}), 3.99 (m, 4H, H^{G2}), 4.48 (s, 4H, H^F), 4.65 (m, 4H, H^{G1}), 7.30 (s, 4H, H$^{P2, P3, P5, P6}$), 7.33 (m, 4H, H^{C5}), 7.73 (d, *J* 4.5 Hz, 4H, H^{C6}), 8.08 (t, *J* 7.5 Hz, 4H, H^{C4}), 8.21 (s, 4H, H^{D3}), 8.52 (d, *J* 8.0 Hz, 4H, H^{C3}).

^{13}C NMR (125 MHz, CD$_3$CN) δ_C 69.8 (C^{G2}), 70.5 (C^{G4}), 71.0 (C^{G1}), 71.5 (C^{G3}), 73.4 (C^F), 111.1 (C^{D3}), 123.9 (C^{C3}), 128.4 (C^{C5}), 128.8 (C^{P2,P3,P5,P6}), 139.0 (C^{P1,P4}), 142.2 (C^{C4}), 148.8 (C^{C6} and C^{C2}), 152.0 (C^{D2}), 172.4 (C^{D4}).

MS (ESI) m/z = 927.5 [**M**-BF$_4$]$^+$ (calc. 927.5), 420.3 [**M**-2BF$_4$]$^{2+}$ (calc. 420.5).

IR (solid, $\tilde{\nu}$/cm^{-1}): 3114w, 3083w, 2865w, 2359w, 1611w, 1600w, 1573w, 1558w, 1478w, 1439w, 1429w, 1349w, 1224w, 1165w, 1053m, 1034m, 1030m, 1021m, 1012m, 974w, 933w, 863w, 845w, 792w, 747w, 728w, 700w, 661w, 637w, 621w.

UV/VIS (CH$_3$CN):λ_{max}/ nm (ε_{max}, M^{-1} cm^{-1}) 243 (76 x 10^3), 274 (60 x 10^3), 310 (34 x 10^3), 323 (35 x 10^3).

Elemental Analysis . Found: C, 53.63; H, 4.27; N, 8.92. Calc. for C$_{46}$H$_{44}$B$_2$F$_8$N$_6$O$_6$Zn·H$_2$O·0.5CH$_3$CN: C, 53.54; H, 4.54; N, 8.63%.

CHAPTER 5

Synthesis of a tritopic 4'-substituted- 2,2':6',2''-terpyridine ligand and its heteroleptic trinuclear ruthenium(II) complex

5.1 Introduction
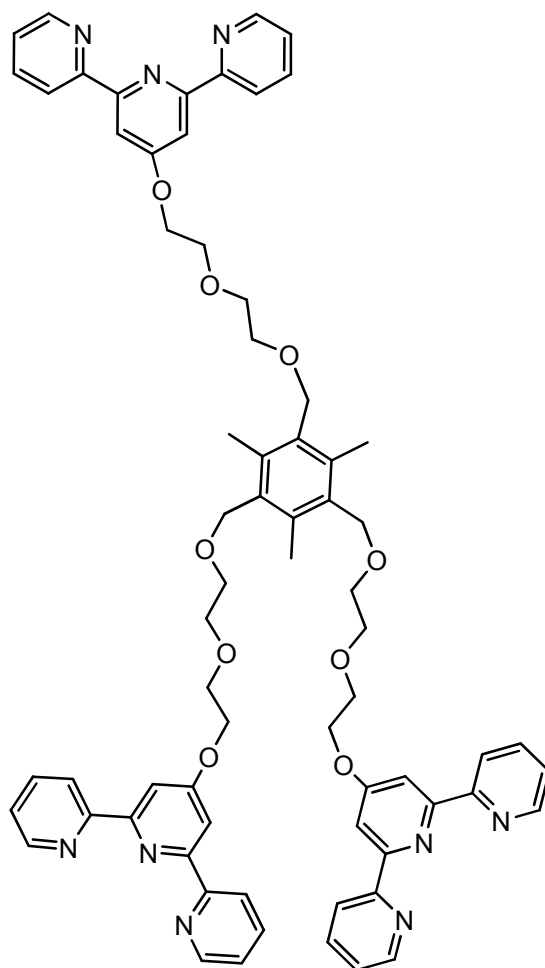
Scheme 5.1. New tritopic ligand **L5**.

In the introduction it was shown that more than one or two 2,2':6',2''-terpyridine domains can be used to synthesize different groups of ligands (see Section 1.3). Bridged ligands containing three, four or six tpy domains can be used as the core for the synthesis of metallostars[83,84] and metallodendrimers.[85]

In this chapter the synthesis of new tritopic ligand **L5** based on a mesitylene unit connected to three 4'-substituted-2,2':6',2''-terpyridine moieties through diethylene glycol spacers is discussed (**Scheme 5.1**).

In Chapter 3, the interesting properties of the complexes of 2,2'-bipyridine and 2,2':6',2''-terpyridine derivatives were discussed. The synthesis, as well as the photochemical and photophysical properties, of new dinuclear ruthenium(II) complexes of ditopic 4'-substituted- 2,2':6',2''-terpyridine ligands have been described in this thesis in Chapter 3. In Chapter 5, a new tritopic 4'-substituted- 2,2':6',2''-terpyridine ligand **L5** was introduced and characterized. In this chapter, a heteroleptic trinuclear ruthenium(II) complex of ligand **L5** is discussed (**Scheme 5.2**). This ruthenium(II) complex [(**L5**)(Ru)$_3$(tpy)$_3$][PF$_6$]$_6$ was designed such that one ruthenium ion goes to each binding site to create an M$_3$L species. The monotopic tpy ligands "close" the complex at all three sites and prevent polymerization.
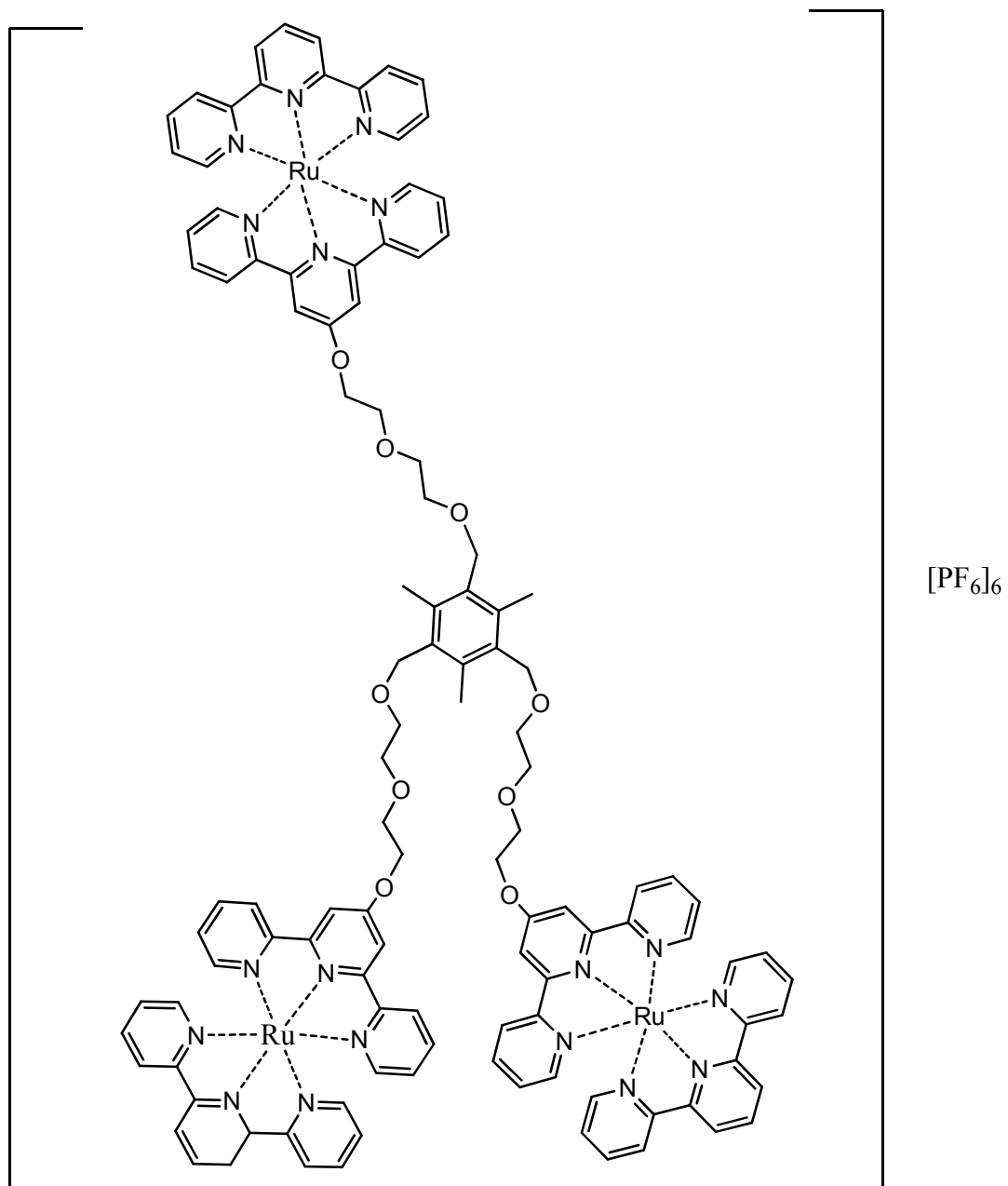
Scheme 5.2. Heteroleptic trinuclear ruthenium(II) complex of tritopic 4'-substituted-2,2':6',2''-terpyridine ligand.

5.2.1 Synthesis of a tritopic ligand L5

Ligand **L5** was prepared in three steps by nucleophilic substitution reactions. In the first step commercially accessible mesitylene was bromomethylated in reaction with *para*-formaldehyde and potassium bromide (**Scheme 5.3**). The benzene ring functionalized with three diethylene glycol chains was obtained (**L5a**) by nucleophilic substitution of the tribromobenzene derivative (**Scheme 5.3**). In the last step, a nucleophile was generated by deprotonation of three terminal hydroxyl groups, these were then reacted further with Cl-tpy (**Scheme 5.5**). 4'-Chloro-2,2':6',2"-terpyridine (Cl-tpy) was prepared as previously reported in the literature.[102]
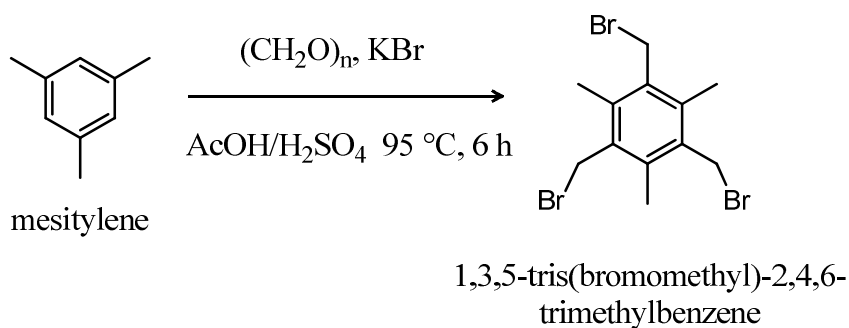
Scheme 5.3. Synthesis of 1,3,5-tris(bromomethyl)-2,4,6-trimethylbenzene.

The conversion of mesitylene involves bromomethylation with *para*-formaldehyde and KBr in hot 1:1 mixture of concentrated sulfuric and acetic acids (**Scheme 5.3**).

136
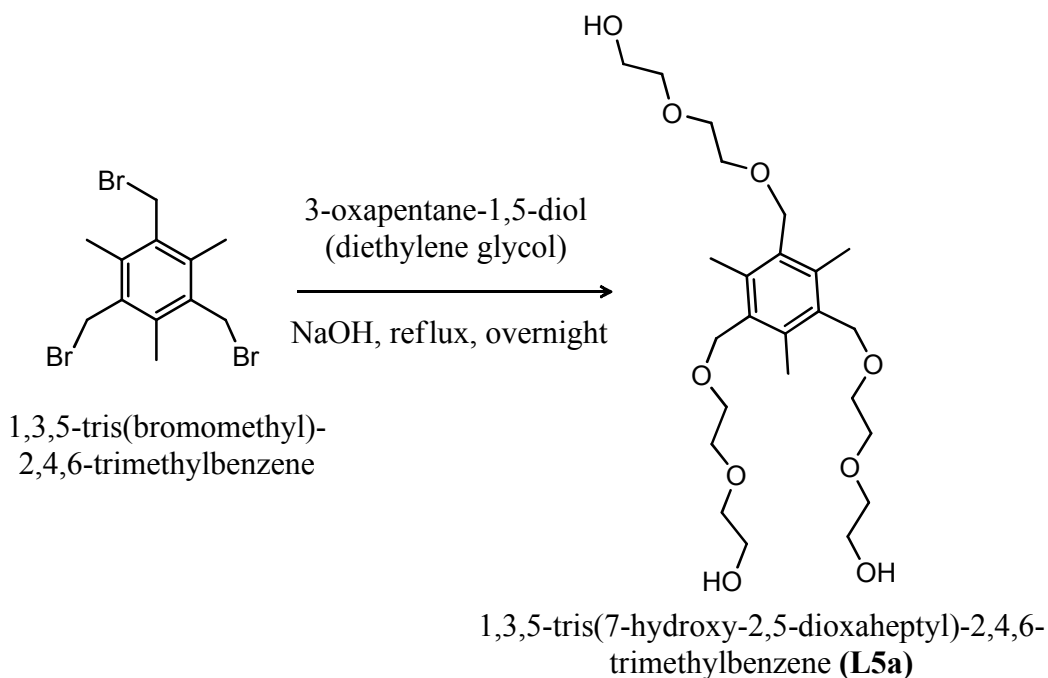
Scheme 5.4. Synthesis of **L5a**.

L5a was prepared from 1,3,5-tris(bromomethyl)-2,4,6-trimethylbenzene, which was heated under reflux in the diethylene glycol with sodium hydroxide overnight (**Scheme 5.4**).

In the next step, after deprotonation of three terminal hydroxyl groups with potassium hydroxide in hot DMSO, intermediate product **L5a** was reacted further with Cl-tpy. After three days the desired product was obtained in 89% yield after work up (**Scheme 5.5**).

1,3,5-tris(8-(4'-(2,2':6',2"-terpyridyl))-2,5,8-trioxaoctyl)-
2,4,6-trimethylbenzene **(L5)**
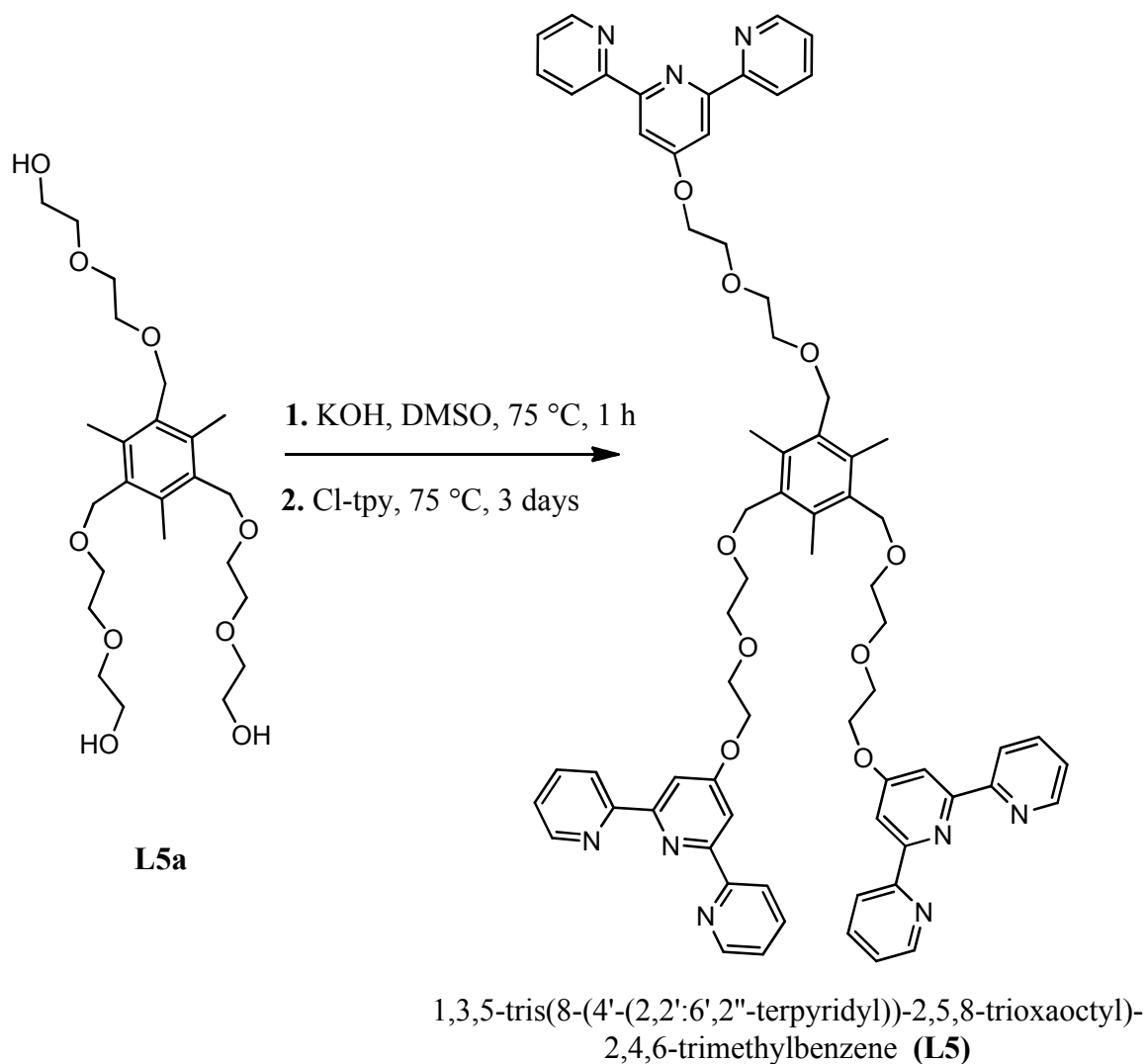
Scheme 5.5. Synthesis of ligand **L5**.

5.2.2 Synthesis of ruthenium(II) complex of L5 (Ru₃L5)

A heteroleptic trinuclear ruthenium(II) complex of ligand **L5** was prepared stepwise in a Biotage microwave reactor. First one equivalent of $RuCl_3 \cdot 3H_2O$ and one equivalent tpy

(**Scheme 5.6**) were heated under microwave conditions in ethanol at 135 °C for 15 minutes. Then 0.3 equivalents of tritopic 4'-substituted- 2,2':6',2''-terpyridine ligand **L5** and the reducing agent *N*-ethylmorpholine (NEM) were added and the mixture was again heated under microwave conditions at 135 °C for 15 minutes (**Scheme 5.6**). The red ruthenium(II) complex was precipitated from solution with excess aqueous NH_4PF_6 and then filtered and collected, yielding $[(\mathbf{L5})(Ru)_3(tpy)_3][PF_6]_6$ in 90% yield, without further purification.
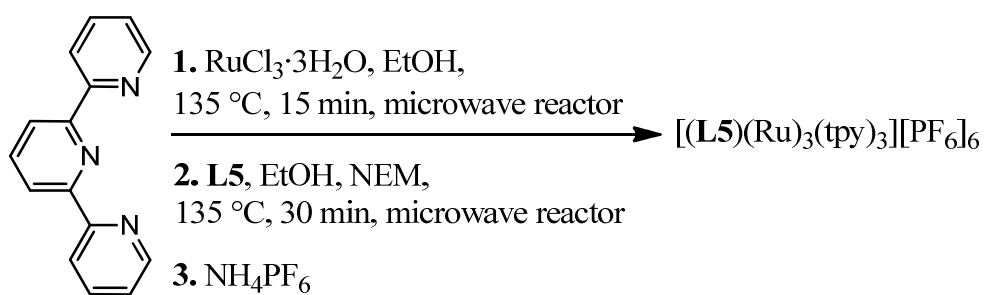
Scheme 5.6. Synthesis of $[(\mathbf{L5})(Ru)_3(tpy)_3][PF_6]_6$.

5.3.1 ^{1}H NMR spectroscopy of L5a and L5

L	$H^{G2\text{-}G4}$	H^{G1}	H^F	H^{OH}	H^P/H^{Me}
L1a	3.59–3.76 (m)	3.57 (m)	4.56 (s)	3.34 (br)	7.18-7.39 (m)
L5a	3.65-3.85 (m)	3.55 (m)	4.59 (s)	1.71 (br)	2.41 (s)

Table 5.1. ^{1}H NMR spectroscopic data, δ_H [ppm], (400 MHz, 295 K, CDCl$_3$) for **L1a** and **L5a** (see page 140 for scheme of labeling)**.**

Intermediate product **L5a** (**Scheme 5.7**) and ligand **L5** (**Scheme 5.8**) were characterized by ^{1}H NMR spectroscopy in CDCl$_3$. In **Table 5.1** the proton signals of intermediate **L5a** are compared with those of compound **L1a.**
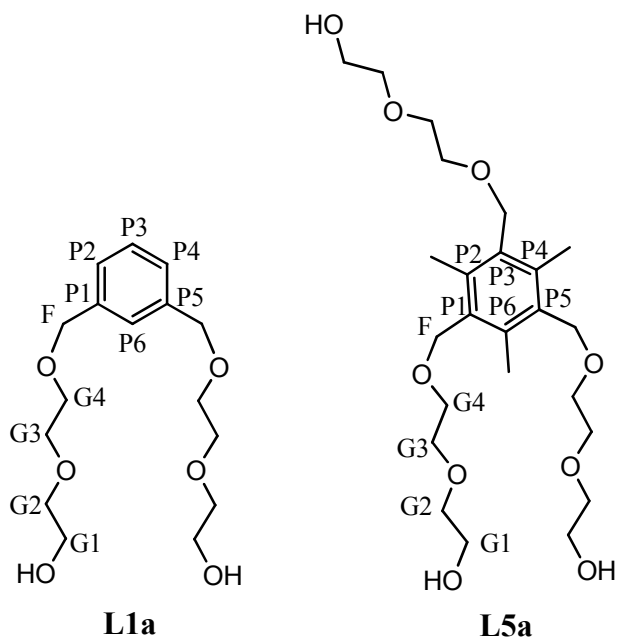
Scheme 5.7. Labeling for **L1a** and **L5a** intermediates.

All of **H^P** protons on the benzene ring of **L5a** are substituted with CH$_3$ groups, therefore a singlet for nine mesitylene protons **H^{Me}** is observed at δ 2.41 ppm. All of the signals corresponding to the diethylene glycol chain **H^{G1-G4}** of **L5a** can be found, as expected in the aliphatic region at δ 3.55-3.85 ppm. The signal for **H^{G1}** is the strongest shifted downfield due to its close proximity to the tpy unit. The signals of the **H^{G2}**, **H^{G3}** and **H^{G4}** protons of ligand **L5** overlap and give a multiplet. The signal at δ 4.59 ppm is assigned to **H^F** from the -CH$_2$- bridge connecting the benzene ring to the diethylene glycol chain.

After the substitution of the three terminal hydroxyl groups on the diethylene glycol chains of **L5a** with Cl-tpy some of changes in chemical shifts can be observed (**Tables 5.2** and **5.3**).

140
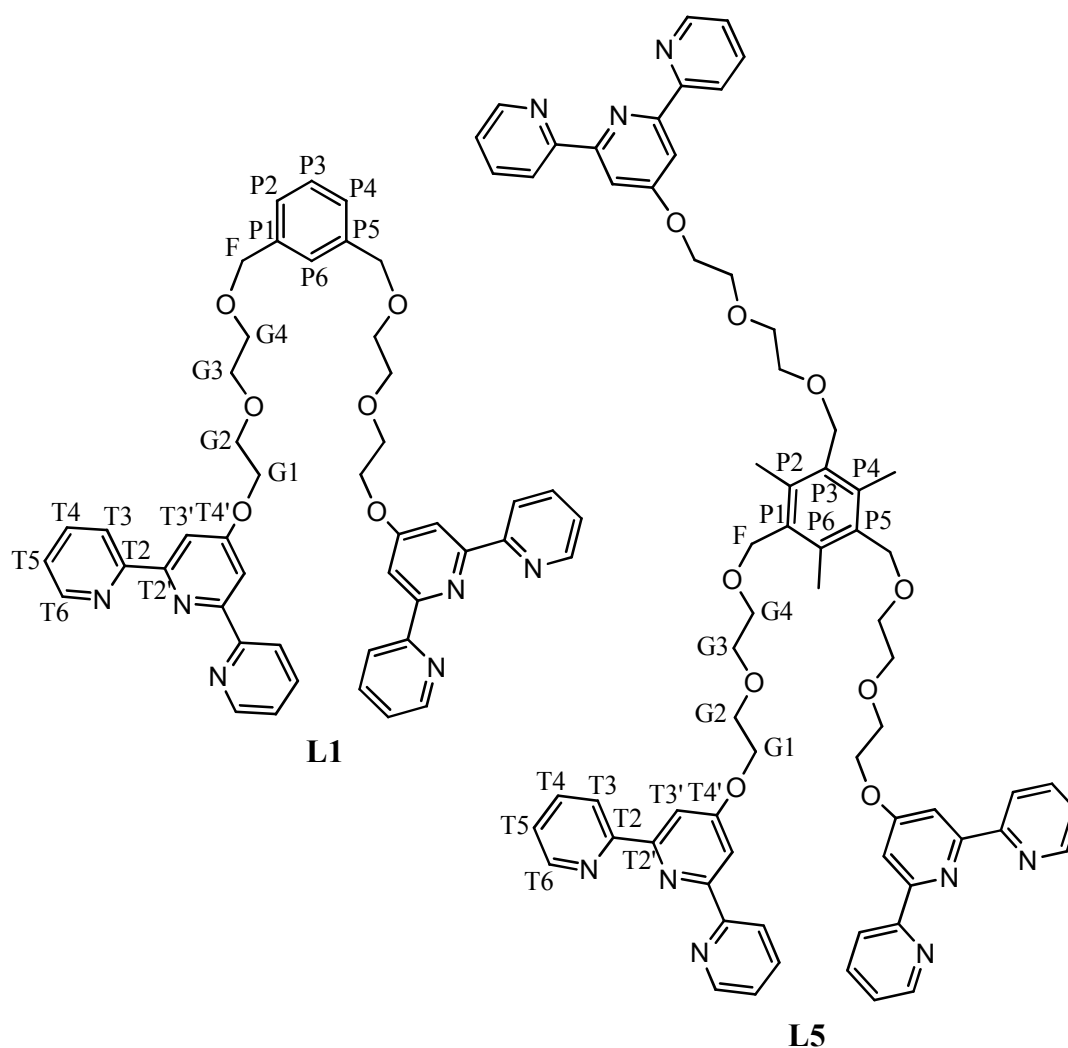
Scheme 5.8. Labeling for ligands **L1** and **L5**.

For comparison, **Table 5.2** shows chemical shifts of the protons on diethylene glycol chains $\mathbf{H}^{\mathbf{G1\text{-}G4}}$ and the -CH$_2$-bridge $\mathbf{H}^{\mathbf{F}}$ of ligands **L1** and **L5**. The aromatic protons from tpy of ligands **L1** and **L5** are shown in **Table 5.3**.

All of the signals corresponding to the diethylene glycol chain $\mathbf{H}^{\mathbf{G1\text{-}G4}}$ of **L5** are slightly shifted upfield in comparison to the proton signals $\mathbf{H}^{\mathbf{G1\text{-}G4}}$ of **L1**. The singlet at δ 4.54 ppm is assigned to $\mathbf{H}^{\mathbf{F}}$ from the -CH$_2$- bridge connecting the benzene ring to the ethylene glycol chain. The splitting of the methyl signal in the ligand **L5** (and the complex) indicates that the two atropisomers only interconvert slowly in solution (see **Figure5.1** and **5.3**).

L	H^{G4}	H^{G3}	H^{G2}	H^{G1}	H^F
L1	3.63 (m)	3.75 (m)	3.91 (m)	4.37 (m)	4.54 (s)
L5	3.61 (m)	3.68 (m)	3.85 (m)	4.34 (m)	4.54 (s)

Table 5.2. ^{1}H NMR spectroscopic shift data, δ_H [ppm], (500 MHz, 295 K, CDCl$_3$) for **L1** and **L5** (see page 141 for scheme of labeling)**.**

The five signals in the aromatic region for both ligands **L1** and **L5**: $\mathbf{H^{T6}}$, $\mathbf{H^{T3}}$, $\mathbf{H^{T3'}}$, $\mathbf{H^{T4}}$, $\mathbf{H^{T5}}$ have almost the same chemical shifts in the two compounds.

L	H^{T5}	H^{T4}	$H^{T3'}$	H^{T3}	H^{T6}
L1	7.27-7.31 (m)	7.81 (td) J 1.5, 7.8 Hz	8.02 (s)	8.58 (d) J 8.0 Hz	8.65 (d) J 4.1 Hz
L5	7.27-7.32 (m)	7.79 (t) J 7.5 Hz	7.99 (s)	8.56 (d) J 7.9 Hz	8.65 (d) J 3.9 Hz

Table 5.3. ^{1}H NMR spectroscopic shift data, δ_H [ppm], (500 MHz, 295 K, CDCl$_3$) for **L1** and **L5** (see page 141 for scheme of labeling)**..**

The ^{1}H NMR spectrum of ligand **L5** (**Figure 5.1**) shows five signals in the aromatic region for the protons on tpy: $\mathbf{H^{T5}}$, $\mathbf{H^{T3}}$, $\mathbf{H^{T3'}}$, $\mathbf{H^{T4}}$, $\mathbf{H^{T5}}$. In the aliphatic region, in the ^{1}H NMR spectrum of ligand **L5,** there is one singlet for the $\mathbf{H^F}$ proton at δ 4.54 ppm and four well separated multiplets from the $\mathbf{H^G}$ protons on the diethylene glycol chains. The signal for $\mathbf{H^{G1}}$ is the strongest shifted downfield due to its close proximity to the tpy unit. The assignment of the $\mathbf{H^{G1}}$, $\mathbf{H^{G2}}$, $\mathbf{H^{G3}}$ and $\mathbf{H^{G4}}$ protons of the **L5** ligand were made using the COSY technique (**Figure 5.2**). The signal for $\mathbf{H^{G1}}$ gives a COSY cross peak to the signal $\mathbf{H^{G2}}$ at δ 3.85 ppm (**Figure 5.2**). The signal for $\mathbf{H^{G3}}$ gives a COSY cross peak to

the signal at δ 3.61 ppm, and this signal is assigned to $\mathbf{H^{G4}}$ (**Figure 5.2**). The singlet for nine mesitylene protons $\mathbf{H^{Me}}$ is observed at δ 2.38 ppm.
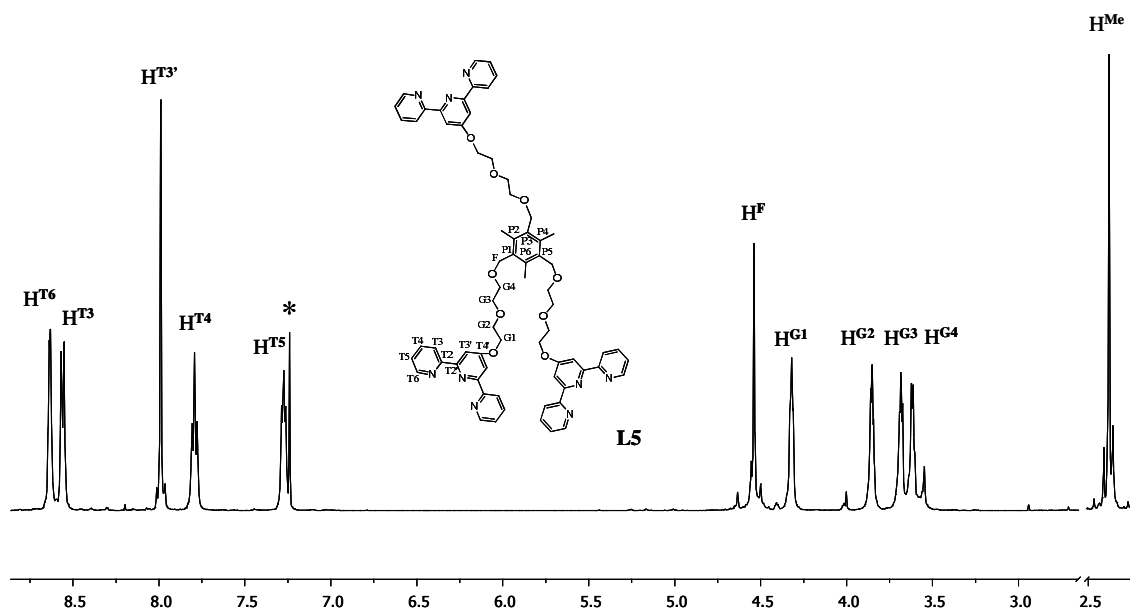
Figure 5.1. ^{1}H NMR spectrum (500 MHz, 295 K) of **L5** in CDCl$_3$. The signal marked with * is the signal for CHCl$_3$. Spectrum exhibits some residues of the starting material, which could not be removed by column chromatography or other purification methods.
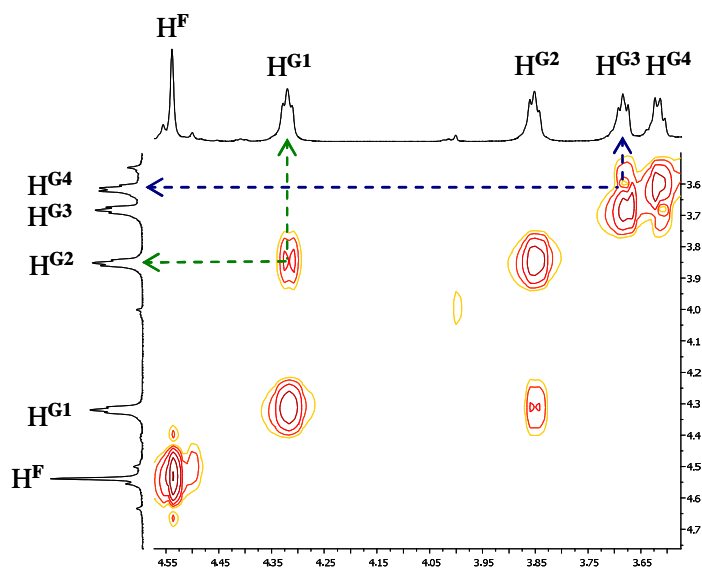
Figure 5.2. Aliphatic region of the COSY spectrum (500 MHz, 295 K) of **L5** in CDCl$_3$.

5.3.2 ^{1}H NMR spectroscopy of Ru$_3$L5
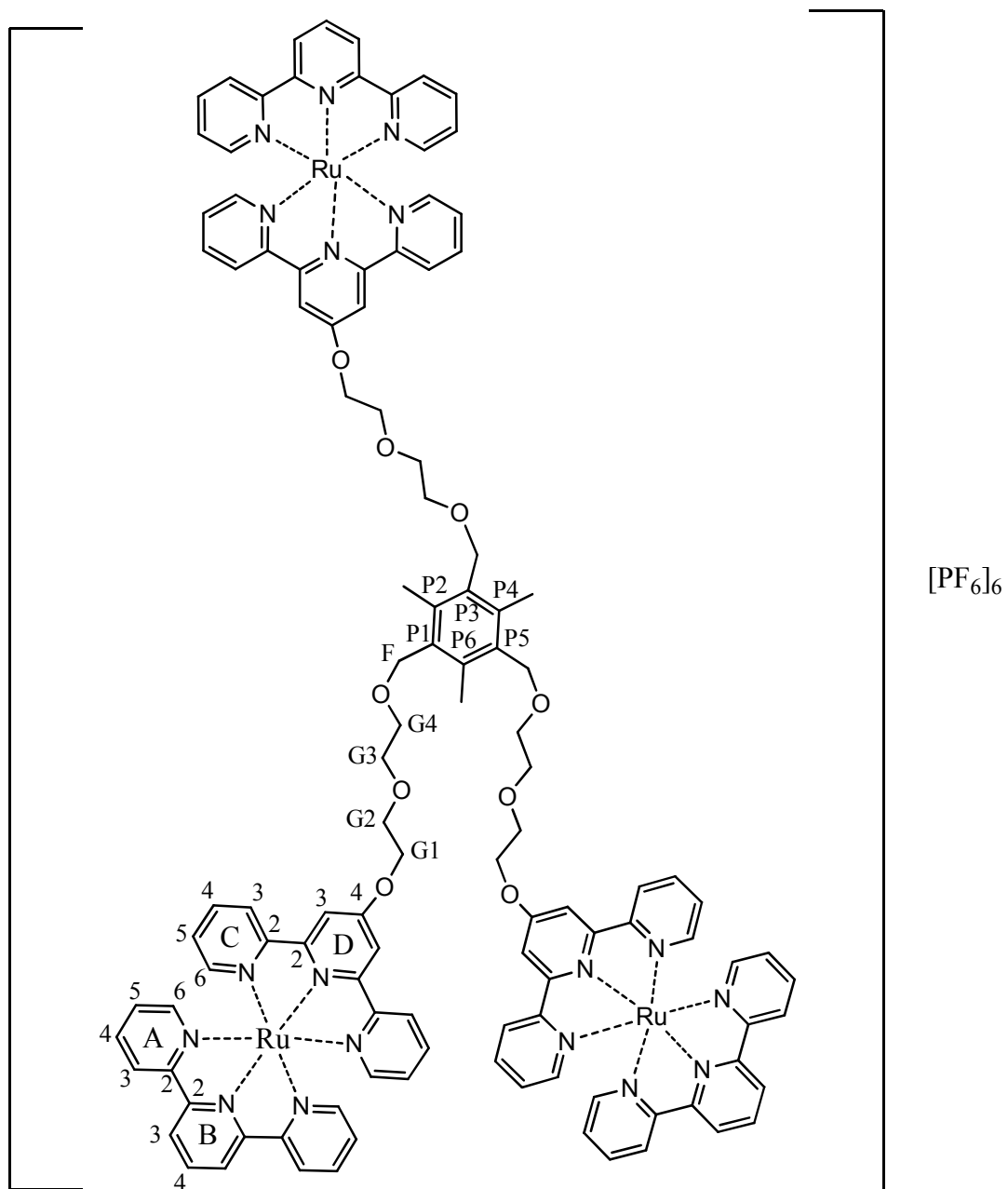
Scheme 5.9. Labeling for the ruthenium(II) complex of tritopic 4'-substituted- 2,2':6',2"-terpyridine ligand [(**L5**)(Ru)$_3$(tpy)$_3$][PF$_6$]$_6$.

The complex [(**L5**)(Ru)$_3$(tpy)$_3$][PF$_6$]$_6$ was characterized by ^{1}H NMR spectroscopy in CD$_3$CN solution. Assignments have been made using COSY and NOESY experiments and by comparison with the spectra of heteroleptic dinuclear ruthenium(II) complexes of ditopic 4'-substituted- 2,2':6',2''-terpyridine ligands **L1**, **L2**, **L4**, **L6** and **L7** described in Chapter 3 in this thesis.
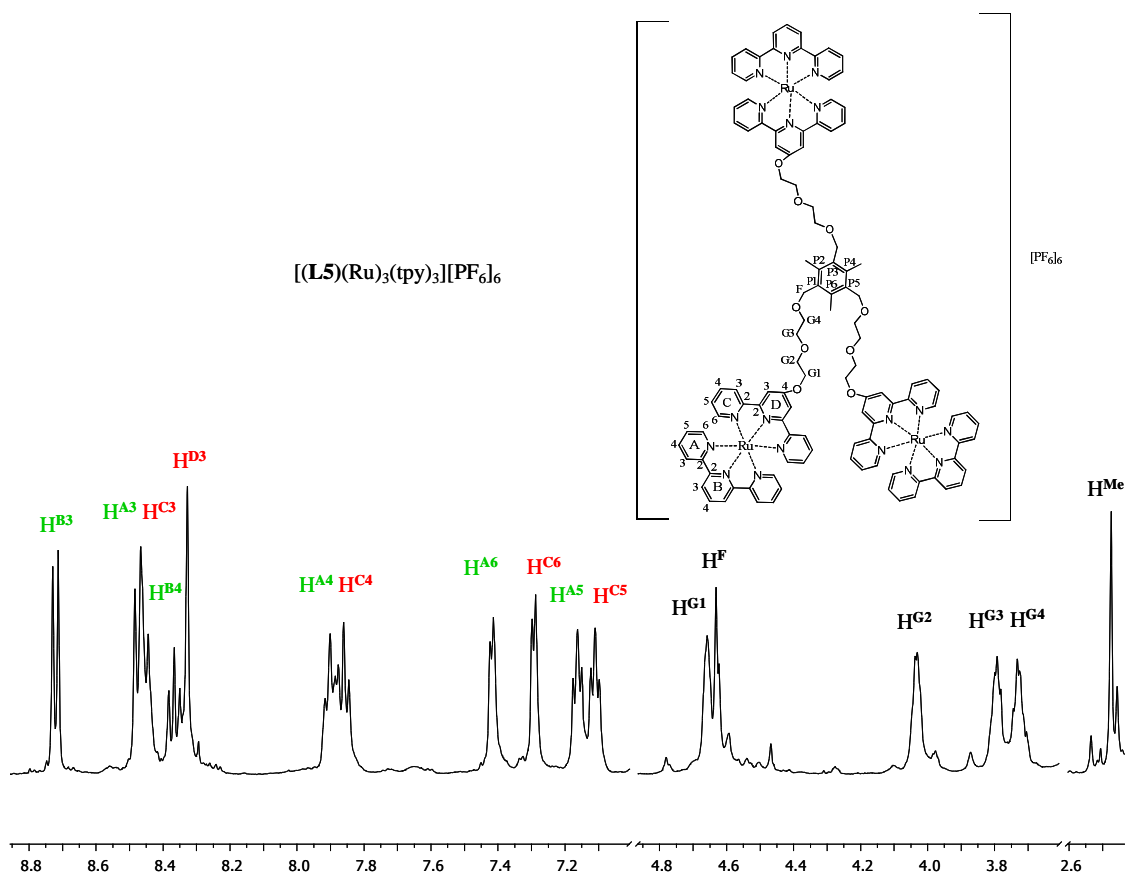
Figure 5.3. ^{1}H NMR spectrum of [(**L5**)(Ru)$_3$(tpy)$_3$][PF$_6$]$_6$ in CD$_3$CN. Spectrum exhibits some residues of the starting material, which could not be removed by column chromatography or other purification methods.

In **Figure 5.3** the ^{1}H NMR spectrum of [(**L5**)(Ru)$_3$(tpy)$_3$][PF$_6$]$_6$ in CD$_3$CN is shown. The proton signals from rings A and B of the unsubstituted tpy are highlighted in green, the proton signals from rings C and D of ligand **L5** in red.

	H^{G4}	H^{G3}	H^{G2}	H^{G1}	H^{F}
L5	3.61 (m)	3.68 (m)	3.85 (m)	4.34 (m)	4.54 (s)
Ru₃L5	3.73 (m)	3.79 (m)	4.03 (m)	4.66 (m)	4.63 (s)

Table 5.4. ^{1}H NMR spectroscopic data, δ_H [ppm] for **L5** (500 MHz, 295 K, CDCl₃) and [(**L5**)(Ru)₃(tpy)₃][PF₆]₆ (500 MHz, 295 K, CD₃CN) (see page 144 for scheme of labeling)**.**

Tables 5.4 and **5.5** as well as **Figure 5.3** show how the ^{1}H NMR spectrum of ligand **L5** changes after complexation with ruthenium(II). All of the signals are influenced by addition of ruthenium(II) to the system.

	H^{T5}/H^{C5}	H^{T4}/H^{C4}	$H^{T3'}/H^{D3}$	H^{T3}/H^{C3}	H^{T6}/H^{C6}
L5	7.27-7.32 (m)	7.79 (t) J 7.2 Hz	7.99 (s)	8.56 (d) J 7.9 Hz	8.65 (d) J 3.9 Hz
Ru₃L5	7.11 (m)	7.82-7.94 (m)	8.33 (s)	8.46 (m)	7.29 (d) J 5.2 Hz

Table 5.5. ^{1}H NMR spectroscopic data, δ_H [ppm] for **L5** (500 MHz, 295 K, CDCl₃) and [(**L5**)(Ru)₃(tpy)₃][PF₆]₆ (500 MHz, 295 K, CD₃CN) (see page 144 for scheme of labeling)**.**

In the aliphatic region of the ^{1}H NMR spectra of ligand **L5** and complex [(**L5**)(Ru)₃(tpy)₃][PF₆]₆ there are a few significant differences. After complexation all of the proton signals **H^{G}** and **H^{F}** are shifted downfield, protons **H^{G4}, H^{G3}** and **H^{F}** by around 0.10 ppm, and mostly affected signals assigned to the protons **H^{G2}** and **H^{G1}** by 0.18 and 0.32 ppm, respectively (**Table 5.4**). The assignment of the **H^{G1}, H^{G2}, H^{G3}** and **H^{G4}** protons of complex [(**L5**)(Ru)₃(tpy)₃][PF₆]₆ were made using the ^{1}H-^{1}H COSY technique (**Figure 5.5**).

146
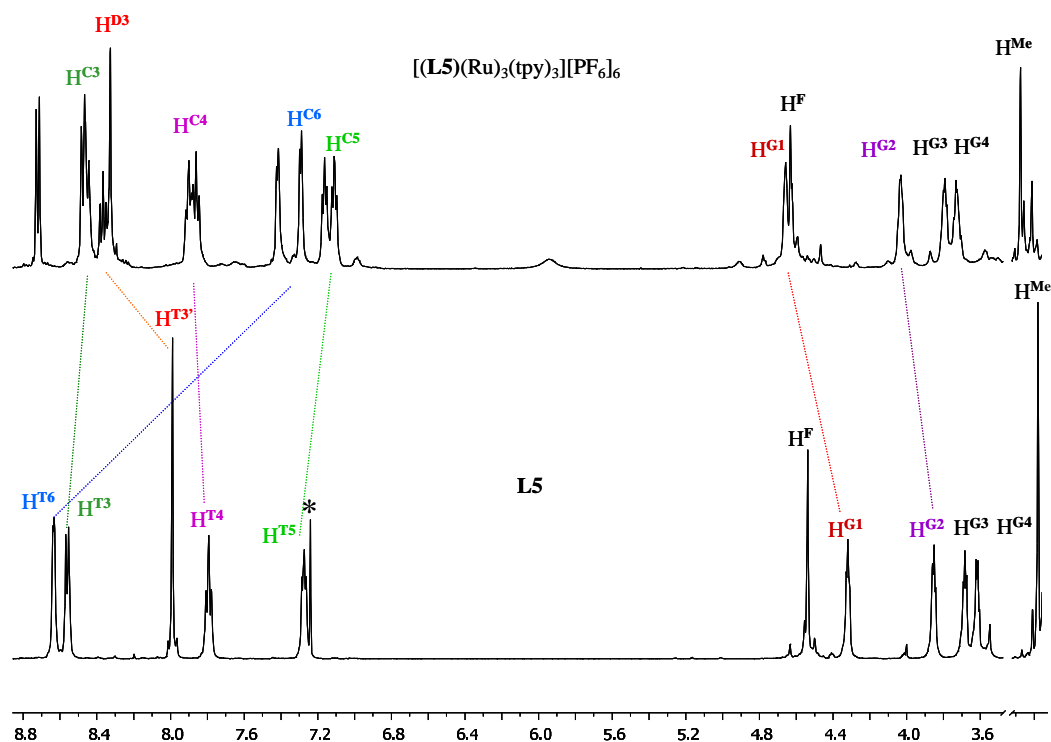
Figure 5.4. ^{1}H NMR spectrum (500 MHz, 295 K) of **L5** (below) in CDCl$_3$ and [(**L5**)(Ru)$_3$(tpy)$_3$][PF$_6$]$_6$ (above) in CD$_3$CN. The signal marked with * is the signal for CHCl$_3$.
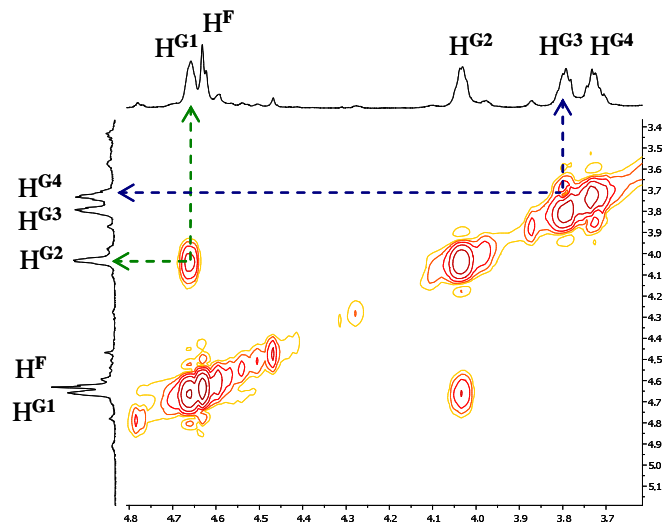
Figure 5.5. Aliphatic region of the ^{1}H-^{1}H COSY spectrum (500 MHz, 295 K) of [(**L5**)(Ru)$_3$(tpy)$_3$][PF$_6$]$_6$ in CD$_3$CN. Spectrum exhibits some residues of the starting material, which could not be removed by column chromatography or other purification methods.

For comparison, all of the terpyridine proton signals of ligand **L5** and ruthenium(II) complex $[(\mathbf{L5})(\mathrm{Ru})_3(\mathrm{tpy})_3][\mathrm{PF}_6]_6$ are shown in **Table 5.5**. The signals for the $\mathbf{H^{T3}}$, $\mathbf{H^{T5}}$ and $\mathbf{H^{T6}}$ protons of ligand are all shifted upfield and the mostly affected signal assigned to the proton $\mathbf{H^{T6}}$ by 1.36 ppm. The signals for protons $\mathbf{H^{C4}}/\mathbf{H^{T4}}$ and $\mathbf{H^{D3}}/\mathbf{H^{T3'}}$ of complex $[(\mathbf{L5})(\mathrm{Ru})_3(\mathrm{tpy})_3][\mathrm{PF}_6]_6$ are shifted downfield, respectively by around 0.09 and 0.34 ppm, in comparison to ligand **L5**.

5.4.1 ^{13}C NMR spectroscopy of L5a and L5

Table 5.6 shows the ethylene glycol $\mathbf{C^G}$, $\mathbf{C^F}$ and phenyl $\mathbf{C^P}$ carbon signals for ligands **L1** and **L5** in CDCl$_3$ solution. All of the terpyridine carbon signals are shown in the **Table 5.7**. The assignments were made using HMQC and HMBC techniques.

L	$\mathbf{C^{G1}}$	$\mathbf{C^{G2}}$	$\mathbf{C^{G3}}$	$\mathbf{C^{G4}}$	$\mathbf{C^F}$	$\mathbf{C^P}/$ $^{(\#)}\mathbf{C^P}$ (quaternary)
L1	68.0	69.8	71.2	69.7	73.4	127.3 127.3 128.7 $^{(\#)}$138.6
L5	68.0	69.6	71.3	69.6	68.1	$^{(\#)}$132.5 $^{(\#)}$138.5

Table 5.6. ^{13}C NMR spectroscopic shift data, δ_C [ppm], (125 MHz, 295 K, CDCl$_3$) for **L1** and **L5** (see page 141 for scheme of labeling)**.**

Almost all of the carbon signals in the aliphatic region of ligand **L5** are shifted upfield, in comparison to the carbon signals of ligand **L1**, but most changed is the carbon signal C^F of ligand **L5**, which is shifted by 5.3 ppm.

L	$C^{T3'}$	C^{T3}	C^{T5}	C^{T4}	C^{T6}	C^{T2}	$C^{T2'}$	$C^{T4'}$
L1	107.7	121.5	124.0	136.9	149.2	156.3	157.3	167.2
L5	107.6	121.5	124.0	136.9	149.2	156.2	157.2	167.1

Table 5.7. ^{13}C NMR spectroscopic shift data, δ_C [ppm], (125 MHz, 295 K, CDCl$_3$) for **L1** and **L5** (see page 141 for scheme of labeling)**.**
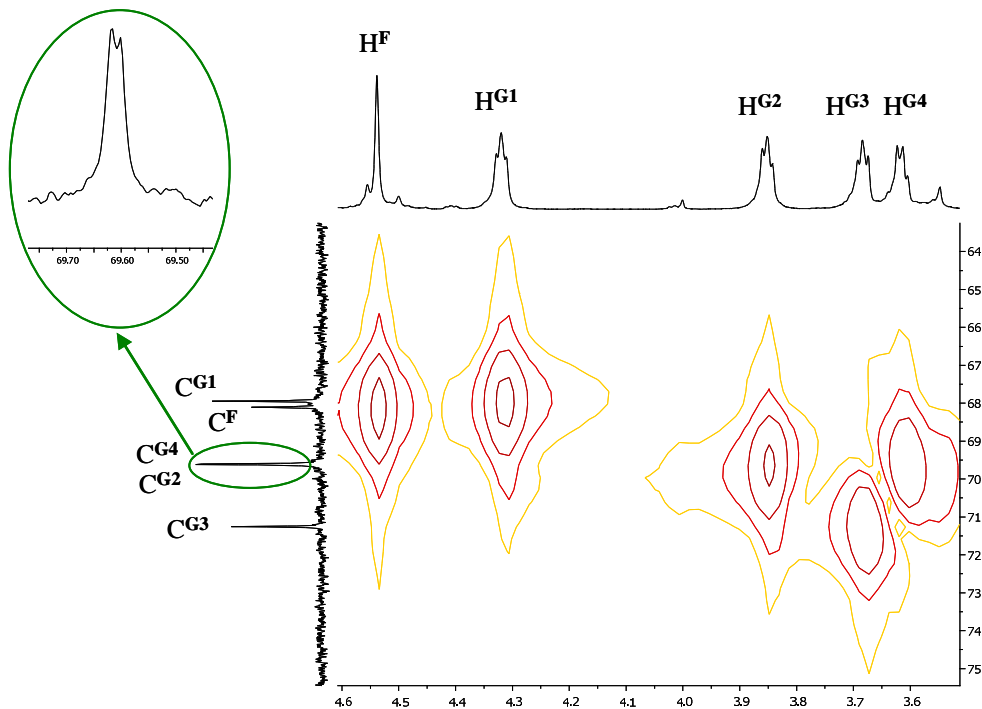
Figure 5.6. Part of the HMQC spectrum (500 MHz, 295 K) of **L5** in CDCl$_3$ showing the aliphatic region. Spectrum exhibits some residues of the starting material, which could not be removed by column chromatography or other purification methods.

In **Figure 5.6** the aliphatic region of HMQC spectrum of ligand **L5** in CDCl$_3$ is shown. The proton signals for $\mathbf{H^{G2}}$ and $\mathbf{H^{G4}}$ couple with the almost overlapping signals for carbons $\mathbf{C^{G2}}$ and $\mathbf{C^{G4}}$, giving the cross peaks.

The signal for the quaternary carbon $\mathbf{C^P}$ of ligand **L5,** to which the glycol chains are attached through a -CH$_2$- bridge, is slightly shifted upfield.

For the terpyridine carbon signals of ligands **L1** and **L5,** almost no differences are observed, except the signal assigned to the carbon $\mathbf{C^{T4'}}$ of ligand **L5**, which is shifted upfield by 0.1 ppm.

5.4.2 ^{13}C NMR spectroscopy of Ru$_3$L5

Table 5.8 shows the ethylene glycol $\mathbf{C^G}$, $\mathbf{C^F}$ and phenyl $\mathbf{C^P}$ carbon signals for the heteroleptic trinuclear ruthenium(II) complex of ligand **L5** in CD$_3$CN solution. All of the terpyridine carbon signals, from both types of tpy units – from tritopic ligand **L5** and monotopic tpy ligand - are shown in **Tables 5.9** and **5.10**. The assignments were made using HMQC and HMBC techniques. The terpyridine carbon signals are comparable to ruthenium(II) complexes described in Chapter 3 and other related terpyridine systems.

In the aliphatic region of the ^{13}C NMR spectrum after complexation, all of the carbon signals $\mathbf{C^G}$ and $\mathbf{C^F}$ as well as signals of carbons on the benzene ring $\mathbf{C^P}$ are shifted downfield, in comparison to free ligand **L5**. The mostly affected signals assigned to the carbons $\mathbf{C^{G1}}$ and $\mathbf{C^{G4}}$ are shifted by around 3 and 1 ppm, respectively (**Table 5.8**).

	C^{G1}	C^{G2}	C^{G3}	C^{G4}	C^{F}	C^{P}
L5	68.0	69.60	71.3	69.6	68.1	132.5 138.5
Ru₃L5	70.9	70.0	71.7	70.6	68.4	134.0 139.0

Table 5.8. ^{13}C NMR spectroscopic data, δ_C [ppm], (125 MHz, 295 K) for **L5** in $CDCl_3$ and $[(\textbf{L5})(Ru)_3(tpy)_3][PF_6]_6$ in CD_3CN (see page 144 for scheme of labeling).
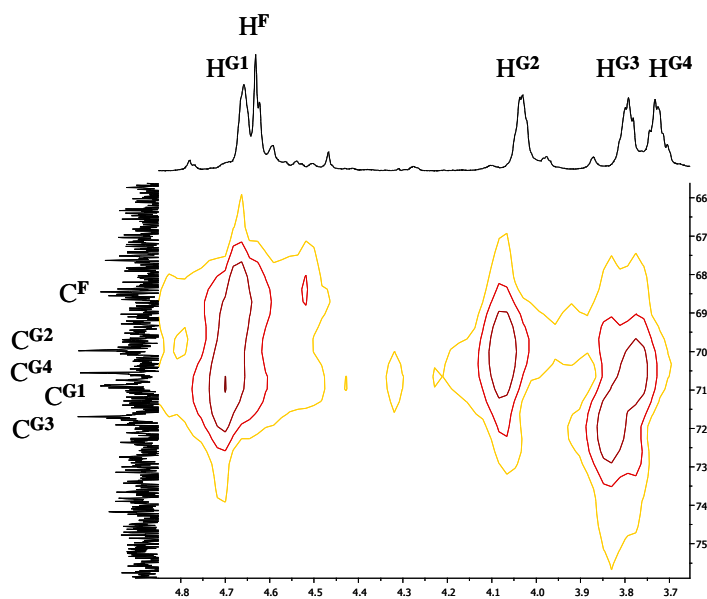
Figure 5.7. Part of the HMQC spectrum (500 MHz, 295 K) of complex $[(\textbf{L5})(Ru)_3(tpy)_3][PF_6]_6$ in CD_3CN showing the aliphatic region. Spectrum exhibits some residues of the starting material, which could not be removed by column chromatography or other purification methods.

In **Figure 5.7** the aliphatic region of HMQC spectrum of complex $[(\textbf{L5})(Ru)_3(tpy)_3][PF_6]_6$ in CD_3CN is shown. Five cross peaks of proton signals for $\textbf{H}^{\textbf{G}}$ and $\textbf{H}^{\textbf{F}}$ to carbon signals $\textbf{C}^{\textbf{G}}$ and $\textbf{C}^{\textbf{F}}$ were found.

All of the terpyridine carbon signals of complex [(**L5**)(Ru)$_3$(tpy)$_3$][PF$_6$]$_6$ in comparison to tritopic ligand **L5** are shifted downfield (**Table 5.9**).

In **Table 5.10** the terpyridine carbon signals of complex [(**L5**)(Ru)$_3$(tpy)$_3$][PF$_6$]$_6$ from monotopic tpy ligand (see aromatic rings A and B on **Figure 5.3**) are shown.

	C^{T2} /C^{C2}	C^{T3} /C^{C3}	C^{T4} /C^{C4}	C^{T5} /C^{C5}	C^{T6} /C^{C6}	$C^{T2'}$ /C^{D2}	$C^{T3'}$ /C^{D3}	$C^{T4'}$ /C^{D4}
L5	156.2	121.5	137.0	124.0	149.2	157.2	107.6	167.1
Ru$_3$L5	157.0	125.5	139.0	128.5	153.8	159.1	112.1	167.4

Table 5.9. ^{13}C NMR spectroscopic data, δ_C [ppm], (125 MHz, 295 K) for **L5** in CDCl$_3$ and [(tpy)Ru(**L5**)(Ru)$_2$(tpy)$_2$][PF$_6$]$_6$ in CD$_3$CN (see page 144 for scheme of labeling)**.**

	C^{A2}	C^{A3}	C^{A4}	C^{A5}	C^{A6}	C^{B2}	C^{B3}	C^{B4}
Ru$_3$L5	156.9	125.3	138.9	128.5	153.3	159.3	124.7	136.2

Table 5.10. ^{13}C NMR spectroscopic data, δ_C [ppm], (125 MHz, 295 K) for [(**L5**)(Ru)$_3$(tpy)$_3$][PF$_6$]$_6$ of monotopic tpy ligand in CD$_3$CN (see page 144 for scheme of labeling)**.**

5.5.1 Mass spectrometric characterization of L5a and L5

Electrospray ionization (ESI) and MALDI-TOF mass spectrometry, both in positive mode, were also used to characterize intermediate **L5a** and ligand **L5**. The $[\text{L+H}]^+$ peak was found as the major peak: 475.5 $[\text{L5a+H}]^+$ (calc. 475.5), 1169.3 $[\text{L5+H}]^+$ (calc. 1169.5). The simulated spectra match the experimental ones.

5.5.2 Mass spectrometric characterization of Ru₃L5
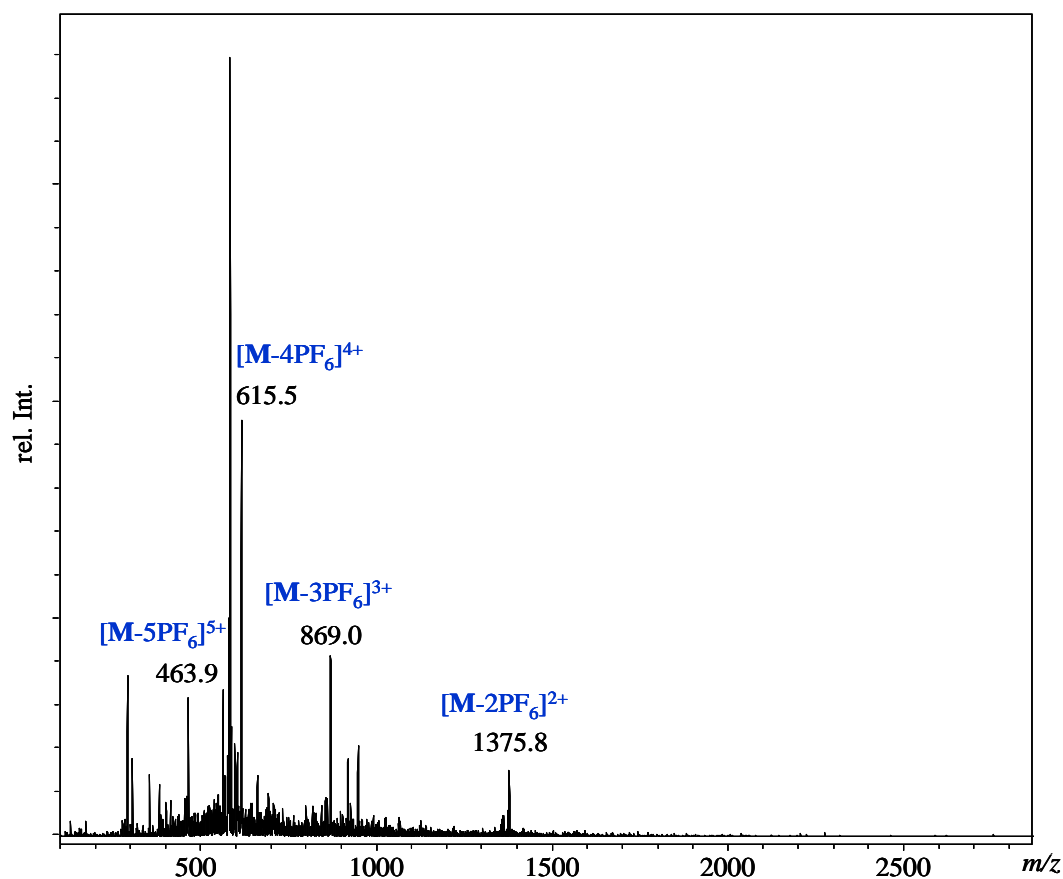
Figure 5.8. ESI-MS spectrum of $[(\text{L5})(\text{Ru})_3(\text{tpy})_3][\text{PF}_6]_6$.

Electrospray ionization mass spectroscopy (ESI-MS) was used to characterize the new heteroleptic trinuclear ruthenium(II) complex of ligand **L5** - [(**L5**)(Ru)$_3$(tpy)$_3$][PF$_6$]$_6$. The peaks are observed as the ratio of mass to the charge of the species (*m/z*), hence allowing one to distinguish between ions carrying different charges.

In **Figure 5.8** the ESI-MS spectrum of [(**L5**)(Ru)$_3$(tpy)$_3$][PF$_6$]$_6$ is shown. The second highest signal is a peak at *m/z* 615.5 and was assigned to [**M**-4BF$_6$]$^{4+}$. The other three signals at *m/z* 1375.8, 869.0 and 463.9 correspond to [**M**-2PF$_6$]$^{2+}$, [**M**-3PF$_6$]$^{3+}$ and [**M**-5PF$_6$]$^{5+}$, respectively. Also shown are expansions of peaks at *m/z* 1375.8, 869.0 and 615.5 (**Figure 5.9**). The peaks show the typical isotope pattern of three ruthenium ions. Confirming the nuclearity of the complex.
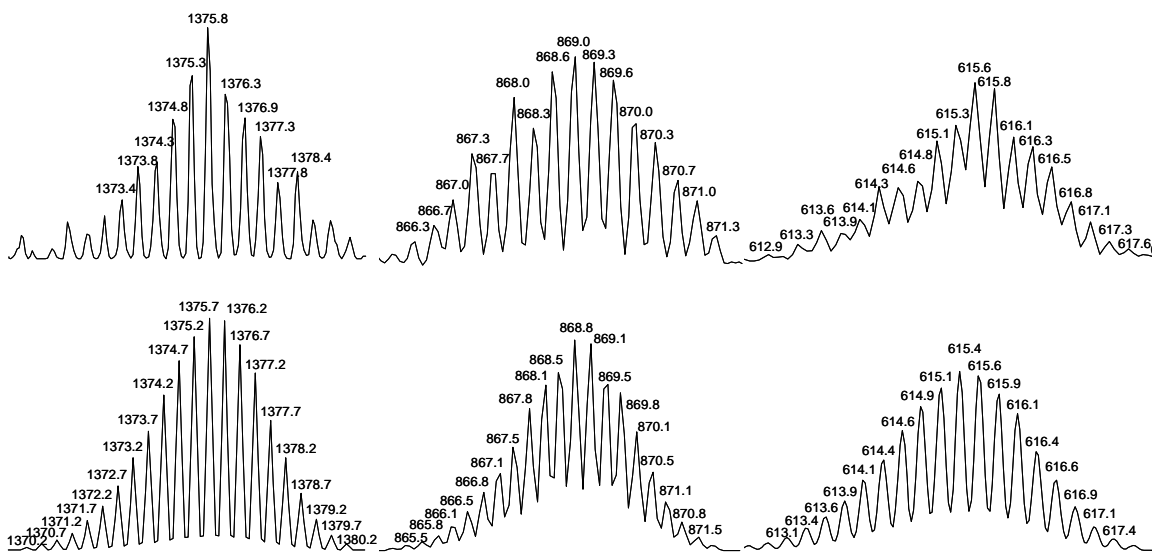
Figure 5.9. Measured (above) and simulated (below) isotopic pattern of +4, +3 and +2 charged cations from [(**L5**)(Ru)$_3$(tpy)$_3$][PF$_6$]$_6$. The *m/z* ratio is also reflecting in the line spacing.

154

5.6.1 Absorption spectroscopic characterization of L5

The electronic spectrum of the tritopic 4'-substituted-2,2':6',2''-terpyridine ligand **L5** was recorded in HPLC grade dichloromethane solution.
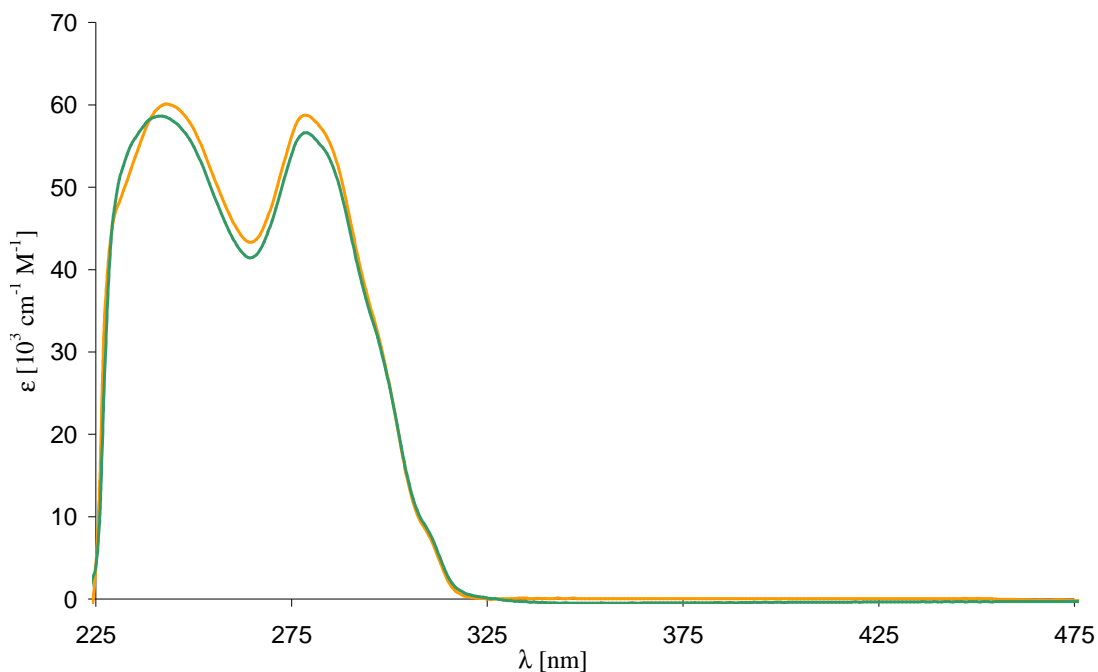
Figure 5.10. Absorption spectra of ligand **L4** in CH_2Cl_2 (in green) and ligand **L5** in CH_2Cl_2 (in orange).

In **Figure 5.10** absorption spectra of ligand **L4** (1,4-bis(8-(4'-(2,2':6',2''-terpyridyl))-2,5,8-trioxaoctyl)benzene, see Section 2) (in green) and ligand **L5** (in orange) are shown for comparison. The UV-Vis spectra of both ligands **L4** and **L5** look almost identical. There are two bands in the high energy UV region, assigned to ligand-centered (LC) π^* ← π transitions with λ_{max} at 241 and 279 nm. Both bands have almost the same intensity, ($\varepsilon_{max}/10^3$ M^{-1} cm^{-1} : 56.8 and 55.3 for ligand **L4,** 57.0 and 55.6 for ligand **L5**).

5.6.2 Absorption spectroscopic characterization of Ru₃L5

The electronic spectrum of the heteroleptic trinuclear ruthenium(II) complex [(**L5**)(Ru)$_3$(tpy)$_3$][PF$_6$]$_6$ was recorded in HPLC grade acetonitrile solution. The four very intense bands with λ_{max} at 233, 241, 269 and 305 ($\varepsilon_{max}/10^3$ M^{-1} cm^{-1} : 120.0, 122.0, 137.0 and 173.0 respectively) nm in the UV region are assigned to the ligand-centered (LC) π^* $\leftarrow$ π transitions. [(**L5**)(Ru)$_3$(tpy)$_3$][PF$_6$]$_6$ complex exhibits typical low energy metal-to-ligand charge transfer (MLCT) transition for ruthenium(II) complexes with λ_{max} at 481 nm ($\varepsilon_{max}/10^3$ M^{-1} cm^{-1} : 47.0).
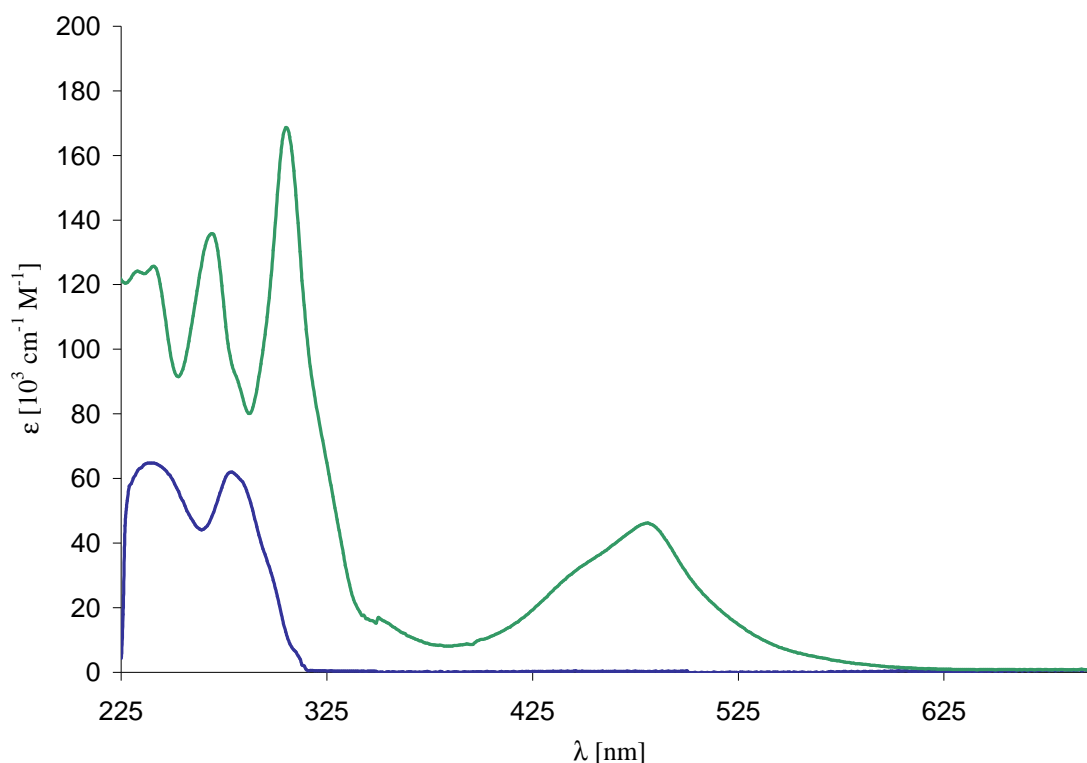
Figure 5.11. Absorption spectra of ligand **L5** in CH$_2$Cl$_2$ (in blue) and [(**L5**)(Ru)$_3$(tpy)$_3$][PF$_6$]$_6$ in CH$_3$CN (in green).

In **Figure 5.11** absorption spectra of ligand **L5** in CH$_2$Cl$_2$ (in blue) and [(**L5**)(Ru)$_3$(tpy)$_3$][PF$_6$]$_6$ in CH$_3$CN (in green) are shown for comparison. The absorption spectrum of uncomplexed ligand **L5,** unlike complex [(**L5**)(Ru)$_3$(tpy)$_3$][PF$_6$]$_6$, shows only

two bands in the high energy UV region, assigned to ligand-centered (LC) $\pi^* \leftarrow \pi$ transitions with λ_{max} at 241 and 279 nm ($\varepsilon_{max}/10^3$ M^{-1} cm^{-1} : 57.0 and 55.6 respectively).

5.7 Electrochemical studies of Ru$_3$L5

The redox properties of ruthenium(II) complex $[(\mathbf{L5})(Ru)_3(tpy)_3][PF_6]_6$ have been investigated using the cyclic voltammetry method (CV).

Potential [V] vs Fc/Fc$^+$	
oxidation	reduction
0.78[a]	-1.68[a], -1.92[a], -2.39[b]

Table 5.11. Redox potentials measured for $[(\mathbf{L5})(Ru)_3(tpy)_3][PF_6]_6$ in argon-purged solutions of acetonitrile. $E_{1/2}$ values are given for reversible processes ([a]) from the cyclovoltametry and for irreversible processes ([b]) from square wave.

The oxidation of ruthenium(II) in this complex occurs at 0.78 V (**Table 5.11**). There are three reduction processes, two of them are reversible, at -1.68 and -1.92 V, one is irreversible, at -2.39 V (**Table 5.11**). The potentials were measured versus Ferrocene^0/Ferrocenium$^+$ (Fc/Fc$^+$).

In **Figure 5.12** the cyclic voltammogram of $[(\mathbf{L5})(Ru)_3(tpy)_3][PF_6]_6$ in degassed acetonitrile is shown.
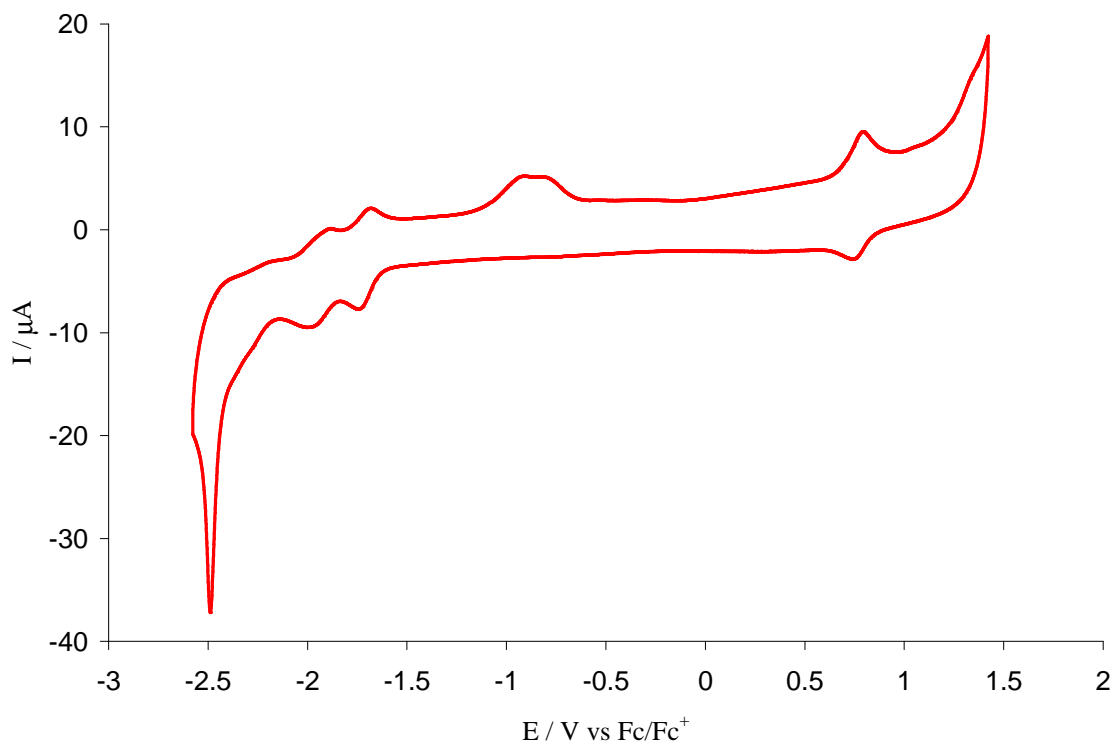
Figure 5.12. Cyclic voltammogram of [(**L5**)(Ru)$_3$(tpy)$_3$][PF$_6$]$_6$ (1 mM) in degassed acetonitrile containing 0.1 M [^{n}Bu$_4$N][PF$_6$], scan rate = 100 mVs^{-1}.

5.8 Conclusion

In this chapter, new tritopic intermediate **L5a**, ligand **L5** and the heteroleptic trinuclear ruthenium(II) complex of tritopic 4'-substituted-2,2':6',2''-terpyridine ligand **L5** have been synthesized and characterized with ^{1}H and ^{13}C NMR spectroscopy, mass spectrometry (ESI-MS and MALDI-TOF), IR spectroscopy, UV-Vis spectroscopy and elemental analysis. To fully characterize the ruthenium(II) complex of ligand **L5,** [(**L5**)(Ru)$_3$(tpy)$_3$][PF$_6$]$_6$, also cyclic voltammetry has been used. The compounds are

based on a mesitylene ring substituted in position 1, 2 and 3 with three diethylene glycol chains connected to 4'-substituted-2,2':6',2''-terpyridine moieties. Experimental data of ligand **L5** have been compared with those of ligand **L1**. Spectroscopic data of ruthenium(II) complex [(**L5**)(Ru)$_3$(tpy)$_3$][PF$_6$]$_6$ have been compared with those of ligand **L5**.

5.9.1 Experimental of L5a and L5

❖ 1,3,5-Tris(7-hydroxy-2,5-dioxaheptyl)-2,4,6-trimethylbenzene (**L5a**)

❖ 1,3,5-Tris(8-(4'-(2,2':6',2''-terpyridyl))2,5,8-trioxaoctyl)-2,4,6-trimethylbenzene (**L5**)

4'-Chloro-2,2':6',2''-terpyridine[102] and 1,3,5-tris(bromomethyl)-2,4,6-trimethylbenzene[106] were prepared as previously reported in the literature.

Schematic reaction for 1,3,5-tris(bromomethyl)-2,4,6-trimethylbenzene is shown below.[106]

1,3,5-tris(bromomethyl)-2,4,6-trimethylbenzene

❖ 1,3,5-Tris(7-hydroxy-2,5-dioxaheptyl)-2,4,6-trimethylbenzene (**L5a**)

1,3,5-tris(bromomethyl)-
2,4,6-trimethylbenzene
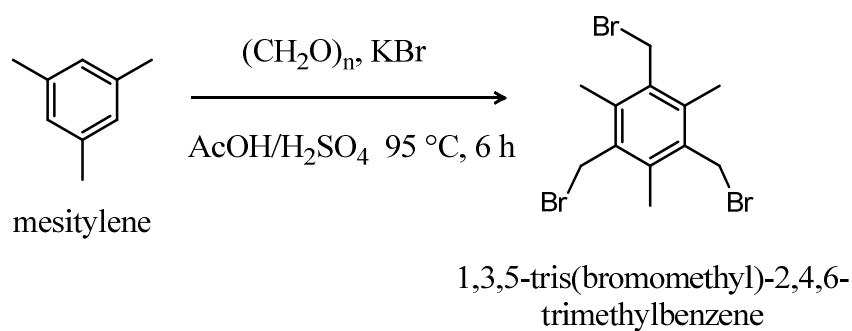
1,3,5-tris(7-hydroxy-2,5-dioxaheptyl)-2,4,6-
trimethylbenzene **(L5a)**
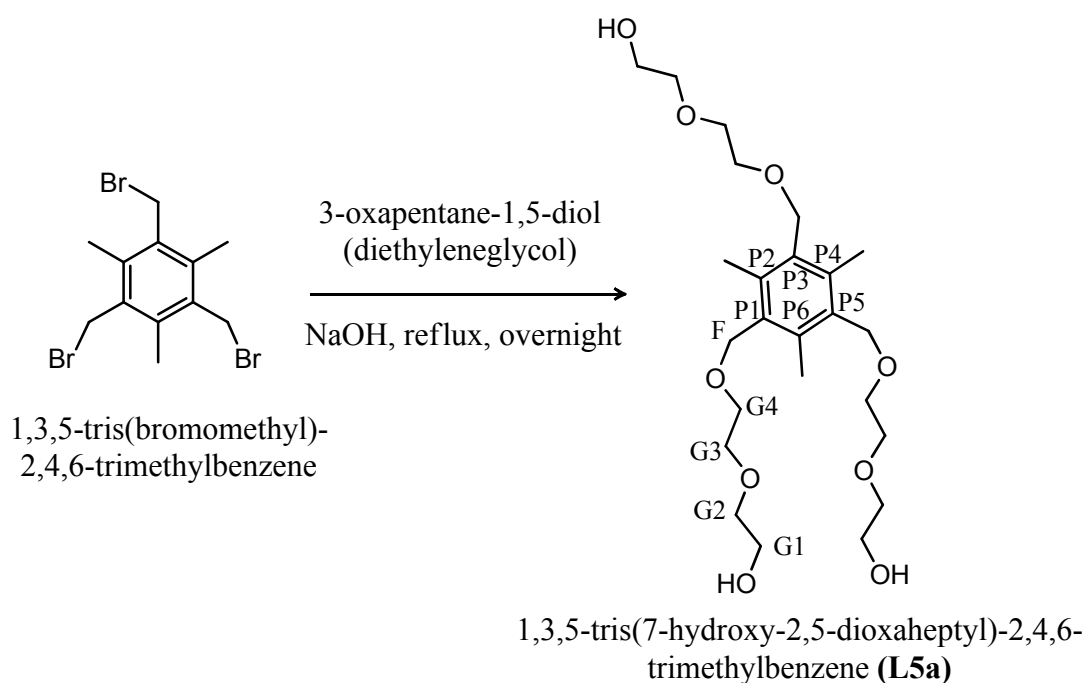
Molecular formula: $C_{24}H_{42}O_9$
Molecular weight: 474.58

1,3,5-Tris(bromomethyl)-2,4,6-trimethylbenzene (1.0 g, 2.5 mmol) was added to a hot suspension of NaOH (0.28 g, 7.0 mmol) in 50 mL diethylene glycol. The reaction mixture was stirred overnight at 125 °C under nitrogen. After 10 h, the reaction mixture was cooled to room temperature and quenched with 100 mL water, then extracted with $CHCl_3$ (4x100 mL). The organic layer was dried ($MgSO_4$), filtered and the solvent was removed *in vacuo* yielding a yellow oil of **L5a** (0.71 g, 1.5 mmol, 60%). The product was used in the next step without further purification.

The reaction could also be performed in a microwave reactor at 125 °C for 15 minutes but on a much smaller scale. 1,3,5-Tris(bromomethyl)-2,4,6-trimethylbenzene (0.10 g, 0.25 mmol) was reacted with NaOH (0.041g, 0.88 mmol) in 10 mL diethylene glycol.

After work up, **L5a** was obtained in 50% yield (0.059 g, 0.13 mmol). Despite the lower yield, this method allowed the reaction time to be shortened from 10 hours to 15 minutes.

^{1}H NMR (400 MHz, CDCl$_3$) δ_H 1.71 (br, 3H, H^{OH}), 2.41 (s, 9H, H^{Me}), 3.55 (m, 6H, H^{G1}), 3.65-3.85 (m, 18H, H$^{G2\text{-}G4}$), 4.59 (s, 6H, H^F),

MS(MALDI-TOF, sinapinic acid): m/z = 475.5 [**L5a**+H]$^+$ (calc. 475.5).

❖ 1,3,5-Tris(8-(4'-(2,2':6',2''-terpyridyl))-2,5,8-trioxaoctyl)-2,4,6-trimethylbenzene (**L5**)

1,3,5-tris(8-(4'-(2,2':6',2''-terpyridyl))-2,5,8-trioxaoctyl)-2,4,6-
trimethylbenzene (**L5**)
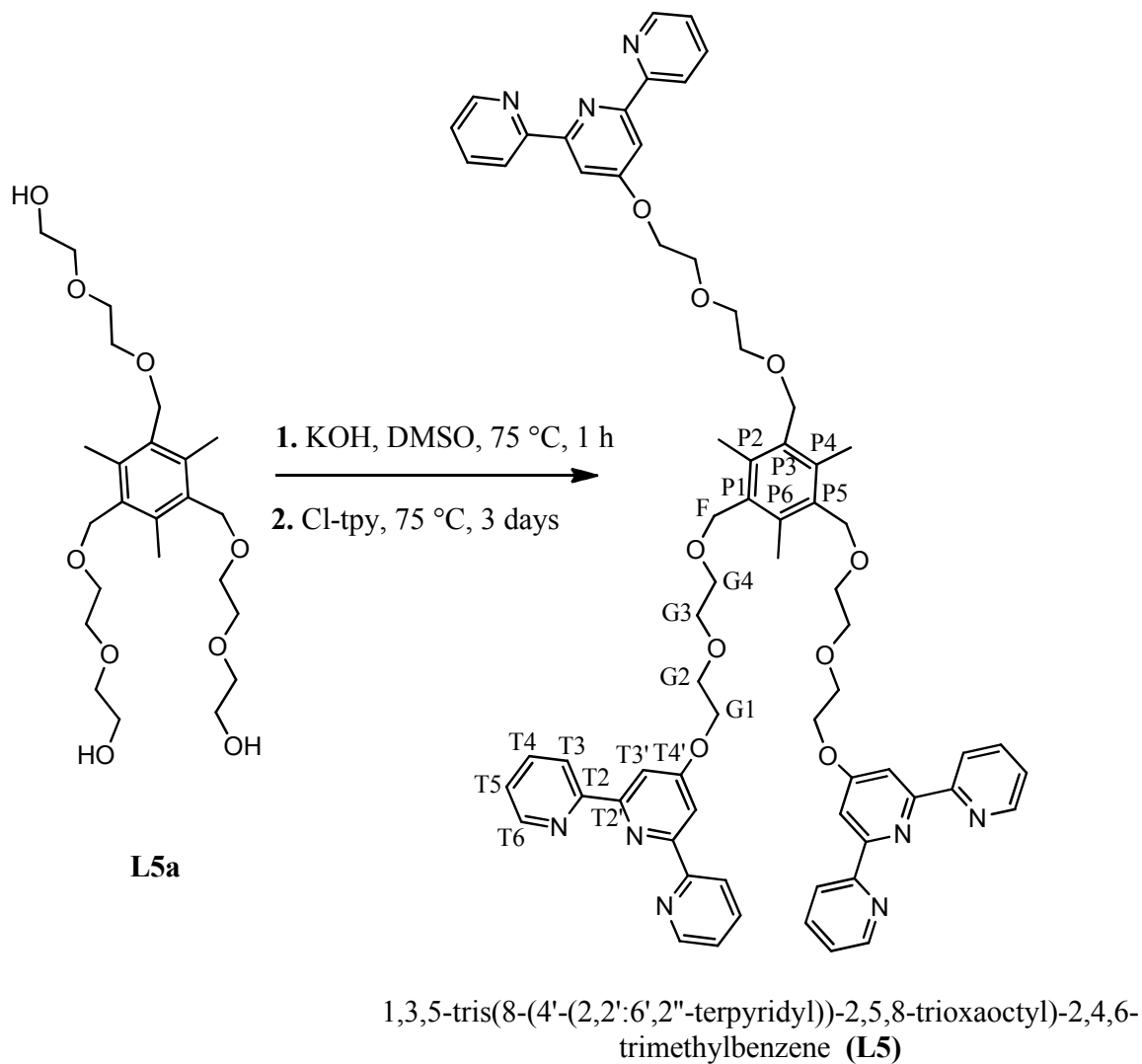
Molecular formula: $C_{69}H_{69}N_9O_9$
Molecular weight: 1168.34

Compound **L5a** (0.71 g, 1.5 mmol, 1.0 eq) was added to a suspension of finely powdered potassium hydroxide (1.6 g, 29 mmol) in 30 mL dry DMSO and the mixture was stirred for 1 h at 70 °C under nitrogen. After 1 h, 4'-chloro-2,2':6',2''-terpyridine (Cl-tpy) (2.5 g, 9.3 mmol, 6.0 eq) was added and the reaction mixture was heated to 70 °C for 3 days. The reaction mixture was cooled to room temperature and quenched with 70 mL of water. The product was then extracted with $CHCl_3$. The organic layer was separated and

163

dried (MgSO$_4$). The crude product was filtered and the solvent was removed *in vacuo*. The pure product **L5** was obtained after column chromatography (Al$_2$O$_3$, CHCl$_3$), isolated as a yellow oil (1.6 g, 1.3 mmol, 89%).

^{1}H NMR (500 MHz, CDCl$_3$) δ_H 2.38 (s, 9H, H^{Me}), 3.61 (m, 6H, H^{G4}), 3.68 (m, 6H, H^{G3}), 3.85 (m, 6H, H^{G2}), 4.32 (m, 6H, H^{G1}), 4.54 (s, 6H, H^F), 7.27-7.32 (m, 6H, H^{T5}), 7.79 (t, *J* 7.5 Hz, 6H, H^{T4}), 7.99 (s, 6H, H$^{T3'}$), 8.56 (d, *J* 7.9 Hz, 6H, H^{T3}), 8.65 (d, *J* 3.9 Hz, 6H, H^{T6}).

^{13}C NMR (125 MHz, CDCl$_3$) δ_C 16.0 (C^{Me}), 68.0 (C^{G1}), 68.1 (C^F), 69.6 (C^{G4}), 69.6 (C^{G2}), 71.3 (C^{G3}), 107.6 (C$^{T3'}$), 121.5 (C^{T3}), 124.0 (C^{T5}), 132.5 (C^{P1,P3,P5}), 136.9 (C^{T4}), 138.5 (C^{P2,P4,P6}), 149.2 (C^{T6}), 156.2 (C^{T2}), 157.2 (C$^{T2'}$), 167.1 (C$^{T4'}$).

MS (ESI) *m/z* = 1169.3 [**L5**+H]$^+$ (calc. 1169.5).

IR (oil, $\tilde{\nu}$/cm^{-1}): 2878w, 1599w, 1582s, 1560s, 1468m, 1441m, 1406m, 1346m, 1252w, 1203m, 1134m, 1092m, 1057m, 1038m, 1013m, 968m, 883w, 868w, 793s, 743s, 698m, 658m, 621m.

UV/VIS (CH$_2$Cl$_2$):λ_{max}/ nm (ε_{max}, M^{-1} cm^{-1}) 241 (57 x 10^3), 279 (55.6 x 10^3).

Elemental Analysis. Found: C, 62.60; H, 5.80; N, 9.15. Calc. for C$_{69}$H$_{69}$N$_9$O$_9$·3H$_2$O·CHCl$_3$: C, 62.66; H, 5.71; N, 9.40%.

5.9.2 Experimental of Ru$_3$L5

[Ru(tpy)Cl$_3$] was prepared as described in Section 3.9. In some cases NaPF$_6$ can be captured in long ethylene glycol chains (see elemental analysis).

❖ [(**L5**)(Ru)$_3$(tpy)$_3$][PF$_6$]$_6$

[PF$_6$]$_6$
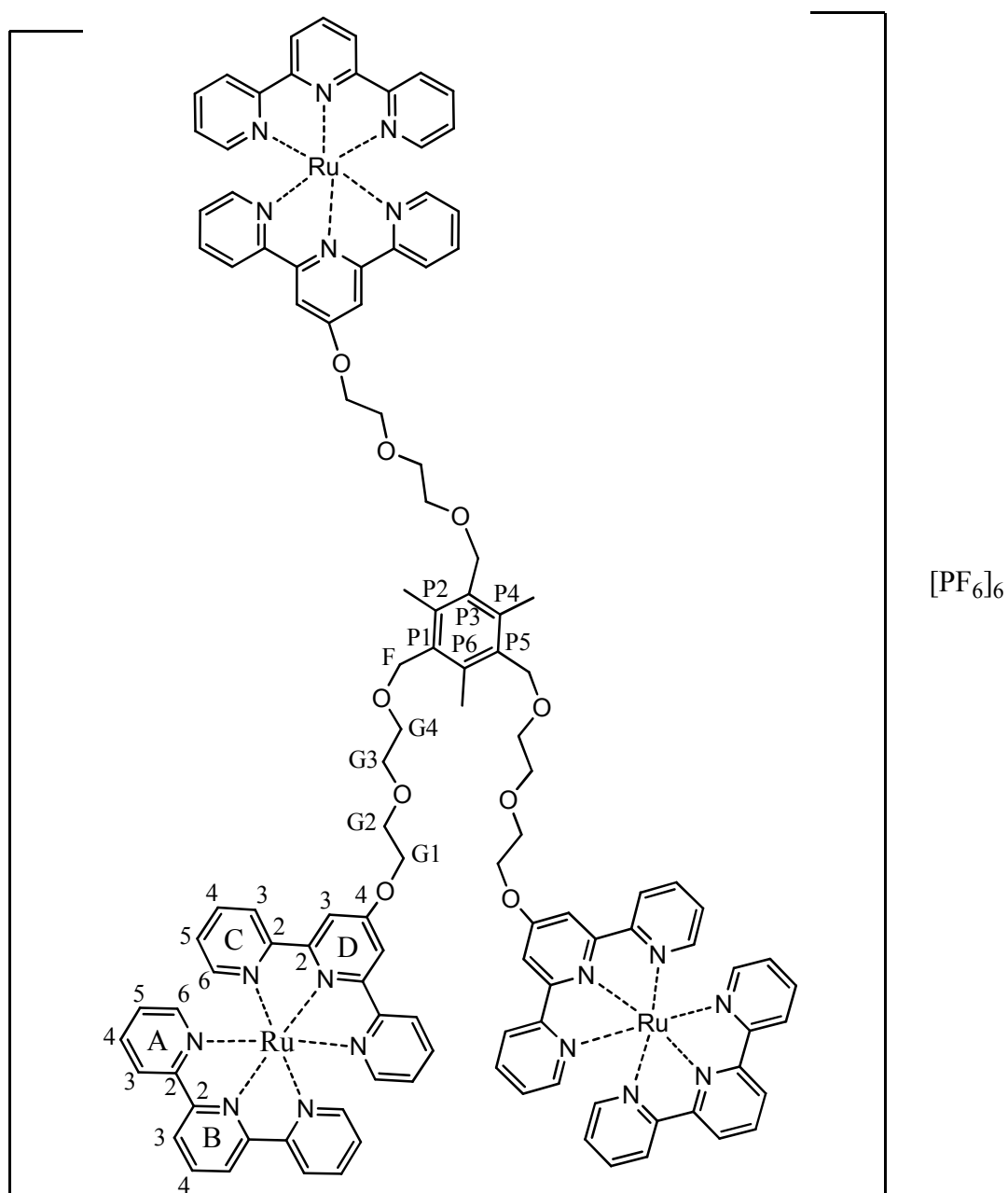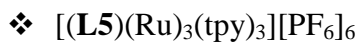
Compound **L5** (0.014 g, 0.012 mmol, 1.0 eq) and [Ru(tpy)Cl₃] (0.016 g, 0.036 mmol, 3.0 eq) with a few drops of *N*-ethylmorpholine (NEM) were heated at 135 °C in 15 mL ethanol in a microwave reactor for 30 minutes. Excess of solid ammonium hexafluorophosphate was added to give a red precipitate. This was collected by filtration through celite, washed with water and diethyl ether, then redissolved in acetonitrile. The solvent was removed *in vacuo* to give a red solid [(**L5**)(Ru)₃(tpy)₃][PF₆]₆ (0.032 g, 0.010 mmol, 90%).
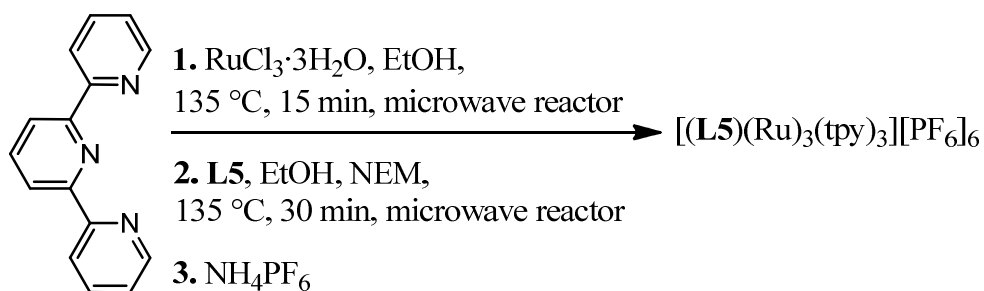
^{1}H NMR (500 MHz, CD₃CN) δ$_H$ 2.47 (s, 9H, H^{Me}), 3.73 (m, 6H, H^{G4}), 3.79 (m, 6H, H^{G3}), 4.03 (m, 6H, H^{G2}), 4.63 (s, 6H, H^F), 4.66 (m, 6H, H^{G1}), 7.11 (m, 6H, H^{C5}), 7.16 (m, 6H, H^{A5}), 7.29 (d, *J* 5.2 Hz, 6H, H^{C6}), 7.42 (d, *J* 5.0 Hz, 6H, H^{A6}), 7.82-7.94 (m, 12H, H^{C4} and H^{A4}), 8.33 (s, 6H, H^{D3}), 8.37 (m, 3H, H^{B4}), 8.46 (m, 12H, H^{C3} and H^{A3}), 8.72 (d, *J* 8.2 Hz, 6H, H^{B3}).

^{13}C NMR (125 MHz, CD₃CN) δ$_C$ 16.1 (C^{Me}), 68.4 (C^F), 70.0 (C^{G2}), 70.6 (C^{G4}), 70.9 (C^{G1}), 71.7 (C^{G3}), 112.1 (C^{D3}), 124.7 (C^{B3}), 125.3 (C^{A3}), 125.5 (C^{C3}), 128.5 (C^{A5} and C^{C5}), 134.0 (C$^{P1/P3/P5}$ or C$^{P2/P4/P6}$), 136.2 (C^{B4}), 138.9 (C^{A4} and C^{C4}), 139.0 (C$^{P1/P3/P5}$ or C$^{P2/P4/P6}$), 153.30 (C^{A6}), 153.8 (C^{C6}), 156.9 (C^{A2}), 157.0 (C^{C2}), 159.1 (C^{D2}), 159.3 (C^{B2}), 167.4 (C^{D4}).

MS (ESI) *m/z* = 463.9 [**M**-5PF₆]$^{5+}$ (calc. 464.0), 615.6 [**M**-4PF₆]$^{4+}$ (calc. 615.5), 869.0 [**M**-3PF₆]$^{3+}$ (calc. 869.0), 1375.8 [**M**-2PF₆]$^{2+}$ (calc. 1375.5).

IR (solid, $\widetilde{\nu}$/cm^{-1}): 3651w, 3310w, 3121w, 3080w, 2870w, 1607m, 1468w, 1448m, 1437m, 1418m, 1387m, 1348w, 1286w, 1248w, 1209m, 1163w, 1094w, 1061w, 1045w, 1028w, 964w, 824s, 785s, 766s, 752s, 741s, 725s, 696m, 663m, 644m, 612w.

Cyclic voltammetry data (CH$_3$CN, 0.1 M [^{n}Bu$_4$N][PF$_6$], Fc/Fc$^+$): +0.78 V, -1.68 V, -1.92 V, -2.39 V.

UV/VIS (CH$_3$CN): λ_{max}/ nm (ε_{max}, M^{-1} cm^{-1}) 233 (120 x 10^3), 241 (122 x 10^3), 269 (137 x 10^3), 305 (173 x 10^3), 481 (47 x 10^3).

Elemental Analysis: Found: C, 40.83; H, 3.25; N, 7.66. Calc. for C$_{114}$H$_{102}$F$_{36}$N$_{18}$O$_9$P$_6$Ru$_3$·2NaPF$_6$: C, 40.54; H, 3.04; N, 7.47%.

CHAPTER 6

Synthesis of homoleptic mononuclear europium(III) and terbium(III) complexes of a tritopic 4'-substituted- 2,2':6',2''-terpyridine ligand

6.1 Introduction

Historical overview[177]
Discovery and isolation of the lanthanides

In 1752, the Swedish mineralogist Cronstedt discovered a new heavy mineral in a mine near Ryddarhyttan in his home country. Gadolin (Finnish), in 1794, isolated an oxide from a heavy black mineral at Ytterby (also in Sweden) and named the oxide 'ytterbia'. Half a century later, in 1842, Mosander further separated 'ytterbia' by oxalate and hydroxide precipitation. He named the three fractions 'yttria', 'erbia' and 'terbia'. The isolation of lanthanum, the lanthanides, yttrium, and scandium was not completed until 1908–1909 owing to the difficulties in separating them by repetitive fractional crystallizations. Charles James, an early expert in the isolation of kilogram quantities of pure lanthanide salts, once performed many thousands of recrystallizations to obtain 'pure' $Tm(BrO_3)_3$. Before the Second World War, a major advance in separating lanthanide ions was made by McCoy, who purified considerable quantities of Eu by reducing Eu^{3+} to Eu^{2+} with Zn amalgam followed by precipitation as $EuSO_4$. The Manhattan project during the Second World War yielded the first large-scale separation methods for lanthanide ions. The ion exchange chromatographic methods developed during this project are based on the (small) differences in the stability of chelates (at the time citrate complexes). Together with the liquid-liquid extraction methods developed in

the early 1950s these methods are still used in the commercial production of lanthanides.[177]

Over the past five years, the lanthanides have attracted great interest, due to their unique magnetic and photophysical properties such as their relatively long-lived luminescence. [178-180]Research in luminescence signaling has developed quickly due to its many possible applications.[181-199] The metal-based complexes can be used as therapeutic drugs, biological probes and assays.[200-212] Furthermore lanthanides have potential applications in medical diagnostics[213,214], optical imaging[215,216] and high technology.[217,218]

Lanthanides have a characteristic 4f open-shell configuration and exhibit small and regular decreases in their ionic radii across the periodic series, (the lanthanide contraction).[219,220] Their most stable oxidation state is +3, with configuration $[Xe]4f^n$ (**Figure 6.3**). They are coordinated by a variety of ligands with high coordination numbers, typically between eight and ten.

Lanthanides are hard metals so they can coordinate to ligands with hard donors, like nitrogen or oxygen. For example, in $[Eu(ClO_4)(L)]^{2+}$, (**Figure 6.1**) the metal ion is coordinated to six oxygen atoms and two nitrogen atoms from cryptand(2.2.2). This type of complexes is very stable due to the chelate effect. The eight-coordinate geometry of the lanthanides allows the self-assembled helicate structure shown in **Figure 6.1** to be formed.[217]
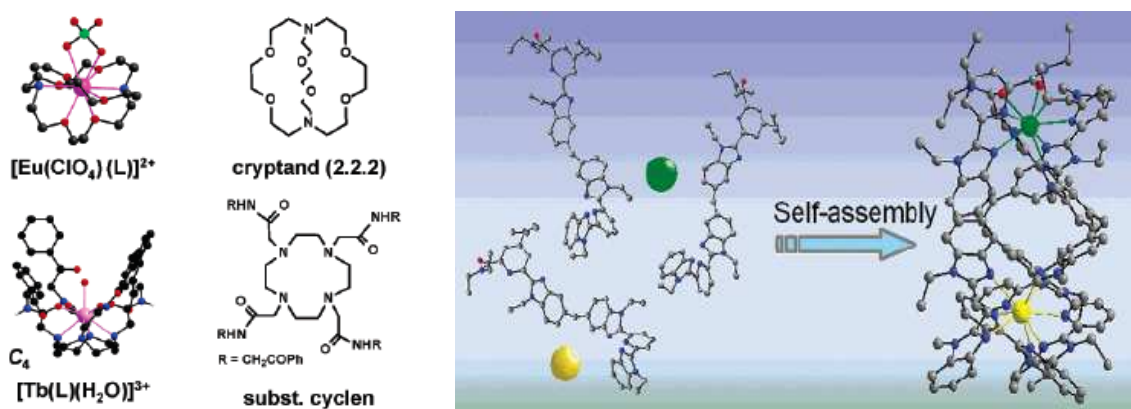
Figure 6.1. Some examples of the structures of lanthanide complexes.[217]

170

For an *f*-orbital, the quantum numbers are $n = 4$ or 5, $l = 3$ and $m_l = +3, +2, +1, 0, -1, -2, -3$. A set of *f*-orbitals is therefore seven-fold degenerate, and the "cubic set" is the most commonly used to present the shapes of these orbitals. **Figure 6.2** shows the three dimensional representation of *f*-orbitals: $4f_{xyz}$, $4f_{x(z^2-y^2)}$, $4f_{y(z^2-x^2)}$, $4f_{z(x^2-y^2)}$, $4f_x^3$, $4f_y^3$ and $4f_z^3$.

In the cubic set of 4*f* orbitals, there are two distinct shapes, each of which possesses a number of planar and conical nodes. None of the 4*f* orbitals possesses radial nodes.

The $4f_{xyz}$, $4f_{x(z^2-y^2)}$, $4f_{y(z^2-x^2)}$, and $4f_{z(x^2-y^2)}$ (bottom two rows in **Figure 6.2**) each have eight lobes. The $4f_{x(z^2-y^2)}$, $4f_{y(z^2-x^2)}$, and $4f_{z(x^2-y^2)}$ orbitals are related to each other by 45° rotations about the *x*, *y*, and *z*-axis respectively. Each orbital has three nodal planes, which for the $4f_{xyz}$ are the *xy*, *xz*, and *yz* planes. The $4f_x^3$, $4f_y^3$, and $4f_z^3$ (top row in **Figure 6.2**) orbitals has a planar node in the *xy* plane and two conical nodes orientated along the *z*-axis. The other two orbitals are related through 90° rotations.

The lanthanides have 4*f* orbitals and the ground state electronic configuration of e.g. europium is $[Xe]4f^7 6s^2$.
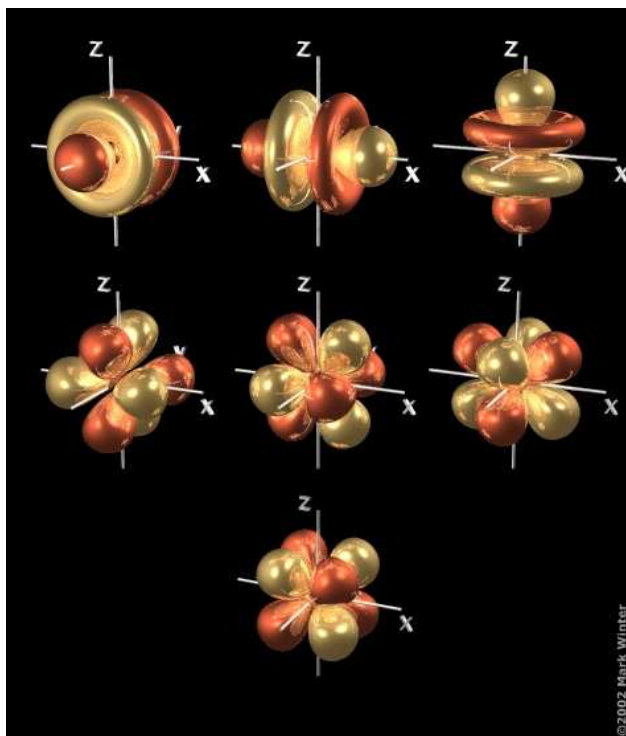
Figure 6.2. The three dimensional representations of the *f* orbitals.[221]

171
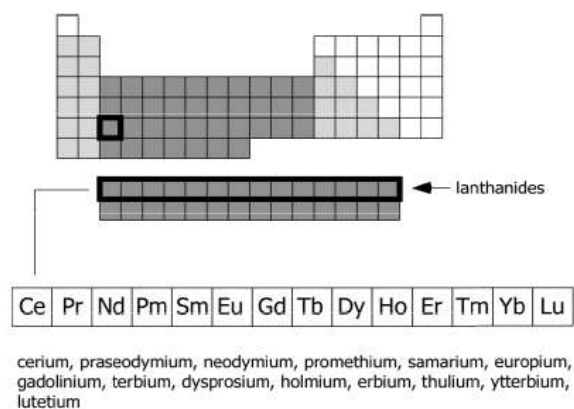
Figure 6.3. The place of the lanthanides in the Periodic Table.[177]

The most interesting spectroscopic properties of lanthanides are an effect of the shielding of the 4*f* orbitals. The characteristic narrow emission bands in the visible and near infrared ranges, as well as very low extinction coefficients in the absorption spectra (ε_{max}, 0.1 M^{-1} cm^{-1})[222] are a result of the spin forbidden f-f electronic transitions. The intensity of these transitions is very low due to very little f-d mixing.
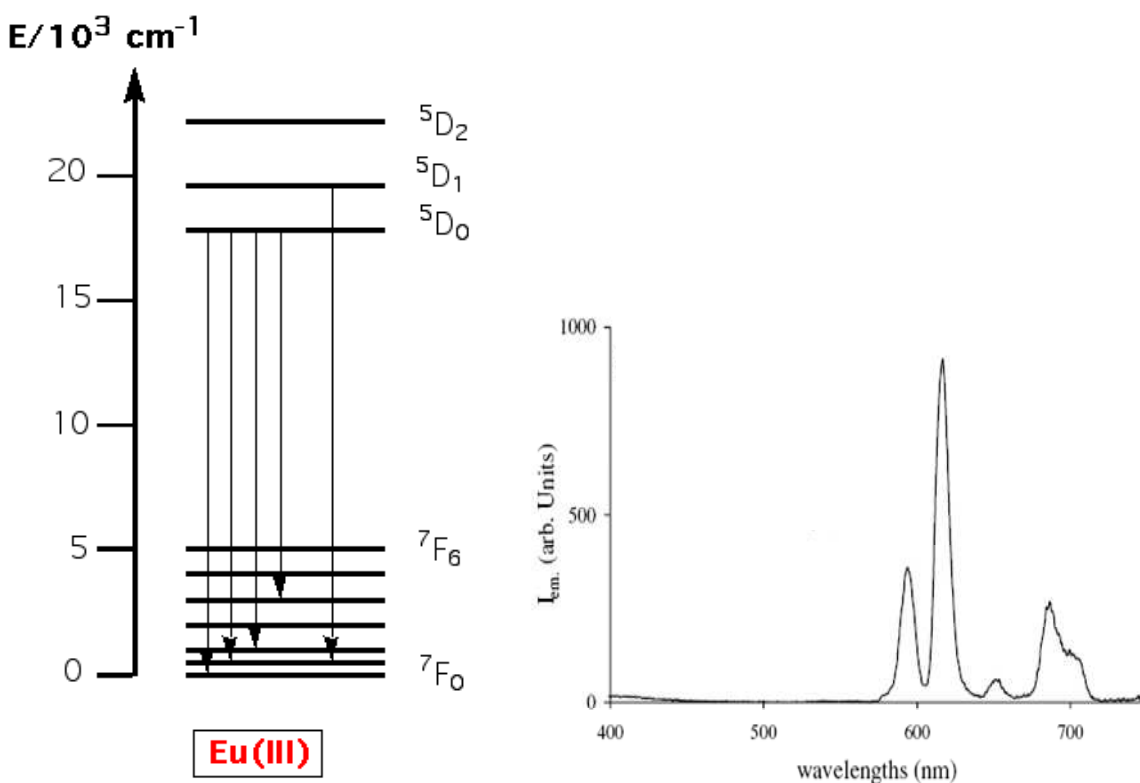
Figure 6.4. Characteristic transitions and emission spectrum of Eu^{3+} complexes.[210]

Most of the lanthanide ions' complexes are luminescent. The exceptions are La(III) (configuration: [Xe]) and Lu(III) (configuration: $[Xe]4f^{14}$) which have no f-f transitions. The "$f-f$" electronic transitions are easily recognizable and almost independent of the chemical environment of the ion. They can be either fluorescent (e.g. Pr(III), Nd(III), Ho(III), Er(III) and Yb(III)) or phosphorescent (e.g. orange Sm(III), red Eu(III), Gd(III) UV, green Tb(III), yellow Dy(III) and blue Tm(III)). Fluorescence occurs when the processes undergo without change in spin, typically $S_1 \rightarrow S_0$ transitions and phosphorescence refers to transitions involving a change in spin, typically $T_1 \rightarrow S_0$.[222]

As their emissions occur in the visible region, Eu(III) and Tb(III) are especially interesting, Eu(III) emits in the red (550–750 nm) (**Figure 6.4**) and Tb(III) emits in the green (450–650 nm) (**Figure 6.5**); the energy gaps: Eu(III) ($\Delta E = 12300$ cm^{-1}, $^5D_0 \rightarrow {}^7F_6$ and Tb(III) ($\Delta E = 14800$ cm^{-1}, $^5D_4 \rightarrow {}^7F_0$).[218]
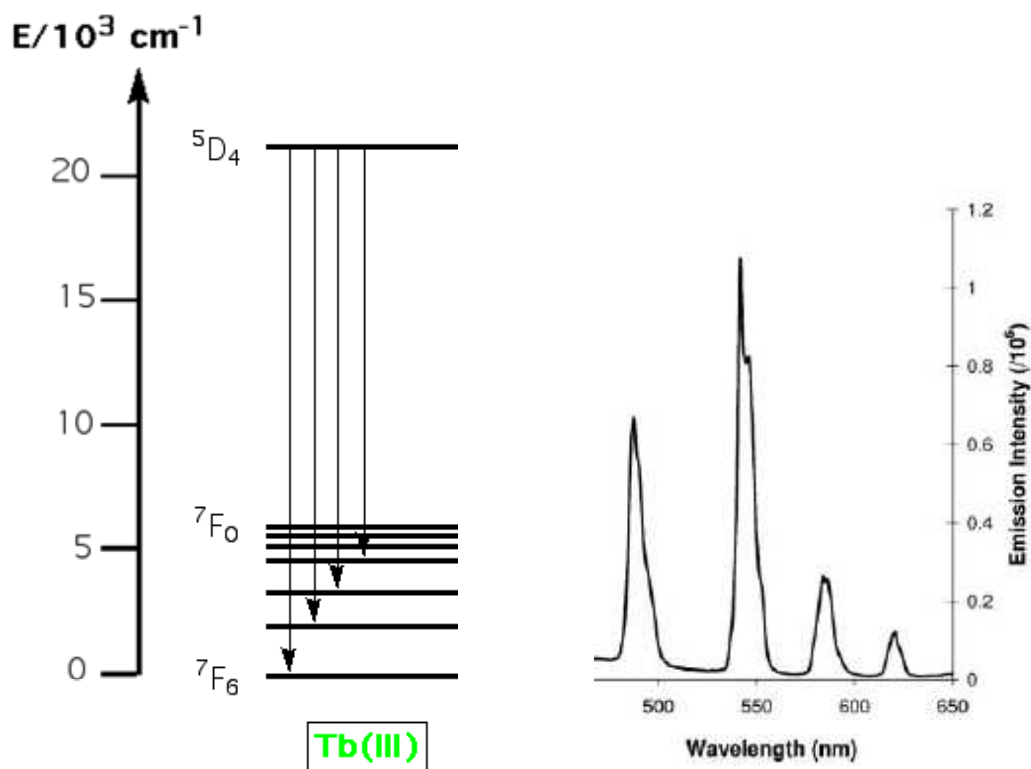
Figure 6.5. Characteristic transitions and emission spectrum of Tb^{3+} complexes.[210]

One of the strongly investigated type of ligands for Ln(III) complexation are receptors bearing the β-diketonate structural motif.[223] Suitable diketonate complexes can be advantageously used for fluoroimmunologic assays[223] and for responsive systems based on luminescence quenching.[224] For example, Zebret and Haamcek from the University of Geneva have prepared a new ligand by introducing terminal carboxylate groups on the Hbpca ((bis(2-pyridylcarbonyl)amine) backbone to achieve Ln(III) coordination in the pentacoordinate cavity (**Figure 6.6**).[225-228] The structure of this coordination site can be compared to some pentadentate ligands, namely derivatized dicarbazone[229,230] and terpyridine ligands[231] used for fluorimetric assays.[223]
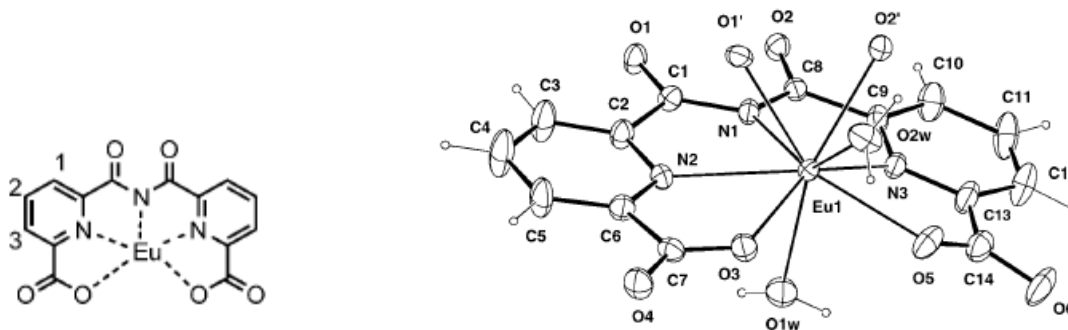
Figure 6.6. View of the coordination environment around Eu(III) cations with the atomic numbering scheme (O1' and O2' – amidic carbonyl groups, O1 and O2.– water molecules).[218]

The X-ray crystal structure of this Eu(III) complex shows that it is formed by three molecules of the ligand shown in **Figure 6.6,** interconnected with three europium cations around a crystallographic threefold axis. Each europium cation in the crystal structure is nine-coordinate with five donor atoms of one ligand (pentacoordinated cavity), two oxygen atoms of the amidic carbonyl groups of the neighboring ligand, and the two remaining positions are occupied by water molecules (**Figure 6.6**). The coordination sphere of Eu(III) can be described as a distorted mono-capped square antiprismatic site, in which one water molecule caps the rectangular face formed by two carbonyl and two carboxylate oxygens.

174

Recently a new approach in lanthanide chemistry has generated great interest. Scientists are trying to control the luminescent properties of multimetallic assemblies exactly by controlling intermetallic communication between two (or more) metal ions inserted into polymetallic edifices, such that directional energy transfer occurs. One may control the properties of one metal ion by tuning the physicochemical properties of the other ion. This strategy is being mostly used for sensitizing Near-IR emitting Ln(III) ions and there are two possibilities : through-bond or through-space directional energy transfer.[206]
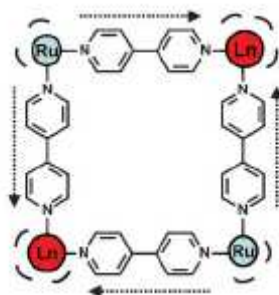
Figure 6.7. Tetrametallic complex exhibiting Ru(II)-to-Ln(III) directional energy transfer.[232]

An example of the first process is given by the tetrametallic square Ru_2Ln_2 complex proposed by Guo *et al.* (**Figure 6.7**).[232] An example of the through-space strategy is shown in **Figure 6.8** for a trimetallic $RuLn_2$, the d- and f-transition metal ions are not directly linked.[233]
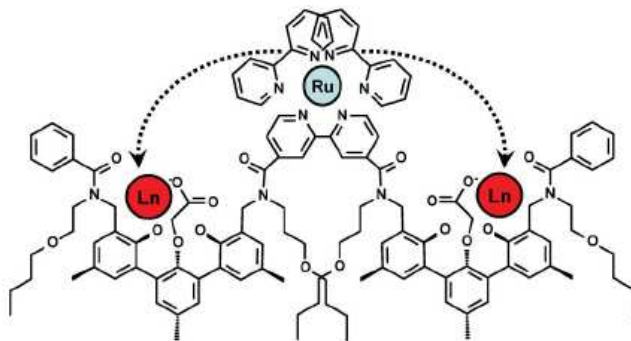
Figure 6.8. Trimetallic complex exhibiting Ru(II)-to-Ln(III) through-space energy transfer.[233]

Following on from these examples of chelating ligands with hard donor atoms and the known Eu(tpy)$_3$ complex[234], ligand **L5** was designed to act as a chelating ligand for one Ln(III) ion. Studies of new homoleptic mononuclear europium(III) and terbium(III) complexes of tritopic 4'-substituted- 2,2':6',2''-terpyridine ligand **L5** described in Chapter 5 will be fully presented in this chapter (**Scheme 6.1**).

Ln = Eu(III) or Tb(III)
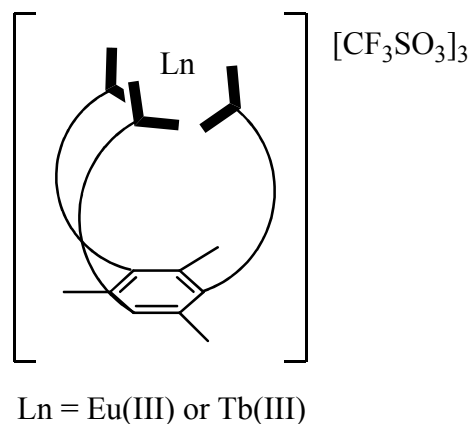
Scheme 6.1. Homoleptic mononuclear lanthanide(III) complex of a tritopic 4'-substituted- 2,2':6',2''-terpyridine ligand.

6.2 Synthesis of [Eu(L5)$_3$]$^{3+}$

The homoleptic mononuclear europium(III) complex of ligand **L5** (**Scheme 6.3**) was easily prepared by reacting one equivalent of ligand **L5** in CHCl$_3$ with one equivalent of Eu(CF$_3$SO$_3$)$_3$ in acetonitrile at room temperature for few minutes. ^{1}H NMR spectrum shows that the reaction occurs almost instantly. The solvent was removed *in vacuo* and the desired product was obtained in 90% yield (**Scheme 6.2**).
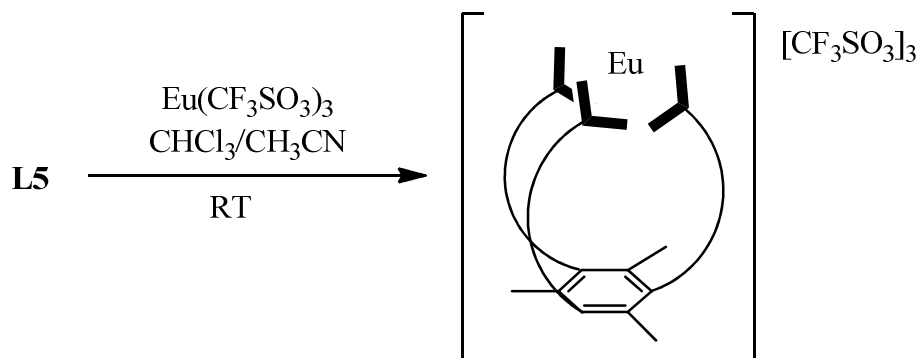
Scheme 6.2. Synthesis of [Eu(**L5**)][CF$_3$SO$_3$]$_3$.

6.3 ^{1}H NMR spectroscopy of [Eu(L5)$_3$]$^{3+}$

Europium(III) has a [Xe]$4f^6$ configuration so it has six unpaired electrons and therefore shows paramagnetic properties. The Eu(III) complex of ligand **L5** - [Eu(**L5**)][CF$_3$SO$_3$]$_3$, was characterized by ^{1}H NMR spectroscopy in CD$_3$CN solution (**Scheme 6.3**) and the spectrum is shown in **Figure 6.9**.
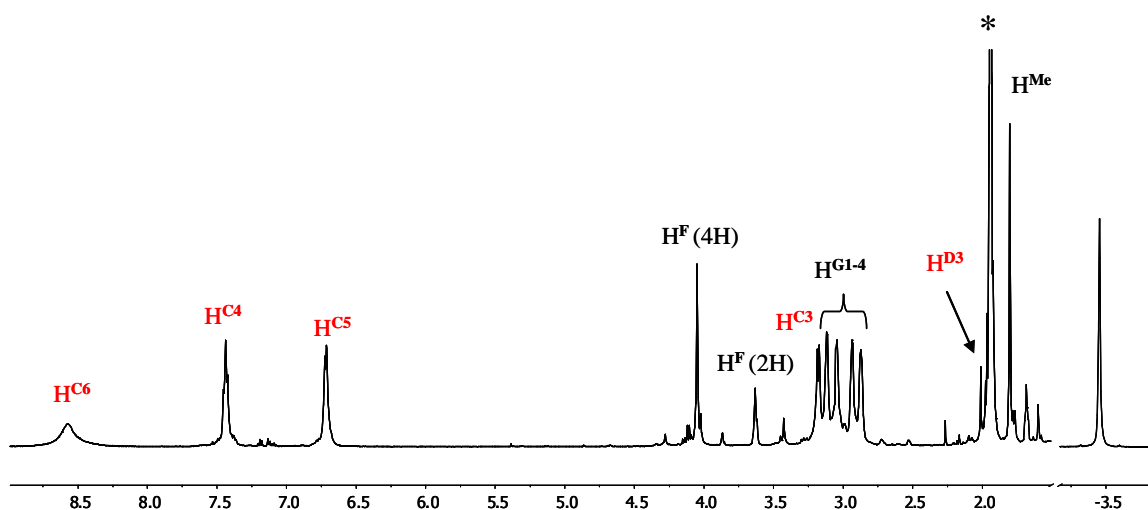
Figure 6.9. ^{1}H NMR spectrum (600 MHz, 295 K) of [Eu(**L5**)][CF$_3$SO$_3$]$_3$ in CD$_3$CN. The signal marked with * is the signal for CD$_3$CN.
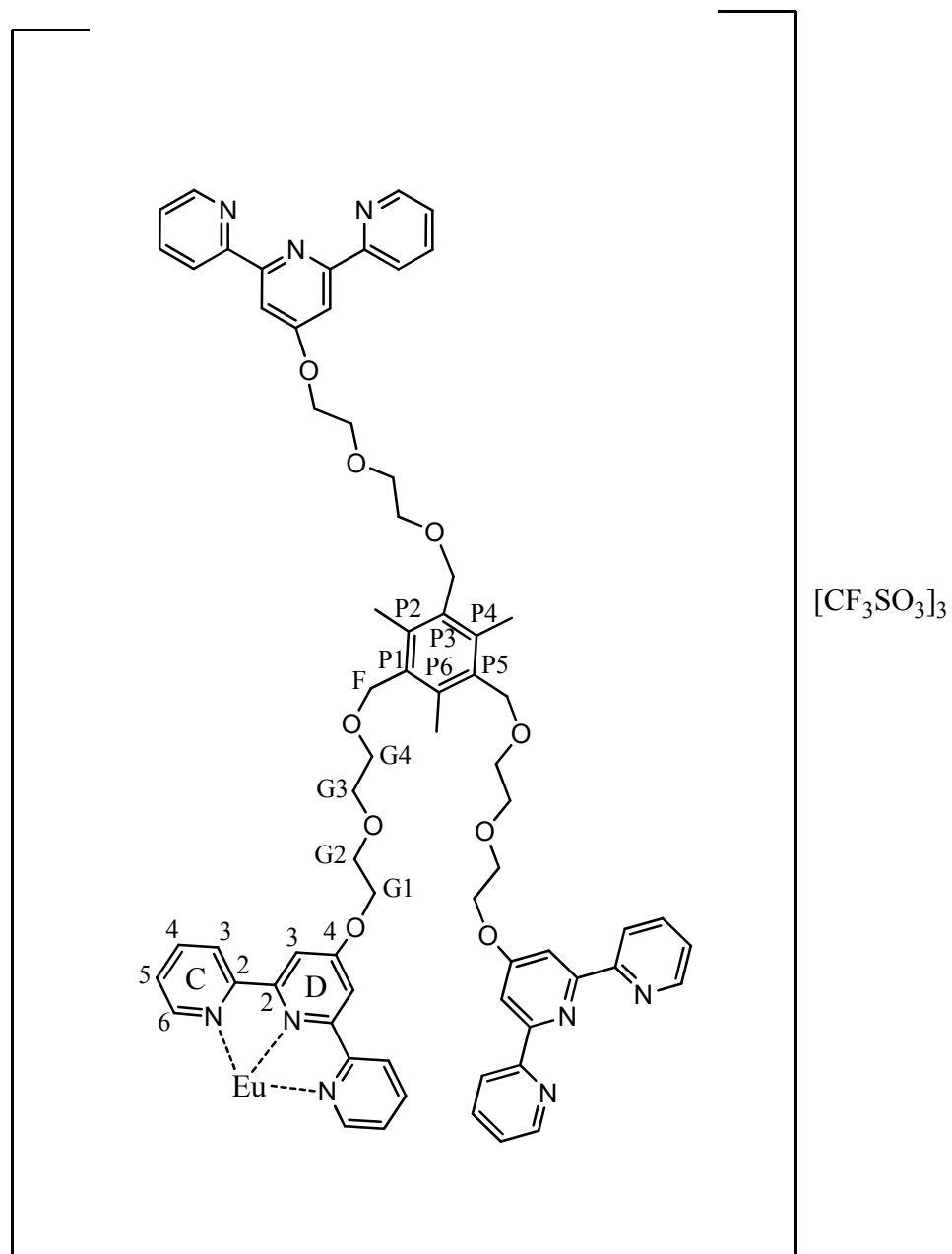
Scheme 6.3. Labeling for [Eu(**L5**)][CF$_3$SO$_3$]$_3$.

The assignment of all of the protons of the europium(III) complex were made using the COSY, NOESY and ROESY (**Figure 6.11**) techniques. Both NOESY and ROESY are very useful for identifying protons that are close in space but ROESY has the advantage that cross peaks are always positive and cannot be zero.[235]

All of the signals corresponding to the diethylene glycol chain $\mathbf{H^{G1\text{-}G4}}$ of [Eu(**L5**)][CF$_3$SO$_3$]$_3$ can be found, as expected, in the aliphatic region between δ 2.85-3.15 ppm. The signals at δ 4.08 and 3.63 ppm are assigned to $\mathbf{H^F}$ from the -CH$_2$- bridge connecting the benzene ring to the diethylene glycol chain. A singlet for the nine mesitylene protons $\mathbf{H^{Me}}$ is observed at δ 1.83 ppm (**Figure 6.9**).

	$\mathbf{H^{C5}/H^{T5}}$	$\mathbf{H^{C4}/H^{T4}}$	$\mathbf{H^{D3}/H^{T3'}}$	$\mathbf{H^{C3}/H^{T3}}$	$\mathbf{H^{C6}/H^{T6}}$
L5	7.27-7.32 (m)	7.79 (t) J 7.2 Hz	7.99 (s)	8.56 (d) J 7.9 Hz	8.65 (d) J 3.9 Hz
[Eu(**L5**)]$^{3+}$	6.72 (d) J 7.2 Hz	7.44 (t) J 7.4 Hz	1.96 (s)	3.20 (m)	8.58 (br)

Table 6.1. ^{1}H NMR spectroscopic data, δ$_H$ [ppm] for **L5** (600 MHz, 295 K, CDCl$_3$) and [Eu(**L5**)][CF$_3$SO$_3$]$_3$ (500 MHz, 295 K, CD$_3$CN) (see pages 141 and 178 for scheme of labeling).
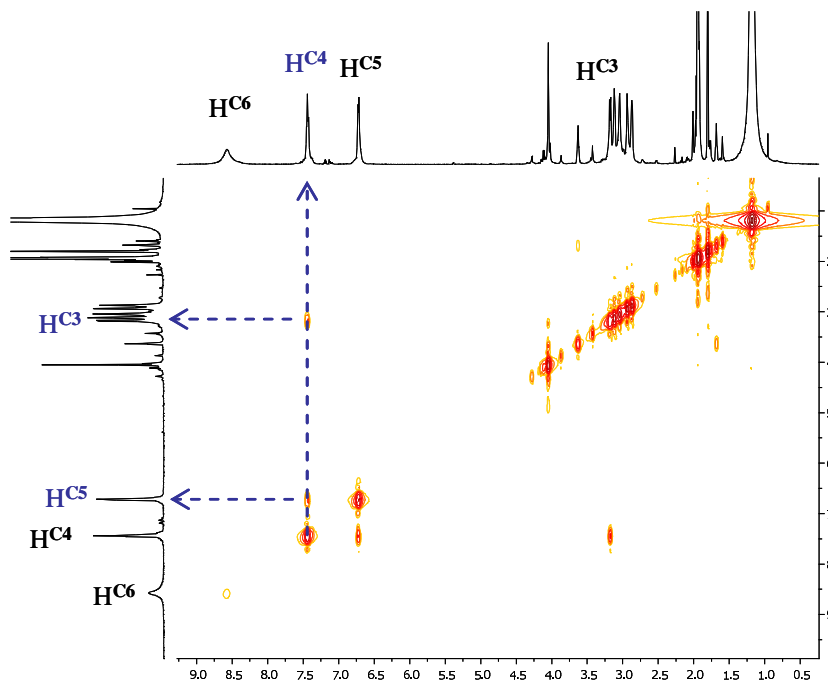
Figure 6.10. Part of the COSY spectrum (600 MHz, 295K) of [Eu(**L5**)][CF$_3$SO$_3$]$_3$ in CD$_3$CN.

A comparison between the chemical shifts of tpy protons of free ligand **L5** in CHCl$_3$ and the europium(III) complex [Eu(**L5**)][CF$_3$SO$_3$]$_3$ in acetonitrile is shown in **Table 6.1**. All of the terpyridine proton signals of ligand **L5** after complexation with europium(III) are shifted upfield. The signals for protons **H^{C4}**/**H^{T4}** and **H^{C6}**/**H^{T6}** of complex [Eu(**L5**)][CF$_3$SO$_3$]$_3$ are not so strongly affected and respectively shifted by 0.35 and 0.07 ppm, in comparison to ligand **L5**. The signals for protons **H^{C3}**/**H^{T3}**, **H^{C5}**/**H^{T5}** and **H^{D3}**/**H$^{T3'}$** are the most shifted upfield by 5.36, 0.57 and more than 6.03 ppm for signal **H^{D3}**/**H$^{T3'}$**. The signals, especially the signal for proton **H^{C6}**/**H^{T6}** are broadened due to the paramagnetic contribution of Eu(III) cation. This very strong upfield shifting is also a result of the paramagnetic metal center.

In **Figure 6.10** the COSY spectrum of complex [Eu(**L5**)][CF$_3$SO$_3$]$_3$ is shown. The signal for **H^{C4}** gives a COSY cross peak to the signal **H^{C3}** at δ 3.20 ppm and **H^{C5}** at δ 6.72 ppm. Due to broadening of the signal and the short relaxation time, the COSY cross peaks of proton **H^{C6}** can not be found.
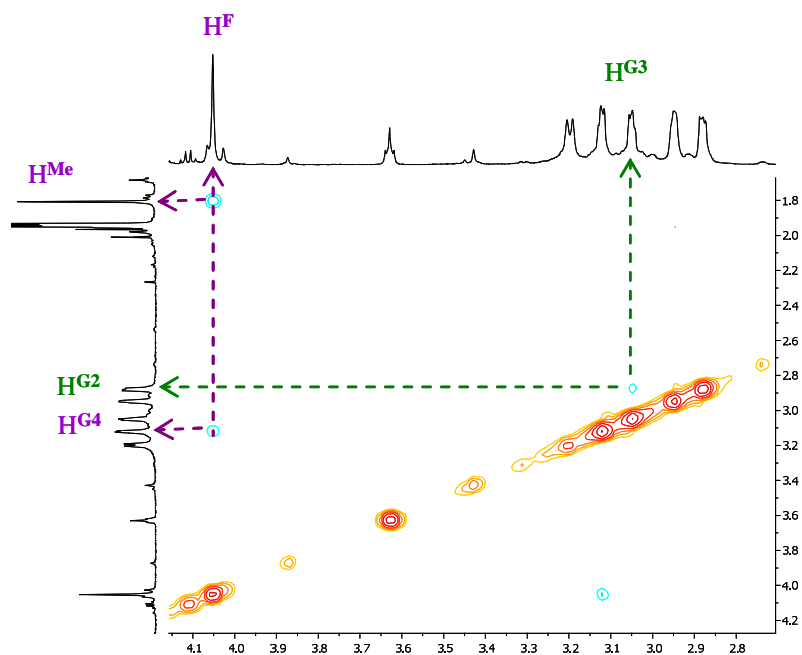
Figure 6.11. Part of the ROESY spectrum (600 MHz, 295K) of [Eu(**L5**)][CF$_3$SO$_3$]$_3$ in CD$_3$CN.

6.4 ^{13}C NMR spectroscopy of [Eu(L5)$_3$]$^{3+}$

For comparison, the diethylene glycol $\mathbf{C^G}$, $\mathbf{C^F}$ and phenyl $\mathbf{C^P}$ carbon signals of europium(III) complex [Eu(**L5**)][CF$_3$SO$_3$]$_3$ as well as the terpyridine carbon signals of this complex were put together with carbon signals of ligand **L5** in **Tables 6.2** and **6.3**. The assignments were made using HMQC and HMBC techniques.

	$\mathbf{C^{G1}}$	$\mathbf{C^{G2}}$	$\mathbf{C^{G3}}$	$\mathbf{C^{G4}}$	$\mathbf{C^F}$	$\mathbf{C^P}$
L5	68.0	69.6	71.3	69.6	68.1	132.5, 138.5
[Eu(**L5**)]$^{3+}$	68.9	69.0	71.1	70.0	68.1 68.9	133.5 138.7

Table 6.2. ^{13}C NMR spectroscopic data, δ_C [ppm], (151 MHz, 295 K) for **L5** in CDCl$_3$ and [Eu(**L5**)][CF$_3$SO$_3$]$_3$ in CD$_3$CN (see pages 141 and 178 for scheme of labeling).

Table 6.2 shows how the $\mathbf{C^G}$, $\mathbf{C^F}$ and $\mathbf{C^P}$ carbon signals of ligand **L5** changes, after complexation with europium(III). The signals $\mathbf{C^{G1}}$, $\mathbf{C^{G4}}$, $\mathbf{C^F}$ and $\mathbf{C^P}$ are slightly shifted downfield after complexation with europium(III) and the carbon signals $\mathbf{C^{G2}}$ and $\mathbf{C^{G3}}$ of europium(III) complex [Eu(**L5**)][CF$_3$SO$_3$]$_3$ are shifted upfield by 0.6 and 0.2 ppm, respectively.

In **Figure 6.12** the cross peaks of the aliphatic protons $\mathbf{H^F}$ (4H) at δ 4.08 ppm and $\mathbf{H^F}$ (2H) at δ 3.63 ppm of the complex [Eu(**L5**)][CF$_3$SO$_3$]$_3$ to the signals for directly attached carbons at δ 68.1 and δ 68.9 ppm are shown. All of the C-H signals could be easily assigned using the HMQC spectrum.

Table 6.3 shows in comparison the terpyridine carbon signals of ligand **L5** and europium(III) complex [Eu(**L5**)][CF$_3$SO$_3$]$_3$. The signals $\mathbf{C^{T4}}$/$\mathbf{C^{C4}}$, $\mathbf{C^{T6}}$/$\mathbf{C^{C6}}$ and $\mathbf{C^{T4'}}$/$\mathbf{C^{D4}}$

are strongly shifted downfield after complexation with europium(III) and the carbon signals C^{T2}/C^{C2}, C^{T3}/C^{C3}, C^{T5}/C^{C5}, $C^{T2'}/C^{D2}$ and $C^{T3'}/C^{D3}$ of europium(II) complex [Eu(**L5**)][CF$_3$SO$_3$]$_3$ are shifted upfield. The signals for carbons C^{C3}/C^{T3}, C^{C6}/C^{T6} and $C^{D3}/C^{T3'}$ are the most shifted, by more than 30 ppm for all three signals. These very strong chemical shifts are a result of the paramagnetic metal center.

	C^{T2} /C^{C2}	C^{T3} /C^{C3}	C^{T4} /C^{C4}	C^{T5} /C^{C5}	C^{T6} /C^{C6}	$C^{T2'}$ /C^{D2}	$C^{T3'}$ /C^{D3}	$C^{T4'}$ /C^{D4}
L5	156.2	121.5	137.0	124.0	149.2	157.2	107.6	167.1
[Eu(**L5**)]$^{3+}$	153.6	90.7	151.1	105.1	184.1	144.3	72.6	175.2

Table 6.3. ^{13}C NMR spectroscopic data, δ_C [ppm], (151 MHz, 295 K) for **L5** in CDCl$_3$ and [Eu(**L5**)][CF$_3$SO$_3$]$_3$ in CD$_3$CN (see pages 141 and 178 for scheme of labeling).
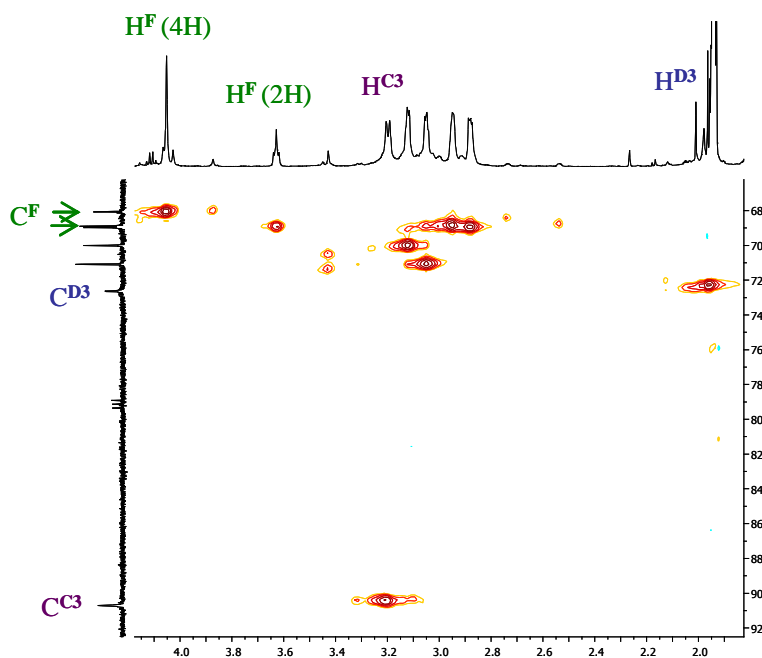
Figure 6.12. Part of the HMQC spectrum (600 MHz, 295 K) of [Eu(**L5**)][CF$_3$SO$_3$]$_3$ in CD$_3$CN.

In the **Figure 6.12** the cross peaks of the terpyridine protons $\mathbf{H^{C3}}$ and $\mathbf{H^{D3}}$ of the complex [Eu(**L5**)][CF$_3$SO$_3$]$_3$ in CD$_3$CN to the directly bound carbon signals are shown.
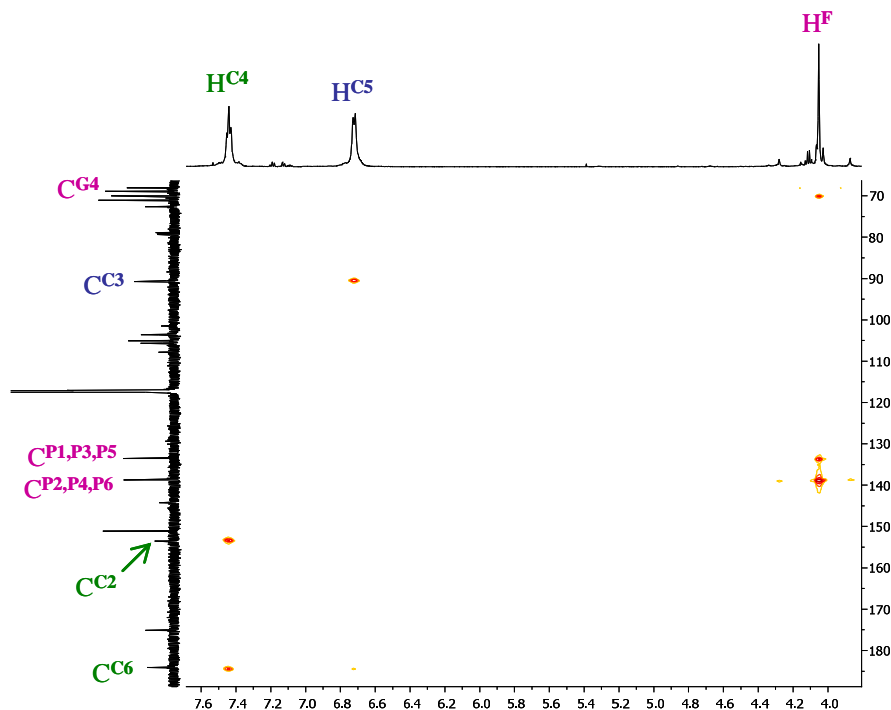
Figure 6.13. Part of the HMBC spectrum (600 MHz, 295 K) of [Eu(**L5**)][CF$_3$SO$_3$]$_3$ in CD$_3$CN

In **Figure 6.13**, the cross peaks of the protons $\mathbf{H^{C4}}$, $\mathbf{H^{C5}}$ and $\mathbf{H^{F}}$ of the europium(III) complex to the carbon signals separated by 2-3 bonds are shown. The signal for proton $\mathbf{H^{C4}}$ couples with the signals for carbons $\mathbf{C^{C2}}$ and $\mathbf{C^{C6}}$, the signal for proton $\mathbf{H^{C5}}$ couples with a signal for a carbon $\mathbf{C^{C3}}$ and the signal for proton $\mathbf{H^{F}}$ couples with the signals for carbons $\mathbf{C^{G4}}$, $\mathbf{C^{P1,P3,P5}}$ and $\mathbf{C^{P2,P4,P6}}$, giving the cross peaks.

The complex [Tb(**L5**)][CF$_3$SO$_3$]$_3$ could not be studied in the solid state. However, preliminary NMR studies suggesting the presence of a paramagnetic species and photochemical investigation (see section 6.5) of the complex in solution confirm the existence of the proposed terbium(III) complex.

6.5   Photochemical characterization

In order to determine conditional stability constants, spectrophotometer titrations of ligand **L5** 10^{-5} M with europium(III) and terbium(III) trifluoromethanesulfonate solutions 5×10^{-3} M were performed. UV-vis spectra were recorded after each addition of Ln(III) starting from 0.01 eq/0.05 eq up to a total concentration ratio $R = $ Ln(III)/**L5** = 5. All of the titrations were conducted in acetonitrile solution (**Figures 6.14 and 6.15**).

Addition of the Ln(III) salt results in the appearance of a new band at around 320 nm with a increase in the insentity of two bands of ligand **L5** at 241 and 279 nm. The band at 241 nm is additionally red shifted. After $R = $ Ln(III)/**L5** = 1 further addition of Ln(III) does not significantly modify the shape of the spectrum. UV-vis spectra recorded during the titration of **L5** with Ln(III) display only one well defined isosbestic point at 300 nm (**Figures 6.14 and 6.15**).
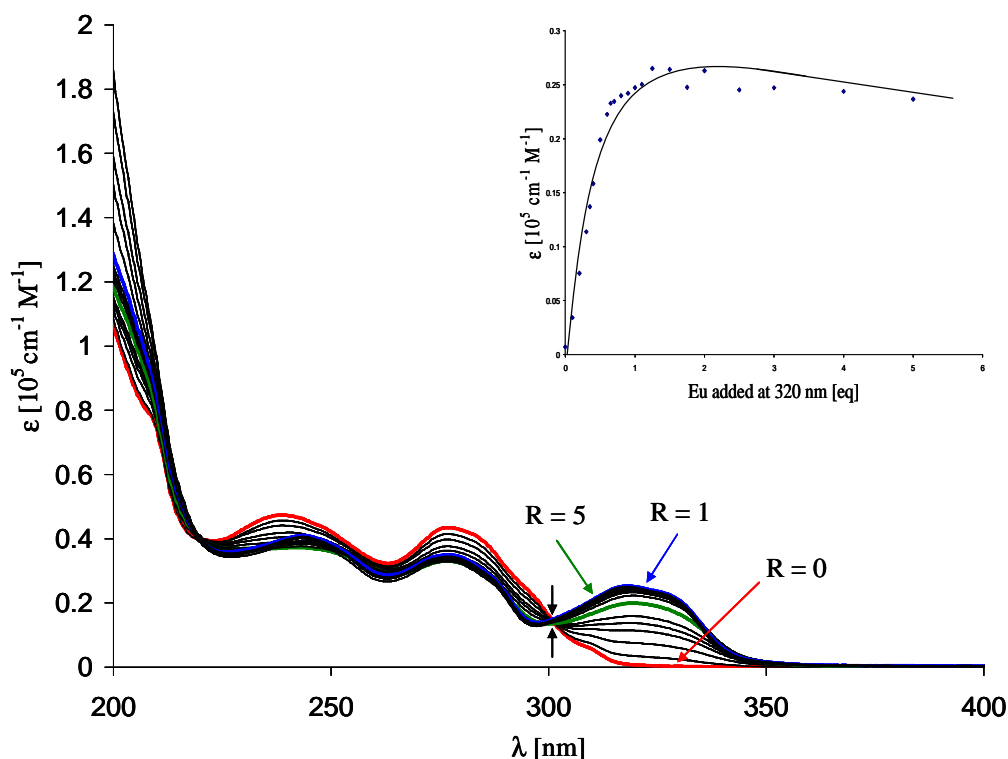
Figure 6.14. UV-vis spectra of ligand **L5** 10^{-5} M in acetonitrile and 298 K in the presence of increasing amounts of Eu(CF$_3$SO$_3$)$_3$, double arrows denote isosbestic point. The inset shows relation between ε [10^5 cm^{-1} M^{-1}] and added amount of metal [eq].
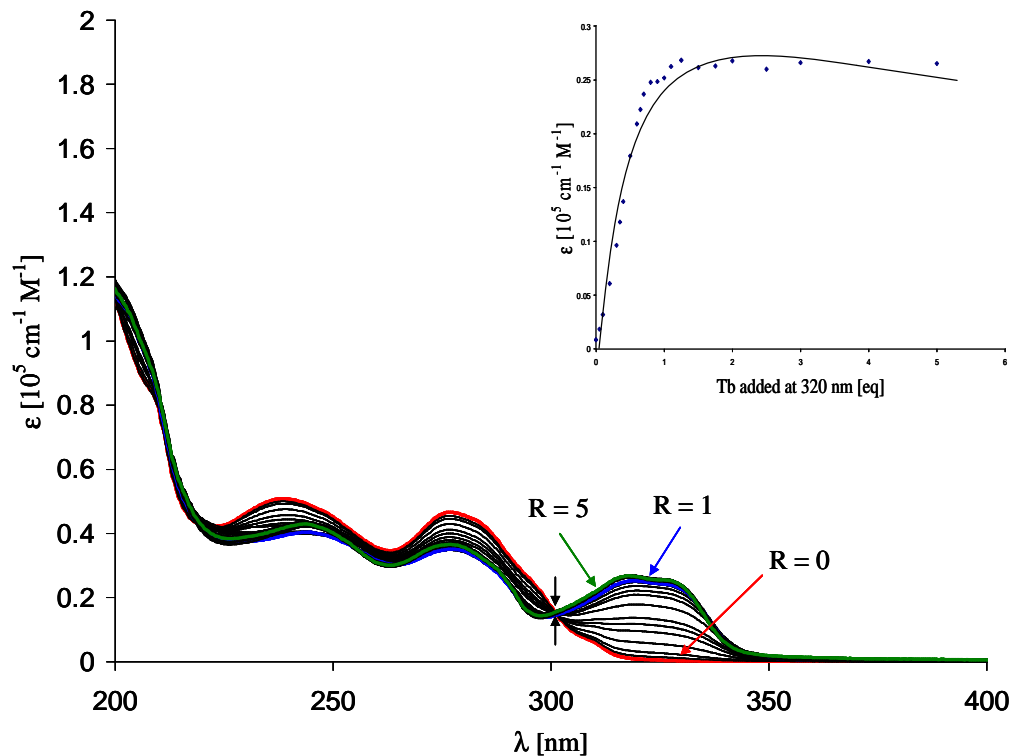
Figure 6.15. Absorption spectra of ligand **L5** 10^{-5} M in acetonitrile and 298 K in the presence of increasing amounts of $Tb(CF_3SO_3)_3$, double arrows denote isosbestic point. The inset shows relation between ε [10^5 cm^{-1} M^{-1}] and added amount of metal [eq].

Emission (fluorescence and phosphorescence) spectra were also recorded after each addition of Ln(III) starting from 0.01 eq/0.05 eq up to a total concentration ratio R = Ln(III)/**L5** = 5. The titrations were performed in acetonitrile solution.

In **Figures 6.16** and **6.17** the emission spectra of ligand **L5** titrated with a solution of $Eu(CF_3SO_3)_3$ are shown. In red, the spectrum of ligand **L5** is shown, before addition of the metal salt, the ligand exhibits no emission. Increasing the amount of europium(III) salt in the solution causes the appearance of an emission spectrum typical for this lanthanide (see **Figure 6.4**). The five bands at 591, 615, 650, 690 and 700 nm correspond to five transition processes: $^5D_1 \rightarrow {}^7F_1$, $^5D_0 \rightarrow {}^7F_0$, $^5D_0 \rightarrow {}^7F_1$, $^5D_0 \rightarrow {}^7F_2$ and $^5D_0 \rightarrow {}^7F_4$, respectively.

Figure 6.16. Emission (fluorescence) spectra of ligand **L5** 10^{-5} M in acetonitrile and 298 K in the presence of increasing amounts of $Eu(CF_3SO_3)_3$.
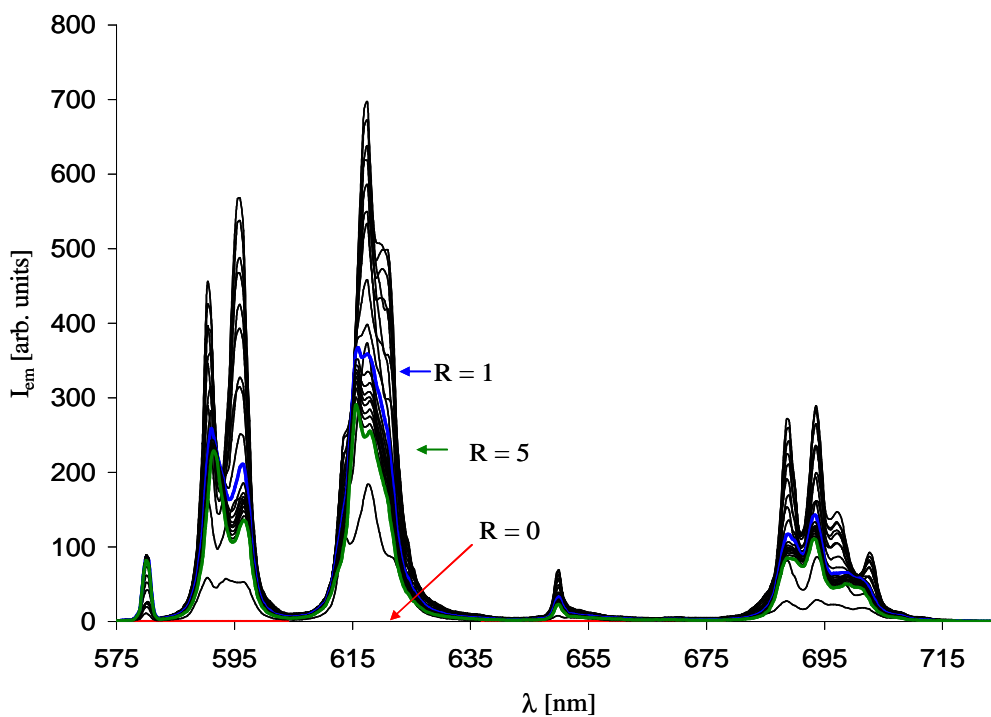
Figure 6.17. Emission (phosphorescence) spectra of ligand **L5** 10^{-5} M in acetonitrile and 298 K in the presence of increasing amounts of $Eu(CF_3SO_3)_3$.

In both **Figures 6.16** and **6.17** the spectra of the species with R = 1 and R = 5 are highlighted, in blue for R = 1 and in green for R = 5. None of the spectra, neither R = 1 nor R = 5, have maximum emission intensity, especially in the fluorescence spectra (**Figure 6.16**), but these data can not be treated as quantitative and the above observation suggests only that an intermediate has a stronger emission that dominates the 1:1 species.

In **Figures 6.18** and **6.19** the emission spectra of ligand **L5** titrated with a solution of $Tb(CF_3SO_3)_3$ are shown. The spectrum of ligand **L5** before addition of the metal salt exhibits no emission and is shown in red. Upon addition of terbium(III) salt, the typical emission spectrum appears (see **Figure 6.5**). The four bands at 490, 544, 584 and 621 nm correspond to four transition processes: $^5D_4 \rightarrow {}^7F_6$, $^5D_4 \rightarrow {}^7F_5$, $^5D_4 \rightarrow {}^7F_4$ and $^5D_4 \rightarrow {}^7F_3$, respectively.

In the case of titration of ligand **L5** with the terbium(III) salt, the spectra with R = 1 and R = 5 almost overlap with each other and are very close to the spectrum with the maximum emission intensity, especially in the fluorescence spectra (**Figure 6.18**).
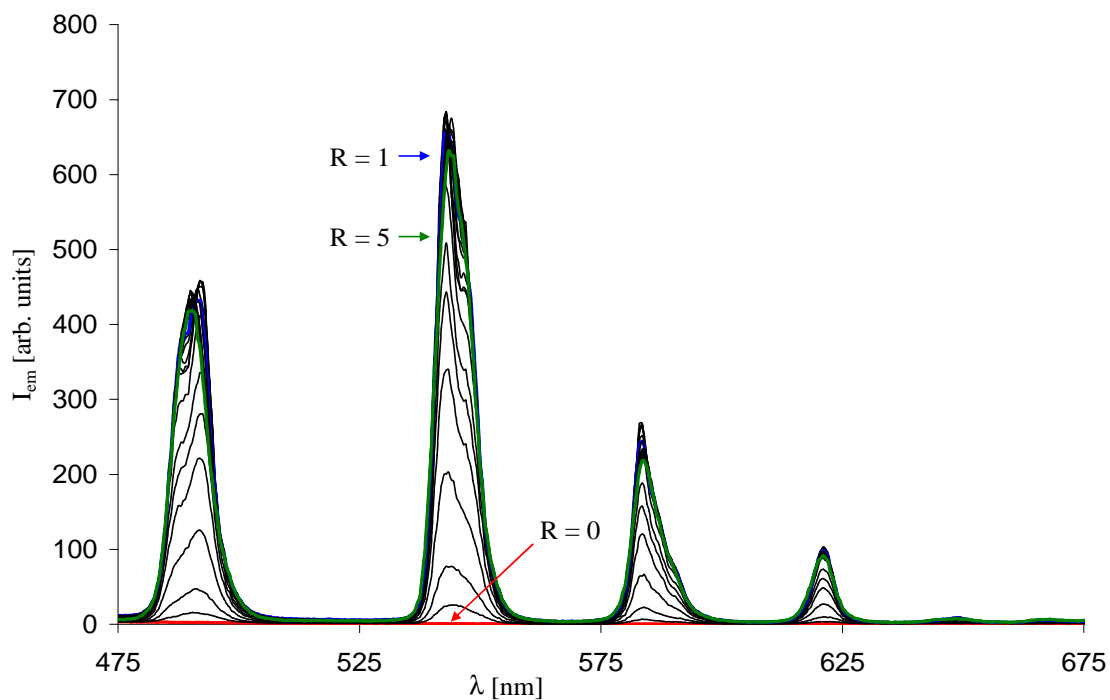
Figure 6.18. Emission (fluorescence) spectra of ligand **L5** 10^{-5} M in acetonitrile and 298 K in presence of increasing amounts of Tb(CF$_3$SO$_3$)$_3$.
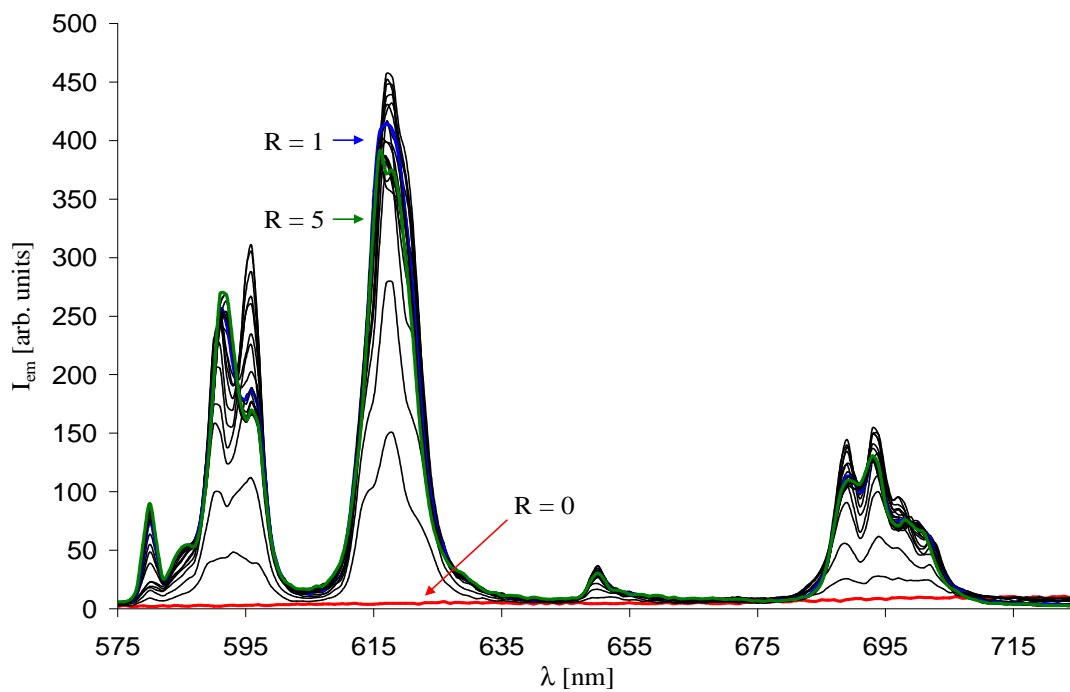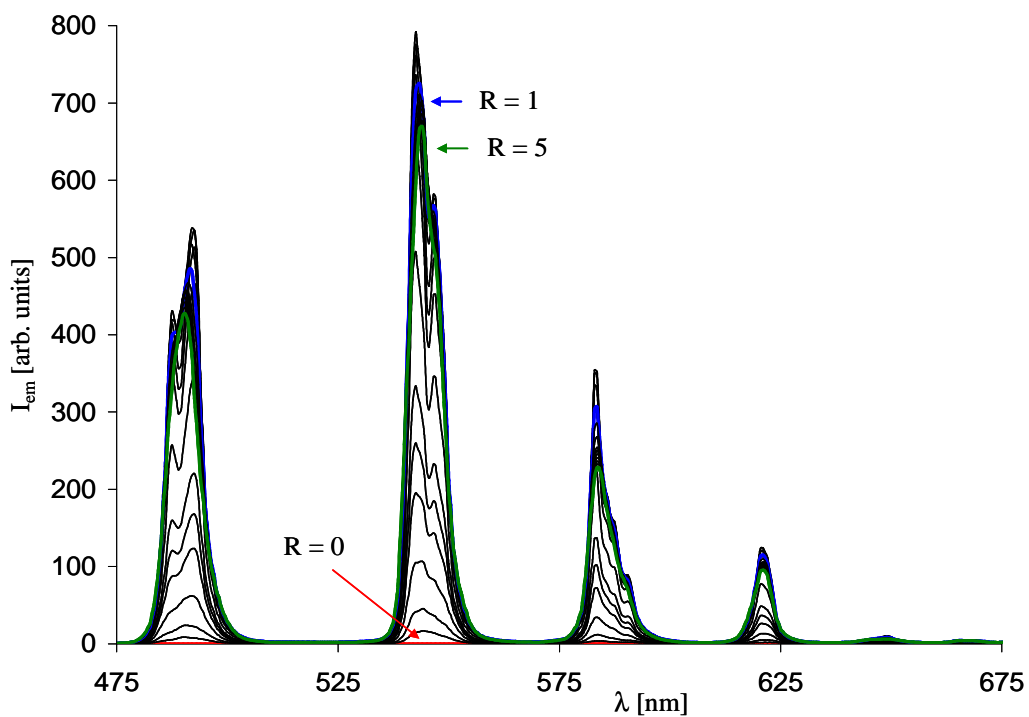

Figure 6.19. Emission (phosphorescence) spectra of ligand **L5** 10^{-5} M in acetonitrile and 298 K in presence of increasing amounts of Tb(CF$_3$SO$_3$)$_3$.

Mathematical treatments of the data with SPECFIT[®236,237] allowed the determination of conditional stability constants corresponding to the following general equation:

$$m \, Ln^{3+} + n \, \textbf{L5} \rightleftharpoons [(Ln)_m(\textbf{L5})_n]^{3m+} \qquad \beta_{nm} = [\{(Ln)m(\textbf{L5})_n\}^{3m+}] / [Ln^{3+}]^m \cdot [\textbf{L5}]^n$$
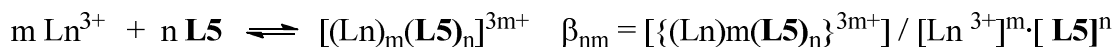
The model used for SPECFIT approximation suggests that in solution are four absorbing species, nevertheless only three could be defined: ligand and the 1:2 and 1:1 Ln:$\textbf{L5}$ species. Data were fitted by non-linear least-squares techniques to the following set of equations:

$$Ln^{3+} + 2 \, \textbf{L5} \rightleftharpoons [Ln(\textbf{L5})_2]^{3+} \qquad \log \beta_{21}$$

$$Ln^{3+} + \textbf{L5} \rightleftharpoons [Ln\textbf{L5}]^{3+} \qquad \log \beta_{11}$$
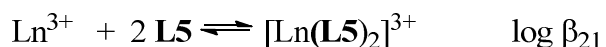
In **Table 6.2** conditional stability constants of 1:2 and 1:1 Eu:$\textbf{L5}$ species are shown. Data fitted based on UV-vis and phosphorescence titrations give comparable values for stability constants $\log\beta_{21}$ (around 16), for $\log\beta_{11}$ (around 25), whereas stability constants fitted by treating fluorescence data are by two orders of magnitude smaller.

	UV-Vis	Luminescence Fluor./Phosp.
$\log\beta_{21}$	16.04	13.88/16.02
$\log\beta_{11}$	24.63	22.07/25.08

Table 6.2. Conditional stability constants for $[Eu(L)_2]^{3+}$ and $[EuL]^{3+}$. Estimated errors $\pm$ 2 log K units.

In **Table 6.3** conditional stability constants of 1:2 and 1:1 Tb:$\textbf{L5}$ species are shown. Data could be fitted only based on UV-vis and fluorescence titrations. The observations made

during interpretation of data for europium(III) complexes (see above) suggest that values for stability constants $\log\beta_{21}$ (around 14) and $\log\beta_{11}$ (around 22), fitted by treating UV-vis data are more credible.

	UV-Vis	Luminescence (Fluorescence)
$\log\beta_{21}$	13.80	15.92
$\log\beta_{11}$	21.52	24.42

Table 6.3. Conditional stability constants for $[Tb(L)_2]^{3+}$ and $[TbL]^{3+}$. Estimated errors $\pm$ 2 log K units.

Recalculated spectra of the ligand and 1:2 and 1:1 Ln:**L5** species match satisfyingly the experimental ones.
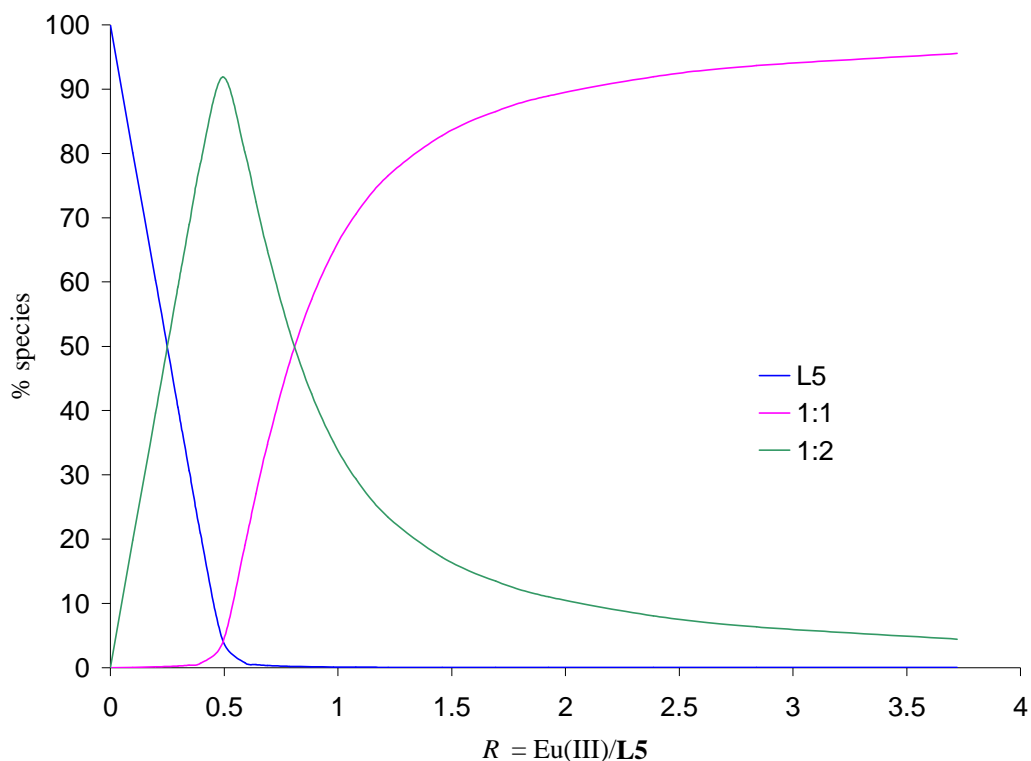
Figure 6.20. Distribution diagram for europium(III).

190

Distribution diagrams drawn from the conditional stability constants are presented in **Figures 6.20** and **6.21**. When the ratio *R* reaches a value 0.5, the 1:2 Ln(III)/**L5** complex become predominant. For europium(III) 1:2 Eu(III)/**L5** species at R = 0.5 is present in solution in 90%, for terbium, around 70%. Furthermore, when *R* is larger than 1.5 for $[EuL]^{3+}$ and 1 for $[TbL]^{3+}$, the 1:1 complexes represent the most abundant species in solution.

In the distribution diagram for europium(III) at *R* = 1, the 1:1 Eu(III)/**L5** species represents only 70% of the total solution species and the 1:2 Eu(III)/**L5** species is present in solution, comprising 30% of the total solution species. Significant excess of europium(III) salt is needed to shift an equilibrium towards 1:1 Eu(III)/**L5** complex, at *R* = 2.5, 1:1 complex represents the most abundant species in solution (95%) (**Figure 6.20**).
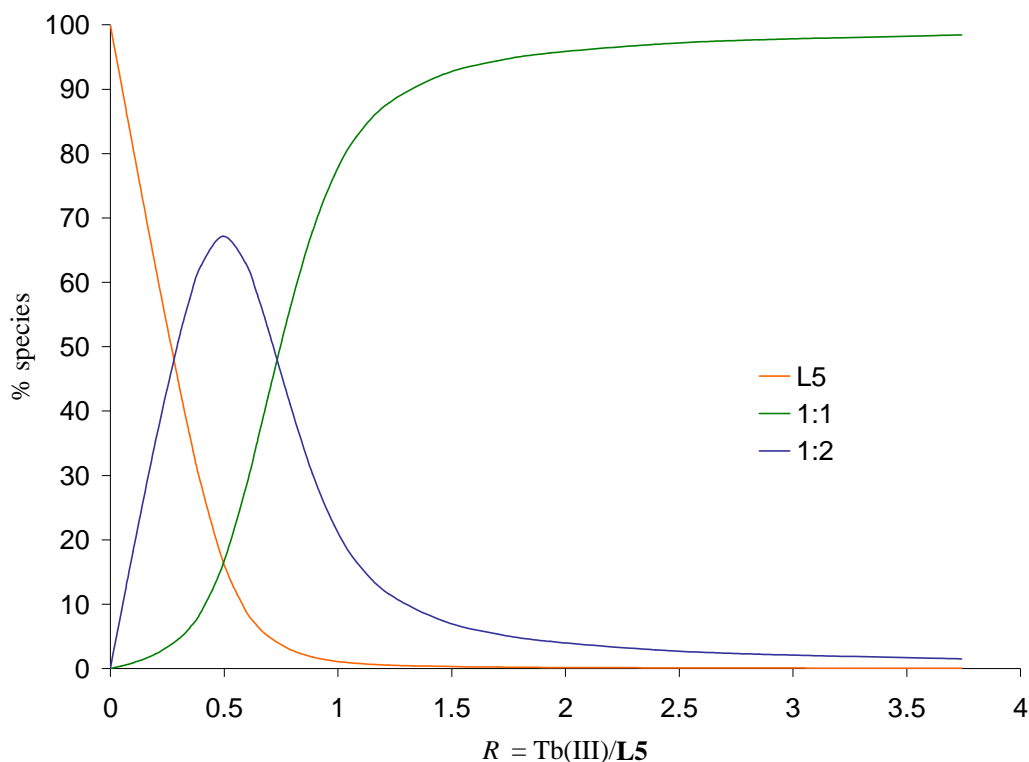
Figure 6.21. Distribution diagram for terbium(III).

In the distribution diagram for terbium(III) at $R = 1$, the 1:1 Tb(III)/**L5** species comprises 80% of the total solution species and there is only a trace amount of free ligand left. The 1:2 Tb(III)/**L5** complex represents only 20% of the solution species. At $R = 1.5$, the 1:1 complex becomes completely predominant in solution (95%) (**Figure 6.21**).

6.6 Conclusion

The homoleptic mononuclear europium(III) and terbium(III) complexes of tritopic 4'-substituted- 2,2':6',2''-terpyridine ligand **L5** have been synthesized. The photophysical properties of both complexes [Eu(**L5**)][CF$_3$SO$_3$]$_3$ and [Tb(**L5**)][CF$_3$SO$_3$]$_3$ were fully investigated. The absorption and emission spectra of both complexes have been recorded. The europium(III) complex [Eu(**L5**)][CF$_3$SO$_3$]$_3$ was characterized by ^{1}H and ^{13}C NMR spectroscopy.

6.7 Experimental

❖ [Eu(**L5**)][CF$_3$SO$_3$]$_3$

❖ [Tb(**L5**)][CF$_3$SO$_3$]$_3$

Ligand **L5** was prepared as described in Chapter 5. Eu(CF$_3$SO$_3$)$_3$ and Tb(CF$_3$SO$_3$)$_3$ are commercially available compounds and were used as received (Sigma Aldrich, 98%)

❖ [Eu(**L5**)][CF$_3$SO$_3$]$_3$
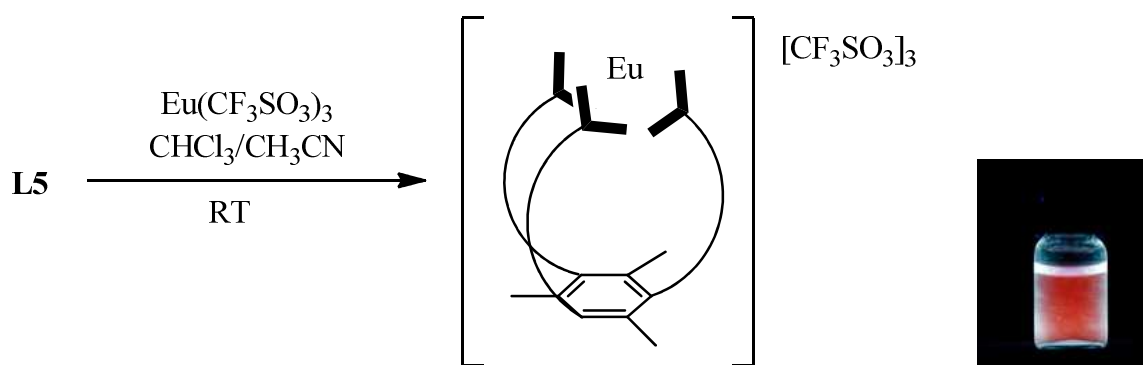
Compound **L5** (0.14 g, 0.12 mmol) dissolved in 10 mL CHCl$_3$ was added to a solution of Eu(CF$_3$SO$_3$)$_3$ (0.072 g, 0.12 mmol) in 30 mL CH$_3$CN. The mixture was stirred 10 minutes at room temperature. The solvent was removed *in vacuo* to give a yellowish oil (0.19 g, 0.11 mmol, 90%).

^{1}H NMR (600 MHz, CD$_3$CN) δ_H 1.83 (s, 9H, H^{Me}), 1.96 (s, 6H, H^{D3}), 2.88 (m, 4H, H^{G2}), 2.95 (m, 4H, H^{G1}), 3.05 (m, 4H, H^{G3}), 3.12 (m, 4H, H^{G4}), 3.20 (m, 6H, H^{C3}), 3.63 (s, 2H, H^F), 4.08 (s, 4H, H^F), 6.72 (d, *J* 7.2 Hz, 6H, H^{C5}), 7.44 (t, *J* 7.4 Hz, 6H, H^{C4}), 8.58 (br, 6H, H^{C6}).

^{13}C NMR (151 MHz, CD$_3$CN) δ_C 15.7 (C^{Me}), 68.1 (C^F), 68.9 (C^{G1} and C^F), 60.0 (C^{G2}), 70.0 (C^{G4}), 71.1 (C^{G3}), 72.6 (C^{D3}), 90.7 (C^{C3}), 105.1 (C^{C5}), 133.5 (C^{P1,P3,P5}), 138.7 (C^{P2,P4,P6}), 144.3 (C^{D2}), 151.1 (C^{C4}), 153.6 (C^{C2}), 175.2 (C^{D4}), 184.1 (C^{C6}).

❖ [Tb(**L5**)][CF$_3$SO$_3$]$_3$
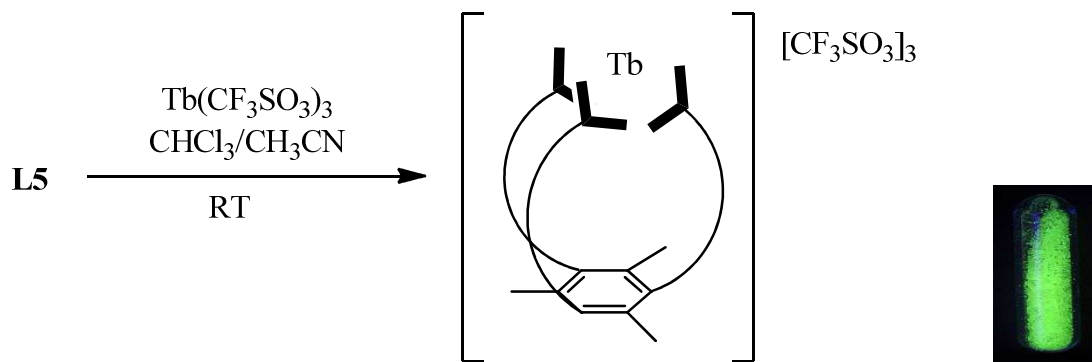
Complex [Tb(**L5**)][CF$_3$SO$_3$]$_3$ was synthesized according to the same procedure as for [Eu(**L5**)][CF$_3$SO$_3$]$_3$ with ligand **L5** (0.14 g, 0.12 mmol) and Tb(CF$_3$SO$_3$)$_3$ (0.073 g, 0.12 mmol). The mixture was stirred 10 minutes at room temperature. The solvent was removed *in vacuo* to give a yellowish oil (0.20 g).

^{1}H NMR (400 MHz, CD$_3$CN): Preliminary results show the presence of a paramagnetic species.

CHAPTER 7

References

1.   J. F. Stoddart, D. Philp, *Angew. Chem. Int. Ed.* **1996**, *35*, 1154-1196.
.
2.   J.-M. Lehn, *Supramolecular Chemistry*, VCH, Weinheim, **1995**.

3.   J.-M. Lehn, *Science,* **1985***, 227*, 849.

4.   J.-M. Lehn, *Angew. Chem. Int. Ed.* **1990**, *29*, 1304.

5.   D. Philips, J. F. Stoddart, *Angew. Chem. Int. Ed*. **1996**, *35*, 1154.

6.   J. S. Lindsay, *New J. Chem.*, **1991**, *15*, 153.

7.   J.-M. Lehn, A. Rigault, J. Siegel, J. Harrowfield, B. Chevrier, D. Moras,   *Proc. Natl. Acad. Sci. USA* **1987**, *84*, 2565.

8.   W. Zarges, J. Hall, J.-M. Lehn, C. Bolm, *Helv. Chim. Acta* **1991**, *74*, 1843.

9.   C. J. Pedersen, *Angew. Chem. Int. Ed.* **1988***, 27*, 1021.

10.   M. Fujita. J Yazaki, K. Ogura, *J. Am. Chem. Soc.* **1990,** *112,* 5645.

11.   M. Fujita, J. Yazaki, K. Ogura, *Chem. Leu.* **1991**, 1031.

12.   M. L. Merlau, M. Del Pilar Mejia, S. T. Nguyen, J. T. Hupp, *Angew. Chem. Int. Ed.* **2001**, *40*, 4239-4242.

13.   C. E. Housecroft, A. G. Sharpe, *Inorganic Chemistry*, 3 ed., Pearson Education.

14.   V. Chaurin, E. C. Constable, C. E. Housecroft, *New J. Chem.* **2006**, *30*, 1740-1744.

15.   D. Philp, J. F. Stoddart, *Synlett* **1991**, 445.

16.   P. Gaviña, J.-P. Sauvage, *Tetrahedron Lett.* **1997**, *38*, 3521.

17.   N. Armaroli, V. Balzani, J.-P. Collin, P. Gaviña, J.-P. Sauvage, B. Ventura, *J. Am. Chem. Soc.* **1999**, *121*, 4397.

18. V. Balzani, A. Credi, F. M. Raymo, J. F. Stoddart, *Angew. Chem. Int. Ed.* **2000**, *39*, 3348.

19. The name "catenane" is derived from the Latin word "catena" meaning chain 1941. In chemical terms, such molecules can be viewed as being composed of two or more macrocycles that are connected mechanically but not by any covalent chemical bond. The prefix indicates the number of interlocked components. Thus a [2]catenane contains two interlocked rings.

20. H. L. Frisch. E. Wasserman, *J. Am. Soc.* **1961**, *83*, 3789.

21. D. M. Walba, *Tetrahedron* **1985,** *41*, 3161.

22. C. O. Dietrich-Buchecker, J.-P. Sauvage, *Biorg. Chem. Front.* **1991**, *2*, 195.

23. C. Weber, *New J. Chem.* **1993**, *17*, 627.

24. D. B. Amabilino, W. Parsons, J. F. Stoddart, *Trends Polym. Sci.* **1994**, *1*, 146.

25. M. Cesario, C. O. Dietrich-Buchecker, J. Guilhem, C. Pascard, J. P. Sauvage, *Chem. Commun.* **1985**, 244.

26. M. Beyler, V. Heitz, J.-P. Sauvage, *Chem. Commun.* **2008**, 5396 - 5398.

27. C. A. Hunter. M. N. Meah, J. K. M. Sanders, *J. Am. Chem. Soc.* **1990,** *112*, 5773.

28. H. L. Anderson, C. A. Hunter, M. N. Meah, J. K. M. Sanders, *J. Am. Chem. Soc.* **1990**, *112*, 5780.

29. H. L. Anderson, J. K. M. Sanders*, Angew. Chem.* **1990,** *102,* 1478.

30. H. L. Anderson, J. K. M. Sanders, *Angew. Chem. Int. Ed.* **1990**, 29, 1400.

31. H. L. Anderson, *J. Am. Chem. Soc.* **2007**, *129*, 4291-4297.

32. H. L. Anderson, *J. Am. Chem. Soc.* **2007**, *129*, 13370-13371.

33. H. L. Anderson, *Angew. Chem. Int. Ed.* **2007**, *46*, 3122 –3125.

34. P. N. W. Baxter, J. M. Lehn, J. Fischer, M. T. Youinou, *Angew. Chem.* **1994,** *106*, 2432.

35. P. N. W. Baxter, J-M. Lehn, J. Fischer, M. T. Youinou, *Angew. Chem. Int. Ed.* **1994**, *33*, 2284.

36. H. Sleiman, P. N. W. Baxter, J. M. Lehn, K. Rissanen, *J. Chem. Soc. Chem. Commun.* **1995**, 715.

37.	G. S. Hanan, C. R. Arana, J.-M. Lehn, D. Fenske, *Angew Chem.* **1995**, *107*, 1191.

38.	S. Hanan, C. R. Arana, J.-M. Lehn, D. Fenske, *Angew. Chem. Int. Ed.* **1995**, *34*, 1122.

39.	A. A. Schilt, S. W. Wong, *J. Coord. Chem.* **1984**, *13*, 331-339.

40.	J. I. Bullock, P. W. G. Simpson, *J. Chem. Soc. Faraday Trans. 1* **1981**, *77*, 1991-1997.

41.	B. Whittle, S. R. Batten, J. C. Jeffery, L. H. Rees, M. D. Ward, *J. Chem. Soc. Dalton Trans.* **1996**, 4249.

42.	M. E. Padilla-Tosta, J. M. Lloris, R. Martónez-Máñez, A. Benito, J. Soto, T. Pardo, M. A. Miranda, M. D. Marcos, *Eur. J. Inorg. Chem.* **2000**, 741.

43.	D. Armspach, E. C. Constable, F. Diederich, C. E. Housecroft, J.-F. Nierengarten, *Chem. Eur. J.* **1998**, *4*, 723.

44.	D. Armspach, E. C. Constable, F. Diederich, C. E. Housecroft, J.-F. Nierengarten, *Chem. Commun.* **1996**, 2009.

45.	U. Siemoling, U. Vorfeld, B. Neumann, H.-G. Stammler, M. Fontani, P. Zanello, *J. Organomet. Chem.* **2001**, *733*, 637-639.

46.	J. M. Haider, M. Chavarot, S. Weidner, I. Sadler, R. M. Williams, L. de Cola, Z. Pikramenou, *Inorg. Chem.* **2001**, *40*, 3912.

47.	J. M. Haider, Z. Pikramenou, *Eur. J. Inorg. Chem*. **2001**, 189.

48.	J. M. Haider, Z. Pikramenou, *Chem. Commun.* **1998**, 1473.

49.	G. Albano, V. Balzani, E. C. Constable, M. Maestri, D. R. Smith, *Inorg. Chim. Acta* **1998**, 225, 277.

50.	E. C. Constable, E. Figgemeier, C. E. Housecroft, J. Olsson, Y. C. Zimmermann, *Dalton Trans.* **2004**, 1918.

51.	E. C. Constable, C. E. Housecroft, M. Neuburger, A. G. Schneider, B. Springler, M. Zehnder, *Inorg. Chim. Acta* **2000**, *49*, 300-302.

52.	E. C. Constable, C. E. Housecroft, M. Neuburger, A. G. Schneider, M. Zehnder, *J. Chem. Soc. Dalton Trans.*, **1997**, 2427.

53.	L. Flamigni, F. Barigelletti, N. Armaroli, J.-P. Collin, I. M. Dixon, J.-P. Sauvage J. A. G. Williams, *Coord. Chem. Rev.* **1999**, *671*, 190-192.

54.   J.-P. Collin, A. Harriman, V. Heitz, F. Odobel, J.-P. Sauvage, *Coord. Chem. Rev.* **1996**, *148*, 63.

55.   A. Harriman, F. Odobel, J.-P. Sauvage, *J. Am. Chem. Soc.* **1995**, *117*, 9461.

56.   J.-P. Collin, V. Heitz, J.-P. Sauvage, *Tetrahedron Lett.* **1991**, *32*, 5977.

57.   E. C. Constable, R. Handel, C. E. Housecroft, M. Neuburger, E. R. Schofield, M. Zehnder, *Polyhedron* **2004**, *23*, 135.

58.   E. Figgemeier, V. Aranyos, E. C. Constable, R. W. Handel, C. E. Housecroft, C. Risinger, A. Hagfeldt, E. Mukhtar, *Inorg. Chem. Commun.* **2004**, *7*, 117.

59.   E. C. Constable, B. Kariuki, A. Mahmood, *Polyhedron*, **2003**, *22*, 687.

60.   L.–X. Zhao, T. S. Kim, S.–H. Ahn, T.–H. Kim, E.–K. Kim, W.–J. Chao, H. Choi, C.–S. Lee, J.–A. Kim, T. C. Jeong, C.–J. Chang, E.–S, Lee, *Bioorg. Med. Chem. Lett.* **2001**, *11*, 2659.

61.   S. Encinas, L. Flamigni, F. Barigelletti, D. Fenske, M. Neuburger, J. G. Vos, M. Zehnder, *Chem. Eur. J.* **2002**, *8*, 137.

62.   E. C. Constable, T. Kulke, M. Neuburger, M. Zehnder, *Chem. Commun,* **1997**, 489.

63.   G. Baum, E. C. Constable, D. Fenske, C. E. Housecroft, T. Kulke, *Chem. Commun.* **1998**, 2659.

64.   E. C. Constable, C. E. Housecroft, T. Kulke, C. Lazzarini, E. R. Schofield, Y. Zimmermann, *J. Chem. Soc. Dalton Tran.* **2001**, 2864.

65.   E. C. Constable, S. M. Elder, J. Healy, D. A. Tocher, *J. Chem. Soc. Dalton Trans.* **1990**, 1669.

66.   E. C. Constable, T. Kulke, M. Neuburger, M. Zehnder, *New J. Chem.* **1997**, *21*, 1091.

67.   M. Schütte, D. G. Kurth, M. R. Linford, H. Cölfen, H. Möhwald, *Angew. Chem. Int. Ed.* **1998**, *37*, 2891-2893.

68.   T. E. Janini, J. L. Fattore, D. L. Mohler, *J. Organomet. Chem.* **1999**, *578*, 260-263.

69.   D. G. Kurth, R. Osterhout, *Langmuir* **1999**, *15*, 4842-4846.

70.   S. Kelch, M. Rehahn, *Chem. Commun.* **1999**, 1123-1124.

71.   S. Kelch, M. Rehahn, *Macromolecules* **1999**, *32*, 5818-5828.

72.   D. G. Kurth, P. Lehmann, M. Schütte, *Proc. Natl. Acad. Sci. USA* **2000**, *97*, 5704-5707.

73.   J. A. Barron, S. Glazier, S. Bernhard, K. Takada, P. L. Houston, H. D. Abruña, *Inorg. Chem.* **2003**, *42*, 1448-1455.

74.   D. Hinderberger, O. Schmelz, M. Rehahn, G. Jeschke, *Angew. Chem. Int. Ed.* **2004**, *43*, 4616-4621.

75.   A. Lindner, M. Menzel, F. Renz, D. G. Kurth, A. F. Thünemann, *Hyperfinen Interact.* **2005**, *166*, 465-468.

76.   F. S. Han, M. Higuchi, D. G. Kurth, *Adv. Mater.* **2007**, *19*, 3928-3931.

77.   F. S. Han, M. Higuchi, Y. Akasaka, Y. Otsuka, D. G. Kurth, *Thin Solid Films* **2008**, *516*, 2469-2473.

78.   F. S. Han, M. Higuchi, D. G. Kurth, *J. Am. Chem. Soc.* **2008**, *130*, 2073-2081.

79.   H. S. Chow, E. C. Constable, C. E. Housecroft, M. Neuburger, *Dalton Trans.* **2003**, 4568-4569.

80.   H. S. Chow, E. C. Constable, R. Frantz, C. E. Housecroft, J. Lacour, M. Neuburger, D. Rappoport, S. Schaffner, *New J. Chem.* **2009**, *33*, 376-385.

81.   H. S. Chow, E. C. Constable, C. E. Housecroft, M. Neuburger, S. Schaffner, *Polyhedron* **2006**, *25*, 1831-1843.

82.   H. S. Chow, Ph.D. Thesis, University of Basel, **2005**.

83.   E. C. Constable, A. M. W. Cargill Thompson, *J. Chem. Soc. Chem. Commun.* **1992**, 617.

84.   E. C. Constable, A. M. W. Cargill Thompson, *J. Chem. Soc. Dalton Trans.* **1992**, 3476.

85.   E. C. Constable, C. E. Housecroft, M. Cattalini, D. Phillips, *New. J. Chem.* **1998**, 193.

86.   E. C. Constable, P. Harverson, *Inorg. Chim. Acta* **1996**, *252*, 9.

87.   A. Juris, V. Balzani, F. Barigelletti, S. Campagna, P. Belser, A. Von Zelewsky, *Coord. Chem. Rev.* **1988**, *84*, 85-277.

88.   S. Bonnet, J.-P. Collin, *Chem. Soc. Rev.* **2008**, *37*, 1207-1217.

89.   V. Balzani, *Photochem. Photobiol. Sci.* **2003**, *2*, 459-476.

90.   A. Abbotto, C. Barolo, L. Bellotto, F. De Angelis, M. Graetzel, N. Manfredi, C. Marinzi, S. Fantacci, J.-H. Yum, M. K. Nazeeruddin, *Chem. Commun.* **2008**, 5318-5320.

91.   M. Graetzel, *Nature* **2003**, *421*, 586-587.

92.   M. Graetzel, *Nature* **2001**, *414*, 338-344.

93.   B. O'Regan, M. Graetzel, *Nature* **1991**, *353*, 737-740.

94.   Y. Bai, Y. Cao, J. Zhang, M. Wang, R. Li, P. Wang, M. Zakeeruddin Shaik, M. Graetzel, *Nature Mater.* **2008**, *7*, 626-630.

95.   P. Wang, M. Zakeeruddin Shaik, E. Moser Jacques, K. Nazeeruddin Mohammad, T. Sekiguchi, M. Graetzel, *Nature Mater.* **2003**, *2*, 402-407.

96.   A. M. W. Cargill Thompson, *Coord. Chem. Rev.* **1997**, 160.

97.   N. W. Alcock, P. R. Barker, J. M. Haider, M. J. Hannon, C. L. Painting, Z. Pikramenou, E. A. Plummer, K. Rissanen, P. Saarenketo, *J. Chem. Soc. Dalton Trans.* **2000**, 1447.

98.   E. C. Constable, C. E. Housecroft, T. Kulke, C. Lazzarini, E. R. Schofield, Y. Zimmermann, *J. Chem. Soc. Dalton Trans.* **2001**, 2864.

99.   E. C. Constable, T. Kulke, M. Neuburger, M. Zehnder, *New J. Chem.* **1997**, *21*, 1091.

100.   C. E. Housecroft, A. G. Sharpe, *Inorganic Chemistry*, Pearson, Harlow, 2005, Chapter 25.

101.   M. Gerloch, E. C. Constable, *Transition Metal Chemistry*, VCH, New York, **1994**.

102.   E. C. Constable, M. D. Ward, *J. Chem. Soc. Dalton Trans.* **1990**, 1405.

103.   J. A. A. de Boer, J. W. H. M. Uiterwijk, J. Geevers, S. Harkema, D. N. Reinhoudt, *J. Org. Chem.* **1983**, *48*, 4821.

104.   M. Tomoi, O. Abe, M. Ikeda, K. Kihara, H. Kakiuchi, *Tetrahedron Letters* **1978**, *33*, 3031 - 3034.

105.   M. Surowiec, R. Custelcean , K. Surowiec , R. A. Bartach, *Tetrahedron* **2009**, *65*, 7777–7783.

106.   J. Zavada, M. Pankova, P. Holy, M. Tichy, *Synthesis* **1995**, *240*, 1132.

107.   B. Dietrich, *J. Chem. Educ.* **1985**, *62*, 954.

108.   R. J. P. Williams, *Q. Rev. Chem. Soc.* **1970**, *24*, 331.

109.   N. S. Poonia, A. V. Bajaj, *Chem. Rev.* **1979**, *79*, 389.

110.   C. J. Pedersen, *J. Am. Chem. Soc.* **1967**, *89*, 7017.

111.   B. Dietrich, J.-M. Lehn, J.-P. Sauvage, *Tetrahedron Lett.* **1969**, 2885-2889.

112.   J. Morita, S. Tsuchiya, *Heterocycles* **2010**, *80*, 1103-1123.

113.   N. M. Kurochkina, V. E. Baulin, *Russian Journal of Coordination Chemistry* **2010**, *36*, 241-248.

114.   K. I. Ishimori, S. Mori, *Talanta* **2009**, *78*, 1272-1279.

115.   G. L. Starova, A. S. Denisova, *Russian Journal of General Chemistry* **2007**, *77*, 274-277.

116.   W. J. Doherty, R. Friedlein, *Journal of Chemical Physics* **2007**, *26*, 1562.

117.   W. Huang, H. F. Qian, *Journal of Molecular Structure* **2005**, *741*, 155-158.

118.   C. Dietrich-Buchecker, J.-P. Sauvage, *Chemical Communications* **1999**, *7*, 615-616.

119.   S. Capone, A. D. Robertis, C. D. Stefano, R. Scarella, *Talanta* **1985**, *32*, 675.

120.   J. Ghasemi, M. Shamispur, *J. Coord. Chem.* **1992**, *26*, 337.

121.   T. Madrakian, A. Afkhami, J. Ghasemi, M. Shamsipur, *Polyhedron* **1996**, *15*, 3647-3652.

122.   R. H. Holyer, C. D. Hubbard, S. F. Kettle, R. G. Wilkiss, *Inorganic Chemistry* **1966**, *5*, 622.

123.   A. Juris, V. Balzani, F. Barigelletti, S. Campagna, P. Belser, A. von Zelewsky, *Coord. Chem. Rev.* **1988**, *84*, 85.

124.   V. Balzani, A. Juris, *Coord. Chem. Rev.* **2001**, *211*, 97.

125.   M. Plevoets, F. Vögtle, L. De Cola, V. Balzani, *New J. Chem.* **1999**, *23*, 63.

126.   A. De Nicola, Y. Liu, K. S. Schanze, R. Ziessel, *Chem. Commun.* **2003**, 288.

127.   P. R. Ashton, V. Balzani, O. Kocian, L. Prodi, N. Spencer, J. F. Stoddart, *J. Am. Chem. Soc.* **1998**, *120*, 11190.

128.   P. R. Ashton, R. Ballardini, V. Balzani, E. C. Constable, A. Credi, O. Kocian, S. J.Langford, J. A. Preece, L. Prodi, E. R. Schofield, N. Spencer, J. F. Stoddart, S. Wenger, *Chem. Eur. J.* **1998**, *4*, 2413.

129.   P. R. Ashton, R. Ballardini, V. Balzani, A. Credi, K. R. Dress, E. Ishow, C. J.Kleverlaan, O. Kocian, J. A. Preece, N. Spencer, J. F. Stoddart, M. Venturi, S. Wenger, *Chem. Eur. J.* **2000**, *6*, 3558.

130.   R. Ballardini, V. Balzani, M. Clemente-León, A. Credi, M. T. Gandolfi, E. Ishow, J.Perkins, J. F. Stoddart, H.-R. Tseng, S. Wenger, *J. Am. Chem. Soc.* **2002**, *124*, 12786.

131.   M. Venturi, F. Marchioni, V. Balzani, D. M. Opris, O. Henze, A. D. Schlüter, *Eur. J. Org. Chem.* **2003**, 4227.

132.   A. González-Cabello, P. Vázquez, T. Torres, D. M. Guldi, *J. Org. Chem.* **2003**, *68*, 8635.

133.   H. Wolpher, M. Borgström, L. Hammarström, J. Bergquist, V. Sundström, S. Styring, L. Sun, B. Åkermark, *Inorg. Chem. Commun.* **2003**, *6*, 989.

134.   O. Johansson, M. Borgström, R. Lomoth, M. Palmblad, J. Bergquist, L. Hammarström, L. Sun, B. Åkermark, *Inorg. Chem.* **2003**, *42*, 2908.

135.   V. Aranyos, A. Hagfeldt, H. Grennberg, E. Figgemeier, *Polyhedron* **2004**, *23*, 589.

136.   J. A. Moss, J. C. Yang, J. M. Stipkala, X. Wen, C. A. Bignozzi, G. J. Meyer, T. J. Meyer, *Inorg. Chem.* **2004**, *43*, 1784.

137.   H. Wolpher, O. Johansson, M. Abrahamsson, M. Kritikos, L. Sun, B. Åkermark, *Inorg. Chem. Commun.* **2004**, *7*, 337.

138.   R. T. F. Jukes, V. Adamo, F. Hartl, P. Belser, L. De Cola, *Inorg. Chem.* **2004**, *43*, 2779.

139.   V. Balzani, A. Juris, M. Venturi, S. Campagna, S. Serroni, *Chem. Rev.* **1996**, *96*, 759.

140.   J.-P. Sauvage, J.-P. Collin, J.-C. Chambron, S. Guillerez, C. Coudret, V. Balzani, F.Barigelletti, L. De Cola, L. Flamigni, *Chem. Rev.* **1994**, *94*, 993.

141. J.-P. Collin, A. Harriman, V. Heitz, F. Odobel, J.-P. Sauvage, *Coord. Chem. Rev.* **1996**, *148*, 63.

142. J.-P. Collin, P. Gaviña, V. Heitz, J-P. Sauvage, *Eur. J. Inorg. Chem.* **1998**, 1.

143. L. Flamigni, F. Barigelletti, N. Armaroli, J.-P. Collin, I. M. Dixon, J.-P. Sauvage, J. A. G. Williams, *Coord. Chem. Rev.* **1999**, *190-192*, 671.

144. J.-P. Collin, S. Guillerez, J.-P. Sauvage, F. Barigelletti, L. De Cola, L. Flamigni, V. Balzani, *Inorg. Chem.* **1991**, *30*, 4230.

145. E. C. Constable, A. J. Edwards, R. Martínez-Máñez, P. R. Raithby, A. M. W. Cargill Thompson, *J. Chem. Soc. Dalton Trans.* **1994**, 645.

146. E. C. Constable, A. M. W. Cargill Thompson, *J. Chem. Soc. Dalton Trans.* **1994**, 1409.

147. B. Whittle, S. R. Batten, J. C. Jeffery, L. H. Rees, M. D. Ward, *J. Chem. Soc. Dalton Trans.* **1996**, 4249.

148. G. Albano, V. Balzani, E. C. Constable, M. Maestri, D. R. Smith, *Inorg. Chim. Acta* **1998**, 277, 225.

149. D. Armspach, E. C. Constable, F. Diederich, C. E. Housecroft, J.-F. Nierengarten, *Chem. Eur. J.* **1998**, *4*, 723.

150. A. Harriman, M. Hissler, A. Khatyr, R. Ziessel, *Chem. Commun.* **1999**, 735.

151. N. W. Alcock, P. R. Barker, J. M. Haider, M. J. Hannon, C. L. Painting, Z. Pikramenou, E. A. Plummer, K. Rissanen, P. Saarenketo, *J. Chem. Soc. Dalton Trans.* **2000**, 1447.

152. E. C. Constable, R. W. Handel, C. E. Housecroft, A. F. Morales, L. Flamigni, F. Barigelletti, *Dalton Trans.* **2003**, 1220.

153. U. Siemeling, J. V. der Brüggen, U. Vorfeld, B. Neumann, A. Stammler, H.-G. Stammler, A. Brockhinke, R. Plessow, P. Zanello, F. Laschi, F. F. de Biani, M. Fontani, S. Steenken, M. Stapper, G. Gurzadyan, *Chem. Eur. J.* **2003**, *9*, 2819.

154. V. W.-W. Yam, K. M.-C. Wong, N. Zhu, *Angew. Chem. Int. Ed.* **2003**, *42*, 1400; E. C. Constable, C.E. Housecroft, M. Neuburger, P. J. Rösel, S. Schaffner, J. A. Zampese, *Chem. Eur. J.* **2009**, *15*, 11746-11757.

155. R. Passalacqua, F. Loiseau, S. Campagna, Y.-Q. Fang, G. S. Hanan, *Angew. Chem. Int. Ed.* **2003**, *42*, 1608.

156.	J. M. Haider, R. M. Williams, L. De Cola, Z. Pikramenou, *Angew. Chem. Int. Ed.* **2003**, *42*, 1830.

157.	A. C. Benniston, A. Harriman, D. J. Lawrie, S. A. Rostron, *Tetrahedron Lett.* **2004**, *45*, 2503.

158.	E. C. Constable, R. W. Handel, C. E. Housecroft, M. Neuburger, E. R. Schofield, M. Zehnder, *Polyhedron* **2004**, *23*, 135.

159.	E. Figgemeier, V. Aranyos, E. C. Constable, R. W. Handel, C. E. Housecroft, C. Risinger, A. Hagfeldt, E. Mukhtar, *Inorg. Chem. Commun.* **2004**, *7*, 117.

160.	E. C. Constable, *Adv. Inorg. Chem. Radiochem.* **1987**, *30*, 69;
	E.C. Constable, A.M.W. Cargill Thompson, D.A. Tocher, M.A.M. Daniels, *New J. Chem.* **1992**, *16*, 855-867.

161.	M. Maestri, N. Armaroli, V. Balzani, E. C. Constable, A. M. W. Cargill Thompson, *Inorg. Chem.* **1995**, *34*, 2759

162.	S. C. Yu, C. C. Kwok, W. K. Chan, C. M. Che, *Adv. Mater.* **2003**, *15*, 1634–1647.

163.	S. C. Chang, J. Bharathan, Y. Yang, R. Helgeson, J. R. Reynolds, *Appl. Phys. Lett.* **1998**, *72*, 2561–2563.

164.	V. N. Bliznyuk, S. A. Carter, J. C. Scott, G. Klaerner, R. D. Miller, D. C. Miller, *Macromolecules* **1999**, *32*, 361–369.

165.	C. Xia, R. C. Advincula, *Macromolecules* **2001**, *34*, 5854–5859.

166.	R. Dobrawa, M. Lysetska, P. Ballester, M. Grüne, F. Würthner, *Macromolecules* **2005**, *38*, 1315–1325.

167.	Y.-Y. Chen, Y.-T. Tao, H. C. Lin, *Macromolecules* **2006**, *39*, 8559–8566.

168.	Y.-Y. Chen, H. C. Lin, *J. Polym. Sci. Part A: Polym. Chem.* **2007**, 3243–3255.

169.	U. S. Schubert *J. Phys. Chem. C* **2008**, *112,* 18651–18660.

170.	S.-H. Hwang, C. N. Moorefield, P. Wang, J.-Y. Kim, S.-W. Lee, G. R. Newkome, *Inorg. Chim. Acta* **2007**, *360*, 1780–1784.

171.	S.-H. Hwang, *Inorganica Chimica Acta* **2007**, *360*, 1780–1784.

172.	L. Pazderski, T. Pawlak, J. Sitkowski, L. Kozerski E. Szlyk, *Magn. Reson. Chem.* **2010**, *48*, 450-457.

173. H. Elsbernd, J.K. Beattie, *J. Inorg. Nucl. Chem.* **1972**, *34*, 771-774.

174. S. Castellano, H. Günther, S. Ebersole, *J. Phys. Chem.* **1966**, *69*, 4166-4176.

175. P.-T. Chou, Y. Chi, *Chem. Eur. J.* **2007**, *12*, 380–395.

176. N. M. Logacheva, V. E. Baulin, A. Y. Tsivadze, E. N. Pyatova, I. S. Ivanova,Y. A. Velikodny, V. V. Chernyshev, *Dalton Trans.*, **2009**, *3*, 2482–2489.

177. Martinus H.V. Werts, *Science Progress* **2005**, *88*, 101–131.

178. T. Gunnlaugsson, F. Stomeo, *Org. Biomol. Chem.* **2007**, *5*, 1999.

179. T. Gunnlaugsson, J. P. Leonard, *Chem. Comm.* **2005**, 3114.

180. B. Alpha, J.-M. Lehn, R. Ballardini, V. Balzani, S. Perathoner, N. Sabbatini, *Photochem. Photobiol.* **1990**, *52*, 299.

181. J. F. Callan, A. P. de Silva, D. C. Magri, *Tetrahedron* **2005**, *36*, 8551.

182. T. Gunnlaugsson, H. D. P. Ali, M. Glynn, P. E. Kruger, G. M. Hussey, F. M. Pfeffer, C. M. G. dos Santos, J. Tierney, *J. Fluoresc.* **2005**, *15*, 287.

183. A. P. de Silva, B. McCaughan, B. O. F. McKinney, M. Querol, *Dalton Trans.* **2003**, *56*, 1902.

184. V. Balzani, *Photochem. Photobiol. Sci* **2003**, *2*, 459.

185. V. Balzani, A. Credi, M. Venturi, *Pure Appl Chem* **2003**, *75*, 541.

186. R. Martínez-Máñez, F. Sancenón, *Chem. Rev.* **2003**, *103*, 4419.

187. F. M. Raymo, *Adv. Mater.* **2002**, *14*, 401.

188. A. P. de Silva, H. Q. N. Gunaratne, T. Gunnlaugsson, A. J. M. Huxley, C. P. McCoy, J. T. Rademacher, T. E. Rice, *Chem. Rev.* **1997**, *97*, 1515.

189. M. Venturi, A. Credi, V. Balzani, *Molecular devices and machines – a journey into the nanoworld* **2003**, Wiley, Weinheim.

190. B. L. Feringa, *Molecular switches* **2001**, Wiley, Weinheim.

191. T. Gunnlaugsson, M. Glynn, G. M. Tocci, P. E. Kruger, F. M. Pfeffer, *Coord. Chem. Rev.* **2006**, *250*, 3094.

192. R. Parkesh, T. C. Lee, T. Gunnlaugsson, *Org. Biomol. Chem.* **2007**, *5*, 310.

193.   T. Gunnlaugsson, P. E. Kruger, P. Jensen, J. Tierney, H: D. P. Ali, G. M. Hussey, *J. Org. Chem.* **2005**, *70*, 1875.

194.   F. M. Pfeffer, T. Gunnlaugsson, P. Jensen, P. E. Kruger, *Org. Lett.* **2005**, *7*, 5375.

195.   T. Gunnlaugsson, J. P. Leonard, N. S. Murray, *Org. Lett.* **2004**, *6*, 1557.

196.   T. Gunnlaugsson, T. C. Lee, R. Parkesh, *Org. Biomol. Chem.* **2003**, *1*, 3265.

197.   T. Gunnlaugsson, B. Bichell, C. Nolan, *Tetrahedron Lett.* **2002**, *43*, 4989.

198.   T. Gunnlaugsson, T. C. Lee, R. Parkesh, *Org. Lett.* **2003**, *5*, 4065.

199.   T. Gunnlaugsson, M. Nieuwenhuyzen, L. Richard, V. Thoss, *Tetrahedron Lett.* **2001**, *42*, 4725.

200.   G. Stochel, A. Wanat, E. Kuli´s, Z. Stasicka, *Coord. Chem. Rev.* **1998**, *171*, 203.

201.   V. Wing-Wah, K. Yam, L. Kam-Ying, *Coord. Chem. Rev.* **1998**, *184*, 157.

202.   L. Thunus, R. Lejeune, *Coord. Chem. Rev.* **1999**, *184*, 125.

203.   L. M. Perry, J. D. Winefordner, *Talanta* **1990**, *37*, 965.

204.   E. F. Gudgin Dickson, A. Pollak, E. P. Diamandis, *J. Photochem. Photobiol. B: Biol.* **1995**, *27*, 3.

205.   J. Coates, P. G. Sammes, R. M. West, *J. Chem. Soc. Perkin Trans.* **1996**, *2*, 1275.

206.   J. Coates, P. G. Sammes, R. M. West, *J. Chem. Soc. Perkin Trans.* **1996**, *2*, 1283.

207.   W. W. E. De Horroks, D. R. Sudnick, *Acc. Chem. Res.* **1981**, *14*, 384.

208.   P. G. Sammes, G. Yahioglu, *Nat. Prod. Rep.* **1996**, *5*, 1.

209.   D. Parker, R. S. Dickins, H. Puschmann, C. Cossland, J. A. K. Howard, *Chem. Rev.* **2002**, *102*, 1977.

210.   J.-C. G. Bünzli, C. Piguet, *Chem. Rev.* **2002**, *102*, 1977.

211.   P. R. Selvin, *J. Am. Chem. Soc.* **2001**, *123*, 7067.

212.   C. Piguet, J.-C. G. Bünzli, *Chem. Soc. Rev.* **1999**, *28*, 347.

213.   E. Toth, L. Burai, A. E. Merback, *Coord. Chem. Rev.* **2001**, *216*, 363.

214.	S. Aime, M. Botta, M. Fasano, E. Terreno, *Chem. Soc. Rev.* **1998**, *27*, 19.

215.	S. Faulkner, J. L. Matthews, Ward MD (ed) *Applications of coordination chemistry. Comprehensive coordination chemistry II* **2003**, *9*, 2nd edn. Elsevier, Amsterdam, 913.

216.	S. Petoud, S. M. Cohen, J.-C. G. Bünzli, K. N. Raymond, *J. Am. Chem. Soc.* **2003**, *125*, 13324.

217.	J.-C. G. Bünzli, *Acc. Chem. Res.* **2006**, *39*, 53.

218.	J.-C.G. Bünzli, C. Piguet, *Chem. Soc. Rev.* **2005**, *34*, 1048.

219.	J.-C. G. Bünzli In: A. Sigel, H. Sigel (ed), *Metal ions in biological systems*, **2006**, *42*, Marcel Dekker, The Netherlands, 39.

220.	A. Sigel, H. Sigel (ed), *The lanthanides and their interrelations with biosystems. Metal ions in biological systems*, **2006**, *40*, Marcel Dekker, New York.

221.	H. G. Friedmom, G. R. Choppin, D. G. Feuerbocherz, *Journal of Chemical Education*, **1964**, *41*, 334.

222.	J.-C. G. Bünzli In: J.-C. G. Bünzli, G. R. Choppin (ed), *Lanthanide probes in life, chemical and earth sciences; theory and practice*, **1989**, Elsevier, New York, 219.

223.	Y. Y. Xu, I. Hemmilä, *Talanta* **1992**, *39*, 759–763.

224.	J.. P. Leonard, C. M. G. dos Santos, S. E. Plush, T. McCabe, T. Gunnlaugsson, *Chem. Commun.* **2007**, *34*, 129–131.

225.	L. R. Melby, N. J. Rose, E. Abramson, J. C. Caris, *J. Am. Chem. Soc.* **1964**, *86*, 5117–5125.

226.	R. C. Holz, L. C. Thompson, *Inorg. Chem.* **1988**, *27*, 4640–4644.

227.	C. R. De Silva, J. R. Maeyer, A. Dawson, Z. Zheng, *Polyhedron* **2007**, *26*, 1229–1238.

228.	Z. Soumaila, N. Dupont,G. Bernardinelli, J. Hamacek, *Chem. Eur. J.* **2009**, *12*, 7–12.

229.	R. C. Palenik, K. A. Abboud, S. P. Summers, L. L. Reitfort, G. J. Palenik, *Inorg. Chim. Acta* **2006**, *359*, 4645–4650.

230.	M. Albrecht, S. Mirtschin, O. Osetska, S. Dehn, D. Enders, R. Froehlich, T. Pape, F. E. Hahn, *Eur. J. Inorg. Chem.* **2007**, *23*, 3276–3287.

231. L. J. Charbonniere, S. Mameri, D. Flot, F. Waltz, C. Zandanel, R. F. Ziessel, *Dalton Trans.* **2007**, *21*, 2245–2253.

232. D. Guo, C. Duan, F. Lu, Y. Hasegawa, Q. Meng, S. Yanagida, *Chem. Commun.* **2004**, *15*, 1486.

233. S. I. Klink, H. Keizer, H. W. Hofstraat, F. C. J. M. Van Veggel, *Synth. Met.* **2002**, *127*, 213.

234. D. A. Durham, G.H. Frost, F. A. Hart, *J. Inorg. Nucl. Chem.* **1969**, *31*, 833-838.

235. U. Shnonis, J. L. Dallas, F. A. Wall, *Inorg. Chem.* **1992**, *31*, 5349.

236. H. Gampp, M. Maeder, C. J. Meyer, A. D. Zuberbühler, *Talanta* **1985**, *32*, 95-101.

237. H. Gampp, M. Maeder, C. J. Meyer, A. D. Zuberbühler, *Talanta* **1986**, *33*, 943-951.

Curriculum Vitae

PERSONAL INFORMATION:

Name, Surname: Paulina, Chwalisz
Date of birth: 08.06.1982
Address: Ryffstrasse 16, 4056Basel, Switzerland
Tel: +41787707734
Email: Paulina.Chwalisz@unibas.ch.

EDUCATION AND TRAINING:

October 2006– Present	Ph.D. studies, University of Basel, Switzerland;
July - September 2006	Practice in laboratory of cytobiochemistry, University of Wrocław;
February – Mai 2006	Socrates/Erasmus exchange student at Katholieke Universiteit Leuven, Belgium. Synthesis of porphyrins and expanded porphyrins;
2001 – 2006	University of Wrocław, chemistry, organic chemistry;
1998-2001	Secondary School in Brzeg Dolny.

PERSONAL AND SOCIAL SKILLS:

Languages:	Polish, native speaker,
	English, fluent,
	German, fluent,
	French, intermediate.
2003-2005	Member of student organization; co-organizing a student conference and chemical workshop for pupils;
2006-2010	Member of Swiss Chemical Society;
September 2009	Elected Vice-president of Swiss Young Chemists' Association.

Publications:

M. Stepien,; L. Latos-Grazynski,; N. Sprutta,; P. Chwalisz; L. Szterenberg,. Expanded porphyrin with a split personality: a Huckel-Mobius aromaticity switch, *Angew. Chem. International Edition* **2007**, 46(41), 7869-7873.

J. E. Beves; P. Chwalisz; E. C. Constable; C. E. Housecroft; M. Neuburger; S. Schaffner and J. A. Zampese, A new polymorph of 4'-tolyl-2,2':6',2"-terpyridine (ttpy) and the single crystal structures of $[Fe(ttpy)_2][PF_6]_2$ and $[Ru(ttpy)_2][PF_6]_2$, *Inorg Chem. Commun.* – accepted.

REFERENCES:

Prof. Dr L. Latos-Grażyński,

University of Wroclaw,
F. Joliot-Curie 14, 50-383 Wrocław, Poland,
Phone +48713757256
llg@wchuwr.chem.uni.wroc.pl

Prof. Dr E. Constable,

Department of Chemistry
University of Basel
Spitalstrasse 51, 4056 Basel, Switzerland
Phone +41612671001
fax +41612671005
edwin.constable@unibas.ch

HOBBIES: music, sport, traveling, challenges.